The Geology, Alteration and Mineralisation of the Beatrice Prospect, western Tasmania

Marcus Hope
Bachelor of Science

UNIVERSITY OF TASMANIA

A Research Thesis submitted in partial fulfilment of the requirements of the Degree of Bachelor of Science with Honours

CODES SRC

School of Earth Sciences, University of Tasmania

November 1999

Abstract

A north trending felsic volcanosedimentary sequence is exposed at the Beatrice Prospect on the southern slopes of Mt Sedgewick, western Tasmania. The exposed sequence, tentatively correlated to the Lynchford Member and Central Volcanic Complex (CVC) dips ~65° to the west, forming the eastern limb of a faulted syncline located west of Itat Creek.

The volcanosedimentary package consists of black shale, coarse and fine felsic volcaniclastics with minor intercalated flow banded quartz phyric lava, conformably overlying a thick unit of quartz feldspar phyric, spherulitic lava correlated with the CVC. The black shale unit incorporates several large lenses of quartz feldspar porphyry, which intruded and possibly burrowed into the wet sediment forming peperitic margins and entraining clastic material.

Three distinct alteration assemblages are recognised. Sericite alteration is ubiquitous, relating to the diagenetic and regional lower greenschist facies metamorphic conversion of originally glassy pumiceous material to sericite. Chlorite alteration correlates with the major mineralising event, showing a systematic increase in intensity toward mineralisation. Potassic alteration overprinted by chlorite + magnetite alteration exists at depth. This assemblage is consistent with alteration associated with Cambrian high K, magnetite series granites.

Uneconomic base metal mineralisation is manifested as veinlets and replacements in the shale unit and is concentrated at the upper contact between fine and coarse volcaniclastic units. The best drillhole intersection was 7m @ 1.07%Pb and 1.65%Zn hosted in fine volcaniclastics in MS1. Textural evidence indicates that sulfides have been recrystallised and mobilised during deformation, resulting in sulfides aligned with cleavage and the remobilisation of base metals into pressure fringes adjacent to pre-existing sulfide grains.

Lead isotopes indicate mineralisation occurred during the Cambrian, with zinc ratios suggesting metals have been transported by a fluid saturated with respect to both lead and zinc. Sulfur isotopes are supportive of a reduced seawater source of sulfur and the possible link to VHMS style mineralisation. Textural evidence indicates mineralisation pre dates Devonian cleavage, however no textural evidence to support strataform mineralisation was observed.

Sulfur isotopes display significant variation associated with *in situ* reduction of evaporite minerals, localising heavy sulfides to a sequence of carbonate and evaporite laminae in the black shale unit.

The absence of stratiform sulfides and abundant veinlet mineralisation may indicate that the conditions necessary to concentrate sulfides on the seafloor was precluded, possibly due to subsurface boiling of the hydrothermal fluid associated with reduced hydrostatic pressure. This interpretation may be supported by the presence of evaporite minerals, indicating a shallow depositional environment.

Table of Contents

List of Figures

List of Tables

List of Plates

Chapter 1
Introduction

1.1 The Beatrice Prospect

The Beatrice Prospect is a Pb-Zn prospect located on the southern and eastern slopes of Mt Sedgewick, 10km north east of Queenstown, western Tasmania (Figure 1.1). The prospect lies within the Pasminco Exploration License 6/98 and is accessible by 4wheel-drive vehicle via a gravel road that originates within the Mt Lyell mine lease.

The prospect ranges from 300 to 1147 metres above sea level. Subalpine scrubby vegetation predominates within exposed areas of the prospect, with rare deciduous beech (*Nothofagus gunnii*) occurring at higher altitudes. Valleys within the prospect, such as Itat and Porphyry Creek support woodland of King Billy Pine (*Anthrotaxis selaginoides*), pandanis (*Richea pandanifolia*) and myrtle (*Nothofagus cunninghamii*).

1.2 Aims

The aims of this study were to:

1. Describe the geology of the Beatrice Prospect.
2. Document the styles of base metal mineralisation at the Beatrice prospect, and to propose a genetic model.
3. Define the styles and distribution of alteration in relation to lithofacies architecture and mineralised zones.
4. Assess the prospectivity of the region and define vectors for further exploration.

1.3 Methods

Five weeks fieldwork were completed in March-April, 1999. During this time detailed mapping at 1:500 scale was completed within the Itat Creek Valley area, which previous exploration had identified as the most prospective area within the tenement. Initially seven diamond drill holes were graphically logged. A further two drill holes were logged through the course of 1999 due to continuation of drilling within the prospect.

During this field work samples from both outcrop and drill core were collected for geochemical and petrographic analysis. Geochemical analyses were conducted by Analabs Pty Ltd, Welshpool, Western Australia. Stable isotope (S,O,C) and radiogenic isotope (Pb)

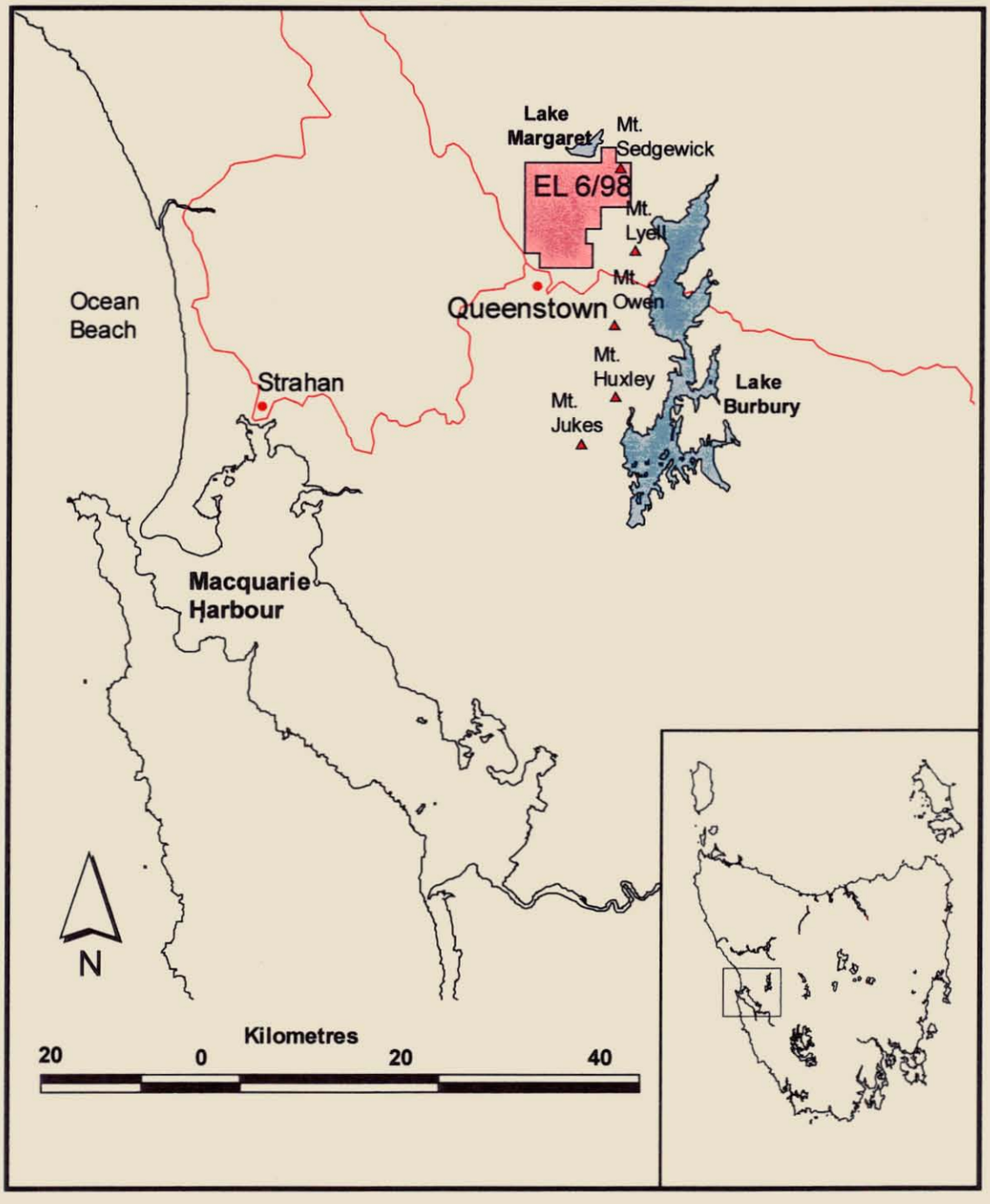

Figure 1.1 Beatrice Prospect (EL 6/98)

5 cm

analyses were conducted at the University of Tasmania and fluid inclusions were analysed at the University of Tasmania and Mineral Resources of Tasmania to determine the compositions, origins and sources of metals and fluids.

1.4 Previous Exploration

Considerable work has been conducted within the prospect since its discovery by the Mount Lyell Mining and Railway Company (MLMRC) in 1974. During the 1976/77 and 1977/78 field seasons 47.5 kilometres of grids were cut, geophysical and soil geochemical surveys were conducted, resulting in a major Pb, Zn and Cu anomaly being identified. This anomalous zone, hosted within a steeply dipping volcanosedimentary sequence running parallel to Itat Creek was termed the Mount Sedgewick Anomalous Zone (MSAZ) during 1978/79. A drilling road was excavated into the prospect and sampled where obvious sulfides existed within the Itat Creek area. An 80m section of the road cutting (near subsequent drill hole MS3) assayed 0.34%Zn, 0.22%Pb, 65ppm Cu and 3.7ppm Ag, with the best interval being 5m at 0.57% Zn, 0.63% Pb, 90ppm Cu and 9ppm Ag. Five drill holes were drilled during 1978-79. MS1, MS2, MS3, MS4 tested the inferred strike length of the MSAZ host shale and volcaniclastic units and MS5 was drilled to test a chargeability anomaly associated with a unit of Quartz Feldspar Porphyry. MS5 intersected black shale that was interpreted to explain the IP anomaly.

A review of the prospect was completed by Goldfields Exploration (Exploration Division of RGC and MLMRC) in 1983. The geology at Beatrice was considered similar to Red Hills. It was also considered that previous drilling inadequately tested the area for VHMS potential, as holes were drilled at a low angle to dip and strike and the southern holes were collared stratigraphically beneath the black shale unit. It was also recognised that potential for mineralisation existed in extensions of the shale and volcaniclastics beneath the Quartz Feldspar Porphyry west of Itat Creek.

There was little further exploration of the Beatrice Prospect until 1989 when BHP conducted a fixed loop UTEM Survey. Only weak conductors were detected and attributed to structures or lithological variations. Relogging of core from holes MS1-MS5 lead to the conclusion that the mineralisation was "partly vein related and partly replacive, and the abundance of associated K-feldspar alteration and absence of major silicification and pyrite suggests that this mineralisation is not of the target VMS style" (Wilde and Kerr, 1990).

RGC Exploration returned to the Beatrice Prospect in search of VHMS style mineralisation in 1993, when a literature review was completed, the area remapped and the core relogged. Boyd's (1994) study of drill core contradicts the interpretations made by BHP. Boyd (1994) stated that "the sulfide exposed in the core is bedded within the black shale and volcaniclastic units and as such is most likely to be syn-sedimentary, thus indicating that some form of seafloor sulfide deposit has occurred at this stratigraphic level". MS6 was drilled in 1996 to test the southern extent of the favourable unit and was located 500m north of the Comstock Valley Fault, which was interpreted to be a synvolcanic growth structure. Drill hole assays were only weakly anomalous with the best intercept being 2.6m at 0.25% Zn.

Pasminco acquired their licence in October 1997 to continue exploration for Pb-Zn deposits and subsequently drilled three holes: MS7, MS8 and MS9. MS7 was drilled as a "stratigraphic" exploration hole encountering weak mineralisation that clearly showed that the prospective horizon extends beneath the quartz feldspar porphyry unit west of Itat Creek. Located roughly 800m north of MS7, MS8 was drilled to test partial leach soil geochemical and IP anomalies and intersected moderate mineralisation with the best interval being 6.6 metre at 1.18%Zn, 0.55%Pb and 12.5ppm Ag. MS9 was targeted on an IP anomaly to the west of MS8, but encountered only very weak sulfide concentrations.

Chapter 2
Regional Geology

2.1 Introduction

The Mount Read Volcanic (MRV) belt (Figure 2.1) is located in western and northwestern Tasmania. The 200km by 15km volcanic belt lies along the eastern margin of the Dundas Trough. The main eastern section, which overlaps the margin of the Precambrian Tyennan rocks, is composed of relatively massive lava rich felsic volcanic sequences. The broader western part of the MRV consists of volcano-sedimentary sequences dominated by volcaniclastic mass flow sandstones and breccias interdigitating with the Cambrian sediments of the west Dundas Trough (Corbett 1992; Figure 2.2).

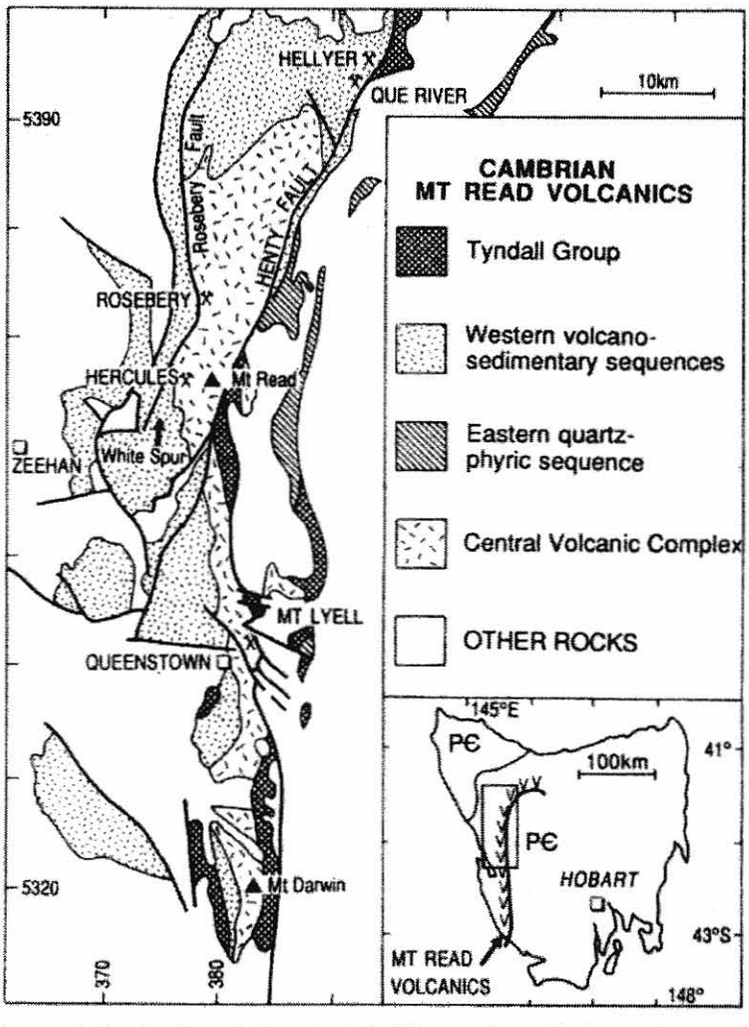

Figure 2.1 Location and distribution of the principle lithostratigraphic formations and major massive sulfide deposits in the Mount Read Volcanic Belt of western Tasmania (McPhie and Allen 1992).

5 cm

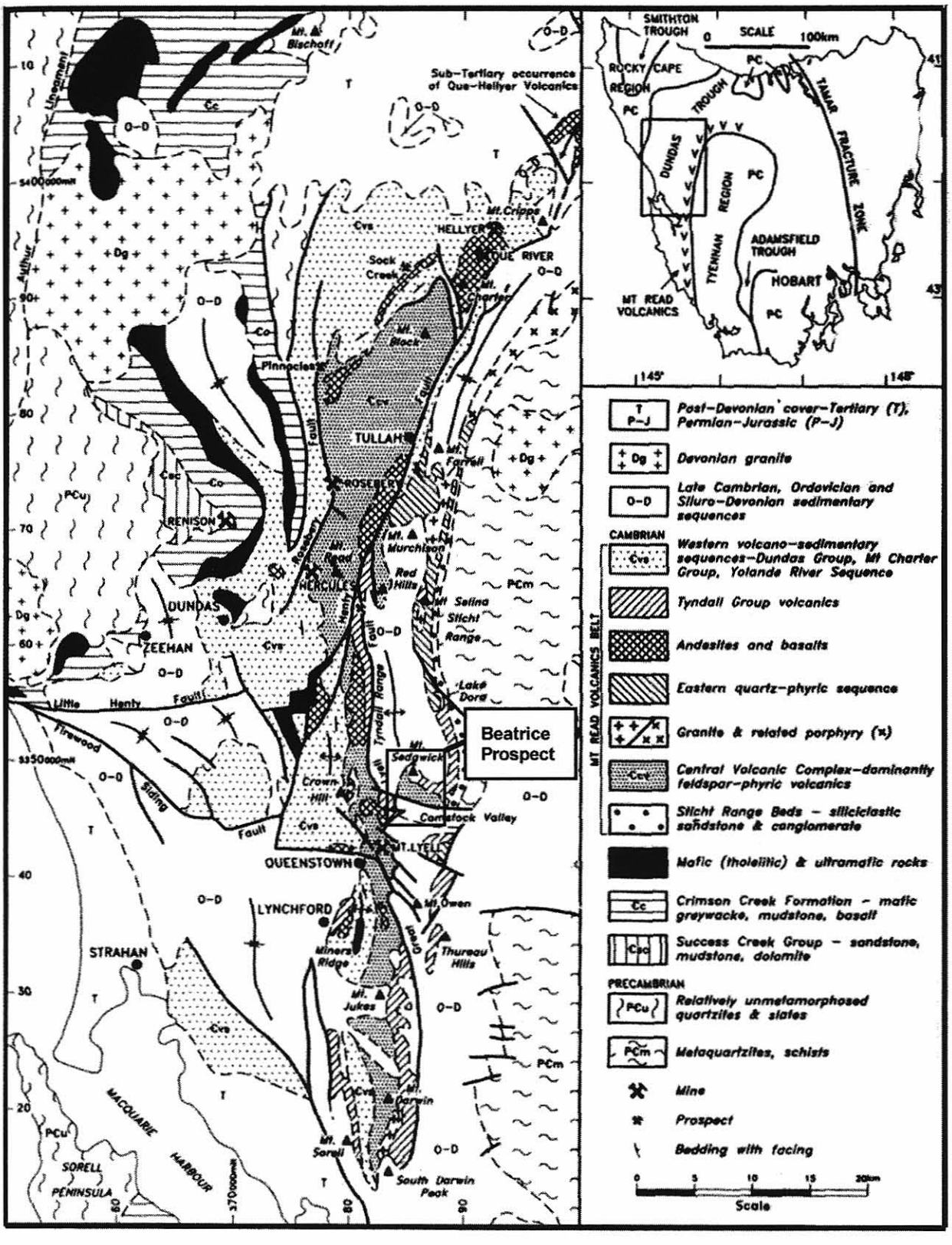

Figure 2.2 Geology of the Dundas Trough and Mount Read Volcanics.
Also shown is the location of the Beatrice Prospect (modified from Corbett 1992).

5 cm

The stratigraphy and correlation between units of the MRV belt is complicated by the NNE trending Henty Fault system which bisects the belt between Mt Read and Mt Charter. The southern portion of the Henty Fault branches into two arcuate splay faults (North and South Henty Faults) that enclose the Henty Fault Wedge, containing sedimentary, volcanic and intrusive rocks including tholeittic basalts, gabbros and ultramafics and calc-alkaline andesites (Corbett 1992). The Great Lyell Fault appears to be another major splay off the Henty Fault system that continues south for some 40km and is offset by a number of west-northwest trending faults near Queenstown.

The Mt Read Volcanics were deposited within a period of 10my or less, during the middle to late Cambrian (Corbett 1992) and (Perkins and Walshe 1993). The environment of deposition for the bulk of lavas and volcaniclastics of the MRV has been interpreted as submarine and largely below wave base (McPhie and Allen 1992). However, *in situ* welded ignimbrites and fossiliferous limestone within the Tyndall Group suggests that at least part of this group was deposited in proximity to subaerial environments (White and McPhie 1996).

Corbett (1992) summarised the Mt Read Belt in terms of seven lithological associations, of which only some can be clearly defined stratigraphically (Figure 2.3). Pemberton and Corbett (1992) acknowledge that the western volcano-sedimentary sequences, Central Volcanic Complex and Eastern Quartz-Phyric Sequence are facies variation of time equivalent units.

2.2 Stratigraphy

2.2.1 The Sticht Range Beds

Lying above a normal unconformity with the Precambrian basement the Sticht Range Beds consist of several hundred metres of a westerly dipping and facing, upward fining sequence of pebble-cobble conglomerate, sandstone and interbedded micaceous siltstone (Corbett 1992). The Sticht Range Formation occupies the eastern margin of the Dundas Trough from Lake Beatrice to north of the Sticht Range (Baillie 1989). Clast content indicates derivation from the Precambrian rocks to the east (Baillie 1989). The presence of minor interbedded volcaniclastic units represents minor input from contemporaneous felsic volcanism (McNeill and Corbett 1992).

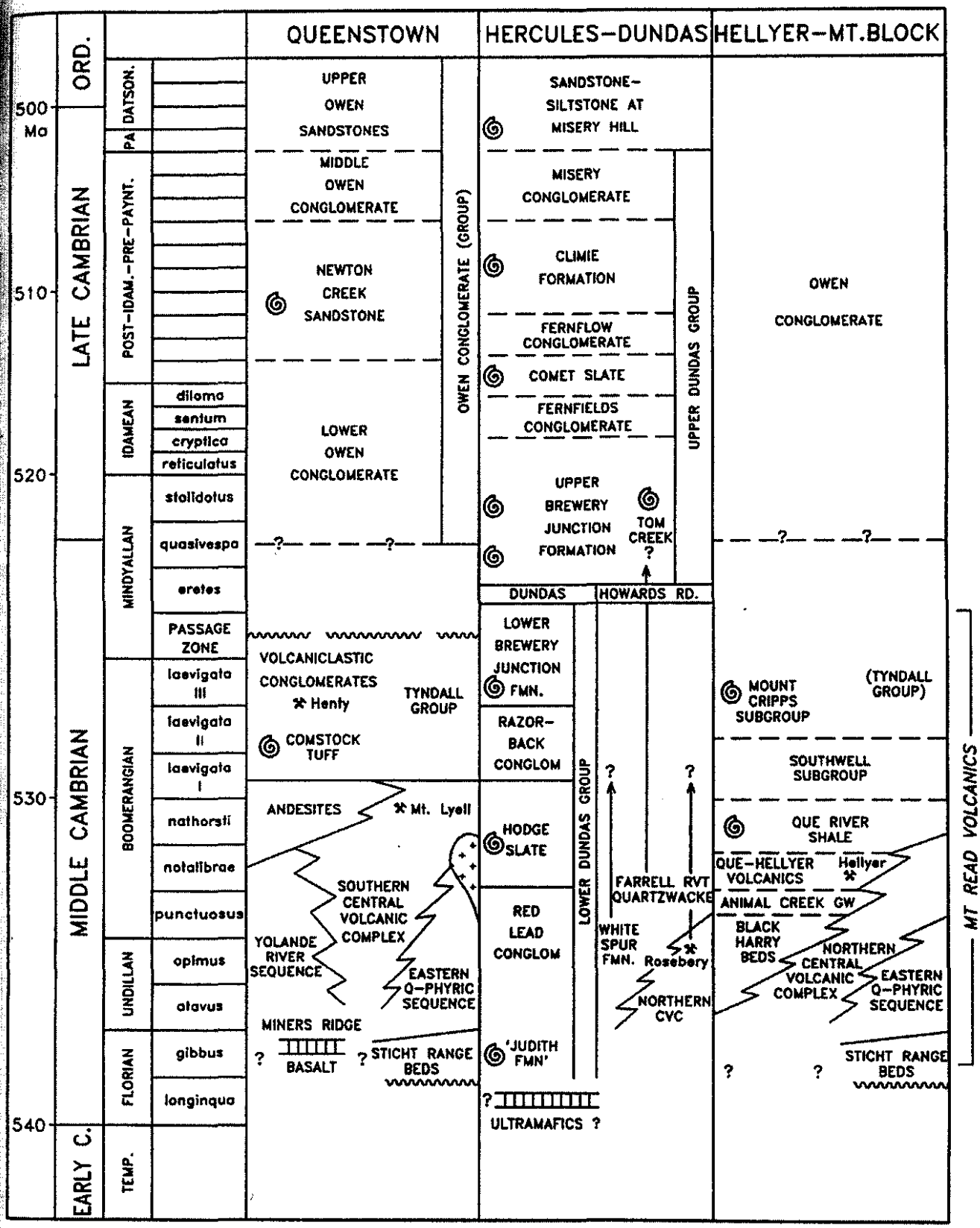

Figure 2.3 Comparative stratigraphic columns for the Queenstown, Hercules-Dundas and Hellyer-Mt Block areas of the Mount Read Volcanics (Corbett 1992).

2.2.2 Central Volcanic Complex

The Central Volcanic Complex (CVC) is a poorly understood assemblage of predominantly feldspar - phyric lavas, pumiceous volcaniclastics and massive dome like lava bodies, extending from Mount Darwin to three kilometres south west of Que River and is bisected by the Henty Fault (Corbett 1992). Although lithologically and compositionally similar, distinct differences exist between the parts that are northwest and south east of the Henty Fault.

The Volcanics of the southern CVC interdigitate with, and are considered coeval to, the eastern quartz - phyric sequence (EQPS). The CVC south of the Henty Fault is mainly rhyodacitic (Crawford et al. 1992), characterised by potash - rich (6 - 9% K_2O) albite rich lavas and is intruded by the Darwin Granite.

Feldspar phyric dacitic - rhyolitic lavas and pumiceous volcaniclastics also dominate the northern CVC, however, the feldspar phyric lavas tend to be rich in plagioclase (Crawford et al. 1992) with only sparse occurrences of potash rich rocks (Corbett 1992). Coeval granites are not known to exist in the northern CVC. Volcanological studies have led to the interpretation that most, if not all of the CVC was deposited within a submarine setting (Corbett 1992, Allen and Cas 1990).

2.2.3 The Eastern Quartz - Phyric sequence

The eastern quartz - phyric sequence (EQPS) consists primarily of rhyolitic, dacitic and minor andesitic quartz feldspar phyric lavas and volcaniclastics, which directly overlies the Sticht Range Beds between Lake Dora and Mount Farrell. The sequence appears to have an interfingering relationship with the feldspar phyric rocks of the CVC (Corbett 1992) and an uncertain relationship with the Tyndall Group. The depositional environment has been interpreted as subaqueous due to the presence of bedded sandstone, siltstone and shard rich mudstone within the sequence and its location between the underlying Sticht Range Beds and the Farrell Slates of which both are probably marine (Corbett 1992).

Numerous quartz feldspar (± biotite) porphyry bodies intrude the Eastern Sequence and the Precambrian basement rocks (Crawford et al. 1992). The Murchison Granite intrudes this sequence within the Murchison Gorge - Mount Murchison area and smaller apophyses of

this granite extend southward to the Mt Selina area (Corbett 1992 and Pemberton and Corbett 1992).

2.2.4 Western Volcano - Sedimentary Sequences

The Western Volcano - Sedimentary Sequences consist of extensive, marine volcano - sedimentary sequences which interfinger with volcanics of the main belt between Mt Darwin and Mt Block. The sequence consists of interbedded tuffaceous, usually quartz feldspar phyric mass-flow units, turbiditic sandstones, shard rich tuffaceous mudstones, miceous siltstones and graphitic black shales. Volcanic derived material is common, however rocks of mixed volcanic-Precambrian metamorphic provenance also exist. Andesitic and minor felsic lavas, and large intrusive porphyry bodies, exist within the sequence, (Pemberton and Corbett 1992).

In the Queenstown area these rocks are known as the Yolande River Sequence. The majority of the sequence dips and faces west but folding has produced eastward dips and facing in the easternmost part. The oldest part of the sequence, exposed in the anticlinal core at Miners Ridge, comprises a siliciclastic sandstone unit underlain by the tholeiitic Miners Ridge basalt (Corbett 1992). The Yolande River Sequence also contains the andesitic-basaltic units of the Lynch Creek basalts and a series of large quartz-feldspar ± biotite porphyries that are intrusive and partly extrusive (Pemberton and Corbett 1992).

2.2.5 Tyndall Group

The Tyndall Group is a middle Cambrian, dominantly submarine, volcano – sedimentary succession representing the uppermost lithostratigraphic unit of the Mt Read Volcanic Belt (White and McPhie 1996). The Tyndall Group is host to the relatively small, high grade Henty gold deposit (±506 000t at 26.9g/t gold). It consists predominantly of felsic to intermediate volcaniclastic breccias, conglomerates, sandstones and mudstones. It also contains subordinate ignimbrite, coherent lavas and/or intrusions and non-volcanic sedimentary rocks including hematitic limestones. The Tyndall Group has variable basal contact relationships with older Mt Read Volcanic rocks. At Mt Darwin and South Darwin Peak the basal beds of the Tyndall Group contain angular to rounded granite and felsic lava clasts indicative of an unconformable contact with the underlying Darwin Granite and CVC. The Tyndall Group, however, conformably overlies the CVC in the Comstock Valley (Corbett, 1992). The Tyndall Group is conformably overlain in places by the

Cambro – Ordovician Owen Conglomerate. The Tyndall Group is thought to reflect the final erosive phase of the Mt Read Volcanics pile, with mixing of basaltic-andesitic debris with felsic-quartz rich material in a shallow water to subaerial environment prior to the deposition of the Owen Conglomerate (Pemberton and Corbett, 1992).

A revision of the stratigraphic nomenclature of the Tyndall Group by White and McPhie (1996) led to the elimination of genetic connotations and the division into two formations; the Comstock Formation (which is further subdivided into the Lynchford and Mount Julia Members) and the overlying Zig Zag Hill Formation (Figure 2.4).

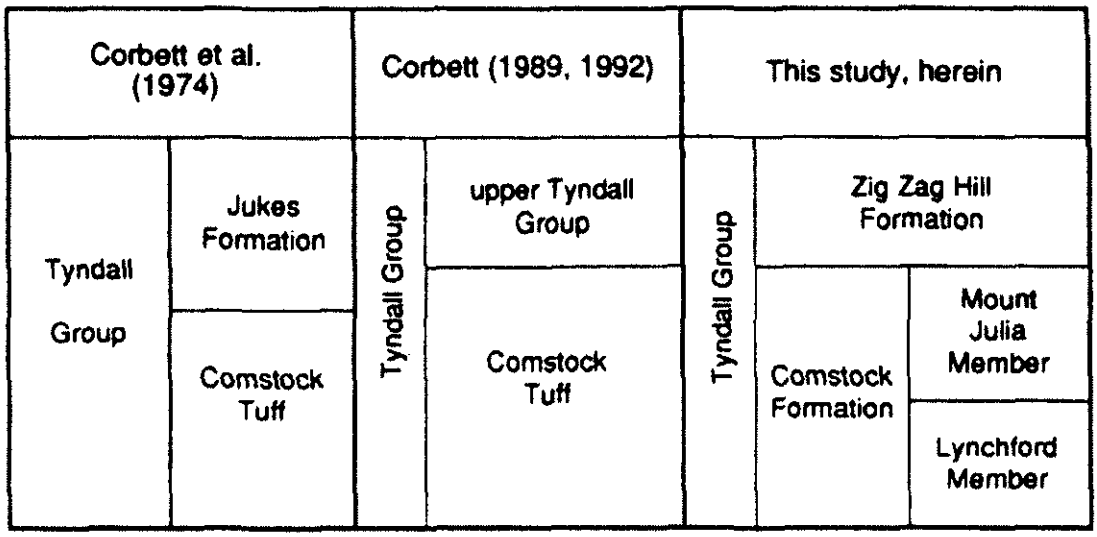

Figure 2.4 Previous and revised stratigraphic schemes used for the Tyndall Group (White and McPhie 1996).

The subdivision of the Comstock Formation into upper and lower members is based on compositional and lithological differences.

The lower, Lynchford Member is approximately 60-200m thick and comprises four main facies:

- Quartz-poor (andesitic to dacitic) crystal ± lithic volcaniclastic sandstone
- Carbonate units dominated by recrystallised calcite ± hematite
- Laminated mudstone and sandstone
- Volcaniclastic lithic breccia

The 150 to 730m thick Mount Julia Member is relatively quartz rich (rhyolitic to dacitic) and comprises four main facies:

- Crystal-rich volcaniclastic sandstone
- Normally graded volcaniclastic breccia-sandstone
- Welded ignimbrite
- Coherent rhyolite

In contrast to the Comstock Formation, which is dominated by syn-eruptive volcaniclastic facies the Zig Zag Hill Formation is comprised of epiclastic deposits derived by reworking of subaerial to shallow marine volcaniclastics. These polymictic deposits are dominated by well-rounded clasts of quartz feldspar phyric volcanic clasts, with subordinate Precambrain quartzite, granite, and sedimentary intraclasts and are believed to have formed from high energy, high-density turbidity currents and/or debris flows (White and McPhie 1996)

2.3 Mineralisation

The Mt Read Volcanic Belt is the principal VHMS mining district in Australia. It contains six major Cambrian base and precious metal orebodies; the Rosebery, Hellyer, Que River, Hercules, Mt Lyell and Henty deposits. The Hellyer and Que River deposits occur within an andesite-basalt succession hosted within the Western Volcano Sedimentary Sequence. The Rosebery and Hercules orebodies are hosted within a pyroclastic-rich felsic sequence in the basal western part of the CVC (Corbett and Solomon 1989). Recent Studies by McPhie and Allen (1992) however, suggest a correlation of the hanging wall quartz-phyric unit at Rosebery with the basal Southwell Subgroup at Que River. Therefore suggesting that the ore position at Rosebery is just below the Que River Shale and perhaps of similar age to the Que River and Hellyer deposits.

The genesis of mineralisation at Mt Lyell is still in debate. Generally Cu-Au mineralisation occurs as disseminated or stringer-type associated with a very large zone of sericite-chlorite altered, felsic Central Volcanic Complex rocks. The small massive sulfide deposits mined at Comstock near Mt Lyell are located within a 500m thick unit of andesitic lavas and breccias lying above felsic Central Volcanic Complex rocks and below the Tyndall Group (Corbett 1992). This stratigraphic relationship has also been interpreted to be of possible correlation with the Southwell Subgroup. Pemberton and Corbett (1992) suggest a

relationship of pre-Tyndall Group - Southwell Subgroup position with the "andesite connection" as a favourable position for VHMS mineralisation.

The relatively small gold rich deposits at Henty are hosted in volcaniclastic, possibly hyaloclastic dacites associated with interbedded carbonates and marly sandstone located at the base of the Tyndall Group or top of the CVC (Callaghan 1998).

Mineralisation within the Mount Read Volcanics was not restricted to VHMS style mineralisation within the Cambrian. A second type of mineralisation formed during the Cambrian consists of sulfide veins, stockworks and disseminations associated with the emplacement of granitoids at depth. The Cambrian granites of the Mt Read Volcanics form a narrow (2-4km), semi-continuous body extending for over 60km along the eastern margin of the belt from Mt Darwin to the Murchison Gorge (Large et al. 1996). Paralleling this linear body, are a series of uneconomic copper pyrite prospects that extend from Mt Darwin to Mt Lyell, incorporating the Lake Dora and Selina Prospects.

Deformation during the Devonian together with coeval fluid circulation has resulted in both mineralogical and textural modification of the Cambrian massive sulfide deposits at Mt Lyell and Rosebery (Corbett and Solomon 1989). The emplacement of post-kinematic ilmenite series granitoids during the Devonian, resulted in the formation of major tin deposits (eg Renison) and associated fluid circulation has resulted in the formation of Pb-Zn ores such as Mt Farrell, Murchison lodes and the Zeehan Mineral Field.

Chapter 3
Geology of the Beatrice Prospect

3.1 Introduction

This chapter documents the local geology of the Beatrice Prospect (Figure 3.1) with particular emphasis on the Mount Sedgewick Anomalous Zone (MSAZ) and its host rocks. Descriptions of lithologies are based on observations from both drillcore logging and mapping within the Itat Creek Valley. Lithological and contact descriptions occurring outside the field of study are based primarily on the work of previous authors, including Boyd (1994) and through personal communication with Pasminco Exploration staff. Figure 3.2 is a simplified stratigraphic column showing the major units throughout the prospect. Figure 3.3 is an interpretative geological map of the Itat Creek area, based on outcrop mapping, structural measurements and the projection of drillhole data.

At the Beatrice Prospect, the host rocks to the MSAZ consist of north trending felsic volcaniclastics, black shale and minor felsic, flow banded lava which are tentatively correlated to the Lynchford Member. This sequence conformably overlies dacitic lava of the Central Volcanic Complex (CVC) and is host to the elevated base metal values known as the Mount Sedgewick Anomalous Zone. This sequence is exposed in a 2x5km window parallel to Itat Creek. A large flow banded quartz feldspar porphyry body dominates the area to the west of Itat Creek. Lying unconformably above the Quartz Feldspar Porphyry and volcano-sedimentary package are volcaniclastics assigned to the Zig Zag Hill Formation of the Tyndall Group and siliciclastic rocks of the Owen Conglomerate. Another unconformity surface exists at the head of the Itat Creek Valley where Permian tillite overlies Owen Conglomerate representing the widely developed late Palaeozoic erosive surface and the deposition of glacial sediments. Jurassic dolerite forms the summit of Mount Sedgewick and produces the large columnar jointed cliff face at the head of the Itat Creek Valley.

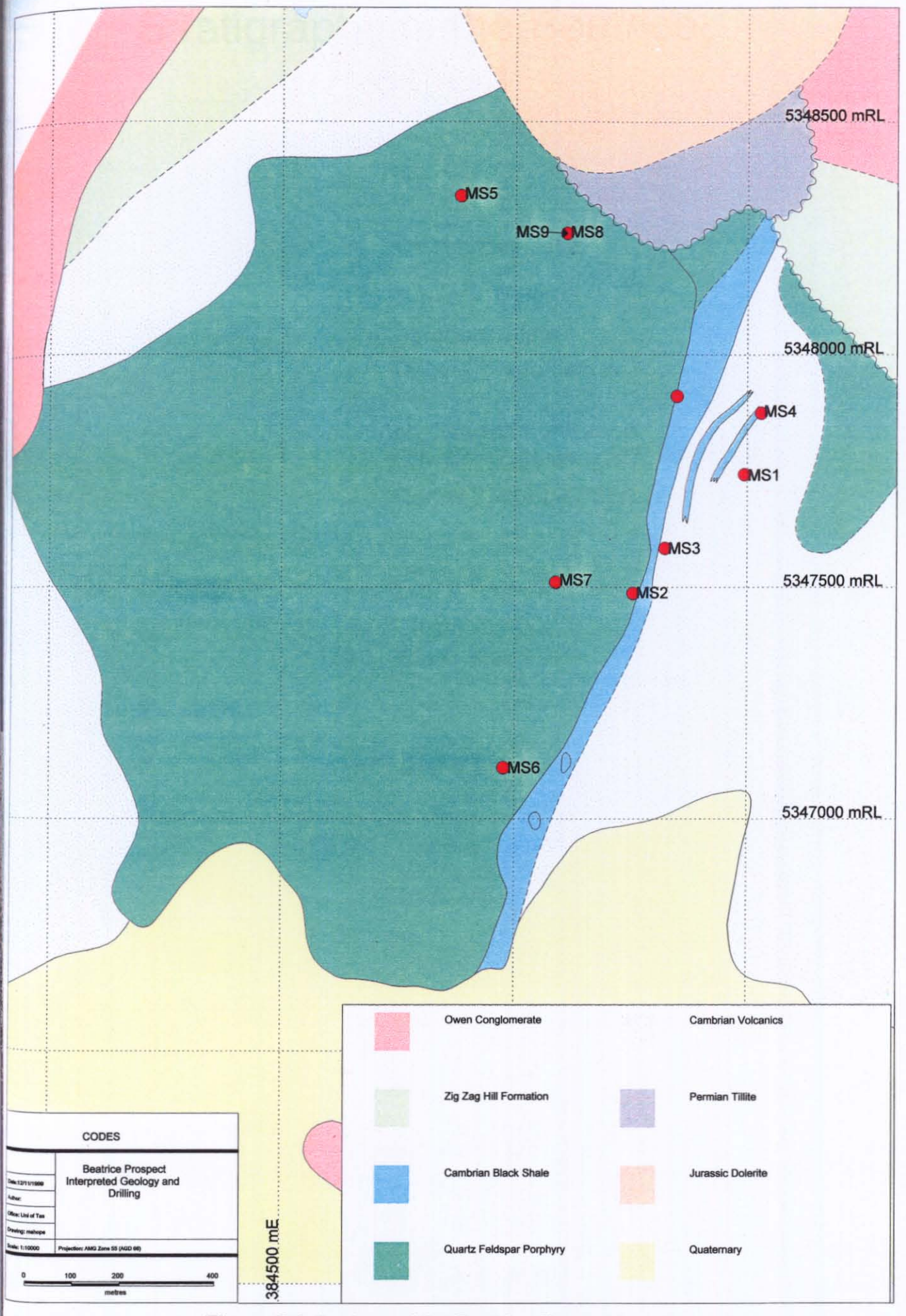

Figure 3.1 Geology of the Beatrice Prospect.

5 cm

Stratigraphy of the Beatrice Prospect

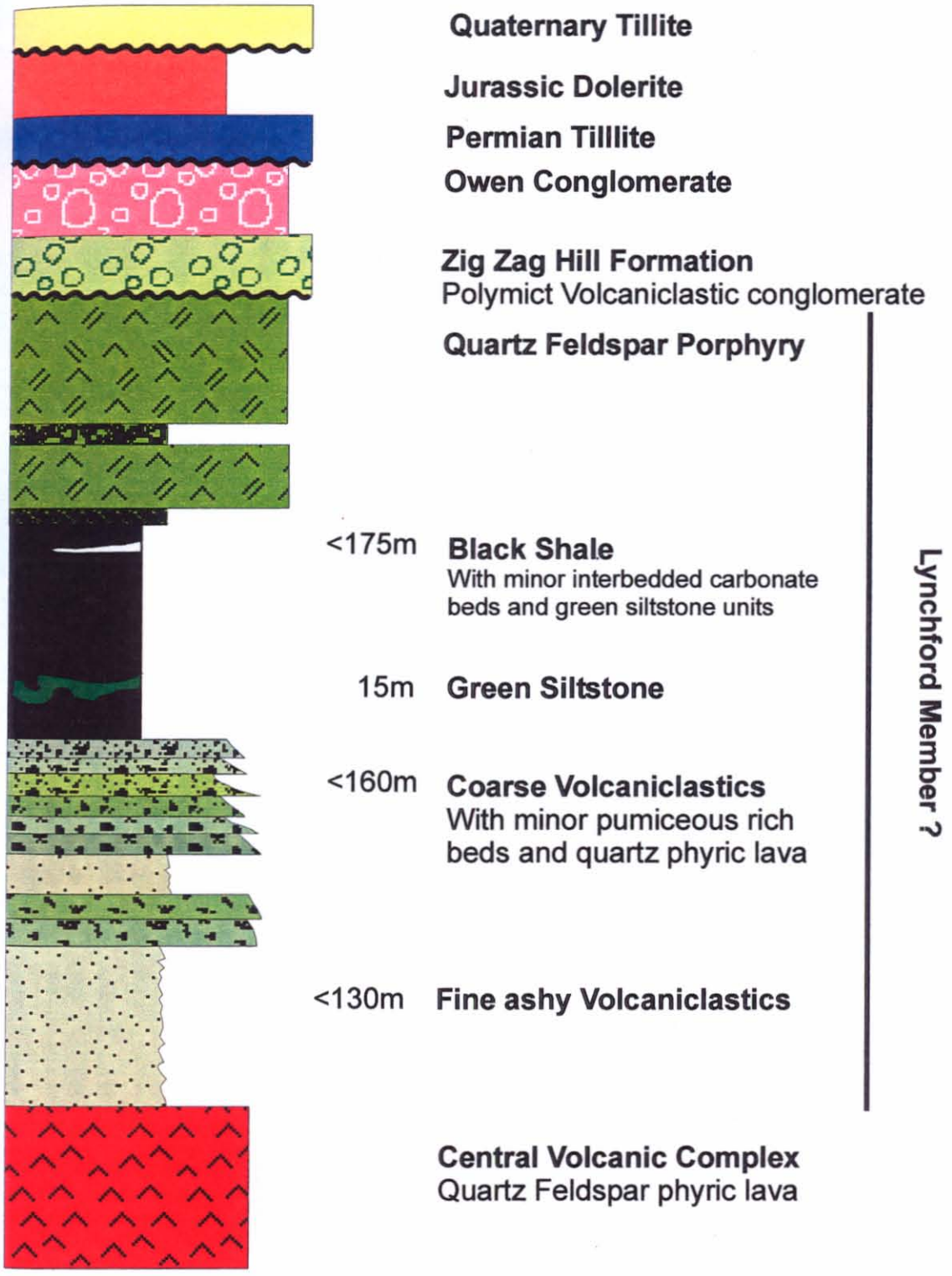

Figure 3.2 Simplified stratigraphic column of the Beatrice Prospect.

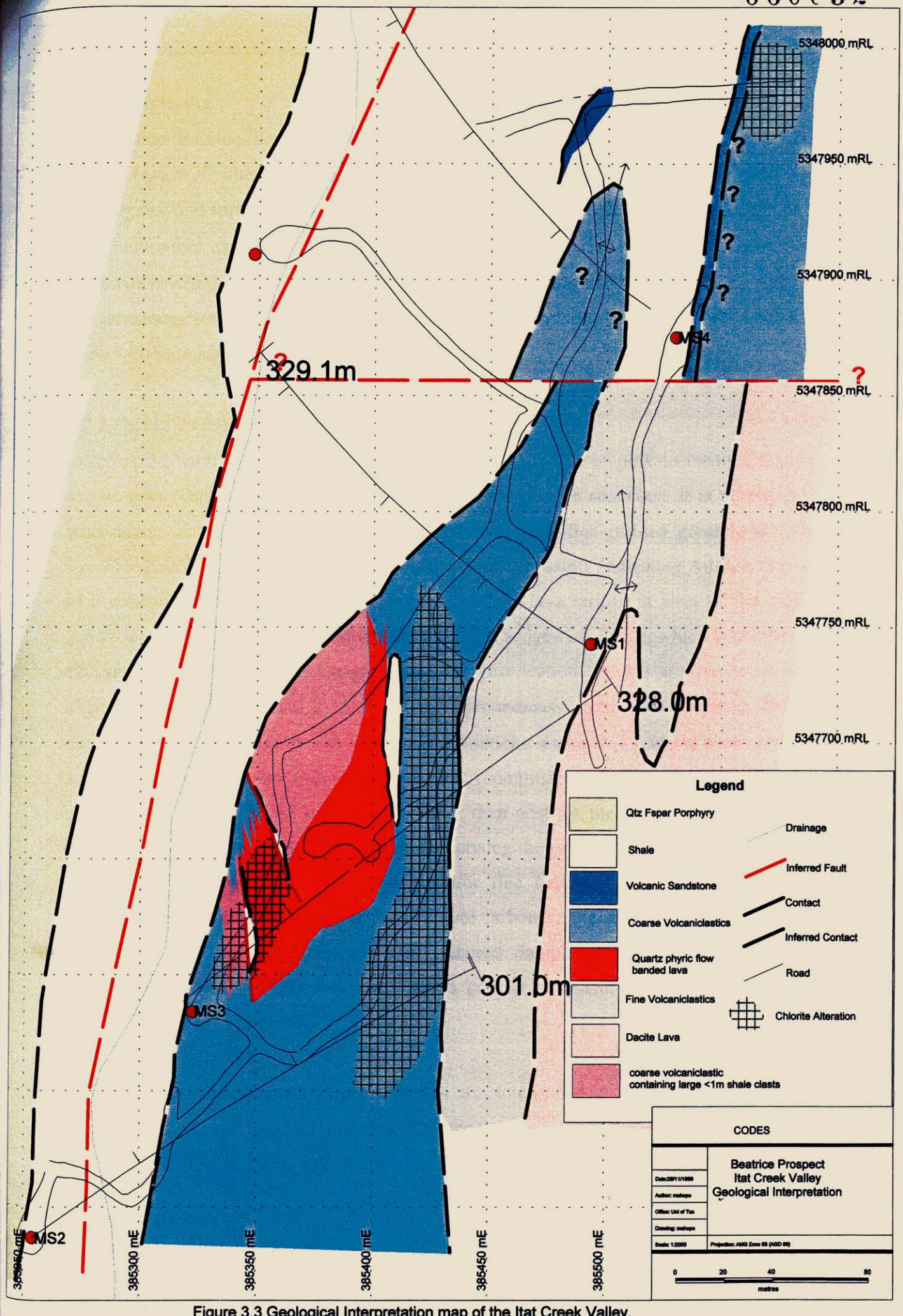

Figure 3.3 Geological Interpretation map of the Itat Creek Valley.
Based on outcrop mapping and the projection of drill hole data

5 cm

3.2 Stratigraphy

This section describes the various lithologies observed in drill core and the Itat Creek Valley. Figure 3.2 illustrates the stratigraphic order of these rock units, defined by drill hole logging and surface mapping. The volcanic units within the Beatrice Prospect can be divided into four main facies; 1) Quartz ± feldspar phyric coherent lava, 2) Pumiceous lithic volcaniclastics, 3) Quartz Feldspar Porphyry and 4) Polymict volcaniclastic conglomerate. Sedimentary units are relatively simple, consisting predominantly of black shale with minor internal facies variations.

3.2.1 Quartz ±feldspar phyric lava

Outcropping south of MS1 and extending eastward is a unit of pink to cream coloured dacitic lava. This unit represents the base of the prospective sequence. It is porphyritic, with quartz and less abundant feldspar phenocrysts in a fine-grained groundmass. On weathered surfaces a clastic appearance is developed, possibly indicating autobrecciation of a coherent extrusive lava flow. Spherulitic dacitic lava crops out west of the major quartz feldspar porphyry body and to the east of the Sedgewick Ridge, which is composed of Tyndall Group and Owen Conglomerate. Devitrivication textures are evident in less altered samples (MH40 and 2-15), where the groundmass consists of abundant 250μm quartzo feldspathic spherulites in a fine grained sericite + quartz + feldspar matrix (Plate 3.1). Quartz phenocrysts (~2mm in diameter, comprising ~5modal percent) are the dominant phenocryst phase comprising greater than 65% of the phenocryst population, with euhedral feldspar crystals up to 2mm comprising the rest. The quartz phenocrysts are embayed, containing inclusions of glass and/or fine recrystallised quartz (Plate 3.2). Feldspar crystals are pseudomorphed by a sericite-carbonate alteration assemblage in more altered samples. The groundmass is variably altered. Sample 2.9, being the most altered, consists of a strongly sericitised groundmass containing silicic spherulites and minor domainal K-feldspar alteration.

A lens of fine grained quartz phyric lava was also intersected in MS2, hosted within the coarse volcaniclastic unit, this unit may be observed forming the large knoll north-east of the MS3 collar. Flow banding distinguishes this unit from the coarse volcaniclastic unit.

3.2.2 Volcaniclastic Units

The volcaniclastic package exposed within the central portion of the Itat Creek Valley and intersected in drill core has a maximum thickness of ~280 metres. Although showing some degree of interbedding, the upper portion of the volcaniclastic package is dominated by coarse volcaniclastic breccias reaching a maximum thickness of approximately 160m. It is underlain by a fine ashy volcaniclastic unit with a thickness of approximately 130m. The basal contact of the fine ashy volcaniclastic unit and the underlying CVC quartz feldspar phyric lava appears conformable.

Within the Itat Creek Valley the coarse volcaniclastic unit forms prominent rounded outcrops with rough, cream to grey weathering surfaces. Large angular to rounded lithic fragments are evident on these surfaces (Plate 3.3). Lithic clasts are composed of well-bedded, fine-grained ashy volcanic rocks, aphyric and quartz phyric lava clasts, carbonate clasts and relict pumice. Large shale clasts (<1metre) exist, hosted within coarse to fine volcaniclastics north of the MS3 collar. This distinctive unit was not observed in drill core, possibly due to being mistaken for interbeds of shale. Diffuse grading in the coarse volcaniclastic units are evident in the access track east of MS3 where large mass flow units display finely bedded tops indicating facing to the west.

Outcrops of fine volcaniclastics are typically subdued. In the road cutting south of MS4 the fine volcaniclastic unit displays well-developed bedding (10 to 25cm thick) dipping to the east. In thin section the fine volcaniclastic unit appears as an extremely fine-grained quartz sericite composite containing fine (generally less than 1-2mm) angular quartz grains.

3.2.3 Black Shale

Black shale units are exposed within the Itat Creek Valley and intersected in all drill holes, shale float was also observed within the Quartz Feldspar Porphyry to the west of MS5. The black shale and underlying volcaniclastic sequence is host to the MSAZ and represents the most prospective unit.

In drill core the shale is typically featureless, silty, with a well developed bedding-plane fissility. In the lower part, fine carbonate beds are common. These light coloured beds are up to 8cm thick, coarser grained and contain fine pyrite. Large, slightly silicic, carbonate poor, dark spherical concretions, up to 8cm occur in holes MS8 and MS9, with

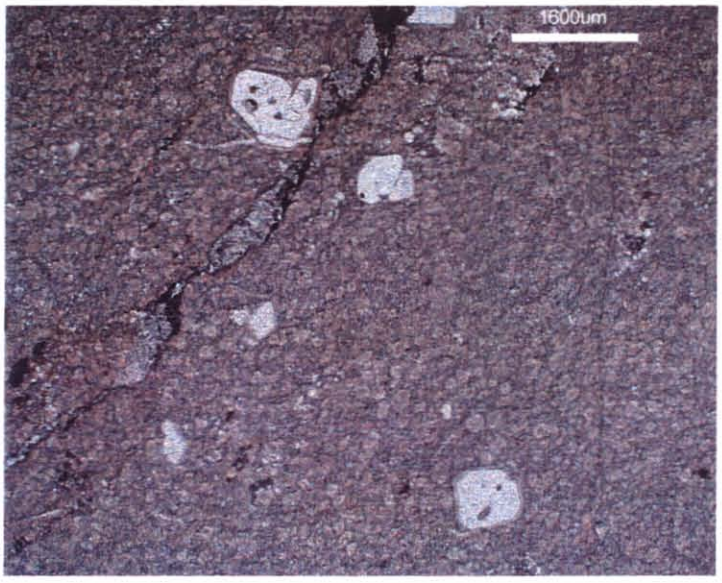

Plate 3.1: Relatively unaltered quartz phyric, coherent lava, containing embayed and inclusion rich quartz phenocrysts in a fine grained spherulitic groundmass.

Photo taken in plane polarised light

Sample MH2-15

Plate 3.2: Embayed quartz crystal within strongly sericite altered, quartz feldspar phyric dacite. The microcrystalline quartz crystals within the embayments are interpreted to reflect the devitrification and crystallisation of original glassy material.

Photo in cross polarised light

Sample MH2-9

Plate 3.3: Well rounded, bedded, ashy volcanic clast within the coarse volcaniclastic unit.

carbonate/pyrite rich beds displaced around them (Plate 3.4). Irregular shaped carbonate nodules and layers were intersected in MS8 that consist predominantly of high Mg calcite and typically displace the sediment around them. Due to the discontinuity of the layers and lack of styolitic features, these carbonate beds are interpreted to reflect shallow subsurface nucleation and growth of carbonate, not the dissolution of original carbonate beds. These carbonate structures preferentially host pyrrhotite, arsenopyrite, pyrite and sphalerite occurring as haloes and as internal veinlets.

Also present within the 6-metre carbonate rich interval in MS8 are laminated pyritic beds, which microscopically display replacement textures and "millet seed" or lozenge-like crystal habit (Southgate et al. 1989: Plate 3.5). These features are interpreted to reflect the pseudomorphing of original evaporite minerals, similar to that outlined by Tompkins et al. (1994). Rare interbeds (<30cm) consisting of fine volcanic derived material and abundant siliceous spicules interpreted to reflect fossil sponge spines have also been recorded in MS8 (Plate 3.6).

Fine microfaulting is common in shales intersected in all holes. Within MS5, 1metre thick breccia zones composed of shale clasts with little or no matrix are interpreted to reflect zones of intense syn-sedimentary microfaulting.

In thin section, the shale consists predominantly of an extremely fine matrix of clay – sericite with rare (5%) rounded fine grained quartz grains (up to 0.5mm in diameter), distributed in diffuse beds. Also present are rare rounded to irregular shaped fragments of fine grained quartz aggregates interpreted to be cross sections through the siliceous sponge spicules.

The basal contact of the shale is conformable with the underlying coarse volcaniclastic unit. A thin (2-5m thick) well sorted green sandstone unit containing interbeds of shale and volcanic derived sandstone is found at this contact. This sandstone unit contains thin rafts of shale (<5cm in length) incorporated into the sandstone beds, in addition to well developed flame structures, showing silt injected in to sand. This unit dips steeply to the west just north of the MS4 collar.

Plate 3.4: Photograph of large spherical nodule, with pyritic carbonate beds displaced around it. Nodule contains small amounts of pyrite, indicating it formed during early diagenesis but preceeds the major pyrite formation.

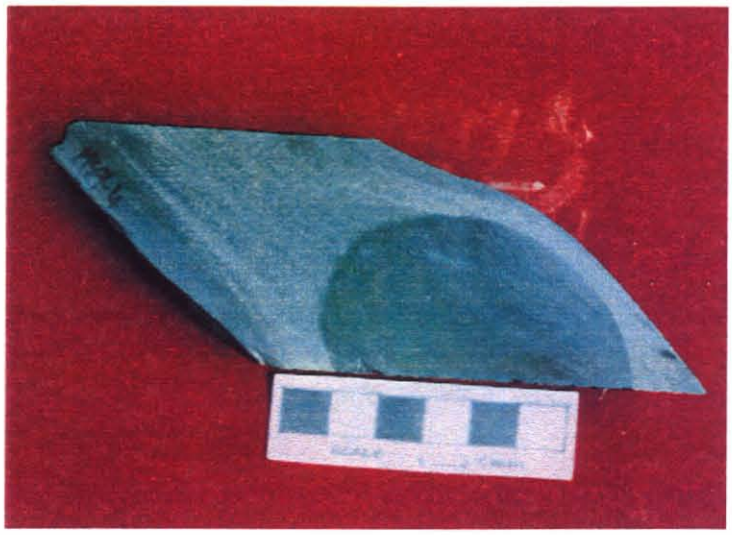

Sample MH8-4

Plate 3.5: Shale unit containing lozenge shaped or "millet seed" crystals of pyrite after gypsum. Also present are bedding subparallel quartz sulfide veins and quartz pressure fringes on gypsum pseudomorphs

Photo taken in plane polarised light

Sample MH8-11

Plate 3.6: Photomicrograph taken within a 30cm mass flow unit in shale, containing ragged pyritic, sericite altered clasts and elongate siliceous fossils interpreted to be sponge spicules.

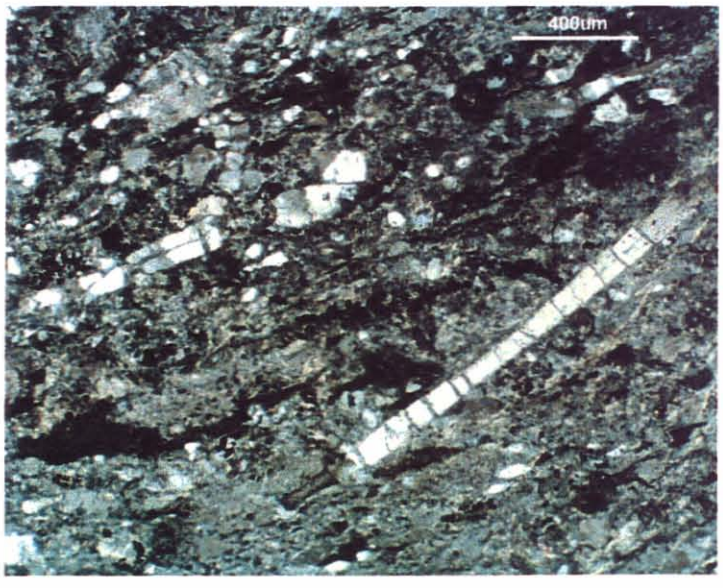

Photo taken in cross polarised light

Sample MH8-14

3.2.4 Green Siltstone

A distinctive green siltstone unit between 4 and 12 metres thick was intersected in MS8, MS1, and MS3, typically near the base of the black shale unit. The unit contains many features similar to the black shale, including dark nodules surrounded by pyrite, discordant quartz carbonate veins and ubiquitous pyrite. In thin section, it appears that its distinctive colouration is due to the presence of fine-grained chlorite in the matrix. Its contact relationship with the shale is unclear, with complex conformable intermixing of the two units.

3.2.5 Quartz Feldspar Porphyry

Quartz feldspar phyric units dominate the central-western portion of the Beatrice Prospect, forming large ridge tops west of Itat Creek and to the north of the prospect. The quartz feldspar phyric unit (hereafter termed Quartz Feldspar Porphyry) typically weathers to a white/cream colour, whereas fresh samples are typically green to pink in colour.

In the Beatrice sequence (Figure 3.2) the Quartz Feldspar Porphyry overlies the shale units exposed in the Itat Creek area and is unconformably overlain by the coarse volcaniclastic conglomerate of the Zig Zag Hill Formation. The Quartz Feldspar Porphyry typically contains ~20% clear, embayed quartz phenocrysts ~5-10mm in diameter. Feldspar population consists of euhedral plagioclase (10%) and potassium feldspar (10%) up to 6mm in size, in a fine silicic groundmass. Alteration is minor, with sericite ± carbonate alteration of feldspars and chlorite + magnetite alteration of subordinant hornblende phenocrysts.

Lenses of the porphyry display peperitic margins at both the top and bottom contacts with shale, indicating shallow intrusion into wet subaqueous sediments. Preferential weathering in outcrop and the alignment of phenocrysts observed in drillcore highlight flow banding within the unit. Two types of clastic zones were identified within the Quartz Feldspar Porphyry unit. Within holes MS8, MS6 and MS2 clastic, clast supported breccia zones, up to 8m thick contain partially rounded polymictic material. Quartz Feldspar Porphyry derived material dominates with quartz feldspar phyric clasts, aphyric clasts, and quartz, feldspar crystals comprising the bulk of the coarse material. The clast population also contains shale clasts. The second type of breccia, observed within MS9, consists of a 35 metre sequence of coherent Quartz Feldspar Porphyry intermixed with zones of monomict

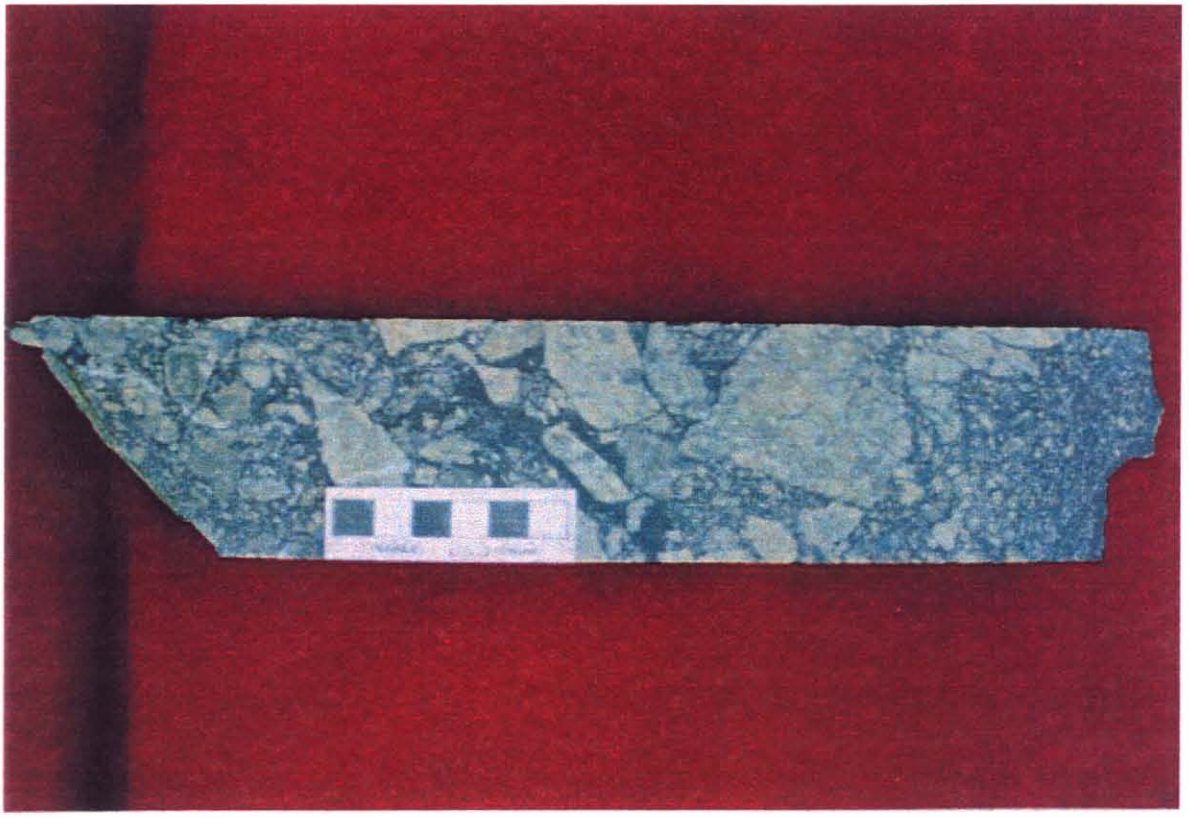

Plate 3-7: Monomict breccia, comprising angular Quartz Feldspar Porphyry clasts in a black shale matrix. Clasts exhibit curviplanar surfaces but do not appear chilled. Breccia also contains areas of well graded material, contained within coherent porphyry.

Sample MH9-3

clasts of Quartz Feldspar Porphyry within a black silty matrix (Plate 3.7). This breccia displays zones of normal grading of angular to subrounded clasts extending from coherent porphyry through a jigsaw fit, clast supported zone through to a matrix-supported top. Clasts commonly display curviplanar surfaces but do not appear to be chilled. Both forms of breccia are enveloped by coherent Quartz Feldspar Porphyry.

3.2.6 Polymict Volcaniclastic Conglomerate

Northeast of Itat Creek, a several hundred metres thick sequence of polymict volcaniclastic conglomerates unconformably overlies both Quartz Feldspar Porphyry and coherent lava units of the CVC.

The matrix supported polymict volcaniclastic conglomerate is composed of large (<15cm), sub to well rounded clasts. The clasts are dominantly quartz-feldspar phyric volcanics and mudstone, with subordinant quartzite, supported in a dark grey to green sandy matrix.

Polymict volcaniclastic conglomerates and sandstones are prominent in the upper Tyndall Group, (White & McPhie, 1996) hence the polymict volcaniclastic conglomerate at Beatrice has been correlated with the Zig Zag Hill Formation of the Tyndall Group (Boyd 1994 and Denwer 1998).

3.4 Discussion

The volcaniclastic and shale units that host elevated base metal mineralisation within the Itat Creek Valley constitute a broadly west facing sequence, interpreted to represent the eastern limb of a syncline located west of the Itat Creek Valley (Figure 3.4). The host sequence is displaced by the north trending Itat Creek Fault. Semi-conformably overlying the host sequence is a series of Quartz Feldspar Porphyry lenses, which have intruded and possibly burrowed into the shale unit forming peperitic margins at both top and bottom contacts. The presence of monomict breccia within the coherent porphyry body suggests the grading and dispersal of fragmented clasts by fluidisation and the envelopment of clastic material by coherent porphyry. However, the presence of polymict breccia suggests that the porphyry was not entirely intrusive and possibly entrained clastic material.

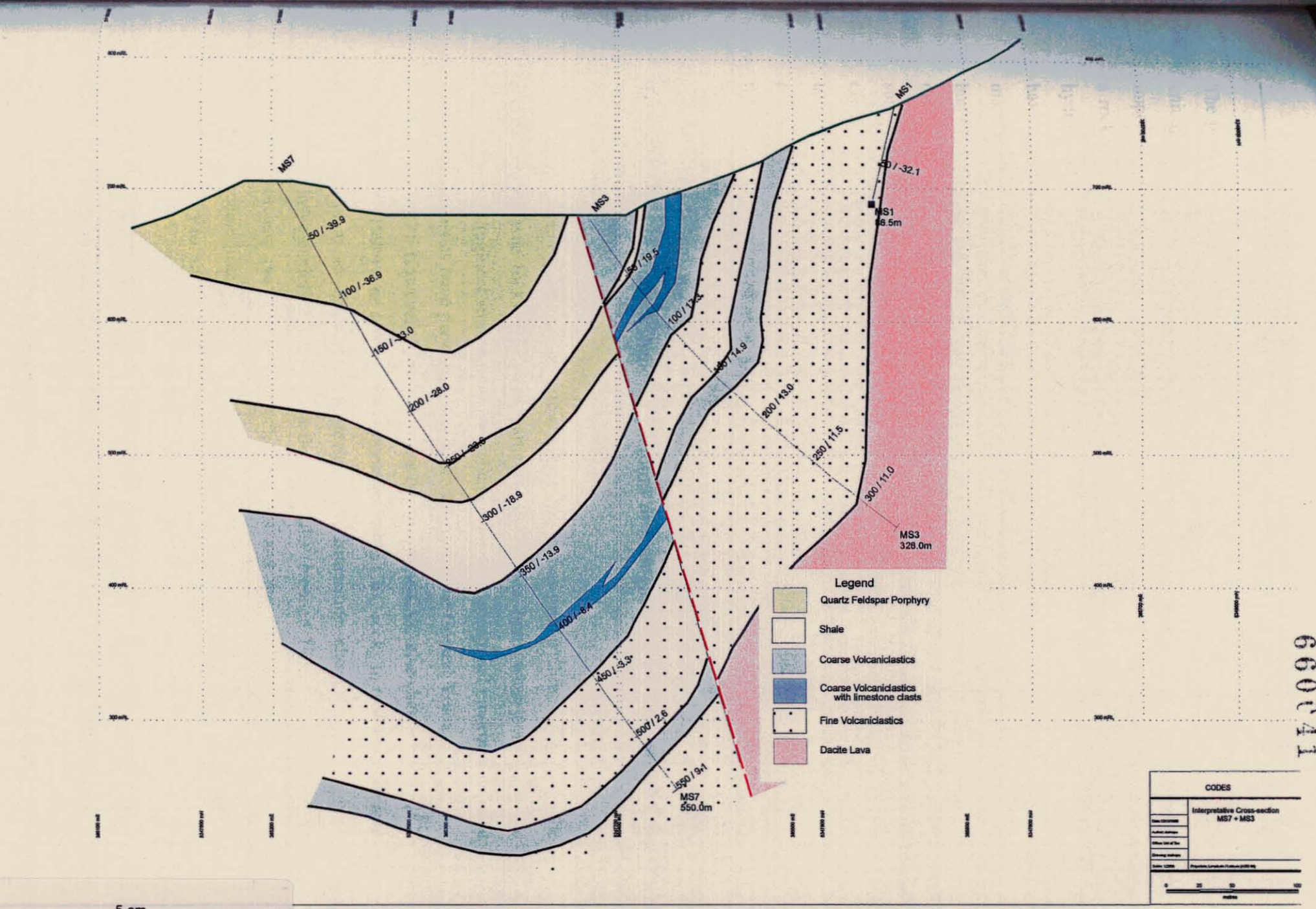

Figure 3.4 Interpretative cross section through the Itat Creek Valley and the MSAZ.

The presence of pyrite after evaporite minerals (gypsum pseudomorphs) within the shale unit appears as a rare finding in rocks of the Mt Read Volcanics, and may be of particular importance in defining a depositional environment. Warren (1996) defines an evaporite as a rock that was originally precipitated from a saturated surface or near-surface brine by hydrologies driven by solar evaporation. The fine (~2mm), precursor gypsum crystals may have formed originally *in situ* on a shallow seafloor experiencing hypersaline conditions or may have formed as "rain from heaven" deposits in deep water environments; less than hundreds of metres depth. (Warren 1996). This "rain from heaven" precipitation of crystals results from the formation at the air-brine interface, when surface water salinities are suitable. Evaporite crystals may grow via solar concentration until they exceed the size capable of being held by surface tension and sink to the basin floor, being deposited as laterally extensive, millimetre scale, laminated beds dominated by fine crystallites. The presence of fine 2-3mm siliceous biogenic material in rare <30cm thick shale hosted mass flow units are interpreted as sponge spicules and hence, indicate a marine environment. The abundant siliceous spicules within the matrix of the evaporitic beds may suggest another scenario, with the evaporite crystals derived from slumped and current reworked deposits sourced from much shallower platforms or from gravitational unstable 'pelagic' salts (Warren 1996).

The presence of fine grained carbonate clasts, interpreted as primary limestone within the coarse volcaniclastic rocks may be of particular importance, both, when correlating the host sequence to regional stratigraphy, and when defining a depostional environment. The coarse volcaniclastics have previously been correlated with the Central Volcanic Complex (Eastoe et al 1987). However, limestone is not typical of the CVC elsewhere, Lees (1987) and Warmeant (1990) note fine-grained carbonate within CVC rocks in the Rosebery area but attribute them to hydrothermal precipitation. Limestone clasts have also been documented in volcaniclastic breccias at the Red Hills (Noonan 1990). Therefore, if the correlation between the coarse volcaniclastic rocks and the CVC is correct, then the presence of coarse limestone clasts within the latter carries implications for the existence of, and proximity to, shallow water depositional environments, at least locally in the CVC.

3.5 Correlation of the Beatrice stratigraphy with the MRV

The polymict volcaniclastic conglomerate, lying above the unconformity to the east of Itat Creek Valley has been correlated with the Tyndall Group (Eastoe et al. 1987). Based on the further subdivision of the Tyndall Group by White and McPhie (1996) this unit has been assigned to the Zig Zag Hill Formation by Boyd (1994) and Denwer (1998).

The felsic volcaniclastics, coherent lava and shale units exposed within the Itat Creek Valley (Section 3.2) have been previously correlated with the Central Volcanic Complex (Eastoe et al. 1987). However, recent opinion suggests that it may occupy the same stratigraphic position as the Lynchford Member of the Tyndall Group (Herrmann 1994). The high quartz content and presence of carbonate clasts within the host sequence is atypical of the CVC elsewhere, perhaps supporting a more suitable correlation with the Lynchford Member. This suggestion however, indicates that an unconformity exists between the basal section of the Tyndall Group and the overlying Zig Zag Hill Formation, due to the presence of the erosive surface on the ridge east of the Itat Creek Valley.

Crawford et al. (1992) subdivided the Mount Read Volcanic Belt into five suites, with most CVC rocks falling into Suites I and II on the basis of immobile element and REE compositions. Figure 3.5 compares the wholerock geochemical data obtained from the Beatrice volcaniclastics and coherent volcanic units with fields defined by Crawford et al. (1992). It is clearly evident that the volcaniclastic rocks are similar to Suite I, with low P_2O_5 values and high silica contents. The disparity between geochemical results and TiO_2/SiO_2 fields and the apparent overlap into the Suite II field defined by Crawford et al. (1992) may be attributable to variable hydrothermal alteration effects. This disparity may also be a function of the variable composition of the volcaniclastic units, with a reduction in SiO_2 concentration, related to the dilution by clasts of variable and non-silicate compositions.

Eastoe et al. (1987) suggested that the stratigraphy and alteration patterns observed within the Beatrice Prospect are similar to that at the Red Hills (and Lake Selina). Reflecting a structurally continuous but largely obscured block of volcanics extending beneath the siliciclastics of the Denison Group, from Mt Farrell to Mount Sedgewick. The association of strongly magnetite + hematite veined Central Volcanic Complex rocks that crop out ~1km east of Itat Creek and the large quartz feldspar porphyry body observed at Beatrice

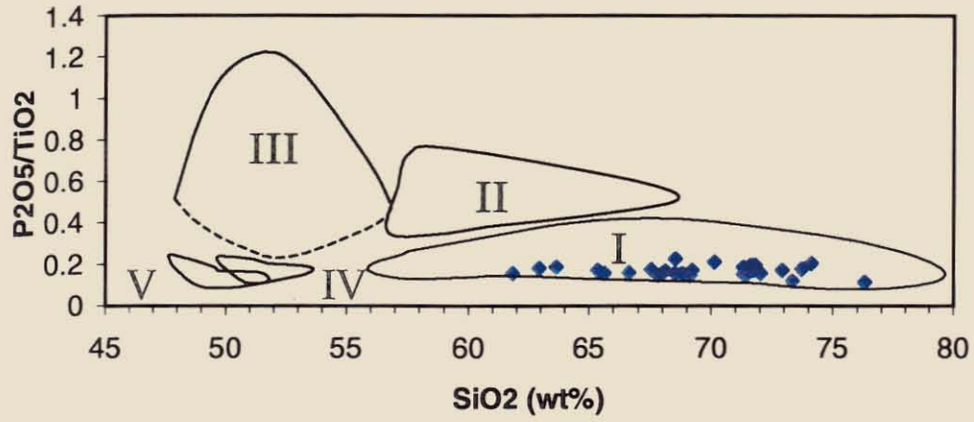

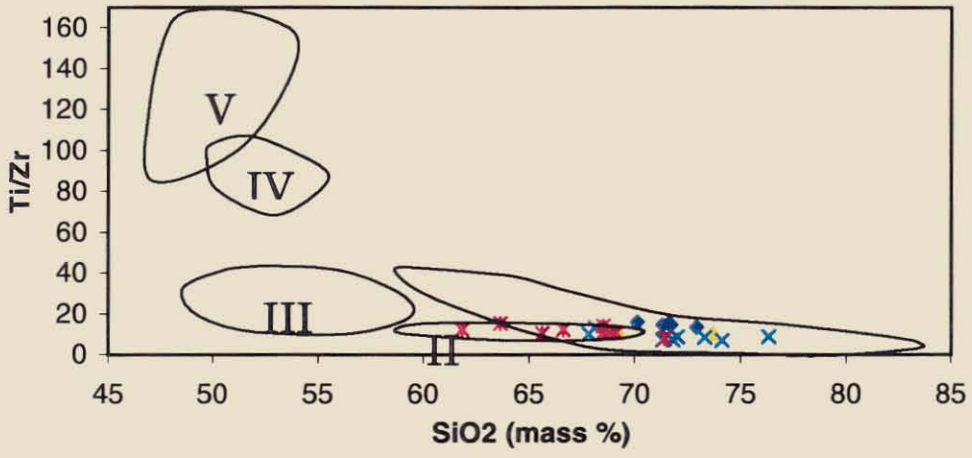

◆ Qtz Fspar Porphyry ▲ chl fspar alt ✕ fine volcaniclastics ✱ coarse volcaniclastics

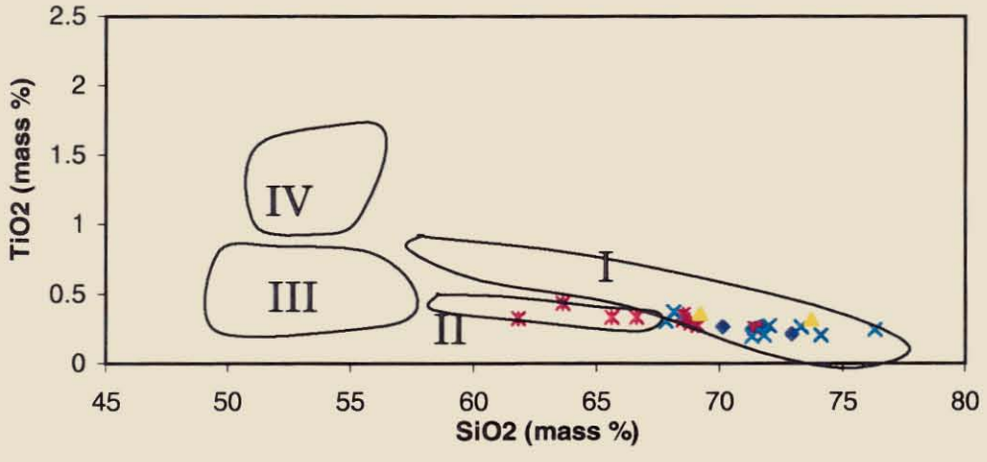

◆ QFP ✱ coarse volcaniclastic ✕ fine volcaniclastic ▲ chl fspar alt

Figure 3.5 P_2O5/TiO_2, Ti/Zr, and TiO_2 versus SiO_2 plots for Beatrice samples with suite fields defined by Crawford et al (1992).

appear very similar to the alteration assemblage associated with the Murchison Granite and the rhyo-dacitic porphyry at Lake Selina described by Hunns (1987). Comparisons between the lithologies observed at the Beatrice Prospect and those noted by Jenkins (1991) and Herrmann (pers. comm. 1999) and Ti/Zr ratios (Noonan 1990) indicate significant similarities between lithologies at Beatrice and Red Hills. The host sequence at Beatrice is dominated by volcaniclastics similar to the polymict breccias that exist at Red Hills, and displays similar Ti/Zr ratios. The volcaniclastics at Beatrice have Ti/Zr ratios; 4-8 appearing similar to the range of 5-7 calculated for volcaniclastics in RH18 and RH19 from the Red Hills. The black shale unit also has similar Ti/Zr ratios; analyses taken from Beatrice samples range from 9 to 13 compared to 10-19 for shale at the Red Hills. The chemostratigraphic similarities between the two areas indicate that the correlation made by Eastoe et al. (1987) may in part be correct, however further immobile element analyses would be needed to further elucidate between these two areas.

Chapter 4
Alteration at the Beatrice Prospect

4.1 Introduction

Alteration assemblages within the Beatrice Prospect are both extensive and variable, and significantly obscure the relationships between rock units. The major alteration minerals are sericite, chlorite, pyrite, K-feldspar, calcite, quartz, manganoan siderite, magnetite, hematite and minor apatite. Observations of outcrop and drill core indicate a variety of assemblages, of which the three most distinct assemblages are: Sericite dominated, chlorite dominated and potassium feldspar + chlorite ± Fe-oxides. The alteration intensity within the prospect is also variable and appears partly lithologically controlled. Figure 4.1 shows the distribution of these alteration assemblages observed on surface within the Itat Creek Valley and Figure 4.2 shows the alteration assemblages being observed at depth based on drill hole logging.

The different volcaniclastic units with the MSAZ appear to have imparted some control on the style and intensity of alteration within the Beatrice Prospect. The fine ashy volcaniclastics have been predominantly sericitised, with localised zones of chloritisation. Sericitisation is also dominant within the coarse volcaniclastic units however selective chlorite alteration of pumice clasts is also evident. Potassium feldspar + chlorite ± carbonate and Fe-oxide alteration is restricted to the volcaniclastics that occur at depth within drill holes MS7, and MS8, and to a lesser extent, the dacitic lava at the base of MS3 and MS2.

4.2 Petrology

This study of alteration applied petrographic, electron microprobe and whole rock geochemical analytical techniques to characterise the different alteration styles and their relationship to mineralisation and litho-stratigraphy.

4.2.1 Sericite

Sericite alteration is ubiquitous within the volcaniclastic units and lavas within the Itat Creek Valley. In outcrop, sericite altered ashy volcaniclastics are typically strongly

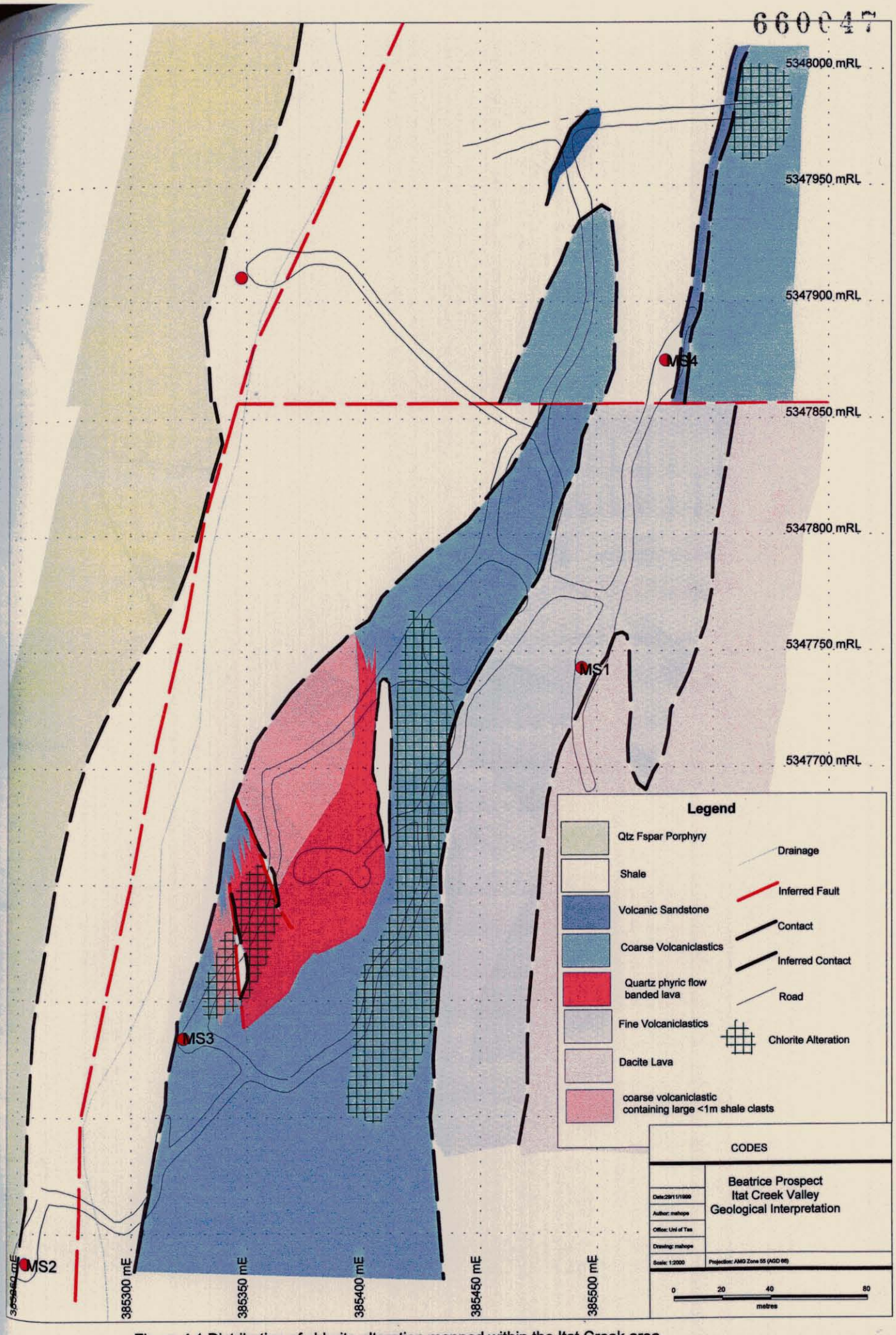

Figure 4.1 Distribution of chlorite alteration mapped within the Itat Creek area.

5 cm

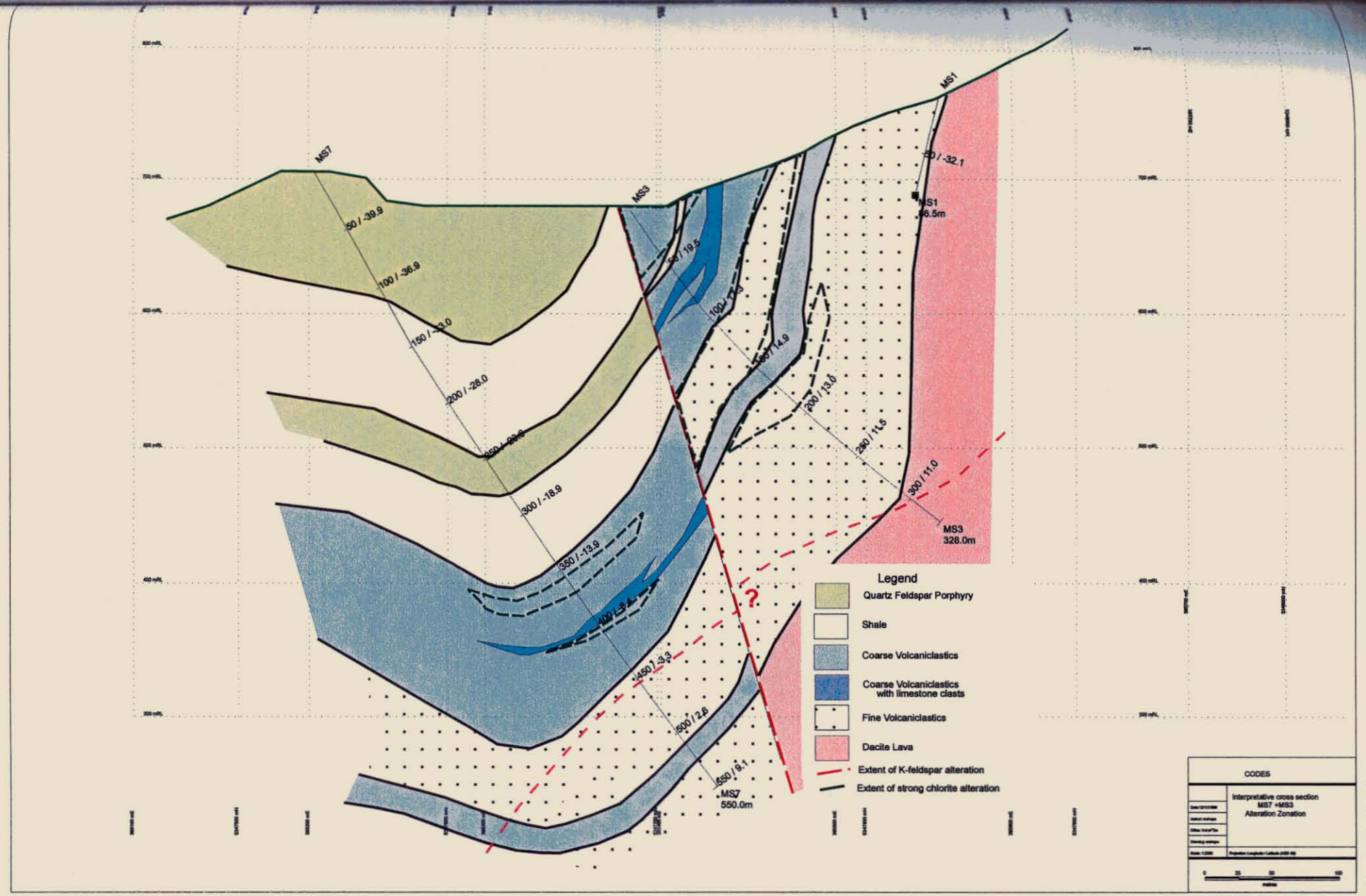

Figure 4.2 Distribution of chlorite and K-feldspar + chlorite + magnetite alteration assemblages with relation to stratigraphy

5 cm

cleaved with weathering rinds consisting of iron oxides and clay. Fresh surfaces are typically pale green-grey in colour.

Within the coarse volcaniclastics, sericitisation of pumice fragments resulted in a well-developed foliation aligned with compaction. In thin section, sericite typically occurs as lenses of fine-grained aggregates, interpreted to reflect the complete sericitisation of original glassy pumice clasts (Plate 4.1). Pervasive sericite + quartz + carbonate alteration imparted a pale brown/green colour to the volcaniclastic groundmass. Sericite alteration of the dacite lava in some thin sections is intense with complete seritisation of the groundmass and the destruction and pseudomorphing of feldspar (Plate 4.2).

Microprobe analysis of sericite indicates that all samples have a homogenous composition, forming a tight cluster with a moderately phengitic composition. No spatial variation in composition was noted for white mica. Figure 4.3 is a ternary diagram showing the composition of white mica based on total cations in tetrahedral and octahedral sites, where M^{2+} includes Ti, Fe, Mg and Cr.

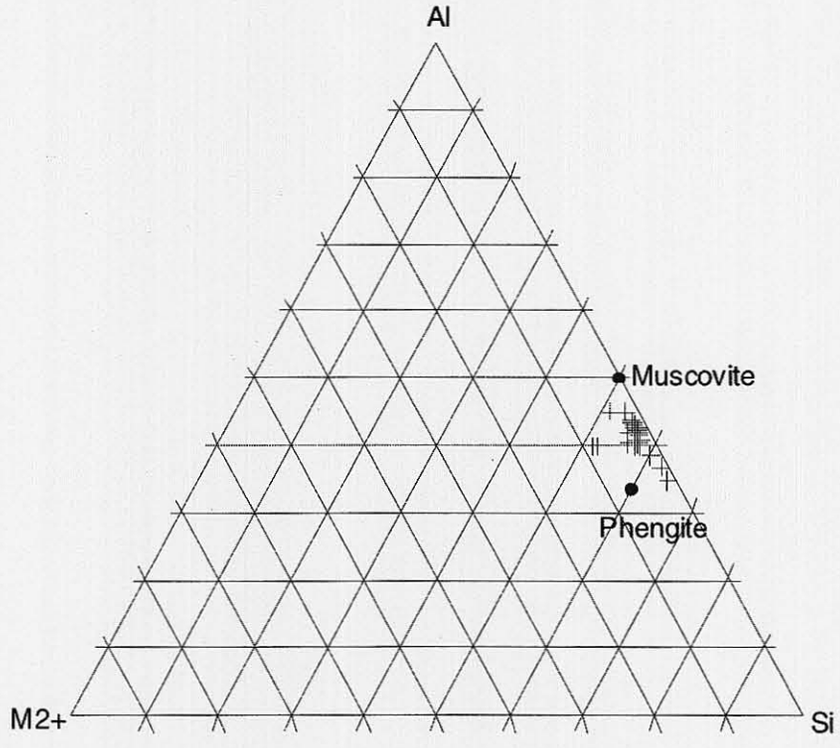

Figure 4.3 Microprobe analyses of white mica from fine and coarse volcaniclastics

4.2.2 Chlorite

Chlorite exists in numerous forms in the volcanic rocks at Beatrice. Selective chloritisation of pumiceous clasts within the coarse volcaniclastics appears to be have been an early alteration feature, similar to the abundant sericitisation and fiamme formation that produced the compaction foliation.

The fine volcaniclastic unit contains spotted fine to medium grained aggregates of chlorite that progressively coalesce to form pervasive zones. This increase in alteration intensity associated with pervasive chlorite typically mirrors the increase in sulfide concentration and appears to represent the major stage of alteration and mineralisation.

Coarse-grained chlorite exists as a late stage, vein controlled, alteration phase best observed in coarsely crystalline quartz + carbonate + chlorite veins in the Quartz Feldspar Porphyry. Chlorite also exists at depth, observed in drill holes MS7 and MS8 as coarse-grained veinlets and disseminated blebs that cross cut and rim pre-existing pervasively K-feldspar altered lava clasts. Chlorite in this assemblage exists in close association with bladed magnetite and calcite. Apatite was also observed within this assemblage as small crystals within the veins. Microprobe analyses indicate anomalous, higher magnesium (Mg number ~34) chlorite exists in a massive sphalerite vein (MH6) that crops out in the Itat Creek Valley. This chlorite microscopically displays anomalous blue interference colours under cross nicols.

4.2.3 Potassium Feldspar

K- feldspar / adularia alteration occurs in numerous samples with varying degrees of intensity. Spherical aggregates of feldspar crystals that exist in some pumice clasts within the coarse volcaniclastic unit are interpreted to reflect diagenetic conversion of zeolite filled amygdales to feldspar.

Of particular interest is the presence of K-feldspar as extremely fine grained aggregates that have pervasively replaced rhyolitic clasts and pumice fragments in the volcaniclastic units, (Plate 4.3). This alteration assemblage is most prevalent at depth, with a K-feldspar + chlorite + magnetite + minor apatite assemblage partially masking the primary volcaniclastic texture at the end of MS7 and MS8. Samples 7-13 and 7-9

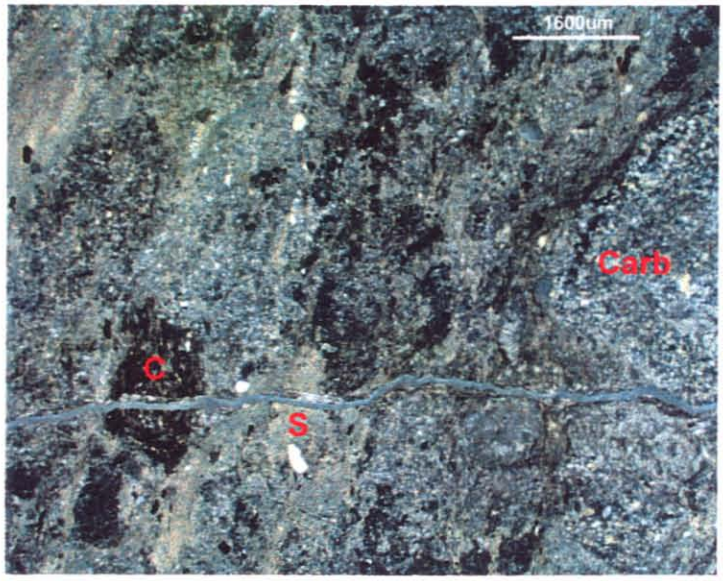

Plate 4.1: Photomicrograph of the coarse volcaniclastic units. Sericite (S) is the dominant alteration phase occurring as ragged fine grained aggregates. Rare chlorite altered clasts (C) are also present, in addition to quartz crystals and carbonate clasts (Carb).

Photo in plane polarised light.

Sample MH1-9

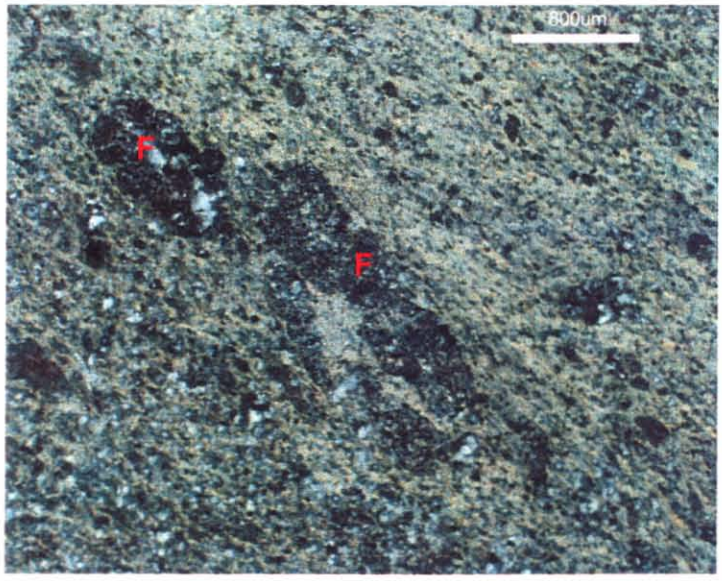

Plate 4.2: Photomicrograph of the strongly sericite altered coherent dacite lava intersected in MS2. The groundmass is intensly sericite altered. Euhedral feldspar phenocrysts (F) have been altered to a fine grained sericite - carbonate assemblage.

Photo in cross polarised light.

Sample MH2-9

Plate 4.3: Coarse volcaniclastic with fine grained potassium feldspar alteration of a quartz phyric lava clast. Groundmass consists of a fine potassium feldspar - chlorite assemblage. Cross cut by late calcite vein.

Scale bar = 6cm

Sample MH7-11

contain K-feldspar altered clasts with rims or cross cutting veins of chlorite indicating that an episode of K-feldspar alteration occurred prior to chloritisation.

This assemblage is similar to alteration associated with Cambrian high K, magnetite series granites mapped by Hunns (1987), Doyle (1990), Jenkins (1991) and Wyman (1998). The presence of potassic alteration overprinted by chlorite alteration containing chlorite + magnetite + carbonate ± pyrite with minor apatite observed at the base of MS7 and MS8 is identical to the typical granite related assemblage occurring sporadically along the eastern boundary of the Mt Read Belt described by Large et al. (1996). A semi continuous subsurface ridge of Cambrian Granite is interpreted to lie at depth to the east of the prospect, as illustrated in Figure 4.4 (Large et al. 1996). The K-feldspar + chlorite + magnetite alteration type observed in DDH MS7 and MS8 is therefore interpreted to be a distal granite related alteration assemblage consistent with the Z_2 alteration zone defined by Large et al. (1996).

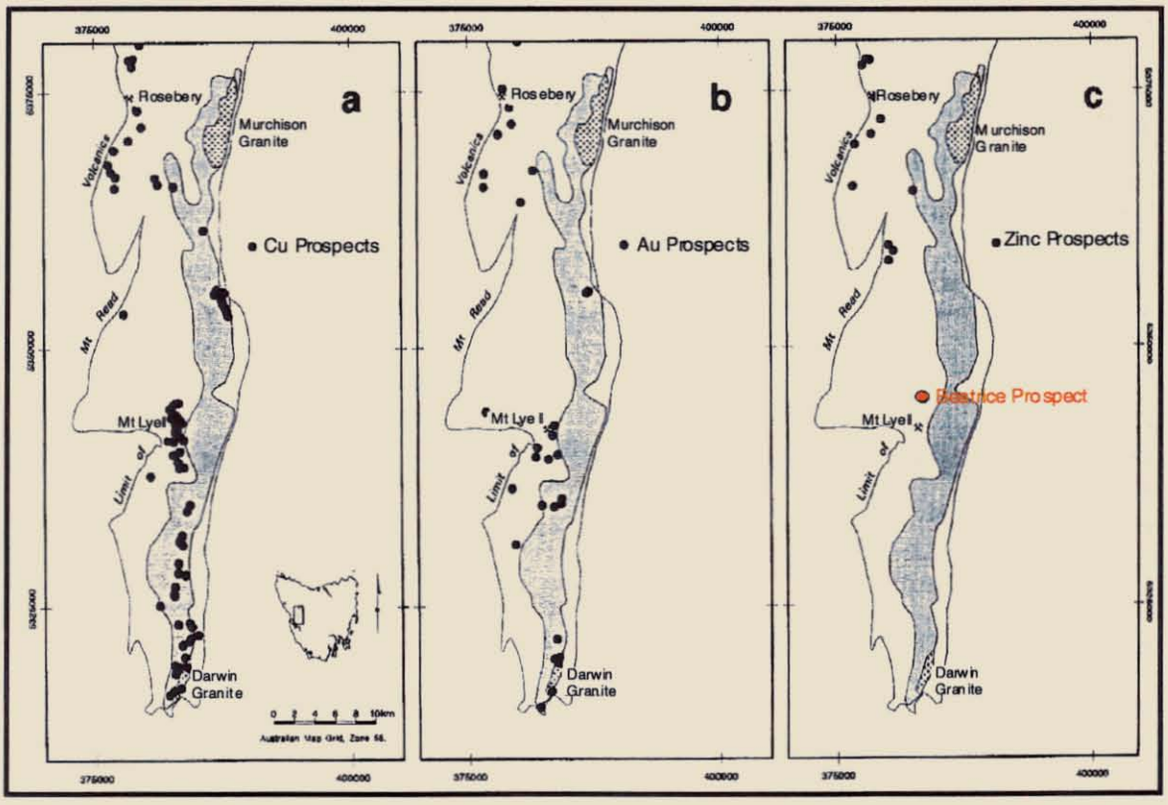

Figure 4.4 Position of copper, gold and zinc deposits and prospects relative to the inferred subsurface granite in the Mt Read Volcanics (shaded area). Field area highlighted in red. (Modified from Large et al. 1996).

5 cm

A second generation of K-feldspar alteration, associated with quartz, carbonate ± chlorite ± sulfide veins was also observed. This fracture-controlled alteration exists in the Quartz Feldspar Porphyry (Plate 4.4) and the volcaniclastic unit, and appears to postdate the major chlorite alteration event.

4.2.4 Carbonate

Carbonate minerals are common in many sections, occurring as beds/concretions, late stage veins, a replacement phase and as a crystalline mosaic intergrown with sulfides. Calcite occurs as euhedral crystals in association with quartz and sulfides in bucky veins (Plate 4.5) and as a recrystallised mosaic aligned with cleavage.

Carbonate compositions show a consistent variation with compositions ranging from calcite, to manganoan siderite and ankerite (Figure 4.5). Plate 4.6 shows the multiple generations of carbonate observed in veins. Manganoan siderite exists as well formed bladed crystals lining vein walls; the interior of veins are composed of coarse calcite (both ferroan and non-ferroan varieties) and remobilised sulfides. Carbonate replacement of feldspar was observed within the dacite lava (sample MH2-15) in association with sericite. Fine ankerite grains were detected within the massive sphalerite vein (MH6) observed at surface within the Itat Creek Valley

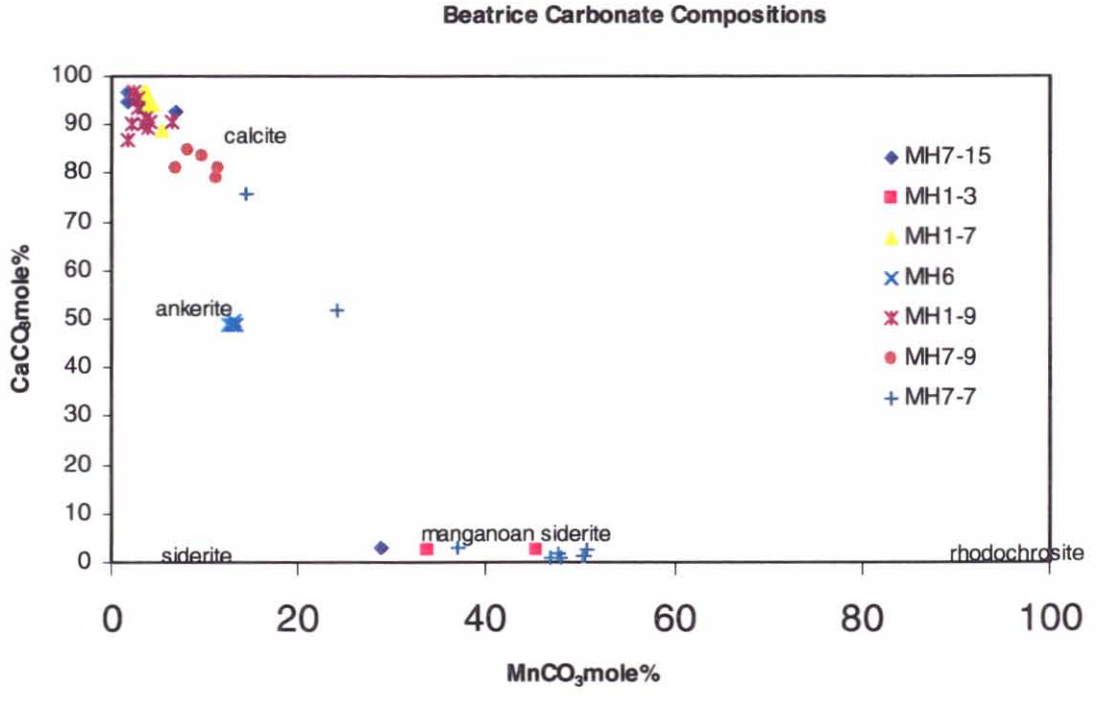

Figure 4.5 Carbonate analyses showing three distinct groups, (manganoan siderite, ankerite and calcite).

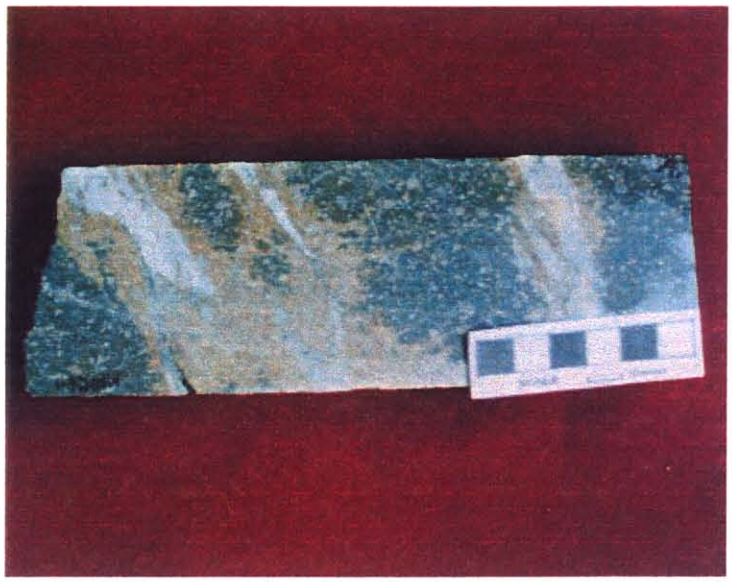

Plate 4.4: Quartz Feldspar Porphyry with late carbonate/quartz vein controlled potassium feldspar alteration.

Scale bar = 6cm

Sample MH6-1

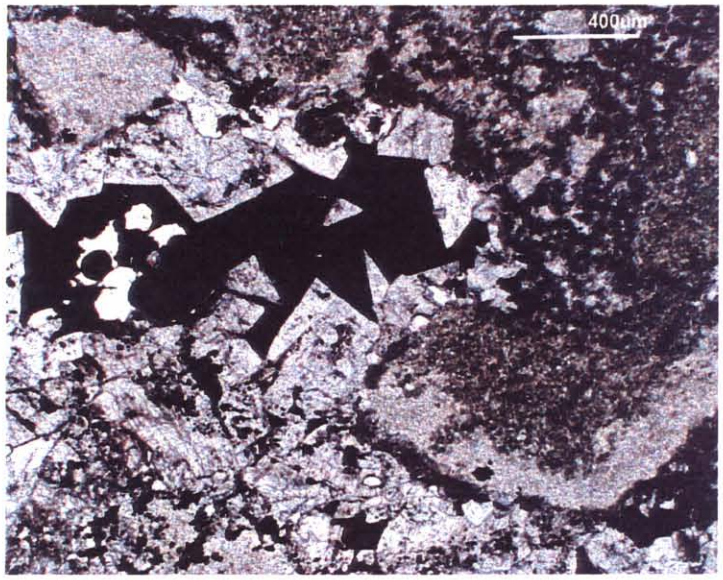

Plate 4.5: Photomicrograph of coarse sparry calcite and galena (opaque phase) in veinlet breccia. Clasts containing chlorite alteration indicate late-stage veining and sulfide mobilisation post dates chloritisation.

Photo in plane polarised light

Sample MH1-1

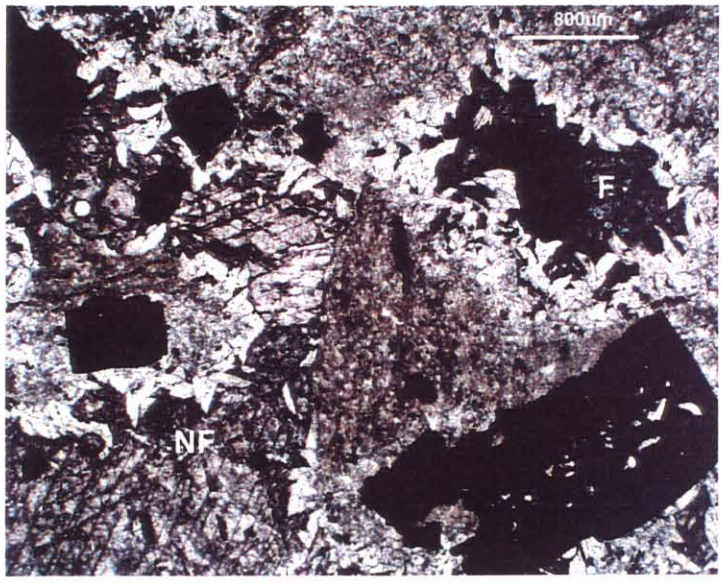

Plate 4.6: Photomicrograph showing veining within shale. Coarse inclusion rich pyrite euhedra are hosted in shale in association with coarse crystalline manganoan siderite with infilling non ferroan (NF) and ferroan (F)calcite.

Photo in plane polarised light

Sample MH8-11

4.3 Whole Rock and Immobile Element Geochemistry

4.3.1 Introduction

A total of 29 samples from Beatrice drill core were submitted for whole rock and trace element analysis. The majority of analytical samples were of unoxidised half or three quarter NQ or BQ drill core sections ~ 0.3m in length. Eleven major elements and six trace elements were analysed by X-ray fluorescence at ANALABS laboratories in Perth, Western Australia. The results of these analyses are presented in Appendix 2, along with two standards (TASGRAN and TASMONZ). Twenty of the samples were volcaniclastics, five were Quartz Feldspar Porphyry and four were black shale. The four shale samples varied in carbonate content and were therefore analysed for both organic C and CO_3 associated with carbonate. Sampling was undertaken to include both unaltered and altered samples in an attempt to constrain both lateral and vertical geochemical variations in both primary compositions and associated with the alteration system.

The aims of the geochemical analysis were to:

1) Characterise the compositions of volcanic rocks in the area.
2) Define protoliths of altered samples and hence assist the understanding of alteration processes.
3) Construct alteration indices to provide possible vectors. (Discussed in section 5.4)
4) Compare the compositions of Beatrice rocks with samples from elsewhere in the MRV.

4.3.2 Results

The major element data for most components (plotted as Harker diagrams in Figures 4.6 and 4.7) shows a broad scatter for volcaniclastic units, with some overlap between the fine and coarse volcaniclastic units.

	SiO_2%	MgO%	Na_2O%	K_2O%	CaO%
Fine V'clastics	68-76	0.48-0.89	0-0.14	1.74-7.8	0.1-0.92
Coarse V'clastics	62-71	0.34-1.59	0-0.16	3.35-7.25	0.05-6.6
Qtz Fspar Porphyry	70-73	0.45-0.75	0.18-3.75	3.15-7.85	0.37-2.95
Shale	58-65	2.75-2.95	0.07-0.21	1.86-3.95	2.3-5.85

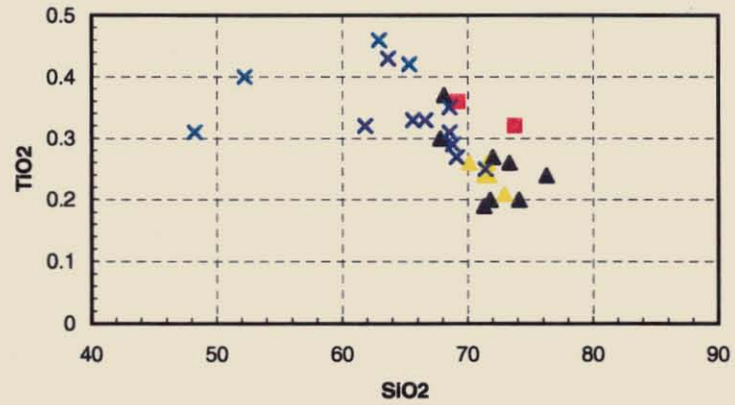

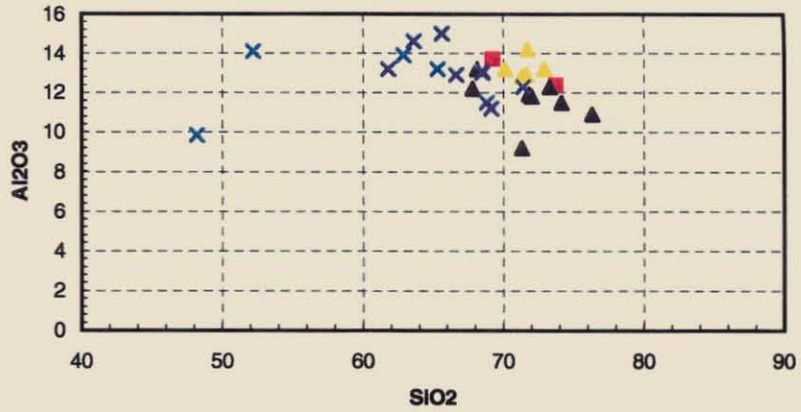

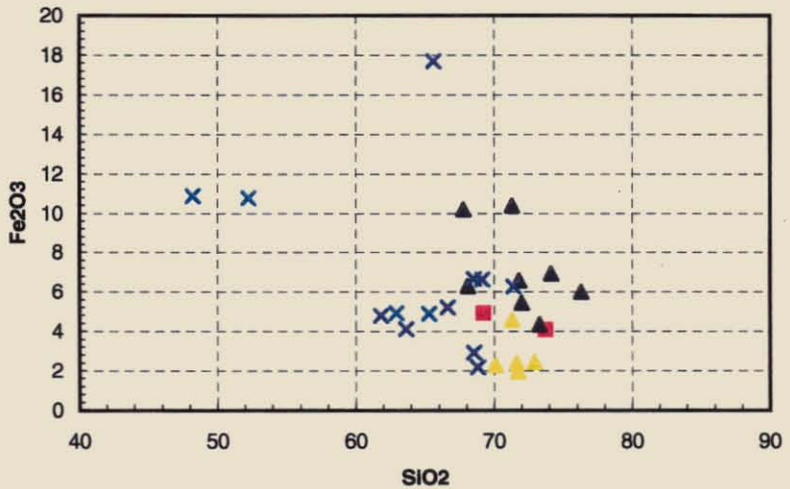

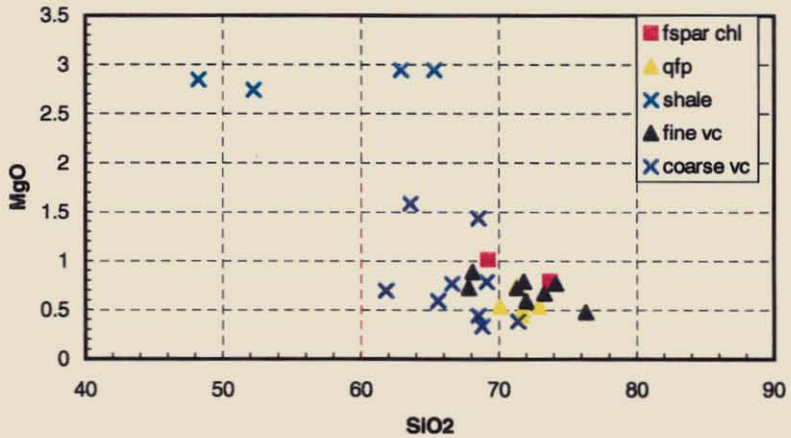

Figure 4.6 Harker diagrams of Fe2O3, MgO, CaO and Na2O for the Beatrice rock samples. All axes in wt%

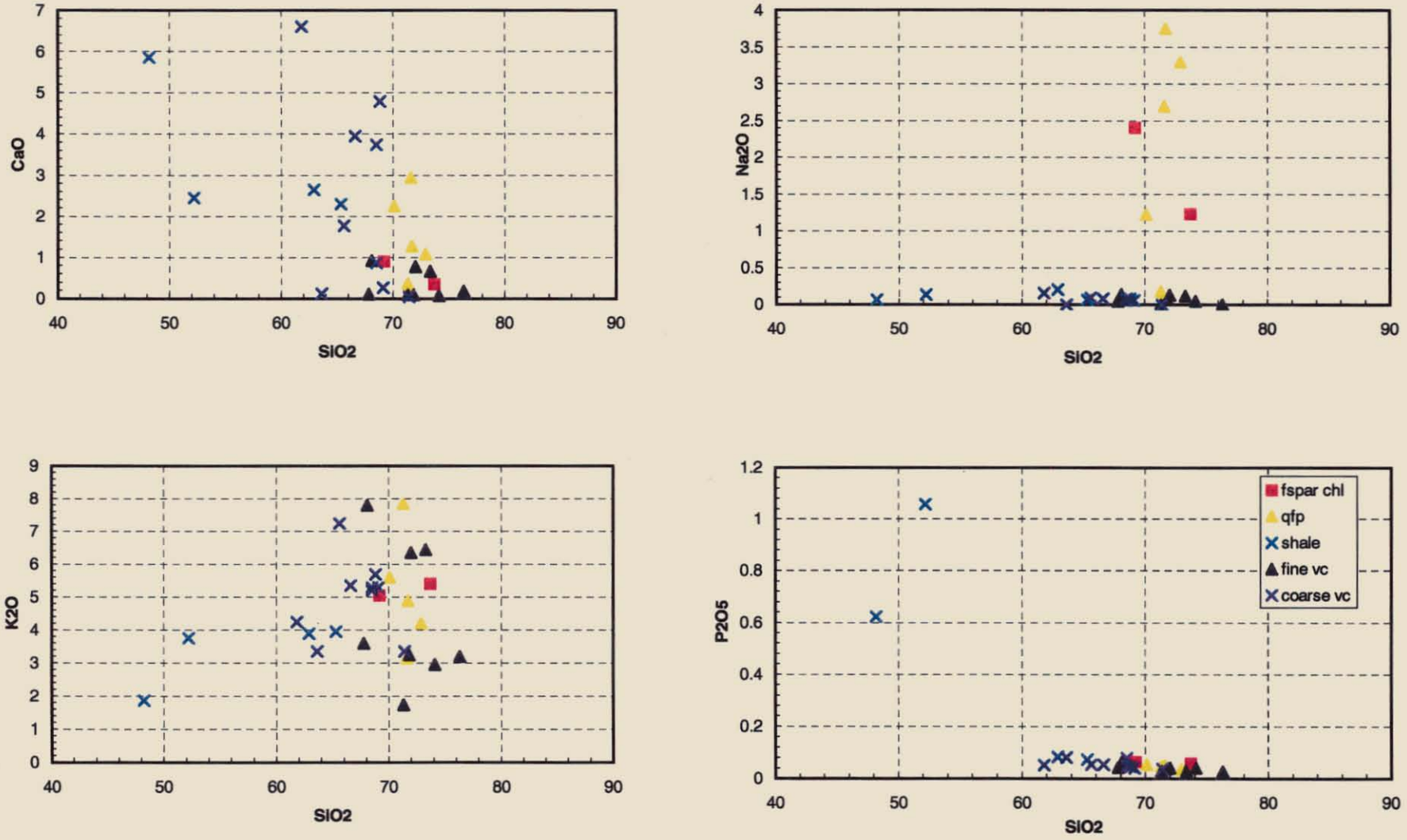

Figure 4.7 Harker diagrams of CaO, Na2O, K2O and P2O5 for the Beatrice rock samples. All axes in wt%

Major element concentrations are typically tightly constrained for the Quartz Feldspar Porphyry samples, indicating the relatively homogenous original composition and absence of significant alteration, with the exception of losses to K_2O and Na_2O, reflecting the partial destruction of feldspar with increasing alteration.

Major element analyses indicated distinct compositional differences between the coarse and fine volcaniclastic units. The fine volcaniclastic unit typically displays higher silica contents than the coarse volcaniclastic unit. The higher concentration and large variation of CaO within the coarse volcaniclastic unit is due to the presence and somewhat random distribution of limestone clasts within the coarse unit.

4.4 Immobile Element Geochemistry

4.4.1 Introduction

A number of elements, including Al, Ti and P and the high field strength elements (HFSE) Zr, Nb and Y are generally considered immobile in rocks which have been subjected to low-grade regional metamorphism and hydrothermal alteration (Barrett and MacLean 1993). The immobility of these elements is however uncertain, under intense hydrothermal alteration. Finlow-Bates and Stumpfl (1981) indicate that although Ti and Zr remain essentially immobile, Y and particularly Nb may be mobile under certain conditions. As a result, the general immobility of Ti and Zr and their contrasting behaviour during fractional crystallisation results in their use in classifying and discriminating between rock types that may have undergone silicic and alkali modification during alteration.

Although immobile element geochemistry is best used on coherent volcanics, they have also been used in this study on volcaniclastic rocks to help identify altered and unaltered units for correlation and to determine the original composition of the volcanic and volcanic derived rocks.

4.4.2 Results

Immobile element plots (Figure 4.8, 4.9) confirm the rhyodacitic composition of the Quartz Feldspar Porphyry (Ti/Zr = 13 to 15). Although showing scatter, the data obtained from the volcaniclastic rocks are consistent with a rhyolitic source, plotting on and below the rhyolitic discrimination line defined by MacLean and Barrett (1993). Fine volcaniclastics display generally lower TiO_2/Zr and Al_2O_3/Zr ratios than

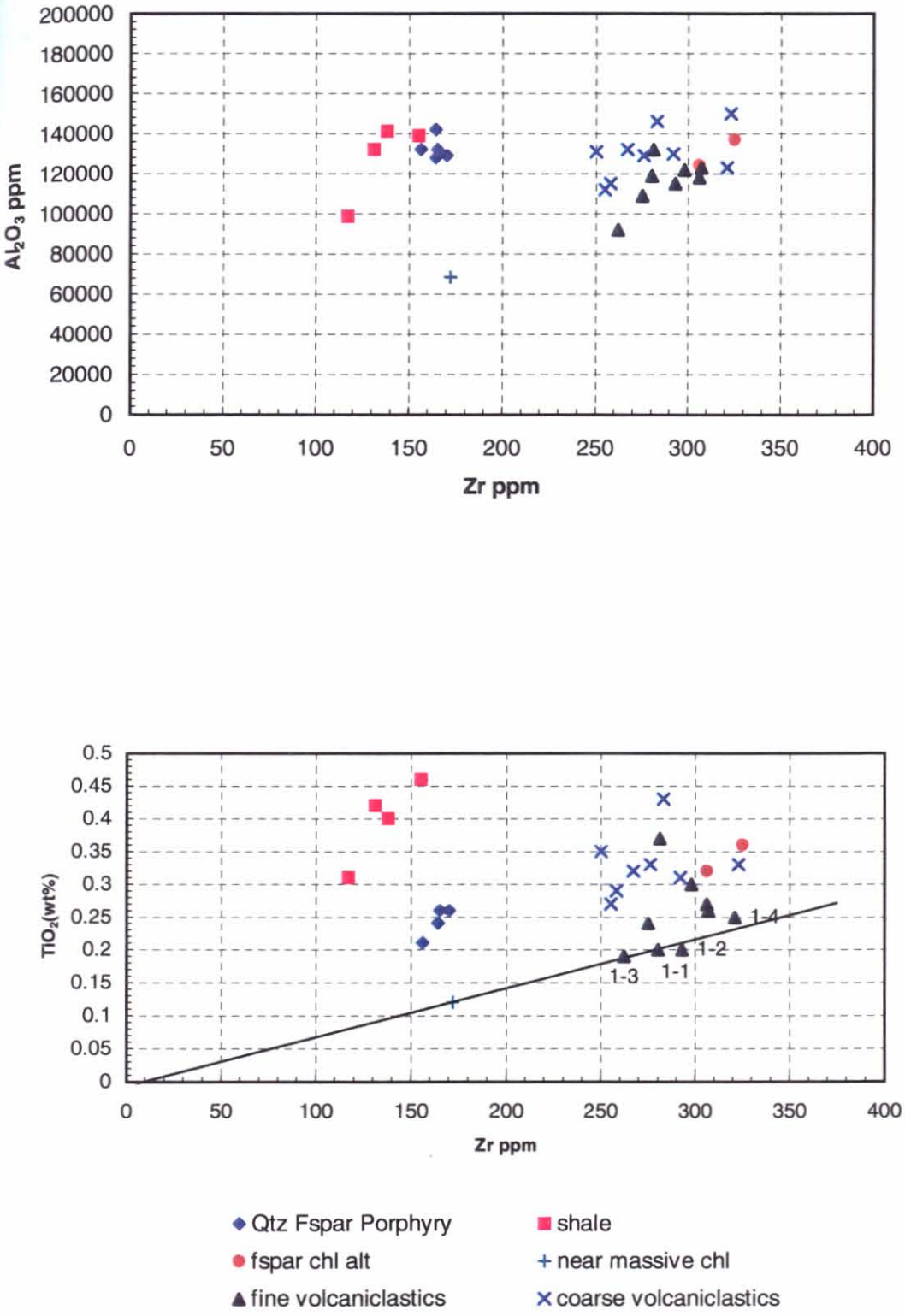

Figure 4.8 "Immobile element' plots: TiO_2-Zr and Al_2O_3-Zr.
Samples MH1-1 to MH1-4 are shown, defining a regression line which passes through the origin suggesting a similar primary composition and relative immobility of Ti and Zr.

the overlying coarse volcaniclastic unit, suggesting a more felsic composition, which is supported by the generally higher silica values obtained from major element analysis.

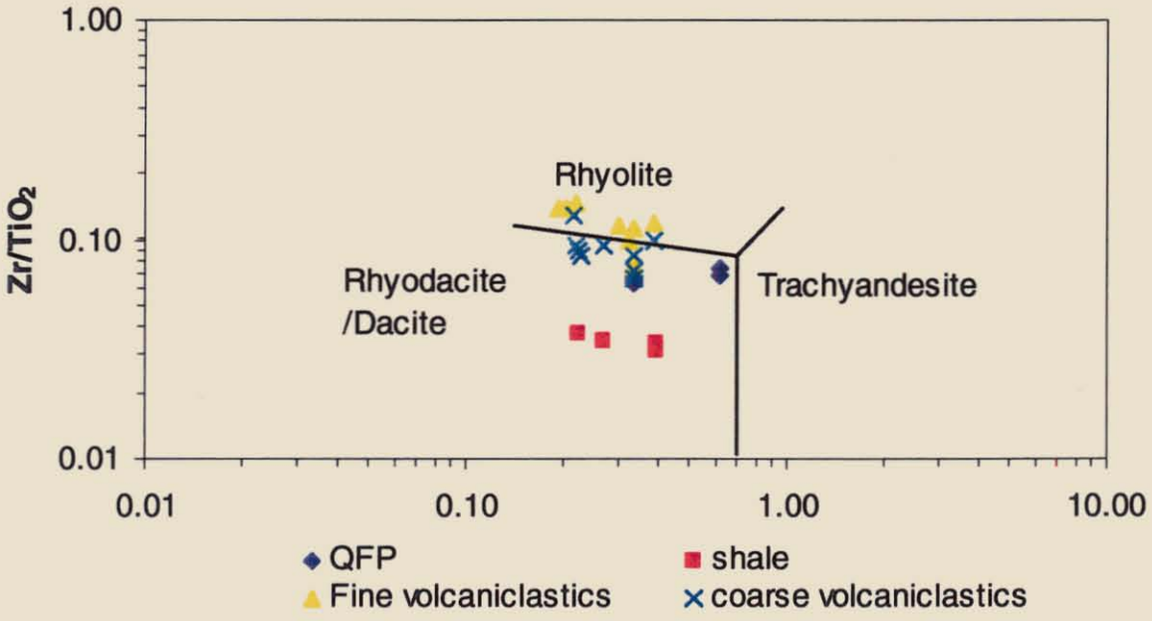

Figure 4.9 Zr/TiO2 vs Nb/Y plot of rock units from the Beatrice Prospect. Discrimination lines defined by Winchester and Floyd (1977).

The use of immobile element ratios may also provide a technique in ascertaining the mass changes undergone due to alteration. Although net mass gains or losses of mobile components associated with hydrothermal alteration can result in changes to the concentrations of immobile elements, their inter-element ratios will be invariable (Herrmann 1998). As a result, scatter plots of immobile element pairs will form highly correlated linear trends reflecting mass gains and losses of the mobile components and hence the concentration or dilution of immobile elements in the altered parts. Mass changes can be calculated for each mobile element based on the dilution or concentration of an immobile component as outlined by MacLean and Barrett (1993). The total mass change of a sample after alteration is calculated using Zr (immobile monitor) concentrations of both the altered sample and an unaltered equivalent, using the formula:

$$\text{Mass Change} = (Zr_{\text{precursor}} / Zr_{\text{altered}} \times \%\ \text{component}_{\text{altered}}) - \%\ \text{component}_{\text{precursor}}$$

This method is a useful tool in the interpretation of alteration effects, but is limited due to its need to calibrate altered samples with an unaltered equivalent. This unaltered equivalent, particularly with respect to the volcaniclastic units, proved difficult to determine due to the regional low-grade alteration and slight primary compositional variation.

4.4.3 Mass Changes in Quartz Feldspar Porphyry

The compositional homogeneity of the Quartz Feldspar Porphyry and the ability to define a sequential progression from unaltered to most altered enabled mass change calculations to be conducted. The intensity of alteration was defined by both visual estimation and major element analysis. Petrographically, both samples MS7-1 and MS5-1 appear relatively unaltered, but have different coloured groundmasses reflecting slightly different primary compositions. As a result MS7-1 was used as the unaltered equivalent for the Quartz Feldspar Porphyry dataset. Mass change calculations (Figure 4.10) show a substantial decrease in SiO_2 and Na_2O with increasing alteration. Absolute Fe_2O_3 and MgO concentrations increase with alteration intensity, as does K_2O. The increase in K_2O and the decrease in Na_2O are due to the destruction of albite and the formation of sericite. The minor increases in Fe_2O_3 and MgO are interpreted to reflect a generally isovolumetric effect associated with the chloritisation of the mafic phase (hornblende). The minor increase is attributed to the hydration of the hornblende, resulting in an increase in volatiles, with no major addition of Fe_2O_3 or MgO.

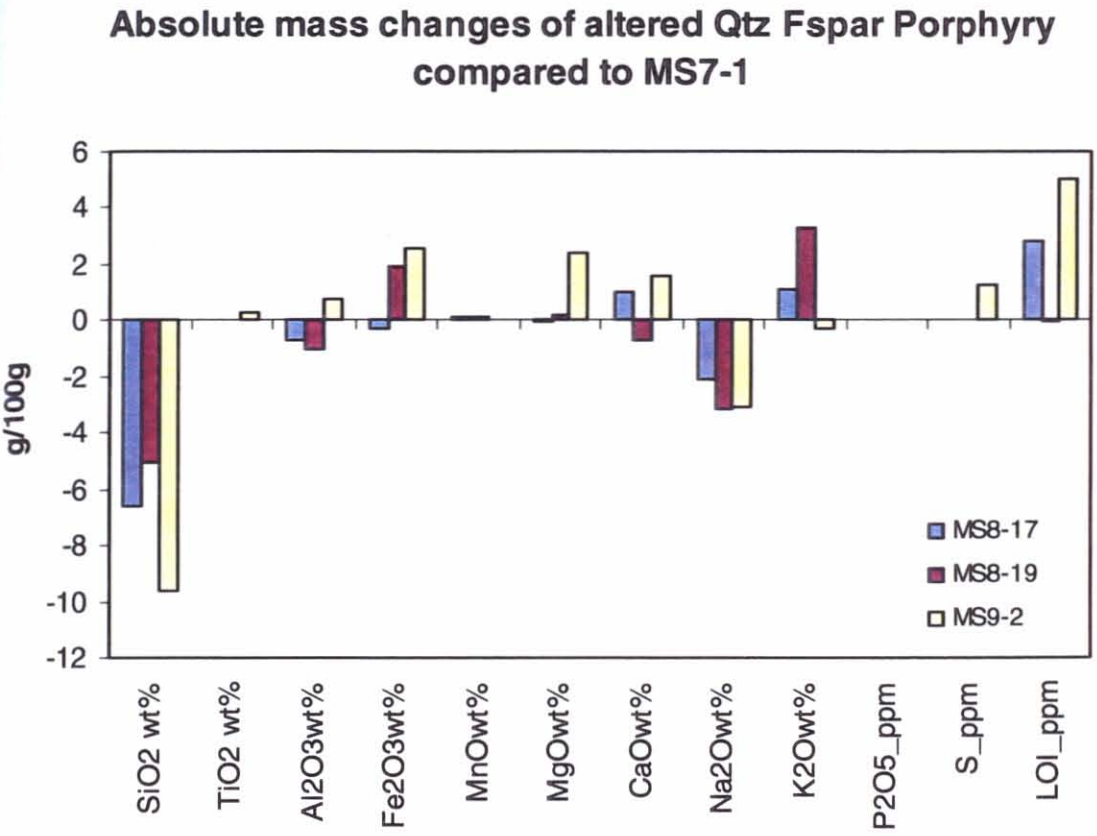

Figure 4.10 Absolute mass changes of Quartz Feldspar Porphyry compared to "unaltered precursor" MS7-1. Mass changes are in g/100g.

4.4.4 Volcaniclastic Units

Due to the interpreted primary compositional variation within the volcaniclastic units care must be taken when calculating mass changes. Based on petrographic analysis and immobile element ratios (Figure 4.8) a suite of four samples from the fine volcaniclastic unit was used in mass change calculations. These four samples, taken from a downhole traverse of MS1 show a visual increase in alteration, which is supported, by their respective location on the AI vs. CCPI boxplot (Figure 4.11). The alteration boxplot; combining the Ishikawa alteration index (AI) with the chlorite/carbonate/pyrite index (CCPI), enables the comparison of whole rock chemistry with alteration mineralogy, and the classification of alteration trends and styles related to VHMS ore deposits (Large 1990). As all samples from the volcaniclastic units have undergone at least weak to moderate alteration, the selection of an unaltered equivalent was impossible. As a result, a least altered equivalent was the next best option, to calibrate the more altered samples. This method will still show the relative movement of elements but will only be a qualitative and not quantitative

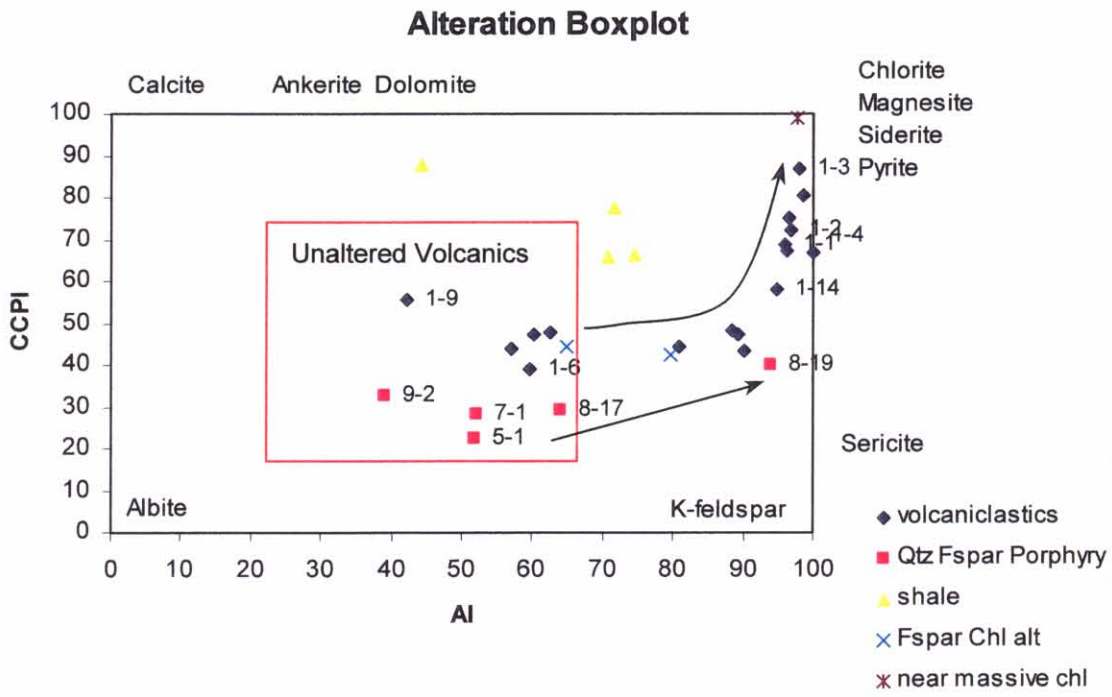

Figure 4.11 Beatrice samples plotted on the AI vs CCPI alteration boxplot. Fine and coarse volcaniclastics show a clear trend from relatively unaltered samples through sericite alteration, to near massive chlorite.

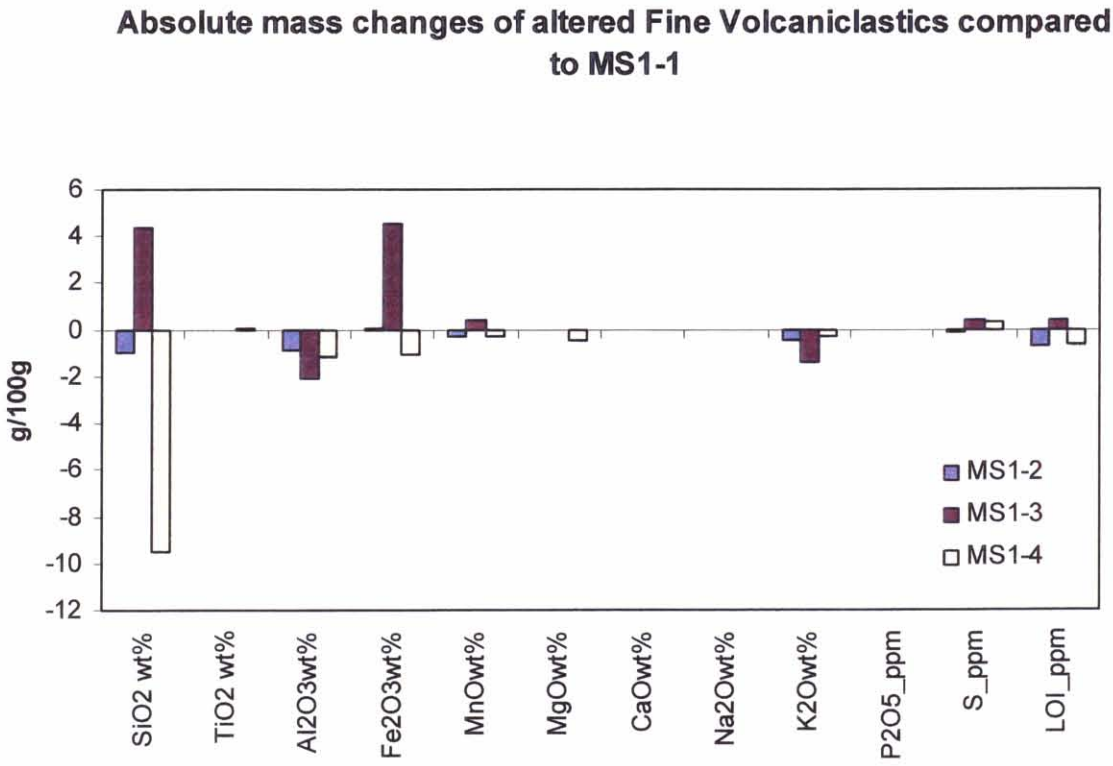

Figure 4.12 Absolute mass changes of altered fine volcaniclastics compared to least altered MH1-1. Mass change units are g/100g.

analysis of their behaviour. Figure 4.12 shows minimal absolute changes associated with increasing alteration. This may be attributed to the difficulties in finding an unaltered precursor, or, as evident by the higher calculated mobility of aluminum, slight variations in original compositions. The minimal calculated changes with progressive alteration can be inferred to reflect the moderate to strong initial alteration of the precursor sample. The absence of any change in sodium reflects that sodium has already been lost from the "least altered" sample. This interpretation is supported by its location on the AI vs CCPI boxplot (Figure 4.11). The moderate increase in iron in MS1-3 relates to the formation of chlorite and pyrite.

4.5 Chlorite Composition

4.5.1 Introduction

Microprobe analyses of chlorite compositions were conducted in an attempt to define compositional variations associated with various chlorite forms or spatial associations with elevated base metal concentrations.

Chlorite exists within the prospect in a variety of forms. It exists within veins, typically associated with quartz + carbonate ± base metal sulfides, and at depth associated with carbonate ± sulfides and also associated with discordant magnetite veins in the zone of moderate to strong K-feldspar alteration. Chlorite exists as selective to pervasive alteration of felsic volcaniclastics and as interstitial grains within the massive sphalerite vein (MH6). As the intensity of pervasive alteration increases towards more mineralised zones within the felsic volcaniclastics, indicating a close spatial relationship to mineralisation, this study of chemical compositions attempted to provide a means of classifying different chlorite generations and providing estimates of temperatures of formation.

Chlorite has the general formula of $Y_6Z_4O_{10}(OH)_8$, where Y and Z represent, respectively, the octahedral and tetrahedral sites. Elements such as Mg, Fe^{2+}, Fe^{3+}, Al, Mn, Zn and Ni may occupy the Y octahedral site and Al, Si, Cr, and Fe^{3+} may be tetrahedrally coordinated by oxygen in the Z site (Deer et al. 1966). The relative substitutions of these elements within the chlorite solid solution may reflect the physio-chemical environment under which these chlorites have formed, and hence may be used as a geothermometer (Walshe, 1986).

4.5.2 Analytical Techniques

Fifty analyses of chlorite compositions from seven samples were obtained using the Cameca SX50 microprobe at the Central Science Laboratory, University of Tasmania. Samples were chosen from a downhole transect reflecting changes in alteration intensity and also within the sphalerite vein associated with potassium feldspar + magnetite ± carbonate alteration

4.5.3 Results and Discussion

Figure 4.13 is an AFM ternary cation plot showing the chlorite solid solution field. Figure 4.14 displays the classification scheme of chlorites, with the vast majority of analyses displaying a tightly constrained range of chlorite compositions plotting within the upper ripidolite field, with the exception of four points, which plot towards the middle of this field. Chlorite compositions have an overall tightly constrained range of compositions, which are particularly iron rich for the Mt Read Volcanic Belt (Eastoe et al. 1987); FeO (25.37-43.75wt%), Al2O3 (19.18-26.46wt%), and MgO (0.14-2.75%), with Mg numbers (100Mg/(Mg+Fe) ranging from (5.56-12). Also analysed were chlorites from within the sphalerite vein (MH6), which displayed anomalous blue interference colours under cross nicols, similar to that noted by Hunns (1987) at the Lake Selina Prospect. When probed these chlorites were significantly more magnesium rich (11.4–14.7wt% MgO), with typically lower iron contents (27.9-32.4wt% FeO) than the rest of the dataset (Table 4.1). Hunns (1987) inferred that these chlorites, were an alteration feature of existing chlorite, however they existed in close association with mineralised areas. The close spatial relationship between these chlorites and pyrite, magnetite ± chalcopyrite ± sphalerite ± galena at Lake Selina may also have genetic implications for their existence at Beatrice. Based on limited exposure, it appears that the massive sphalerite vein containing the anomalous chlorite is discordant to bedding but orientated close to the regional cleavage. This possibly indicates an epigenitic source predating deformation similar to that inferred for Lake Selina.

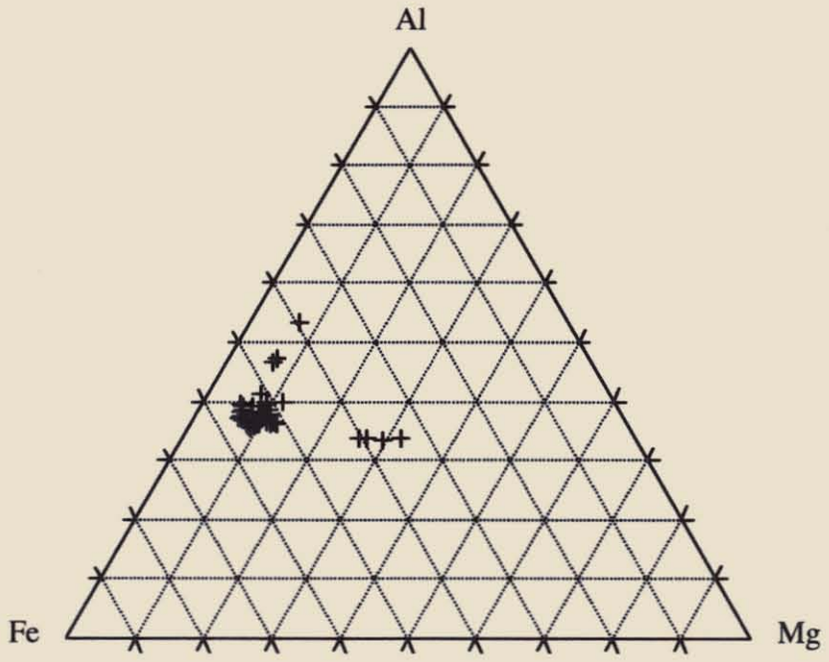

Figure 4.13 Al-Fe-Mg cation plot of chlorite analyses from Beatrice, displaying a tight cluster of low magnesium compositions. Analyses from the massive sphalerite vein plot as a separate clustered field.

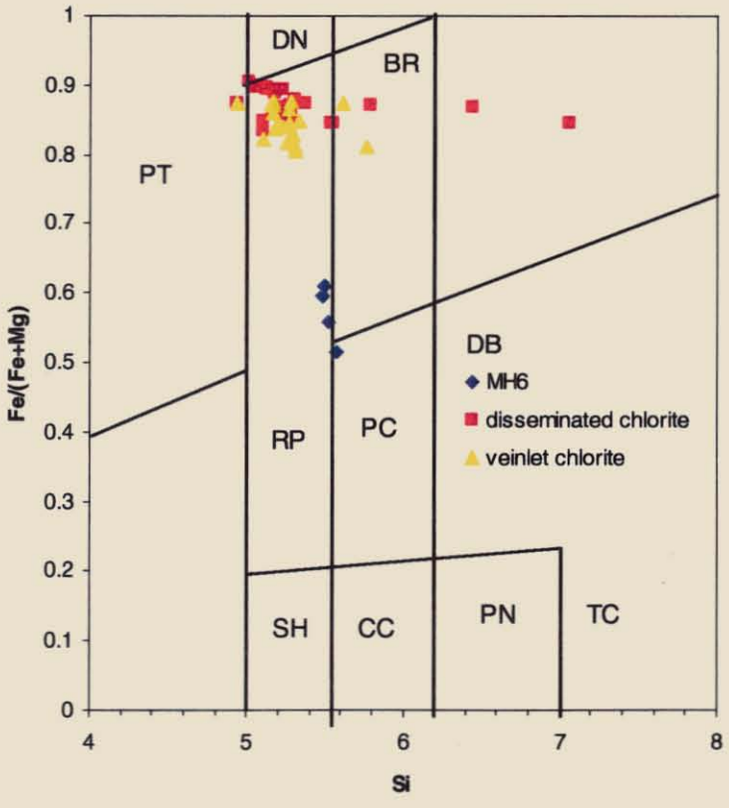

Figure 4.14 Plot of microprobe compositions. Chlorite analyses cluster in the upper ripidolite field. Fields and abbreviations after Hey (1954): Pt, pseudothuringite; CP, corundophilite; DN, daphnite; RP, ripidolite; BR, brunsvigite; SH, sheridanite; PC, pycnochlorite; CC, clinochlore; DD, diabantite; PN, penninite.

Chlorite type	interstital chlorite in massive sphalerite	veinlet chlorite in assoc with Kspar	disseminated chlorite
n	4	21	24
SiO2	26.01	23.26	24.00
TiO2	0.01	0.04	0.05
Al2O3	19.34	20.47	20.85
Cr2O3	0.01	0.01	0.01
FeO	30.60	40.65	40.67
MnO	0.59	0.61	0.67
MgO	13.01	4.22	3.42
CaO	0.01	0.05	0.02
Na2O	0.00	0.03	0.02
K2O	0.02	0.20	0.44
ZnO	0.26	0.14	0.10
NiO	0.01	0.03	0.02
H2O(c)	11.30	10.61	10.71
Sum Ox%	101.17	100.31	100.97
Cations			
Si	5.52	5.26	5.36
Ti	0.00	0.01	0.01
Al/Al IV	2.48	2.74	2.64
Al VI	2.36	2.71	2.86
Al total	4.84	5.45	5.50
Cr	0.00	0.00	0.00
Fe2+	5.43	7.69	7.65
Mn2+	0.11	0.12	0.13
Mg	4.11	1.42	1.15
Ca	0.00	0.01	0.01
Na	0.00	0.01	0.01
K	0.01	0.06	0.12
Zn	0.04	0.02	0.02
Ni	0.00	0.00	0.00
OH	16.00	16.00	16.00
Sum Cat#	36.06	36.05	35.94
XMg	0.43	0.16	0.13
mg no	29.87	9.41	7.80
Al IV corrected	2.88	3.33	3.25
Chlorite temp	323.19	371.49	374.82

Table 4.1 Average microprobe chemical analyses for the three styles of chlorite.

Several models for calculating temperature based on chlorite composition have been proposed by authors including, Walshe (1986), Cathelineau and Nieva (1985) and Kranidiotis and Maclean (1987) and have been critically analysed by Jiang et al. (1994). Walshe (1986) claimed that temperature and oxygen fugacity (fO_2) could be calculated, and where quartz and chlorite and an iron sulfide coexisted, the H_2S content of the fluid could also be calculated. Walshe (1986) indicated that temperatures cannot be determined based on chlorites with a total iron content between 32-40wt% FeO. Samples from the Beatrice Prospect unfortunately have total iron contents in the problematic range outlined by Walshe (1986).

The inherent inaccuracies of geothermometers based on octahedral occupancy and tetrahedral Al have been highlighted by Jiang et al. (1994) and are duly noted here. Jiang et al. (1994) stated that increases in octahedral occupancy and tetrahedral Al is a

function of the decrease in abundance of mixed layers or fine-grained intergrowths associated with an increase in crystal size and homogeneity in prograde sequences. With this in mind, the simpler model of calculating formation temperatures adapted by Kranidiotis and MacLean (1987) from Cathelineau and Nieva (1985) has been used, This geothermometer is based on the equation, corrected for Al^{IV} concentrations, where:

$$Al^{IV}_{corrected} = Al^{IV}_{uncorrected} + 0.7[Fe/(Fe + Mg)_{chl}]$$

$$Temperature\ (T) = 106\ Al^{IV}_{corrected} + 18$$

One assumption for this model to work is that chlorites must be alumina saturated. As can be seen in Figure 4.12 all samples plot on the Al-rich side of the AFM ternary cation plot, indicating alumina saturation. Table 4.2 summarises the temperature ranges calculated, using the Al^{IV} geothermometer for the three major forms of chlorite.

Chlorite type	interstital chlorite in massive sphalerite	disseminated chlorite	veinlet chlorite in assoc with Kspar
Sample numbers	MH6	1-3,1-7,1-9	7-7,7-9,7-15
Number of analyses	4	24	21
Temperature Range	313-328	316-402	315-408
Average temp.	323	375	371

Table 4.2 Summary of temperature calculations based on chlorite composition.

There are significant differences in calculated temperatures between chlorites from the sphalerite vein and those associated with various alteration styles within the volcaniclastic units. The restricted range and similar temperatures calculated from the two alteration styles within the volcaniclastic units suggests two possible explanations:

1) That the two chlorite styles are related, and reflect the original temperature of formation from a hydrothermal fluid, or
2) The composition and hence calculated temperature have been reset by regional metamorphism.

The second possibility appears most plausible given that temperature of ~370°C are consistent with the lower greenschist facies of regional metamorphism. If regional metamorphism was responsible for the resetting of chlorite compositions, the iron and magnesium contents (Mg#) of the chlorite would be expected to re-equilibrate with the whole rock composition, forming a linear relationship (Wyman 1998). Figure 4.15 displays the average Mg# calculated for chlorites plotted against the Mg# of their host rocks for samples MH1-3, MH1-9 and MH7-9. As can be seen there is a clear linear relationship, indicating that chlorites have been reset and equilibrated with their host rocks during regional metamorphism.

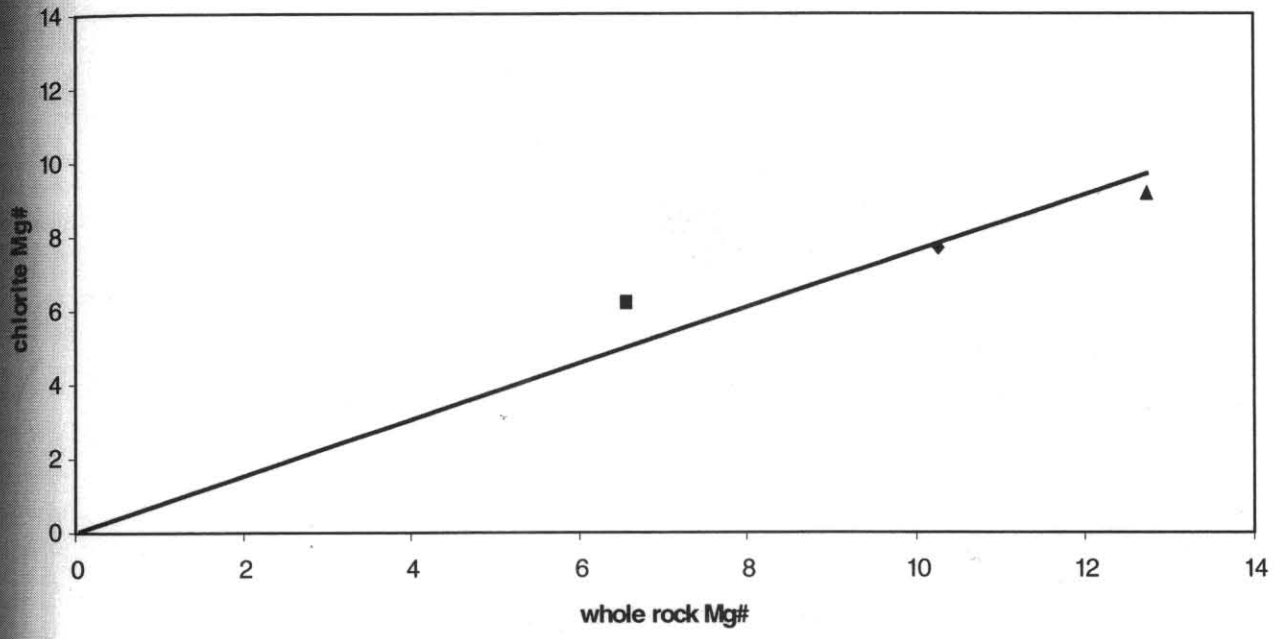

Figure 4.15 Plot of the average Mg# of chlorite compared to the whole rock Mg# of its host rock for samples MH1-3, MH1-9 and MH7-9.

There is however, evidence to suggest that real differences in chlorite composition and formation temperatures do exist within the Beatrice Prospect. The temperatures calculated from chlorites within the sphalerite vein have a narrow range (313-328°C) significantly lower than temperatures calculated for both disseminated chlorite and veinlet chlorite within the feldspar altered zone in MS7, which have similar calculated average temperatures (371 and 374°C respectively). This distinction in calculated temperatures may be a real effect indicating a different alteration fluid, with differing temperature. The anomalous Mg content of the two existing accessory phases may support this interpretation of a separate fluid responsible for the sphalerite vein.

Chlorites within the vein have average Mg numbers roughly three times that of average chlorite from within the prospect (average Mg# 29.9 opposed to 8.5) and also the presence of ankeritic carbonate, which was only observed within this sample. The close association between the massive sulfide vein and both chlorite and carbonate, enriched in magnesium may be used as a possible vector towards mineralisation. The anomalous berlin blue interference colours displayed by these chlorites may also be useful in their recognition, therefore saving on expensive microprobe analyses.

Chapter 5

Mineralisation of the Beatrice Prospect

5.1 Introduction

Known mineralisation at the Beatrice Prospect is confined to the 2 X 5km window of felsic volcaniclastic units and shale exposed in the Itat Creek Valley. The area of elevated base metal values was termed the Mt Sedgewick Anomalous Zone by the Mount Lyell Mining and Railway Company during 1976. The morphology of mineralisation within this zone is controversial. Wilde and Kerr (1990) suggested sulfide occurrences were partly vein related and partly replacive and therefore epigenetic. Boyd (1994) contradicted their interpretation, stating that sulfides are bedded within the shale and volcaniclastic units and as such are most likely of syn-sedimentary formation.

The primary focus of this chapter is to document the various styles of mineralisation observed, and to record the relationship and paragenetic sequence of sulfides at the Beatrice Prospect. As an introduction to this chapter Table 5.1 provides a summary table outlining the best base metal values intersected during drilling within the Beatrice Prospect.

Drill Hole	Depth	Best Grades
MS1	62-68m	7m @ 1.07% Pb, 1.65% Zn, including 2m @ 0.14% Cu, 2.65% Pb, and 5.05% Zn
MS2	60-63.9m	3.9m @ 0.59% Pb and 0.78% Zn
MS3	106.4-118.6m	12.2m @ 0.43% Pb and 0.59% Zn
MS4	142.4-152m	9.6 @ 0.22% Pb and 0.75% Zn
MS7	374-376m	2m @ 0.57% Pb, 0.21% Zn and 357ppm Cu
MS8	540-583.9m	43.4m @ 0.62% Zn, 0.28% Pb, including 6.6m @ 1.18% Zn, 0.55% Pb and 12.5ppm Ag

Table 5.1 Summary table of the best base metal intersections from the Beatrice Prospect. Drill hole locations are illustrated in Figure 5.1. Data compiled from Boyd (1994) and McNeill (written comm. 1999).

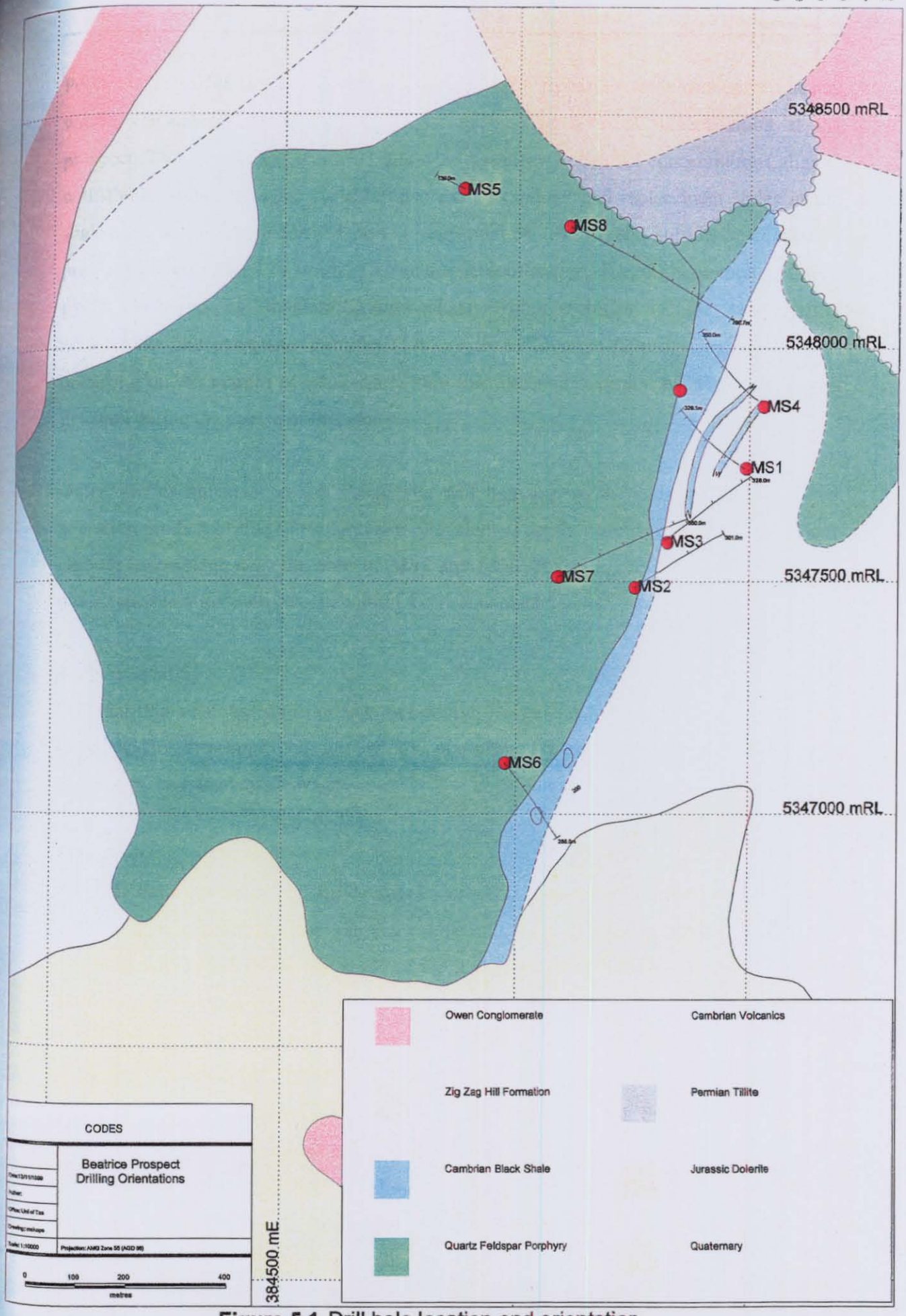

Figure 5.1 Drill hole location and orientation

5 cm

Polymetallic sulfide lenses of sphalerite + galena + pyrite ± rare chalcopyrite, hosted within volcaniclastics, represent the most prospective style of mineralisation at the prospect. These lenses exist in MS1 and MS3 as diffusely banded concentrations aligned with the regional cleavage. Sulfides also exist as veinlet and replacement styles in the shale unit, where pyrite formed prior to deformation. Base metal sulfides also exist in pressure fringes formed by syn-post kinematic remobilisation. The most common sulfide is pyrite, followed by sphalerite, and galena. Minor sulfides include chalcopyrite, arsenopyrite and pyrrhotite. Pontifex (1998) recorded a small (20μm), single gold grain occurring on the margin of sphalerite within the volcaniclastic unit. No visible gold was detected during the course of this study.

Oxide phases are also present. Magnetite and hematite (with hematite forming as an alteration product of magnetite) are more prevalent at depth, occurring with the K-feldspar chlorite assemblage near the base of MS7 and MS8. Rutile is present as a minor oxide phase in association with chlorite within the volcaniclastic units.

5.2 Petrography

Polished thin sections from the fine and coarse volcaniclastic units and shale unit were examined to determine the mineralogy of sulfide assemblages and relationship to lithologies, layering and cleavage.

5.2.1 Pyrite

Pyrite is the most abundant sulfide species present, comprising up to 25% of the rock volume in some intervals within the black shale unit. At least three, possibly four forms of pyrite were observed during the study of the prospect. There is clear evidence that there were at least two stages of pyrite formation. However, paragenetic relations between the differing pyrite morphologies have been difficult to determine and separate pyrite forming generations could not be defined.

As a result pyrite generations are arbitrary unless otherwise stated. Pyrite type 1 exists as fine (~200μm) euhedral grains within carbonate rich beds in the shale unit that probably formed during early diagenesis. A second form of pyrite, type II, typically displays well formed, large (up to 2-3mm), euhedral to subeuhedral crystal shapes and contains abundant quartz inclusions (plate 5.1). This type has been observed in veinlets in the shale unit, and more commonly, as disseminations within both the coarse and fine volcaniclastic units.

There is a clear distinction between the inclusion rich pyrite and a later "clean" generation, in quartz veinlets within the shale unit. This generation of inclusion free pyrite formed as rims, replacements and selvages on the inclusion rich pyrite II grains, (Plate 5.2).

A possible fourth form of pyrite was observed within the K-feldspar, chlorite, Fe oxide altered zone at the base of MS7, existing as an isolated, large (>2cm), subeuhedral crystal within altered volcaniclastics (Plate 5.3).

The pyrite grains, being relatively hard, show evidence of brittle deformation with internal fractures healed by more ductile galena and sphalerite (Plate 5.4). Pyrite grains in shale typically have pressure fringes of elongate quartz fibres, sparry calcite and remobilised sulfides (Plate 5.5)

5.2.2 Sphalerite

Sphalerite is the most common constituent in the higher-grade lens (MH3-10 and MH3-16). It exists as an anhedral massive aggregate intergrown with galena, pyrite and chalcopyrite. Diffuse layering parallel to cleavage has also been observed. Sphalerite also exists in discordant quartz carbonate veinlets in the shale and volcaniclastic units and in voids associated with pressure fringes and quartz fibre development, where it is less common than galena.

Sphalerite appears to occur as coherent clasts within a 1metre diffuse zone of coarse material containing shale and volcanic clasts in MS8 (Sample MH8-15). Microscopically, however, sphalerite appears controlled by veinlets and to have replaced extremely fine quartz sericite volcanic clasts. Sphalerite was also observed in intimate association with galena in coarse quartz carbonate veins in the Quartz Feldspar Porphyry.

Observations under plane polarised light showed that sphalerite is typically dark red brown and less commonly of paler honey brown colour. Sphalerite contains numerous irregular, disseminated blebs of chalcopyrite, often forming rinds around grain boundaries.

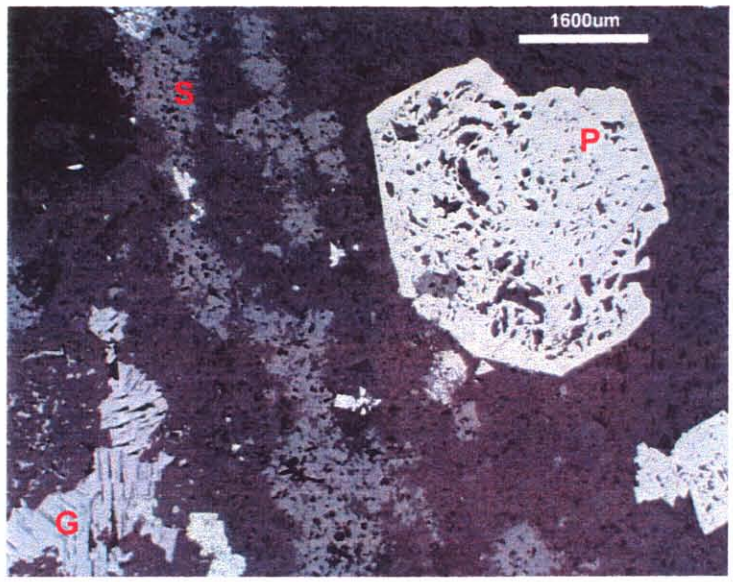

Plate 5.1: Photomicrograph of shale unit with coarse, subeuhedral, inclusion rich pyrite grains (P). Inclusions typically consist of quartz but may also contain rare sphalerite and galena. Also present is a sphalerite rich veinlet (S) and anhedral clot of galena (G) displaying well formed triangular cleavage pits

Photo taken in reflected light.

Sample MH8-10

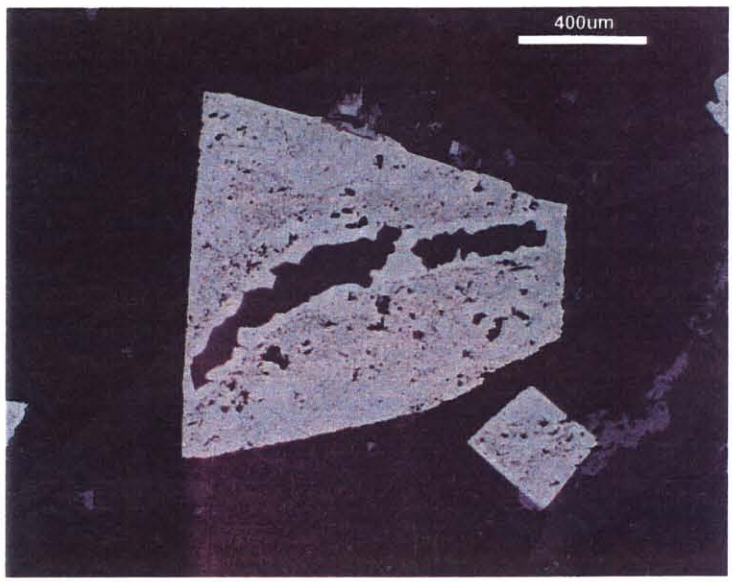

Plate 5.2: Photomicrograph of a euhedral, inclusion rich pyrite grain (Pyrite II) cross cut by fracture controlled reprecipitation of "clean" inclusion free pyrite.

Photo taken in reflected light.

Sample MH4-1

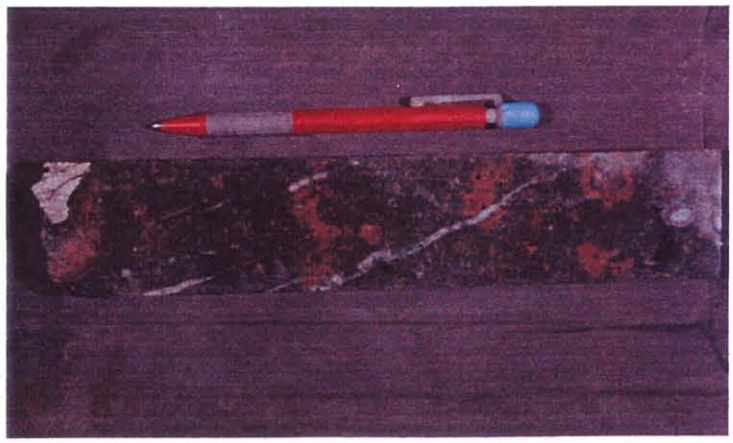

Plate 5.3: Extremely coarse, subeuhedral pyrite grain occurring in isolation within the K-feldspar + chlorite + magnetite/hematite alteration assemblage.

MS7 ~ 487 metres

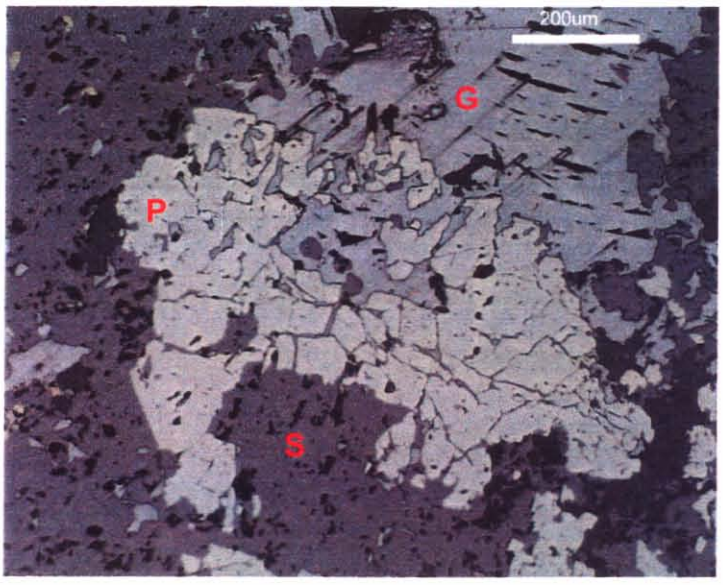

Plate 5.4: Photomicrograph of fractured pyrite (P) grain being annealled and replaced by galena (G) and sphalerite (S).

Photo taken in relected light

Sample MH3-10

Plate 5.5: Euhedral inclusion rich pyrite grain with well formed pressure fringe. Galena with minor sphalerite and chalcopyrite are late infillings with some replacement of fine grained highly corroded pyrite grains.

Photo taken in reflected light

Sample MH4-1

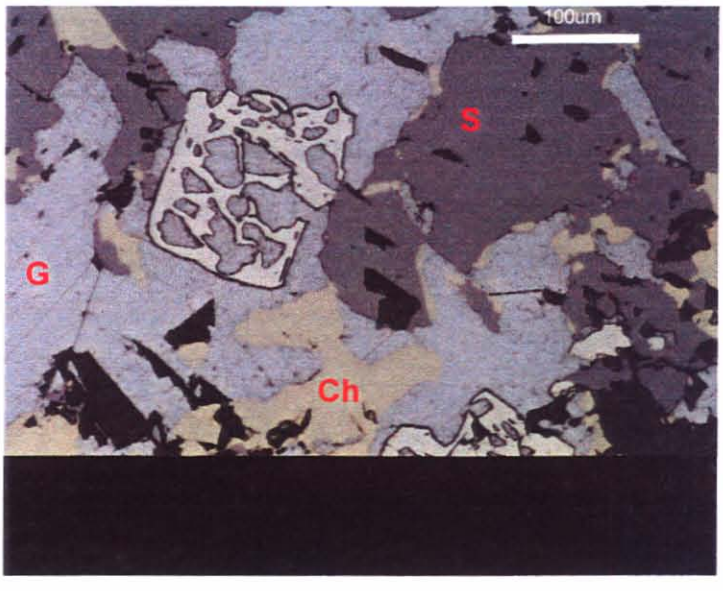

Plate 5.6: Sphalerite (S), pyrite (P), galena (G) and chalcopyrite (Ch) within one of the small polymetallic lenses. Galena is replacing originally euhedral pyrite grains producing a poikolitic texture. Chalcopyrite forms commonly as a selvage on anhedral sphalerite.

Photo taken in reflected light

Sample MH3-10

5.2.3 Galena

Galena is a common constituent of the polymetallic blebs, as coarse anhedral blebs intergrown with sphalerite. It also filled fractures within type II pyrite grains and replaced early formed pyrite forming a poikolitic texture (Plate 5.6). Galena plus minor chalcopyrite and sphalerite, filled voids associated with pressure fringes and quartz fibre development, with sulfides deposited after the formation of coarse sparry calcite crystals.

5.2.4 Chalcopyrite

Chalcopyrite exists as diffusely layered anhedral aggregates often aligned with cleavage within the polymetallic lens. It also occurs as inclusions within pyrite and as an exsolution texture within sphalerite (chalcopyrite disease), forming fine grained <150μm blebs and rims on sphalerite grains. Chalcopyrite occurs as a common but minor constituent within the shale unit, where it is found as fine aggregates, intimately intergrown with remobilised galena filling voids formed during deformation and movement of pyrite grains. It also exists within bedding parallel veins within the shale unit intimately related with anhedral pyrrhotite.

Chalcopyrite abundance appears to be more common at depth, in the K-feldspar-chlorite alteration zone near the end of MS7 and MS8, where it exists in close association with fine wispy pyrite and in discordant quartz chlorite veins.

5.2.5 Arsenopyrite

Arsenopyrite has been observed in the shale unit and in mineralised, quartz carbonate veined zones in the volcaniclastic and Quartz Feldspar Porphyry units. Arsenopyrite in the strongly quartz carbonate veined zones exists as coarse (<6mm) subeuhedral to euhedral crystals. In the shale unit, arsenopyrite formed small (<2mm), rare rhombs. Within the seven metre carbonate bedded section in MS8, fine (~250μm) well-formed arsenopyrite crystals exist as veinlet controlled aggregates preferentially within the carbonate beds. Arsenopyrite is a minor constituent with pyrite in the replacement of beds originally composed of evaporite minerals (gypsum) with some grains exhibiting pressure fringes and quartz fibres on some surfaces.

5.2.6 Pyrrhotite

Pyrrhotite exists as fine grained anhedral masses intimately intergrown with chalcopyrite, sphalerite and galena in the shale unit, forming bedding sub-parallel veins. It is locally abundant within the nodule and bedded carbonate section intersected by MS8, as a replacement of carbonate beds and within discordant carbonate veins (Plate 5.7).

5.2.7 Marcasite

Marcasite exists as a moderately rare sulfide species; it has been observed in intergrowths with pyrite and as selvedges on vein walls in the black shale unit.

5.2.8 Oxides

Magnetite is the most common iron oxide present at the Beatrice Prospect. Magnetite exists as fine disseminated clots or as an alteration product of mafic phases in the Quartz Feldspar Porphyry. Magnetite also exists as radiating aggregates associated with chlorite and carbonate veining in the strongly K-feldspar altered volcaniclastics at depth. Alteration to hematite is common in this zone.

Rutile is a rare accessory mineral phase identified in small concentrations in samples MH1-7, MH1-9 and MH7-15. It exists as disseminated euhedral aggregates in close association with chlorite; typically as fine interlocking crystals, distinguished by their bright internal reflectance.

5.2.9 Quartz Fibres

Quartz fibres (plate 5.8) are features present within shale units and occasionally within the coarse volcaniclastic unit. Typically 100 to 1200μm long, these fibres occur and locally thicken adjacent to hard mineral phases such as pyrite and arsenopyrite grains. In most cases, quartz fibre growth proceeds coarse euhedral calcite growth hosting remobilised galena, chalcopyrite and sphalerite infilling the remainder of the microfracture.

5.2.9.1 Interpretation of Quartz Fibres

Cox and Etheridge (1983) noted that the shape and preferred orientation of fibrous quartz crystals could be attributed to oriented growth mechanisms during successive 'crack-seal' deformational increments. Formed from a heterogeneous strain pattern around the host crystal, these fibrous quartz pressure fringes form in the extension direction of strain.

Plate 5.7: Carbonate layers in shale unit, with discordant carbonate, pyrrhotite and arsenopyrite veins. Pyrrhotite and arsenopyrite have selectively replaced carbonated beds.

MS8 562.9metres

Plate 5.8: Same view as plate 5.5 but in plane polarised light, indicating the well formed pressure fringe adjacent to euhedral pyrite. First formed were quartz fibres (Q) aligned with the dominant cleavage, later infilled by sparry calcite (C) and remobilised sulfides.

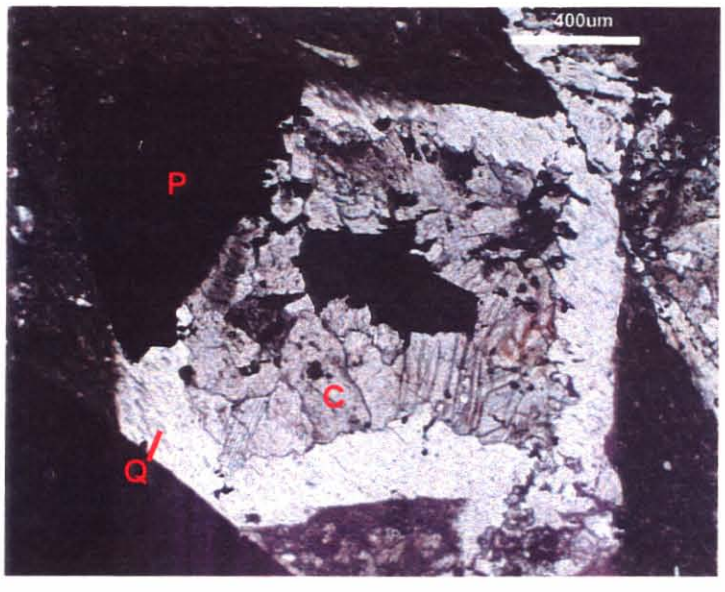

Photo taken in plane polarised light

Sample MH4-1

Plate 5.9: Handspecimen showing anastimosing sphalerite veinlets (S) at the contact between a coarse (C) and fine (F) volcaniclastic unit.

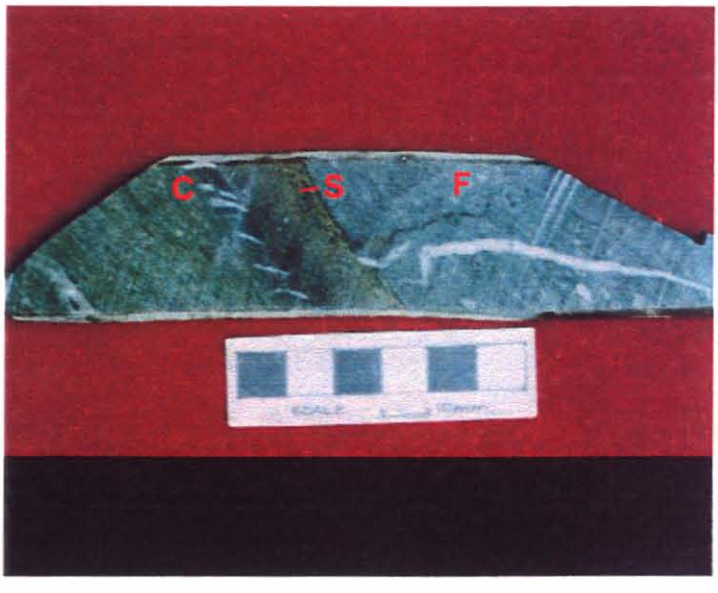

Scale bar = 6cm

Sample MH3-4

The 'crack-seal' deformation process involves the accumulation of elastic strain followed by brittle failure along a discrete surface, solution transfer of material to the microfracture site, and the deposition of material within the opening fracture.

Cox and Etheridge (1983) indicated two possible growth mechanisms for fibres that have developed at or near to, one or both of the detachment surfaces. The first involves fibres occurring as syntaxial overgrowths of grains present in the vein wall. If the fibres are not cleanly detached at successive 'crack-seal' increments, the resulting fibres can record the displacement history during vein growth. The second mechanism involves the formation of non-syntaxial overgrowths which detach cleanly from the vein wall. During each 'crack-seal' increment, the free growth of the fracture-filling phase into the microcrack results in the fibres growing with long axes sub-perpendicular to the microcrack wall. Cox and Etheridge (1983) indicate that this second mechanism is the most likely where quartz fibres develop fringe structures against pyrite euhedra. This feature typically displays an increase in fibre diameter towards the pyrite-quartz interface reflecting the growth of quartz fibres by accretion near the interface. Quartz fibres observed flanking pyrite and arsenopyrite grains from the Beatrice Prospect appear similar to the second style of fibre growth outlined by Cox and Etheridge (1983). The alignment of quartz fibres appears more commonly aligned with the dominant cleavage, however the presence of curved quartz fibres indicate that the host crystal have been partially rotated and subjected to shear stress.

5.3 Paragenesis

Paragenetic relationships between sulfides proved difficult to determine, due to the sparse veinlet morphology and low concentration of sulfides. It was also difficult to establish relations and correlations across lithological boundaries due to differing styles of mineralisation and the different reaction of host rocks to deformation. As a result, a paragenetic sequence for sulfide species can only be generalised and related to individual lithologies.

In the black shale unit, fine grained euhedral pyrite grains formed during early diagenesis, evident by the wrapping of pyritic beds around sedimentary concretions.

The pseudomorphing of original gypsum crystals by pyrite and arsenopyrite appears to have occurred early and prior to deformation, as evident by the rotation and alignment of these crystals into the dominant cleavage and the presence of pressure fringes. These pyrite

and arsenopyrite beds are cross cut by bedding sub-parallel, quartz carbonate veins containing pyrrhotite, with minor chalcopyrite, sphalerite and galena. Apparently cross cutting these veins are coarse siderite, calcite veins containing inclusion rich euhedral pyrite grains together with pyrite-marcasite intergrowths and sphalerite and galena infilling the central portion of the vein. The euhedral pyrite grains exhibit pressure shadows which are infilled by fibrous quartz, then coarse sparry calcite, then galena, sphalerite and chalcopyrite, which are believed to have been remobilised during deformation. This deformation also appears to have resulted in the reprecipitation of pyrite to form selvages and rims of clean inclusion free pyrite around originally inclusion rich crystals.

Mineralised zones within the volcaniclastic units appear simpler, with only four main sulfide species; pyrite, sphalerite, galena and chalcopyrite. Typically sulfides exist within the volcaniclastic units as anastamosing veinlets. Pyrite exists, again as both a coarse, inclusion rich phase and as a clean rim or replacement of the original grain. The contact between pyrite and galena typically shows cusp and caries texture with convex surfaces facing into the pyrite, suggesting the replacement of pyrite by galena (Guilbert and Park, 1986). A similar feature is observed with sphalerite replacing galena. Chalcopyrite is the last mineral phase that formed, as it exists as an exsolution texture within sphalerite and also as rims on anhedral sphalerite grains. Within the polymetallic lens (MH3-10), sulfides exist as diffuse bands aligned to the dominant cleavage defined by ragged chlorite grains in the volcaniclastic host unit. Within the sulfides is a recrystallised mosaic of quartz and carbonate also aligned with the cleavage. The alignment of both sulfide species and gangue minerals is interpreted to reflect syn-kinematic recrystallisation and precipitation. The author considers the known base metal mineralisation within the Beatrice prospect comprises epigenetic veinlet and replacement styles with no evidence of syn depositional mineralisation.

Four distinct vein generations were observed within the Quartz Feldspar Porphyry body, occurring as coarsely crystalline veins ranging in size from 2mm to 40cm thick. Due to the abundance of these veins and their distinct morphology a clear paragenetic sequence can be inferred from cross cutting relationships:

Stage 1: quartz + carbonate + chlorite ± sphalerite ± galena

Stage 2: quartz, carbonate, K-feldspar + chlorite ± sphalerite ± galena

Stage 3: quartz + chlorite + carbonate

Stage 4: carbonate

These vein generations are also present within the underlying shale and volcaniclastic unit, but are far less abundant and distinct, possibly reflecting a competency control on brittle deformation. The veins appear similar to regionally extensive vein styles and therefore, probably related to a later event associated with deformation.

5.4 Metal Zonation and Relationship to Stratigraphy and Alteration

As outlined in Chapter Four, sulfide abundance appears to correlate with the intensity of chlorite alteration, within the fine and coarse volcaniclastic units. The plotting of assay results against lithological and alteration logs provides a method of illustrating the relationship between lithology, style and intensity of alteration, and base metal concentration, and may result in correlations that may be useful in further exploration. This section uses information obtained from both Chapters Four and Five in an attempt to relate metal concentration to lithology and alteration. Three drill holes have been selected for discussion; MS1, MS3 and MS7 (Figures 5.2 to 5.4).

It is apparent in all three logs that the contacts between various lithological units correlate with an increase in lead and zinc. This is particular evident between the fine and coarse volcaniclastic units, where sulfide concentration is greatest within the tops of fine grained volcaniclastic units. This feature is peculiar insofar as the greater porosity and permeability expected for the coarse volcaniclastic units, would be more receptive to hydrothermal alteration and mineralisation. The latter situation has been recognised in handspecimens, where contacts between coarse and fine volcaniclastic beds commonly show a concentration of sulfides at the top of the coarse unit (Plate 5.9), suggesting ponding of hydrothermal fluid below a relatively impermeable layer.

5.4.1 MS1

MS1, collared on the eastern edge of the MSAZ was drilled to the west, intersecting mineralised coarse and fine volcaniclastics. MS1 was drilled subparallel to bedding and drilled up stratigraphy. In Figure 5.2 simplified lithological and alteration logs are illustrated along with graphs displaying metal zonation and concentration and alteration indices defined from whole rock analyses as useful indicators of hydrothermal alteration. In MS1 there are four basic rock types:

- Predominantly fine to moderately coarse volcaniclastic
- Coarse lithic, pumice rich volcaniclastic unit
- Pyritic black shale
- Quartz feldspar porphyry

Alteration within the volcaniclastic units can be categorised into two major types:

- Pervasive sericite alteration
- Disseminated to pervasive chlorite alteration

Sericite alteration is ubiquitous, as moderate pervasive alteration throughout the fine volcanic and as the dominant alteration phase within the coarse volcaniclastic units. It replaced original glassy materials that comprised the bulk of the coarse unit. Chlorite alteration formed small (<1mm) blebs in the fine volcaniclastic unit, increasing in intensity and size, resulting in coalescing of individual chlorite spots to pervasive alteration between 41.3 and 68.4metres and 110.8 and 113.3metres. These two zones of strong chlorite alteration closely correlate to elevated base metal mineralisation, where peak base metal values (greater than 1%Pb and 1.5% Zn) occur in discrete zones at the contacts between fine and coarse volcaniclastic units. These zones of elevated base metal values coincide with fine veinlet mineralisation and also to disseminated sulfides that do not appear veinlet controlled. Also evident in this hole are close correlations between elevated base metal values, chlorite alteration and alteration indices.

The Ishikawa (1976) alteration index (AI), defined as 100 x $(MgO + K_2O)/(MgO + K_2O + CaO + NaO)$ relates to the replacement and destruction of plagioclase and the formation of sericite and chlorite during hydrothermal alteration, however it does not discriminate between sericite and chlorite alteration. Maintaining a consistently high level (>90)

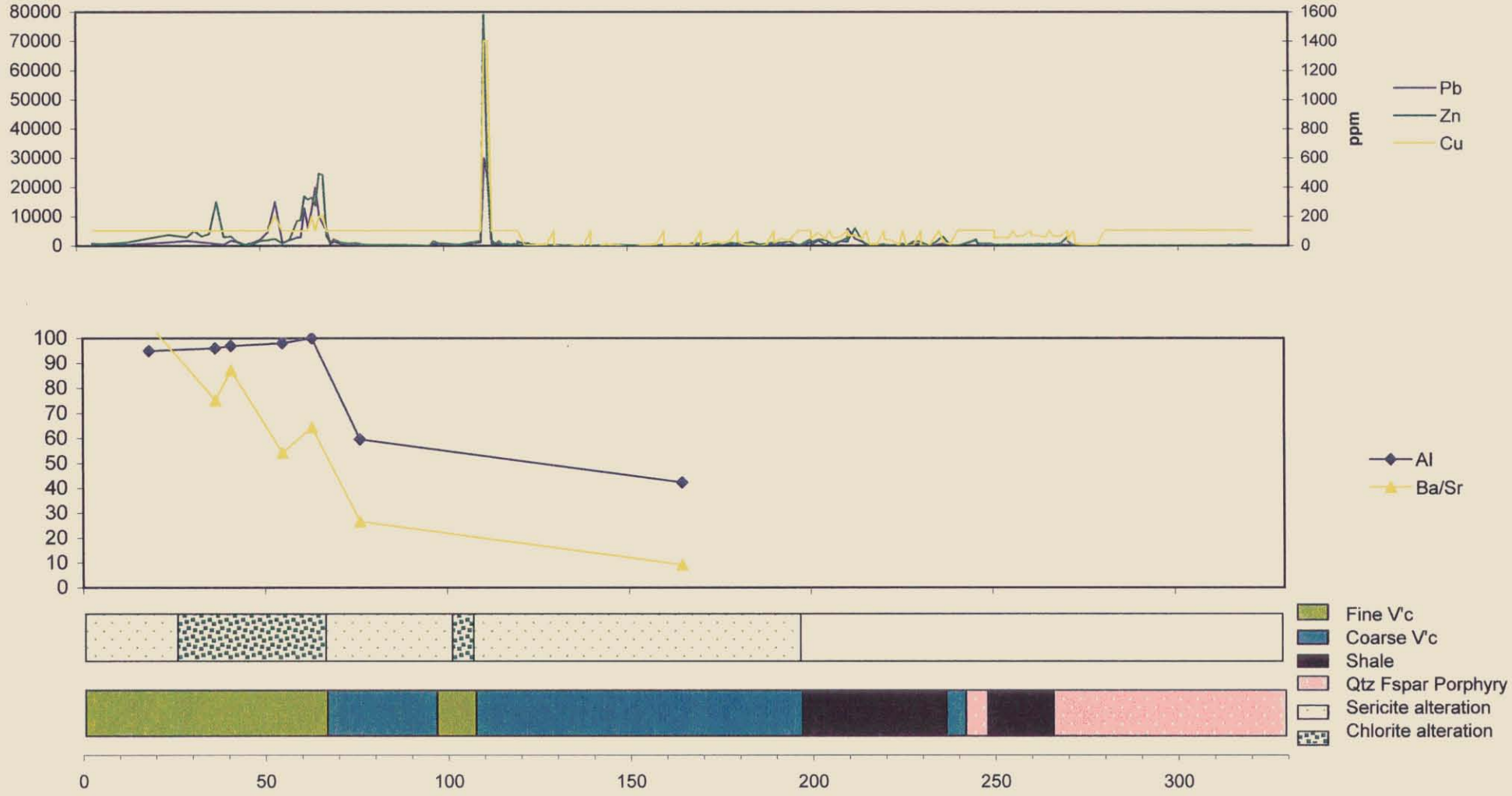

Figure 5.2 Geological and alteration logs with down hole metal assays and alteration indices for MS1

5 cm

throughout the fine volcaniclastic unit, the Ishikawa Alteration Index increases to 100 before falling sharply to 60 within the coarse volcaniclastic unit overlying the mineralised zone at 68.4m. This drop may be partially attributed to the presence of limestone clasts within the coarse volcaniclastics increasing the concentration of CaO. As CaO is in the denominator of the AI formula, the presence of carbonate as an alteration phase or as a primary constituent of the rock results in the lowering of the index. However there is clear evidence, observed petrographically and in hand specimen for a noticeable decrease in alteration intensity between these two units.

There is also a noticeable increase in Ba/Sr ratios across this boundary at 68.4m. This ratio is based on the fact that Ba substitutes for K in the muscovite structure, while Sr is depleted due to plagioclase destruction (Large et al. 1998). The large increase in Ba/Sr is not a direct effect of an increase in Ba in this case, as evident by the actual decrease in barium across this boundary (Appendix 2) but is a function of the almost complete removal of Sr from the altered, mineralised zone.

5.4.2 MS3

MS3 displays many of the same features as MS1 but due to its eastward declination and its collar location (Figure 5.1), MS3 does not intersect the Quartz Feldspar Porphyry, or the shale unit, but rather extends deeper into the stratigraphy, intersecting moderate albite + K-feldspar + chlorite alteration at depth. In figure 5.3 simplified lithological and alteration logs are illustrated along with graphs displaying metal zonation and concentration and useful major element alteration indices as indicators of hydrothermal alteration.

In MS3 there are possibly three different lithological units, consisting of coarse lithic and pumice rich volcaniclastics, fine volcaniclastic sandstone and near the end of MS3 there appears to be a gradational contact into coherent lava. This contact is masked by the presence of pervasive Na + K-feldspar + chlorite alteration that obscures the original rock texture. The alteration assemblages within the volcaniclastic units appear very similar to MS1, with pervasive sericite alteration in the ashy volcaniclastics and as an extensive diagenetic alteration phase in the coarse volcaniclastic units. Chlorite is variable throughout the sequence, but is concentrated within the fine volcaniclastic unit between 111.5 and 150m forming moderate to strong pervasive alteration. This closely correlates with the broad elevated base metal assays from this area. Just as in MS1, these elevated

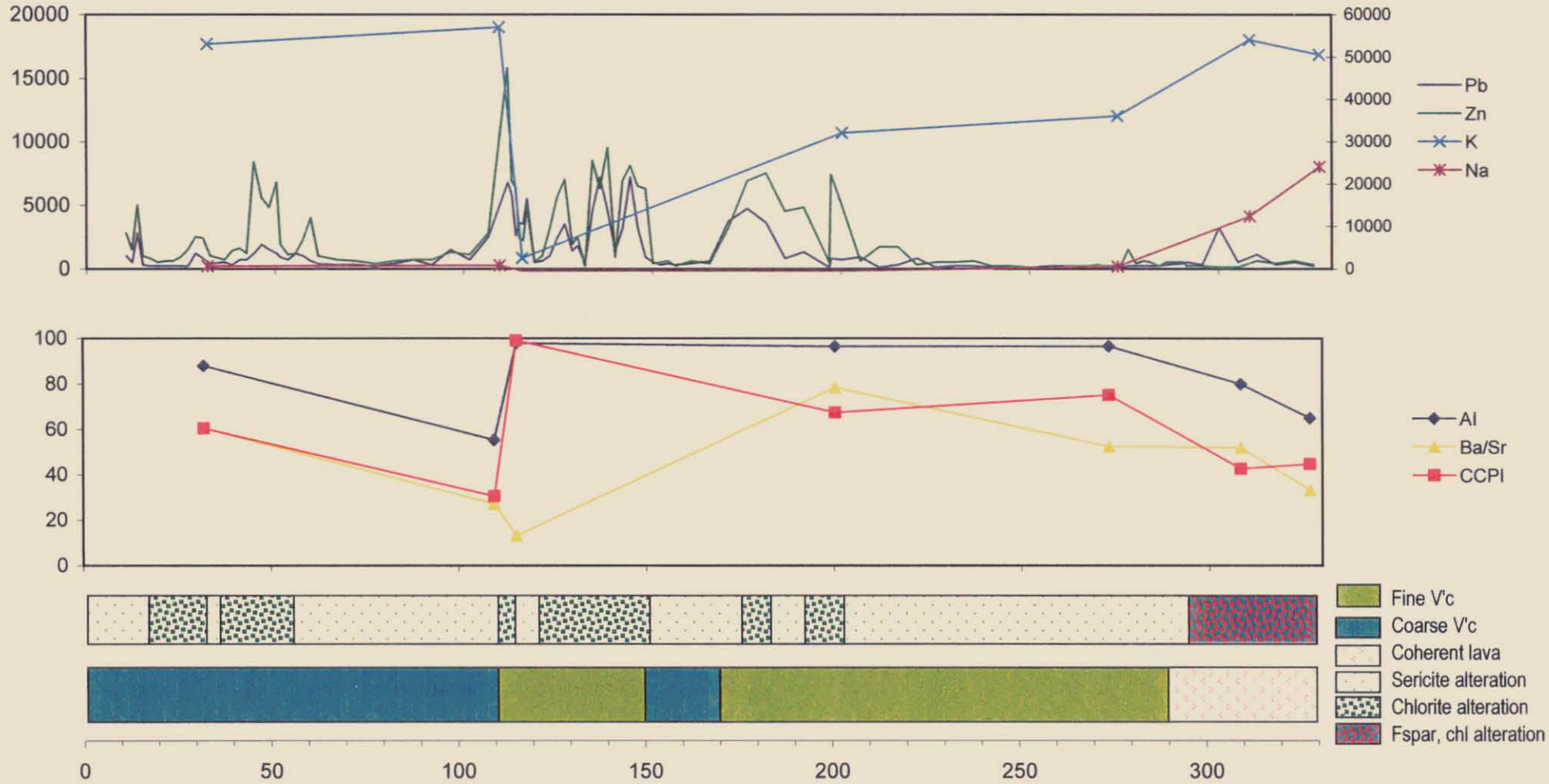

Figure 5.3 Geological and alteration logs with down hole metal assays and alteration indices for MS3.

5 cm

base metal grades, hosted in fine chlorite altered volcaniclastics, are separated by a unit of coarse volcaniclastics that contain only minor base metal concentrations. A distinct change in alteration intensity observed in handspecimen at 111.5m, is supported by a large variation in Ishikawa Alteration Index and Chlorite-Carbonate-Pyrite Index across this contact. The Alteration Index shows an increase from 55 in the coarse pumiceous volcaniclastics to 98 within the fine volcaniclastic unit indicating the destruction of feldspar and the formation of chlorite. The Chlorite-Carbonate-Pyrite Index defined by Large et al. (1998), measures the degree of chlorite, (Fe, Mg) carbonate and/or pyrite alteration. This index shows a systematic increase within the coarse volcaniclastics (from 42 to 99) to the zone of elevated base metals. The mottled feldspar chlorite altered unit at the base of the hole shows generally lower base metal concentrations with lower alteration index values of 65 to 80, associated with the increased sodium and potassium concentrations.

5.4.3 MS7

MS7 was collared in Quartz Feldspar Porphyry and intersected shale, coarse and fine volcaniclastics. Similarly to MS3 the lithologies at the base of MS7 are obscured by the presence of K-feldspar + chlorite ± magnetite and carbonate alteration assemblages that appear as strong selective and veinlet alteration. In figure 5.4 simplified lithological and alteration logs are illustrated along with graphs displaying metal distribution and Ishikawa alteration indices. Also presented are concentrations of magnesium, iron, sodium and potassium to highlight major element variations. In MS7 there are four basic rock types:

- Quartz Feldspar porphyry
- Black shale
- Coarse pumiceous, lithic rich volcaniclastic
- Fine ashy volcanic sandstone

The fine ashy volcanic sandstone is located at the base of the hole, interbedded with the coarse volcaniclastic units. However, K-feldspar + chlorite alteration makes it difficult to distinguish lithological contacts. There are three major alteration assemblages within the volcaniclastic units. Sericite is ubiquitous throughout the coarse volcaniclastic units. Chlorite is concentrated in diffuse zones within the coarse volcaniclastics associated with

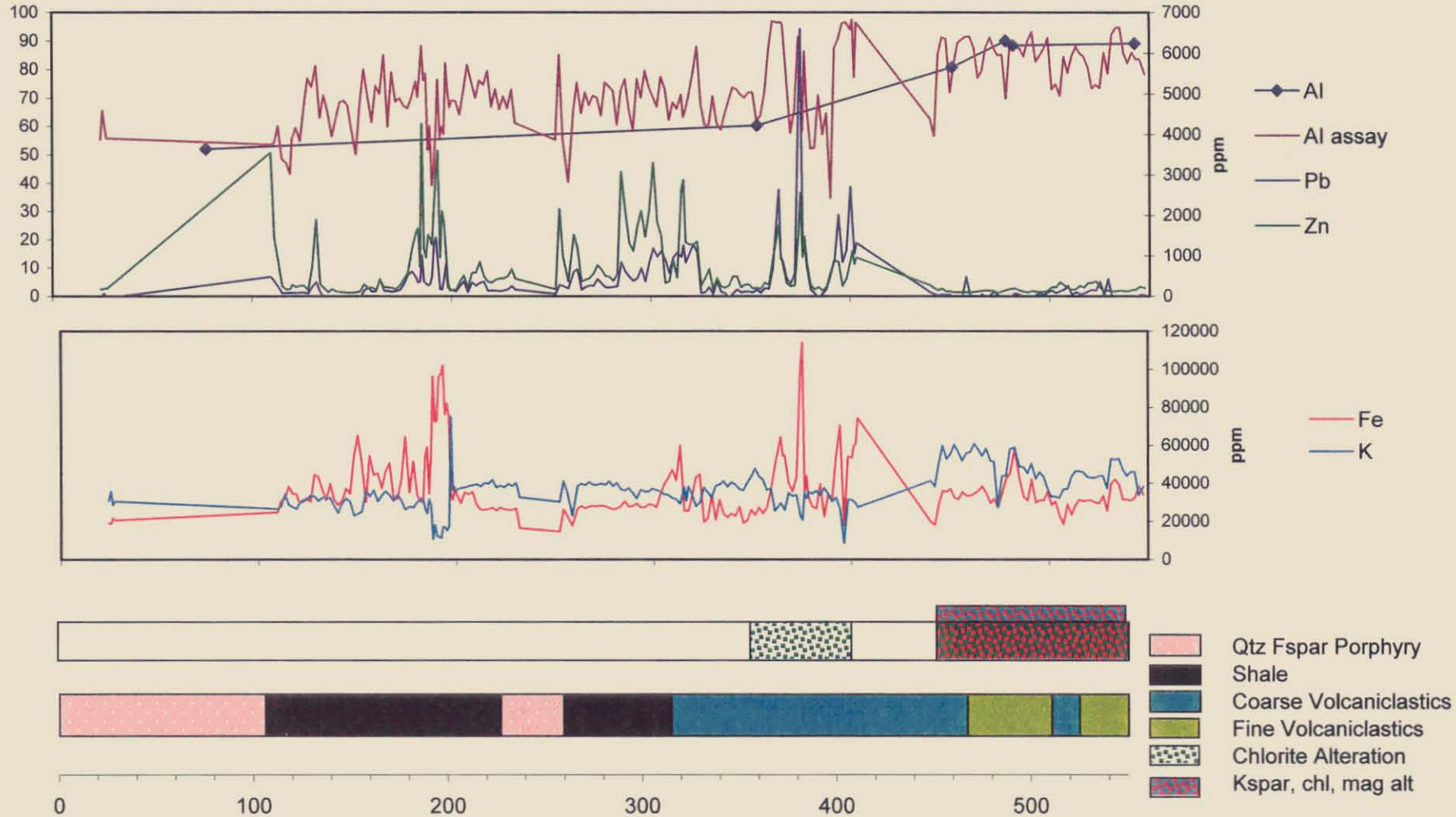

Figure 5.4 Geological and alteration logs with down hole metal assays, Al and element concentrations for MS7

5 cm

zones of elevated base metal concentrations and the K-feldspar + chlorite ± magnetite ± carbonate assemblages exist at depth.

Figure 5.4 illustrates that sulfide concentrations occur in both the shale and the coarse volcaniclastic units. Typically, sulfides in the shale unit are in discordant carbonate veins. Also evident is an association between base metal sulfide concentrations and pyrite within the shale, highlighted by the increase in total Fe within the shale. The elevated metal values between 360 and 406.8m, in the volcaniclastic unit correlate well with the concentration of chlorite alteration observed while logging. This zone is not particularly evident based on Alteration Index due to the high variability in AI. The zone of K-feldspar, chlorite ± magnetite alteration at depth contains low base metal concentrations. However, core logging indicated that chalcopyrite is slightly elevated in this zone. The addition of potassium in the form of K-feldspar is clearly evident within this zone with an increase from 3.4wt% to 4.7wt%.

5.5 Discussion

Analysis of the downhole plots for MS1, MS3 and MS7 indicate a number of interesting features. Sulfides are typically concentrated in the volcaniclastic units at the upper contacts between fine and coarse grained units, existing as fine anastomosing veinlets parallel to the contact. This style of mineralisation is characterised by an associated increase in chlorite abundance and intensity. The close association between elevated base metal results and the existence of moderate to strong chlorite alteration indicates that the two formed from the same hydrothermal fluid. The relationship between the potassic alteration observed at depth, and mineralisation/alteration is however far more diffuse. Chalcopyrite shows a slight increase within the area of K-feldspar + chlorite + magnetite, typically occurring as fine intergrowths with pyrite. This sulfide assemblage, in association with potassic, chlorite and magnetite alteration appears similar to the mineralisation associated with the emplacement of magnetite series granites as discussed in chapter 4.

Distinct differences in sulfide mineralogy occur between the felsic volcaniclastic units and the overlying shale sequence. Pyrite + sphalerite + galena are dominant sulfide species in both sequences. However, within the shale unit base metal sulfides are also associated with arsenopyrite, marcasite and pyrrhotite. In the volcaniclastic units, mineralisation is typically manifested as discordant veinlets. However, rare, small (<3cm) lenses consisting of sphalerite, galena, pyrite and chalcopyrite are also observed in MS1 and MS3. These

lenses also appear as discordant features but have been significantly recrystallised and deformed, indicating that they predate major deformation. In the shale unit, sulfides exist as bedding parallel and discordant veinlets in addition to selective replacements rimming carbonate and evaporite laminae. Sulfides within the shale also exhibit pre to syn deformational features with pyrite and arsenopyrite grains rotated into alignment with the cleavage. These early formed grains exhibit pressure shadows infilled by fibrous quartz, sparry calcite and remobilised sulfides. The existence of sulfides as veinlets and replacement features predating deformation and the common existence of remobilised sulfides indicates a combination of various processes responsible for present sulfide morphologies. Veinlet mineralisation may be a function of primary hydrothermal processes associated with a convecting fluid, analogous to VHMS mineralisation, or to fluids from a granitic source, similar to Lake Selina and Mt Jukes, with isotopic evidence (discussed later) supporting the former interpretation. However, due to remobilisation, their present morphology may be considered both a function of primary precipitation and later modification associated with deformation.

Chapter 6
Fluid Inclusions, Zinc Ratios and Isotope Geochemistry

A limited fluid inclusion and stable isotope study of the Beatrice Prospect was undertaken to investigate the source of the hydrothermal fluids responsible for the mineralised rocks observed within the prospect, and to aid in the formation of a genetic model.

Carbonate minerals existing in veins hosting sphalerite and galena within the Quartz Feldspar Porphyry, shale and volcaniclastic units were analysed for their carbon and oxygen isotopic compositions to determine the timing and isotopic composition of the fluid.

A sulfur isotopic study was conducted on the various forms of sulfides within the prospect to determine the source of sulfur, and to compare $\delta^{34}S$ values with those from other western Tasmanian deposits.

Lead isotope analyses were also conducted to determine the isotopic compositions of galena in an attempt to define the timing of mineralisation. Lead isotopes were also used in conjunction with zinc ratios (100Zn/(Zn + Pb)) to develop a genetic model.

6.1 Fluid Inclusions

6.1.1 Introduction

In this subchapter, microthermometric analyses of fluid inclusions from the Beatrice Prospect are presented. Microthermometric studies may provide information regarding the temperature, salinity, chemical composition and pressure of the mineralising fluid. The data, linked to carbon and oxygen isotope data, has been used in an attempt to determine the physio-chemical conditions and composition of the fluids responsible for mineralisation in the prospect.

This study describes and examines primary fluid inclusions from quartz obtained from bucky quartz carbonate ± chlorite sulfide veins obtained from within the Quartz Feldspar Porphyry and also fluid inclusions from sphalerite obtained from the polymetallic sulfide lenses in the volcaniclastic units.

6.1.2 Sample Preparation and methodology

Four 200μm thick doubly polished thin sections were prepared; two of mineralised (stage II) veins within the Quartz Felspar Porphyry and two from the favourable polymetallic sulfide lenses hosted in the volcaniclastic units (discussed in Chapter 5). Workable fluid inclusions where found in both mineralised vein samples but workable inclusions were only found in one of the slides taken from the small sulfide lenses. Fluid inclusions were described, classified and photographed prior to removal of the rock wafer from the glass slide by immersion in acetone. Microthermometry was performed at the University of Tasmania and Mineral Resources Tasmania.

6.1.3 Fluid Inclusion Classification

In this study, primary and secondary inclusions have been classified based on the criteria of Roedder (1984). Primary fluid inclusions are formed on growth surfaces or within surface irregularities during mineral growth. Secondary fluid inclusions are *epigenetic* and represent fluids trapped along healed fissures that may have formed at anytime after the initial crystallisation of the crystal (Roedder 1984). Due to the ambiquity in the classification of pseudosecondary fluid inclusions, all fluid inclusions of uncertain origin have been classified as secondary. Primary fluid inclusions have been further subdivided based on the observed phase relations outlined by Nash (1976) and modified by Kitto (1994) (Figure 6.1).

6.1.4 Results

Primary fluid inclusions exist in quartz either as isolated inclusions or as three-dimensional clusters typically concentrated within growth zones. Inclusions in quartz vein samples averaged 12μm and were all simple, type 1 (two-phase) inclusions with liquid-vapour ratios between 10 and 30%. Secondary fluid inclusions typically exist along two-dimensional planar structures, defining healed fractures. Secondary inclusions were also simple type 1 inclusions but were typically smaller than primary inclusions (<8μm). Microthermometric measurements were determined only from primary fluid inclusions.

Twenty-four workable primary fluid inclusions were obtained from clear quartz grains in the stage II bucky quartz, carbonate ± sulfide veins that bisect the quartz feldspar porphyry body (Plates 6.1 and 6.2). Due to the inherent change in optical properties during heating and freezing runs, the collection of all three microthermometric standards (T_e=eutectic,

INCLUSION TYPE		PHASES AT 25°C	HOMOGENISATION BEHAVIOUR
Type 1A	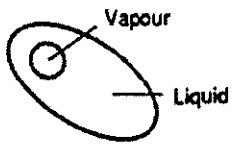	Liquid + vapour	Vapour disappears
Type 1B	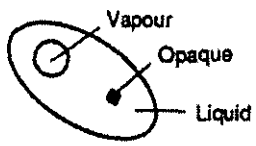	Liquid + vapour + opaque	Vapour disappears
Type 2	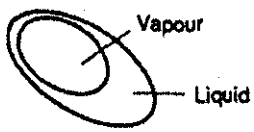	Vapour + liquid	Critical Behaviour
Type 3AD	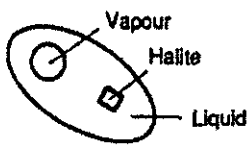	Liquid + vapour + halite (± other daughters)	Vapour disappears
Type 3BV	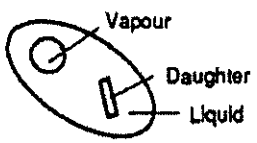	Liquid + vapour + daughter(s) (1 - 5)	Vapour disappears
Type 4	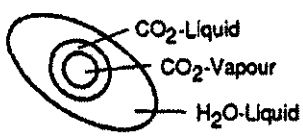	CO_2-liquid + CO_2-vapour + H_2O-liquid	CO_2 disappears
Type 5		Single phase	N.A.

Figure 6.1 Classification of fluid inclusion types observed at room temperature (after Nash 1976 and Kitto 1994).

$T_{m(ice)}$=final ice melting and T_h= homogenisation temperatures) could not be obtained for each sample. Table 6.1 and figure 6.2 illustrate the range of temperatures and salinities obtained from primary fluid inclusions. Two discrete fluid inclusion populations were defined by this study.

	Population I	**Population II**
n	21	3
Th range °C	114 to 168	263 to 276
Th mean °C	148	268
Tm(ice) range °C	-1.9 to -14.9	-7.6 to -12.1
Tm(ice) mean °C	-8.6	-9.7
Salinity range eq. wt%	3.2 to 16.6	11.2 to 16.1
Salinity mean eq. wt%	12.1	13.5
Te range °C	-38.9 to -53.6	-
Te mean °C	-46.0	-

Table 6.1 Summary of primary fluid inclusion populations observed in quartz in Quartz Feldspar Porphyry hosted mineralised veins.

Population one primary inclusions give a range of homogenisation temperatures between 114 and 168°C (mean 148°C), final ice melting temperatures ($T_{m(ice)}$) between –1.9 to –14.9°C giving a range of salinity estimates between 3.2 to 18.6 eq. wt% NaCl. Eutectic temperatures in Population One primary inclusions varied from -38.9 to -53.6°C (mean –45.9°C). The second population of three primary fluid inclusions gives a tightly constrained range of homogenisation temperatures between 263 and 276°C, final ice melting temperatures ($T_{m(ice)}$) between –7.6 and –12.1°C yielding a range of salinity estimates between 11.2 to 16.1 eq. wt% NaCl. No eutectic temperatures were obtained for Population Two fluid inclusions.

Six primary fluid inclusions were found in sphalerite in the sulfide rich zone in sample MH3-10. Three of the inclusions contained daughter crystals, composed of carbonate and/or equant cubic crystals, possibly halite. These Type 3BV inclusions exist typically as angular, large (~20μm) negative crystal inclusions. (Plate 6.3). Due to the opacity of the dark red/brown sphalerite and the reduced optical clarity, the internal phases within these primary inclusions, although clearly evident during petrographic analysis could not be observed during microthermometric analysis at Mineral Resources Tasmania. As a result the study has been restricted to the late stage veins and may not elucidate the nature of fluids responsible for mineralisation within the underlying volcaniclastics and shale.

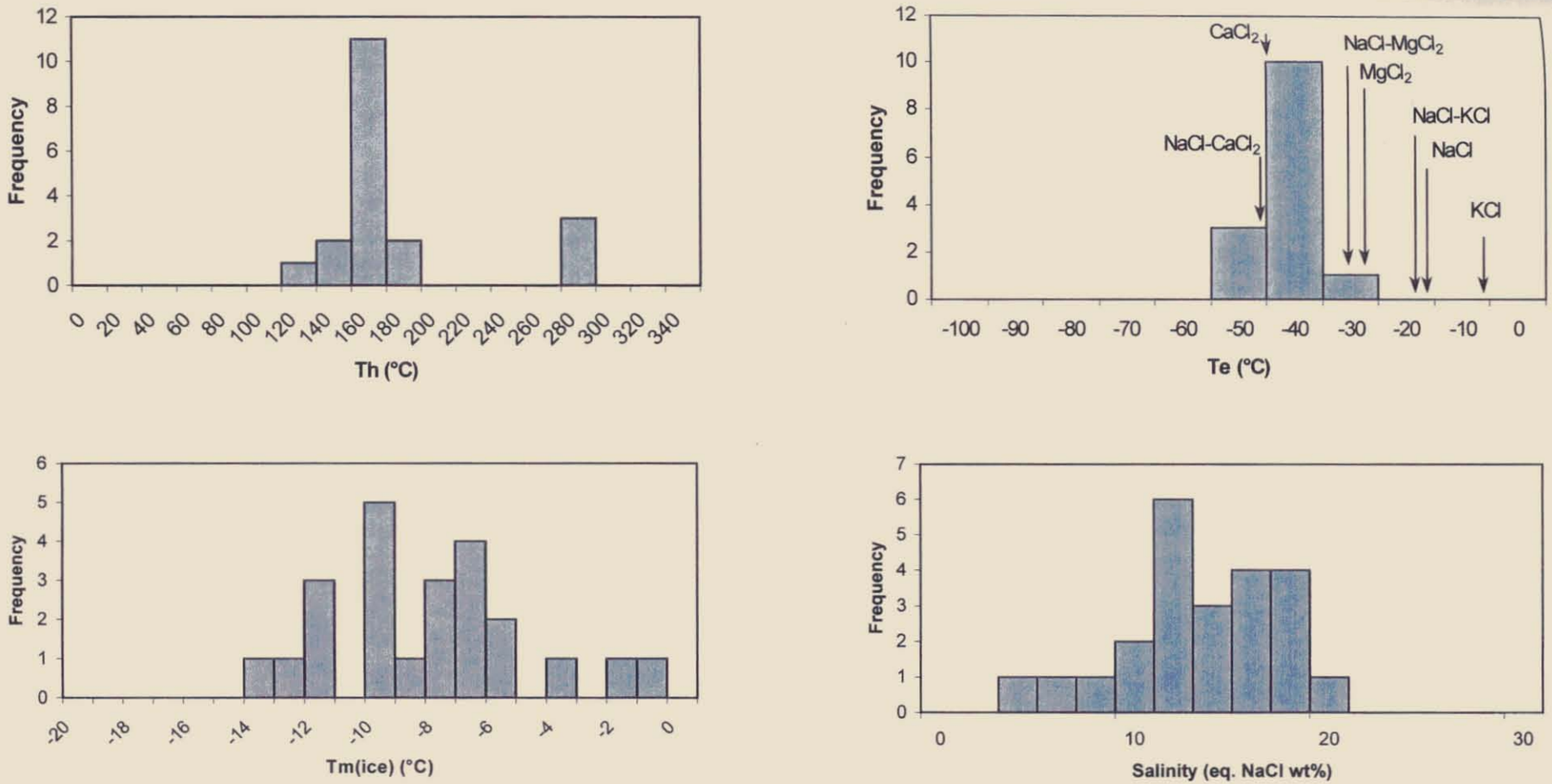

Figure 6.2 Histograms for primary fluid inclusion data obtained from quartz crystals within bucky quartz, carbonate veins within the Quartz Feldspar Porphyry. A) Temperatures of homogenisation. B) Eutectic melting temperatures with principle fluid components. Te for various dissolved salts taken from Zaw and Cooke (1997). C) Final ice melting temperature. D) Calculated salinity in equivalent wt % NaCl.

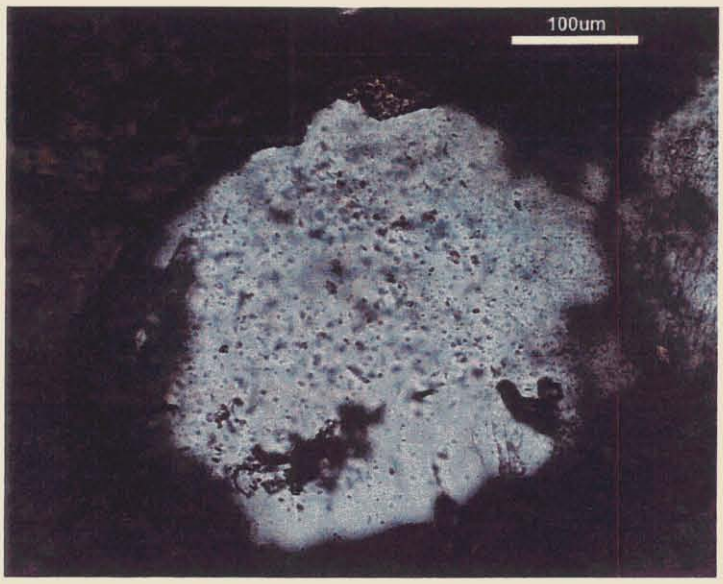

Plate 6.1: Photomicrograph of clear quartz grain hosted in a quartz + carbonate + sphalerite vein within the Quartz Feldspar Porphyry. The quartz grain contains abundant primary and secondary Type 1 fluid inclusions.

Photo taken in plane polarised light.

Sample MH4-11

Plate 6.2: Photomicrograph of a Type 1, primary fluid inclusion within quartz.

Photo taken in cross polarised light.

Sample MH4-11

Plate 6.3: Large Type 3 primary fluid inclusion in sphalerite, existing in oneof the small polymetallic lenses. Note the large rhombic daughter crystal (C), and two small daughters (D) of indeterminate composition.

Photo taken in plane polarised light.

Sample MH3-16

6.1.5 Discussion

The well-formed primary inclusions in sphalerite are clearly of great interest, as this reflects the preserved mineralising fluid trapped within its precipitated host. The study of these observed primary inclusions should be of high priority as the temperature and composition of the mineralising fluid may be determined, it is therefore strongly recommended that further analysis of these inclusions occur using higher quality optics.

Microthermometry analyses of fluid inclusions within the bucky quartz, carbonate ± sulfides veins indicate the possibility of two fluid types present within these late vein generations. Analysis of primary fluid inclusions suggests that mineral preciptiation and sulfide deposition within these veins occurred from a low temperature (110 to 170°C), moderate to high salinity fluid. Average eutectic temperatures (-45.9°C) indicate a fluid composition containing significant quantities of Ca in addition to K, Na, Cl and H_2O. Kharaka et al. (1987) infer that the presence of Ca rich saline fluids may in part be attributed to fluid fluxing through a sedimentary basin containing evaporite and carbonate sequences; both are present in the shale unit which underlies the Quartz Feldspar Porphyry.

The analysis of three primary, Type 1, two phase inclusions gave similar salinity estimates but significantly higher temperatures, (between 263 and 276°C). As these fluid inclusions exist within the same grain as many of the lower temperature inclusions these higher temperature inclusions possibly represent a second type of fluid, however these inclusions are ambiguous and may possibly be secondary inclusions.

Khin Zaw (1991) and Khin Zaw and Large (1992) recognised two fluid types based on inclusion populations within the South Hercules VHMS deposit: a low temperature (125-210°C), low salinity (<4.2 NaCl eq. wt%) fluid, and a variable temperature (125-300°C), higher salinity (up to 15.0 NaCl eq. wt%), CO_2 bearing fluid. The low temperature, low salinity fluids were interpreted as Cambrian fluids of volcanic origin and the cross cutting high salinity fluids were interpreted as inclusions trapped during Devonian metamorphism. The presence of two groups of apparent primary inclusions in bucky quartz carbonate veins in the Quartz Feldspar Porphyry at Beatrice, suggests that precipitation occurred either from:

1) A relatively low temperature, high salinity fluid and later higher temperature fluids possibly associated with deformation.

or:

2) A single high salinity, variable temperature, fluid associated with Devonian metamorphism.

The first interpretation is possible if, like South Hercules, a lower temperature fluid was responsible for mineralisation during the Cambrian. However, unlike South Hercules, such a fluid may have reached significantly higher salinities due to passing through the underlying shale unit, obtaining salts (particularly CaCl) by either shale membrane filtration (Taylor 1979), or through interaction with evaporites. The second interpretation, relating veining and a variable hydrothermal fluid to Devonian deformation, appears the most likely based on textural evidence. The morphology and mineralogy of these vein generations appear similar to that described elsewhere in the region, ie Hellyer (Gemmell and Large 1992), suggesting that the bucky quartz carbonate veins were a late feature, associated with metamorphism.

6.2 Carbon and Oxygen Isotopes

6.2.1 Analytical Techniques

Carbonate materials suitable for carbon/oxygen isotope analysis exist as clasts in the volcaniclastic unit, thin beds in the shale unit and in stage 1-4 veins in the Quartz Feldspar Porphyry. Samples of about 25mg of carbonate (calcite) were hand drilled from veins, clasts and beds. The isotopic compositions of carbon and oxygen for the fifteen samples were analysed using a SIRA series 2, VG isogas stable isotope mass spectrometer at the Central Science Laboratory at the University of Tasmania. Carbonate minerals were first reacted with H_3PO_4 at 25°C for 12 hours to liberate CO_2 as described by McCrea (1950). Results are expressed in the standard δ (‰) notation relative to SMOW (Standard Mean Ocean Seawater) for oxygen and the PDB (Belemnite of the Cretaceous PeeDee Formation) standard for carbon.

6.2.2 Results

Carbon and oxygen isotope results are presented in Appendix 5 and summarised in Table 6.2. The nine $\delta^{18}O_{(SMOW)}$ values of vein carbonate form a tight cluster between 9.0 and 12.7‰ (mean = 10.4‰) and $\delta^{13}C_{(PDB)}$ values between –3.3 to –5.7‰ (mean = -4.3‰). The three carbonate analyses taken from carbonate beds give similar results with $\delta^{18}O_{(SMOW)}$ values of 10.6 to 12.1‰ and $\delta^{13}C_{(PCB)}$ values between –3.8 and –5.8‰.

Sample	Description	Vein stage	^{18}O(SMOW)	^{13}C(PDB)
MH30	Siderite alteration		15.90	-3.43
MS2 MH2	vein	?	10.44	-4.00
MS1 MH11	vein	1	10.89	-3.29
MS3 MH4	vein	?	10.33	-4.34
MS5 MH3	bed		12.11	-5.81
MS6 MH1	vein	2	9.00	-3.21
MS7 MH7	Siderite alteration		13.14	-2.62
MS7 MH17	clast		10.37	-0.83
MS8 MH2	vein	?	9.00	-4.36
MS8 MH3	vein	3	10.98	-5.71
MS8 MH4a	vein	2	10.43	-4.38
MS8 MH4b	vein	1	9.90	-3.40
MS8 MH12a	bed		11.44	-4.73
MS8 MH12b	vein	?	12.75	-5.57
MS8 MH14	bed		10.63	-3.76

Table 6.2 $\delta^{13}C_{(PCB)}$ and $\delta^{18}O_{(SMOW)}$ compositions of carbonates.

The results from carbon and oxygen isotope analyses are illustrated in a $\delta^{13}C_{(PCB)}$ - $\delta^{18}O_{(SMOW)}$ co-variance diagram (Figure 6.3), showing a vague negative trend for the Quartz Feldspar Porphyry hosted calcite veins and beds within the shale unit. Analyses taken from limestone clasts and manganoan siderite alteration plot as separate fields. Figure 6.4 shows the same data relative to the carbonate fields defined by Khin Zaw (1991).

The isotopic difference between a fluid, and a mineral precipitated from the fluid, is referred to as fractionation. Equilibrium fractionation in carbon/oxygen isotopes may occur in response to changes in fluid pH, fO_2 and salinity, however, the most common cause is a change in temperature. Carbon isotope systems are complicated by factors such as changes in speciation that may produce disequilibrium fractionation. Based on the minimum temperature estimate (112°C) derived from fluid inclusion analyses of carbonate veins (MH1-11 and MH4-11) within the Quartz Feldspar Porphyry, it is reasonably assumed that HCO_3^- was negligible and H_2CO_3 was the dominant carbon species (Davidson 1997). The calculation of initial fluid compositions were based on the following equations:

Equation	Reference
$1000\ 1\alpha n\ (CaCO_3 - CO_2) = -3.63 + 1.194(10^6T^{-2})$	Deines et al. 1974 in Longstaff 1988
$1000\ 1\alpha(H_2CO_{3(aq)} - CO_2) = -0.91 + 0.0063(10^6T^{-2})$	Deines et al. 1974 in Longstaff 1988
$1000\ 1\alpha$(calcite – water) = 2.78 x 106T-2 –2.89	Freidman and O'Neil (1977) after O'Neil et al. (1969)

Table 6.3 Equations for the calculation of initial fluid compositions.

Table 6.4 is provided as an example of the method of calculating initial fluid compositions based on known temperatures and isotopic ratios of the precipitated carbonate species. On the basis of temperatures estimated from the low temperature fluid inclusions (mean = 148°C), the calculated $\delta^{13}C$ of the fluid responsible for the precipitation of stage 1-4 quartz carbonate veins ranges from -7.6 to –10.0‰; the $\delta^{18}O$ values of the fluid are negative with values ranging from –0.8 to – 4.5‰. The $\delta^{13}C$ and $\delta^{18}O$ of the fluid calculated from the average of the three higher temperature fluid inclusions (mean = 268°C) gave $\delta^{13}C$ of the fluid as –3.7 to –6.2‰ and $\delta^{18}O$ values from +2.4 to +6.1‰.

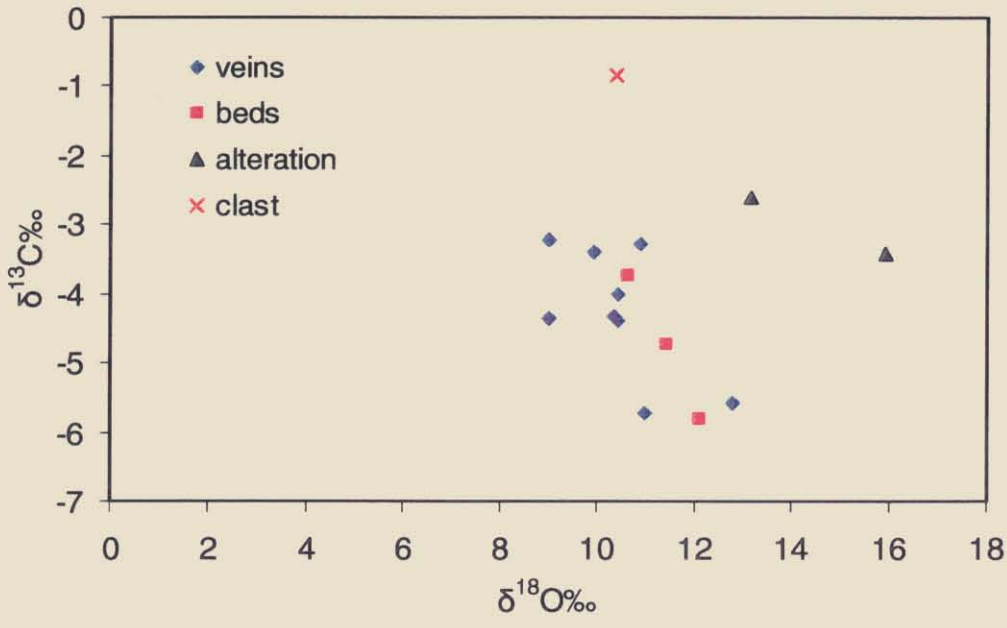

Figure 6.3 Carbon/oxygen isotope compositions of carbonates obtained from the Beatrice Prospect

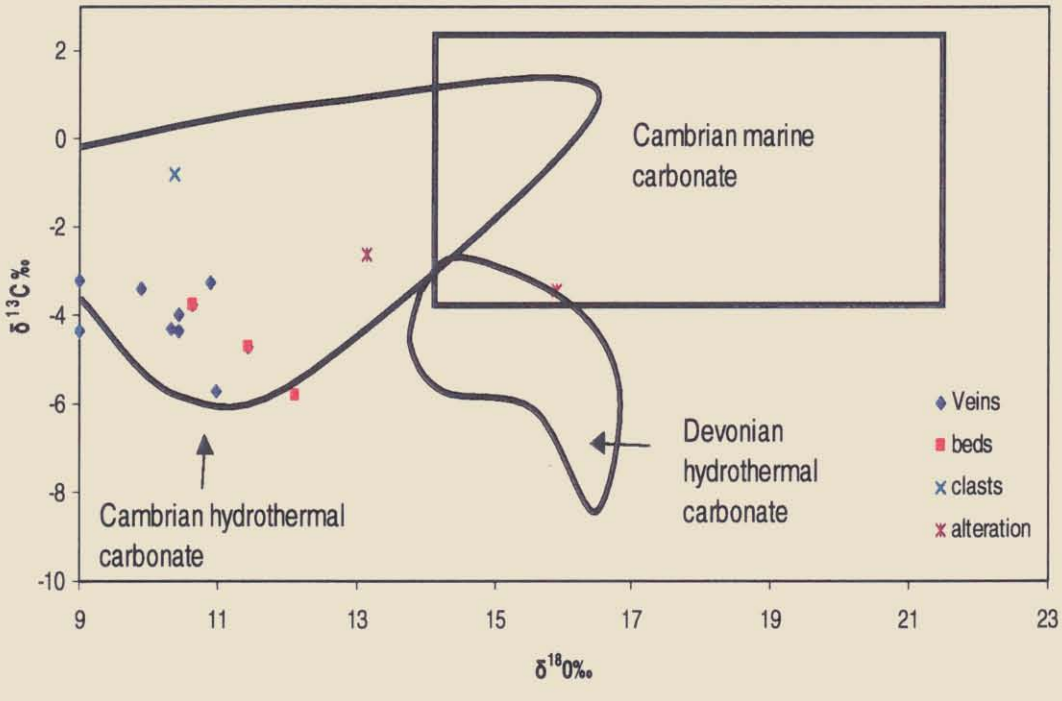

Figure 6.4 Carbon/oxygen isotopic compositons of Beatrice samples with general fields of carbonates (modified from Khin Zaw 1991).

Calculation of initial carbon isotopic composition of an H2CO3 dominant fluid

1) $1000\ 1\alpha n\ (CaCO_3 - CO_2) = -3.63 + 1.194(10^6T^{-2})$
   $\therefore \delta^{13}C_{(calcite)} - \delta^{13}C_{(CO2)} = -3.63 + 1.194(10^6T^{-2})$
   $\therefore \delta^{13}C_{(CO2)} = \delta^{13}C_{(calcite)} - (-3.63 + 1.194(10^6T^{-2}))$
2) $1000\ 1\alpha(H_2CO_{3(aq)} - CO_2) = -0.91 + 0.0063(10^6T^{-2})$
   $\therefore \delta^{13}C_{(H2CO3(aq)-CO2)} = -0.91 + 0.0063(10^6T^{-2})$
   $\therefore \delta^{13}C_{H2CO3(aq)} = -0.91 + 0.0063(10^6T^{-2}) + \delta^{13}C_{(CO2)}$

Tmin = 387K, $\delta^{13}C_{(calcite)} = -3.289$

$\delta^{13}C_{(CO2)} = \delta^{13}C_{(calcite)} - (-3.63 + 1.194(10^6T^{-2}))$
$\therefore \delta^{13}C_{(CO2)} = -3.289 - (-3.63 + 1.194(10^6T^{-2}))$
$\therefore \delta^{13}C_{(CO2)} = -7.6‰$

$\delta^{13}C_{H2CO3(aq)} = -0.91 + 0.0063(10^6T^{-2}) + \delta^{13}C_{(CO2)}$
$\therefore \delta^{13}C_{H2CO3(aq)} = -0.91 + 0.0063(10^6T^{-2}) - 7.6$
$\therefore \delta^{13}C_{H2CO3(aq)} = -8.5‰$

Tmax = 441K, $\delta^{13}C_{(calcite)} = -3.289$

$\delta^{13}C_{(CO2)} = \delta^{13}C_{(calcite)} - (-3.63 + 1.194(10^6T^{-2}))$
$\therefore \delta^{13}C_{(CO2)} = -3.289 - (-3.63 + 1.194(10^6T^{-2}))$
$\therefore \delta^{13}C_{(CO2)} = -5.8‰$

$\delta^{13}C_{H2CO3(aq)} = -0.91 + 0.0063(10^6T^{-2}) + \delta^{13}C_{(CO2)}$
$\therefore \delta^{13}C_{H2CO3(aq)} = -0.91 + 0.0063(10^6T^{-2}) - 5.8$
$\therefore \delta^{13}C_{H2CO3(aq)} = -6.7‰$ (Range: $\delta^{13}C_{H2CO3(aq)} = -6.7$ to $-8.5‰$)

Calculation of initial oxygen isotopic composition of fluid

1) $1000\ 1\alpha(\text{calcite} - \text{water}) = 2.78 \times 10^6T^{-2} - 2.89$
   $\therefore \delta^{18}O_{(calcite)} - \delta^{18}O_{(water)} = 2.78 \times 10^6T^{-2} - 2.89$
   $\therefore \delta^{18}O_{(water)} = \delta^{18}O_{(calcite)} - (2.78 \times 10^6T^{-2}) + 2.89$

Tmin = 387K, $\delta^{18}O_{(calcite)} = 10.891$

$\delta^{18}O_{(water)} = \delta^{18}O_{(calcite)} - (2.78 \times 10^6T^{-2}) + 2.89$
$\therefore \delta^{18}O_{(water)} = 10.891 - (2.78 \times 10^6T^{-2}) + 2.89$
$\therefore \delta^{18}O_{(water)} = -4.8‰$

Tmax = 441K, $\delta^{18}O_{(calcite)} = 10.891$

$\delta^{18}O_{(water)} = \delta^{18}O_{(calcite)} - (2.78 \times 10^6T^{-2}) + 2.89$
$\therefore \delta^{18}O_{(water)} = 10.891 - (2.78 \times 10^6T^{-2}) + 2.8$
$\therefore \delta^{18}O_{(water)} = -0.5‰$ (Range: $\delta^{18}O_{(water)} = -0.5$ to $-4.8‰$)

Table 6.4 The calculation of initial isotopic composition of the fluid based on $\delta^{13}C + \delta^{18}O_{(calcite)}$.

6.2.3 Discussion

As the two siderite samples could not be constrained by paragenetic studies they have been excluded from interpretations. Interpretations are therefore only applicable to carbonate veins constrained by fluid inclusions from stage 1-4 veins within the Quartz Feldspar Porphyry. The $\delta^{13}C$ and $\delta^{18}O$ values of calcite are tightly clustered, displaying a vague negative trend, within the field of Cambrian hydrothermal carbonates as defined by Khin Zaw (1991). In general terms, the variation in $\delta^{13}C$ and $\delta^{18}O$ values of carbonate in a system may be a function of temperature, but may also be attributed to changes in carbon speciation, fluid mixing and wall-rock interaction (Ohmoto and Rye 1979). However, the $\delta^{13}C$ and $\delta^{18}O$ compositions of carbonates precipitated from a fluid of constant composition along a cooling temperature gradient would produce a positive coupled trend lying along the slope outlined by Peter (1986). Conversely, Zheng and Hoefs (1993) indicates that fluid mixing and water/rock interaction are the most viable means of producing negatively coupled O-C trends, such as this dataset. The observations of two fluid inclusion populations within calcite veins in the porphyry may be evidence for the mixing of separate fluid sources.

The calculated initial $\delta^{13}C$ and $\delta^{18}O$ composition for the fluid provide significant insight into the likely sources and hence genetic implications for the carbonate veins within the prospect. The light fluid $\delta^{13}C$ and $\delta^{18}O$ values (-7.6 to –10.0‰ and –0.8 to – 4.5‰, respectively), calculated from population I fluid inclusion temperature estimates, are consistent with meteoric or basinal waters. However, the heavier fluid $\delta^{13}C$ and $\delta^{18}O$ isotopic values (–4.7 to –7.0‰ and +2.4 to +6.1‰ respectively) derived from the higher temperature fluid inclusion data (~268°C) correlate closely with Devonian magmatic/metamorphic hydrothermal fluids of about -6‰ $\delta^{13}C$ and +7‰ $\delta^{18}O$ calculated by Kitto (1994).

Calculated $\delta^{13}C$ and $\delta^{18}O$ values from fluid inclusion Population I and fluid inclusion salinity data suggest a possible similarity to fluids that produce Mississippi Valley Type mineralisation. The $\delta^{18}O$ values of ore stage fluids in MVT style mineralisation tend to be ~ 0‰ with fluids accompanying late stages of mineralisation commonly showing a decrease in $\delta^{18}O$ and salinity. These characteristics are interpreted to be due to dilution of brines by meteoric water (Taylor 1979). In MVT style mineralisation, meteoric fluids become saline during migration through sediments, by both ion exchange-shale membrane

filtration and through interaction with evaporites, acquiring both salt and sulfur (Taylor 1979). The high salinity recorded from mineralised veins in the Quartz Feldspar Porphyry may be attributed to dewatering of the volcaniclastic sediments and shale units. This was possibly driven by the compaction and/or lithostatic pressure exerted by the emplacement of the large quartz feldspar body, as opposed to the convection of brines being driven by sediment compaction in sedimentary basins as described by Beales (1967).

The heavier fluid $\delta^{13}C$ and $\delta^{18}O$ isotopic values (–3.7 to –6.2‰ and +2.4 to +6.1‰ respectively) derived from the higher temperature population II fluid inclusion data (~268°C) correlate closely with Devonian magmatic/metamorphic hydrothermal fluids of about -6‰ $\delta^{13}C$ and +7‰ $\delta^{18}O$ calculated by Kitto (1994). Figure 6.5 displays the carbon and oxygen isotope data obtained from the Beatrice Prospect in addition to the modeled water-rock interaction curve from the equations of Zengh and Hoefs (1993).

$$\delta^{13}C_{calcite} = (\delta^{13}C^{i}_{H2CO3} + \Delta^{13}C^{calcite}_{H2CO3}) - (\delta^{13}C^{i}_{H2CO3} + \Delta^{13}C^{calcite}_{H2CO3} - \delta^{13}C^{i}_{calcite}).e\text{-}(W/R.X_{H2CO3})$$

$$\delta^{18}O_{calcite} = (\delta^{18}O^{i}_{H2O} + \Delta^{18}O^{calcite}_{H2O}) - (\delta^{18}O^{i}_{H2O} + \Delta^{18}O^{calcite}_{H2O} - \delta^{18}O^{i}_{calcite}).e\text{-}W/R$$

where $\delta^{13}C^{i}_{H2CO3}$ = initial $\delta^{13}C$ of hydrothermal fluid.

$\delta^{13}C^{i}_{calcite}$ = initial $\delta^{13}C$ of the rock.

W/R = water rock ratio.

X_{H2CO3}) = mole fraction $H2CO_3$

$\delta^{18}O^{i}_{H2O}$ = initial $\delta^{18}O$ of hydrothermal fluid.

$\delta^{18}O^{i}_{calcite}$ = initial $\delta^{18}O$ of the rock.

$\Delta^{13}C^{calcite}_{H2CO3}$ = equilibrium fractionation factor between calcite and H_2CO_3

$\Delta^{18}O^{calcite}_{H2O}$ = equilibrium fractionation factor between calcite and H_2O.

The modelled data is based on the temperature obtained from population II fluid inclusions and associated calculated $\delta^{13}C$ and $\delta^{18}O$ values as these more likely represent the peak values in the system. The interaction between this magmatic/metamorphic fluid and the felsic host rock (assumed $\delta^{13}C$ of –8 and $\delta^{18}O$ of +12) may produce a negative trend and appears to fit the observed data. The position of observed $\delta^{13}C$ and $\delta^{18}O$ data at high water/rock ratios is consistent for vein carbonates, as interaction between the fluid and host rocks would be minimal. The curve however, is modeled on a $\delta^{13}C$ isotopic composition slightly heavier than typical fresh igneous rocks. However, the modeled data does show

that negative slopes may be achieved for $\delta^{13}C$ and $\delta^{18}O$ values based on the interaction between magmatic/metamorphic fluids and felsic host rocks.

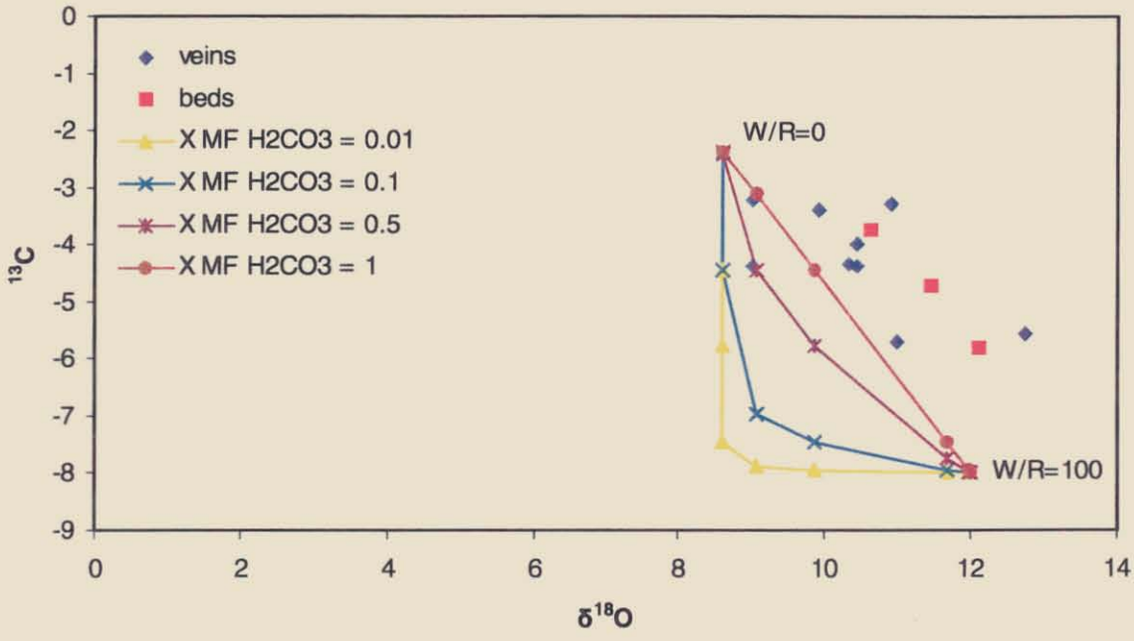

Figure 6.5 Carbon and Oxygen stable isotopes from bedded and veinlet carbonates from the Beatrice Prospect. Modelled carbon and oxygen isotope data is from the equations of Zengh and Hoefs (1993) for a fluid rock interation between a hydrothermal fluid and felsic host rocks.

Although the second interpretation regarding the formation of bucky quartz carbonate veins is based on the smaller fluid inclusion dataset, this interpretation is supported by observations in drill core logging, that veins are mineralogically similar to the regionally distributed late veining associated with Devonian deformation.

6.3 Sulfur Isotopes

6.3.1 Introduction

Studies in sulfur isotope geochemistry have become an integral part of the investigation into sulfide deposit genesis. Variations in sulfur isotope analyses have been used to determine temperatures of sulfide deposition, source of metals and sulfur, and the physiochemical conditions and mechanisms prevailing during sulfide deposition. Studies by Solomon et al. (1988) and Gemmell and Large (1992) on the Mount Read Volcanics have shown that VHMS deposits have a sulfur isotope signature that reflects the supply of sulfur from a combination of reduced seawater sulfate and from volcanic rock sources, resulting in $\delta^{34}S$ values ranging between +5‰ and +20‰.

In this study, a sulfur isotope investigation was undertaken to identify the source of sulfur from base metals within the Beatrice Prospect and to compare them with other values recorded within the Mount Read Volcanics. In addition, the variations of sulfur isotope values within mixed sulfide assemblages were investigated in an attempt to calculate temperatures of deposition.

6.3.2. Sampling and Analytical Techniques

Twenty three analyses taken from eleven samples within the Beatrice Prospect were analysed under the supervision of Keith Harris at the CSL, University of Tasmania using the laser ablation sulfur isotope mass spectrometer analytical method described by Huston et al. (1992). This method involves the generation of SO_2 gas from the ablation of sulfide minerals using an 18 watt Quantronix model 117 Nd:YAG laser. The ablation process liberates SO_2 from a circular area roughly 150-200μm wide and 150μm thick. After cryogenic cleaning the ionic abundance of the SO_2 gas was measured using a VG SIRA Series 11 mass spectrometer.

6.3.3. Results

Table 6.5 lists the mineral, sample description and results of the twenty-three sulfur isotope analyses. The samples were taken from a variety of mineralisation forms, including two small lenses of sphalerite-galena-pyrite hosted within volcaniclastics intersected by MS3. Also included are veinlet sphalerite, pyrite and galena hosted within volcaniclastics and veinlet pyrite, sphalerite, galena and pyrrhotite and pyrite pseudomorphs of gypsum in shale (Chapter 3.2).

Sample ID	Mineral	Discription	$\delta^{34}S$ value
3-10	py	Euhedral pyrite in polymetallic lens	13.7
3-10	gn	anhedral galena in polymetallic lens	14.0
3-10	sph	anhedral sphalerite in polymetallic lens	15.7
3-16	py	Euhedral pyrite in polymetallic lens	12.4
3-16	gn	anhedral galena in polymetallic lens	11.6
3-16	sph	anhedral sphalerite in polymetallic lens	13.8
4-1	py	Euhedral vein controlled inclusion-rich pyrite in black shale	6.3
4-1	sph	sphalerite in shale hosted carbonate veinlet	9.7
MH39	sph	veinlet sphalerite in chloritic volcaniclastic	17.2
MH6	sph	anhedral sphalerite from outcropping vein	19.9
T36721*	py		15.8
T36722*	py		14.9
T36720*	py		15.8
MH38	sph	veinlet anhedral sphalerite in chloritic volcaniclastic	21.5
7-7	py	Euhedral pyrite in coarse volcaniclastic	20.4
7-7	gn	veinlet anhedral galena in coarse volcaniclastic	19.4
8-15	sph	sphalerite replacing clast in shale hosted mass flow	19.6
8-15	py	veinlet pyrite in shale hosted mass flow	12.1
8-10	sph	veinlet sphalerite in shale hosted carbonate bed	25.7
8-10	py	euhedral inclusion rich pyrite in shale hosted veinlet	33.0
8-10	gn	veinlet galena in shale hosted carbonate bed	30.6
4-11	sph	sphalerite in bucky quartz-carbonate vein in QFP	22.9
4-11	gn	galena in bucky quartz-carbonate vein in QFP	14.6
8-11	py	pyrite pseudomorphs after gypsum in shale	31.0
8-11	pø	pyrrhotite in bedding parallel vein	30.3

* RGC data

Table 6.5 Sulfur isotope sample description and results

Sulfur isotope analyses from the various sulfide species and styles of mineralisation have been plotted in Figures 6.6 and 6.7. The overall mean for the entire $\delta^{34}S$ data set is 18.3‰ with a broad standard deviation of 6.99. The polymetallic sulfide lens has a mean $\delta^{34}S$ value of 13.5‰ with a small standard deviation of 1.39. Veinlet mineralisation within the volcaniclastics has a higher mean $\delta^{34}S$ value and standard deviation (18.9‰ and 2.31) and the results from veinlet and bedded samples hosted within shale showed the highest mean $\delta^{34}S$ value (22.0‰) and highly variable population with standard deviations of 10.38.

6.3.4 Geothermometry

The analysis of isotopic values associated with various mineralisation styles and sulfide species was attempted to constrain mineralisation style, source of sulfur and temperature of formation.

As fractionation of $\delta^{34}S$ between coexisting sulfide phases is, in part, a function of temperature, a temperature estimate of equilibrium of sulfide precipitation may be

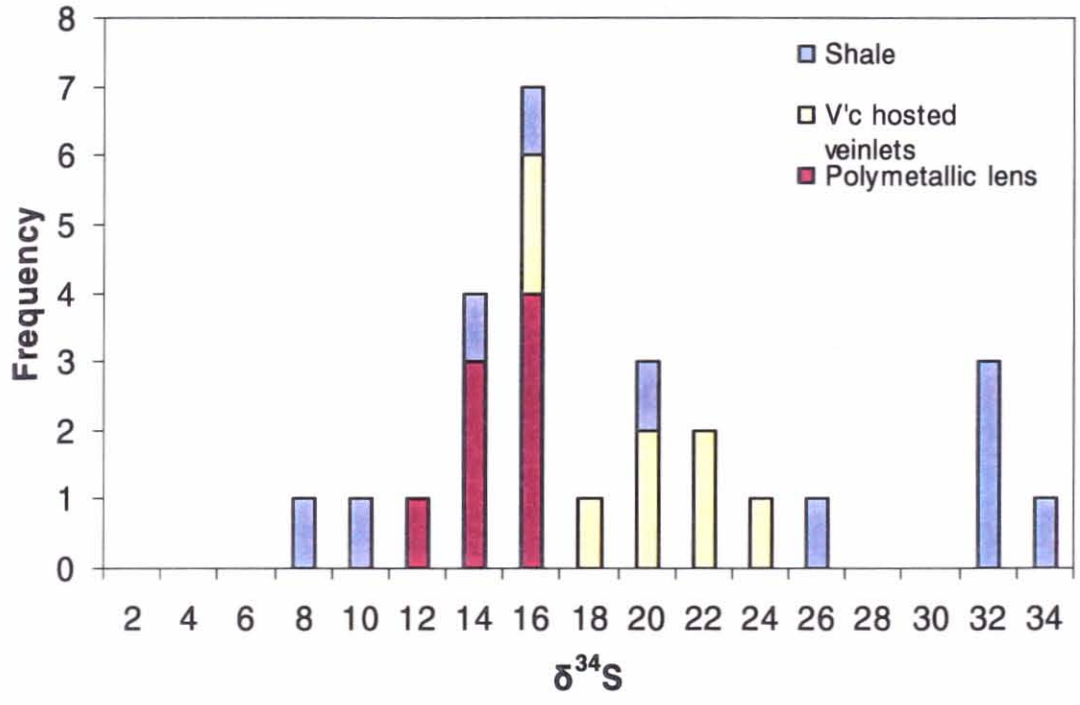

Figure 6.6 Sulfur Isotope Histogram of the Beatrice Prospect with respect to host lithologies.

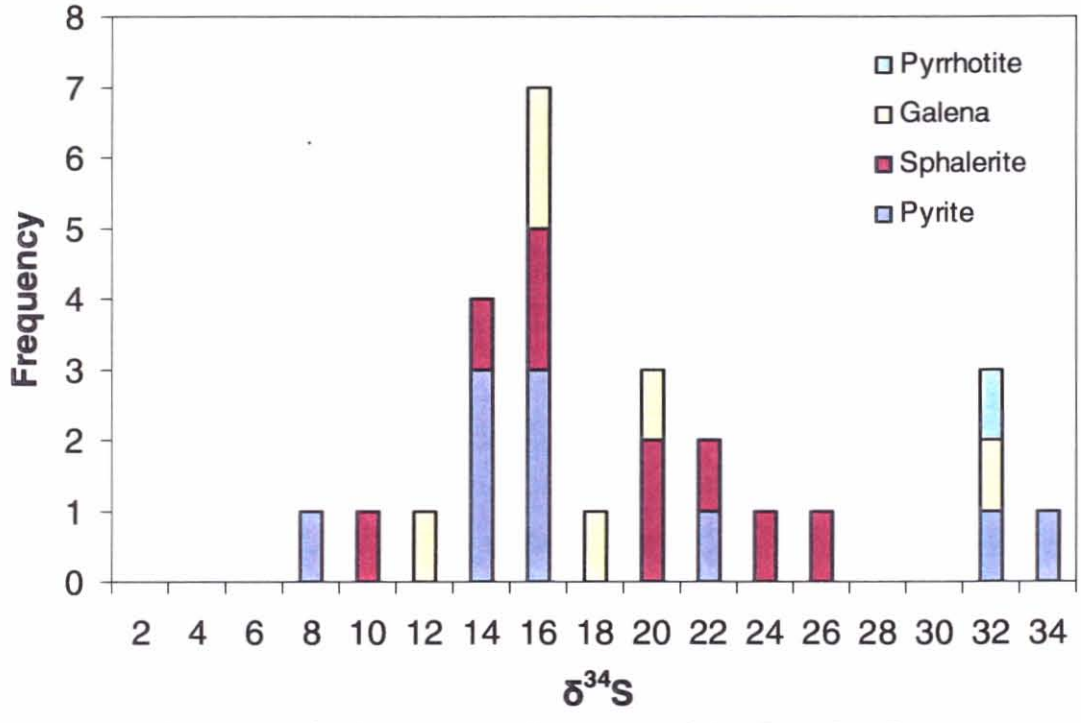

Figure 6.7 Sulfur Isotope Histogram of the Beatrice Prospect with respect to sulfide species.

attempted using the measured difference in the $\delta^{34}S$ of the sulfur-bearing compounds and their known isotopic equilibrium constants (Ohmoto and Rye (1979). Ohmoto and Rye (1979) developed a series of equations for the determination of temperature based on isotopic equilibrium; the three equations used in this study are presented in Table 6.6.

Mineral Pair	Equation
Sphalerite-galena	$T = [(0.85 \pm 0.03) \times 10^3] / \Delta^{½}$
Pyrite-sphalerite (pyrrhotite)	$T = [(0.55 \pm 0.04) \times 10^3] / \Delta^{½}$
Pyrite-galena	$T = [(1.01 \pm 0.04) \times 10^3] / \Delta^{½}$

T = Temperature in Kelvin, $\Delta = \delta^{34}S_{(min\ A)} - \delta^{34}S_{(min\ B)}$

Table 6.6 Sulfur isotopic thermometers (Ohmoto and Rye 1979).

Ohmoto and Rye (1979) noted the importance of isotopic equilibrium for coexisting sulfide species in the interpretation of sulfur isotope data, as it not only has implications for the H_2S concentration of the fluid but also affects temperature estimates. As summarised in Table 6.7 the calculated temperatures from the polymetallic lenses are high but within the upper range limit expected for VHMS mineralisation.

Sample	Py $\delta^{34}S$	Sph $\delta^{34}S$	Gn $\delta^{34}S$	Pair	Temp. range (°C)
MH3-10	+13.67	+15.67	+14.04	Sph-gn	369 to 416
MH3-16	+12.41	+13.77	+11.64	Sph-gn	289 to 330
				Py-gn	830 to 921
MH39		+19.96	+17.15	Sph-gn	217 to 253
MH4-11		+22.94	+14.60	Sph-gn	11 to 32
MH8-11	+31.02	+30.33(Pø)		Py-sph	342 to 438
MH8-10	+33.01	+25.73	+30.62	Py-gn	355 to 406
				Py-sph	-83 to - 54

Table 6.7 Calculated temperatures based on the isotopic thermometers of Ohmoto and Rye (1979).

The large variation in calculated temperature and negative calculated temperatures are possibly attributed to the disequilibrium of precipitated sulfides, resulting in dubious temperature estimates. This is a common feature in VHMS systems due to mineral refining, reprecipitation and replacement. The unrealistic calculated temperatures may also be attributed to differing generations of sulfide species. This interpretation is supported by petrographic analysis (Chapter 5.3). Due to the presence of both galena and sphalerite replacing pyrite, the equations involving pyrite give unreasonable temperature estimates, due to disequilibrium of the sulfide pairs. As discussed in Chapter 5.3, sphalerite and

galena were observed to show cusp and carie replacement textures. However, they appear to give reasonable temperature estimates suggesting that they may have been precipitated close to equilibrium.

6.3.5 Discussion

The consistent parallel variation of sulfur isotope $\delta^{34}S$ ratios of VHMS deposits and coeval marine sulfate deposits noted by Sangster (1968), has been used by Solomon et al. (1988), Green (1983), Gemmell and Large (1992) and others, in support of a mixed sulfur source for VHMS mineralisation. Data from Western Tasmanian VHMS deposits support this interpretation with $\delta^{34}S$ patterns indicative of sulfur sourced from a combination of reduced seawater sulfate and volcanic – rock sulfur.

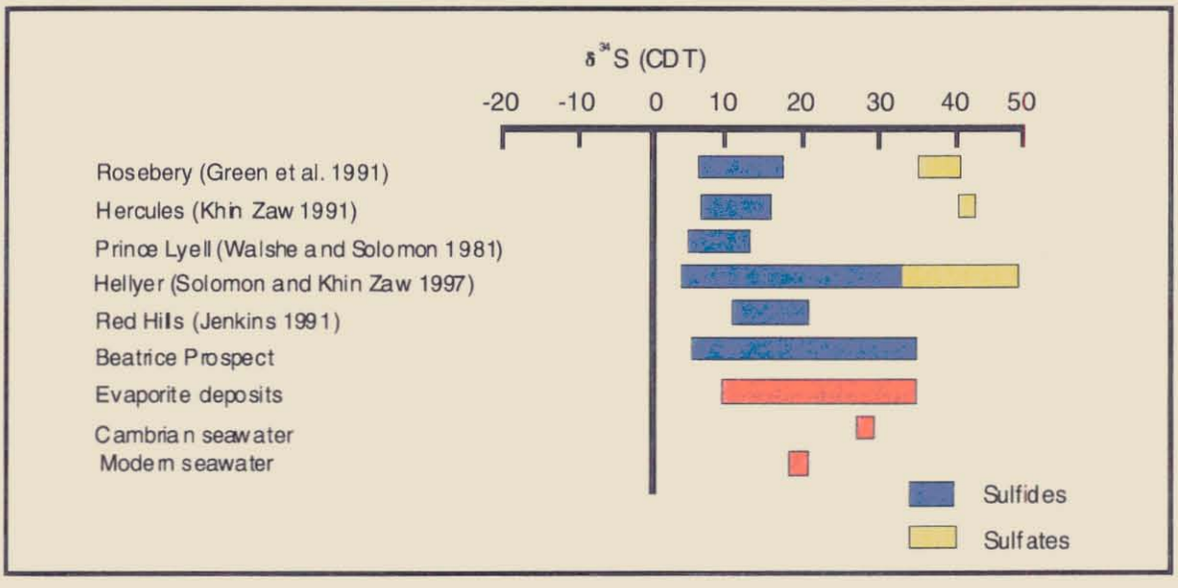

Figure 6.8 Comparison of $\delta^{34}S$ values of sulfides from the Beatrice Prospect with those of other western Tasmanian deposits.

The $\delta^{34}S$ values obtained from the polymetallic sulfide lenses in MS3 (11.6 to 15.8‰) are consistent with values obtained from sulfides deposited during the final stages of formation of the Rosebery deposit (Green et al. 1981) and hence a similar mechanism for the source of sulfur may be suggested. The generally heavier $\delta^{34}S$ values obtained from Rosebery has been interpreted to reflect limited leaching of sulfur from low-sulfur felsic rocks and the comparatively greater reduction of seawater sulfate. An additional factor not considered by Solomon et al. (1988) but suggested by Davidson and Kitto (1997) is the likely higher primary igneous values of 4-8‰ for felsic rocks within the Mt Read Volcanics (based on

their likely arc affinities), as compared to the primitive mantle signature of 0 ± 1‰ for basic rocks within the belt. This feature may lead to higher $\delta^{34}S$ values for sulfide deposits where sulfur has been sourced from an underlying felsic volcanic pile. This relatively greater reduction of seawater sulfate in addition to the predominantly felsic footwall rocks at Beatrice may account for the elevated $\delta^{34}S$ values observed.

The $\delta^{34}S$ values obtained from other mineralisation styles within the Beatrice Prospect are however, far heavier than other major deposits within western Tasmania. The heavier $\delta^{34}S$ values of the veinlet sulfides hosted in the volcaniclastics may indicate an increased involvement of reduced seawater sulfate in the hydrothermal convection system. Studies of the Hellyer deposit by Gemmell and Large (1992) indicate both temporal and spatial controls for the evolution of sulfur isotope values. At Hellyer the massive sulfide ores and main-stage stringer veins have relatively light $\delta^{34}S$ values (4-8‰). However, the sulfides within the barite-rich stratiform ore and the lateral (early and late stage) veins show more positive $\delta^{34}S$ values with variations 5 to 15‰ heavier than the massive sulfide ores (Large 1992). The heavier $\delta^{34}S$ ratios for the sulfides within the lateral stringers and the barite cap have been interpreted to reflect the increasing involvement of reduced seawater sulfate due to mixing of the hydrothermal fluid with heated seawater at the top of the deposit and/or within the lateral stringer zone. This model may be applicable for the higher values obtained from veinlet sulfides at the Beatrice prospect: they may be distal veinlets, in which the greater reduction of seawater sulfate resulted in higher $\delta^{34}S$ ratios.

Within the black shale unit, sulfide species are isotopically highly variable, with values ranging from 6.2 to 33‰. Several processes, including the almost complete reduction of seawater sulfate may cause such heavy values. The heavy $\delta^{34}S$ values recorded from within shale-hosted veins and the pyrite pseudomorphs indicate a complex origin. The fact that several of the values are equal to, and even heavier than Cambrian seawater sulfate ~30‰ (Claypool et al. 1980), indicates the occurrence of sulfate precipitation and the conversion and *in situ* reduction of sulfate minerals to sulfides. The reduction of these sulfate minerals may convert H_2SO_4 to H_2S and precipitate sulfide pseudomorphs or veinlet sulfides with heavy signatures reflecting their sulfate parentage, in a similar fashion to that described by Tompkins et al. (1994) for the MVT style Cadjebut deposit in Western Australia and the Nanisivik lead-zinc deposit discussed by Ghazban et al. (1990). Tompkins et al. (1994)

suggested that sulfide precipitation was initiated by chemical reactions between migrating base metal ore solutions and the evaporitic sulfur. This feature may account for the preferential mineralisation of the carbonate laminae and evaporite-like beds within the 6m interval in MS8.

6.4 Lead Isotopes

6.4.1 Introduction

Detailed studies by Gulson et al. (1987) and Gulson and Porritt (1987) on mineralisation within the Mount Read volcanic belt, have demonstrated the application of lead isotopes in age determination, deposit classification, discrimination of favourable prospects and the improvement in genetic models.

Lead isotope signatures from mineralised occurrences within the Mount Read Volcanics fall into two major isotopic groups, which correspond to different styles and episodes of mineralisation. Cambrian stratiform volcanic hosted massive sulfide Pb-Zn-Ag mineralisation constitute the least radiogenic group ($^{206}Pb/^{204}Pb$ = 18.06 to18.4). Vein style and disseminated Pb-Zn mineralisation that formed in association with Devonian-Carboniferous granitoid emplacement and/or Tabberabberan metamorphism display more radiogenic signatures ($^{206}Pb/^{204}Pb$ = 18.44 to 18.53).

The aim of this study is to determine the isotopic compositions of lead present within the Beatrice Prospect and to make comparisons with western Tasmanian deposits where the metallogenesis and ages are better known.

6.4.2 Analytical Techniques

Five galena samples from the Beatrice Prospect were analysed for their isotopic compositions by Zongshou Yu at the University of Tasmania using the HP4500 inductively coupled plasma mass spectrometer. Two of the samples were polymetallic sulfide blebs hosted within volcaniclastics (MS3MH16 & MS3MH10), two samples consisted of veinlet and clastic galena hosted within shale (MS7MH4 & MS8MH15) and one sample of galena from a bucky quartz carbonate vein within the quartz-feldspar porphyry (MS1MH11).

6.4.3 Results

The results of the lead isotopic study (Appendix 7) are shown in Table 6.8 and plotted in Figure 6.9. The results from the lead isotope study conducted by Actlabs of Perth on behalf of Pasminco Exploration (McNeill writ. comm. 1999) are also included within this study.

Sample No.	Sample Description	$^{206}Pb/^{204}Pb$	$^{207}Pb/^{204}Pb$	$^{208}Pb/^{204}Pb$
MS3-16	polymetallic lens	18.089	15.607	38.005
MS8-15	replacement of clast	18.229	15.583	38.072
MS7MH4	veinlet in shale	18.216	15.609	38.042
MS1MH11	stage 2 vein	18.321	15.671	38.296
MS3-10	polymetallic lens	18.179	15.582	38.050
241738*		18.16	15.65	38.02
241738*		18.19	15.64	38.28
241738*		18.12	15.49	38.05
241738*		18.24	15.69	38.21

* Pasminco Exploration data

Table 6.8 Lead isotope results from this study and from Pasminco Exploration 1999.

Figure 6.9 shows that the isotopic ratios obtained from galena from within the Beatrice Prospect form a discrete field, with $^{207}Pb/^{204}Pb$ values typically tightly constrained between 15.6 and 15.7. $^{206}Pb/^{204}Pb$ ratios span a broader field from 18.086 to 18.321, $^{208}Pb/^{204}Pb$ range from 38.005 to 38.296. The coarse galena sample taken from the quartz carbonate vein in the Quartz Feldspar Porphyry has the highest values in all three ratios.

6.4.3 Discussion

Lead isotopes have been used for distinguishing between VHMS and other styles of uneconomic mineralisation on the West Coast of Tasmania. Gulson & Porritt (1987) indicated that the Cambrian volcanogenic deposits (Mount Lyell, Rosebery, Hercules, Que River and Hellyer) have lead isotope signatures that differ substantially from those associated with post – Cambrian mineralisation. Cambrian stratiform massive sulfide samples exhibit the least radiogenic values ($^{206}PB/^{204}Pb$ = 18.06 to 18.14), Devonian vein-style Pb-Zn-As mineralised samples form the most radiogenic group ($^{206}PB/^{204}Pb$ = 18.44 to 18.53). A third group of values with intermediate radiogenic values come from disseminated and vein-style Pb-Zn mineralised samples associated with quartz porphyry bodies which are considered to post-date the episode of massive sulfide formation (Gulson et al. 1987). Gemmell (1997) noted a variation in lead isotopes within the stringer zone beneath the Hellyer ore body, intermediate to the Cambrian and Devonian fields defined by Gulson et al. 1987).

The Pb isotope signature obtained from the Beatrice galena samples falls within the field typical of Cambrian mineralisation (Figure 6.10). However, the Beatrice signature has a broader distribution than other known VHMS deposits within the Mount Read Volcanics, excluding Hellyer. Gulson and Porritt (1987) proposed that the increasing $^{206}Pb/^{204}Pb$ ratios

A)

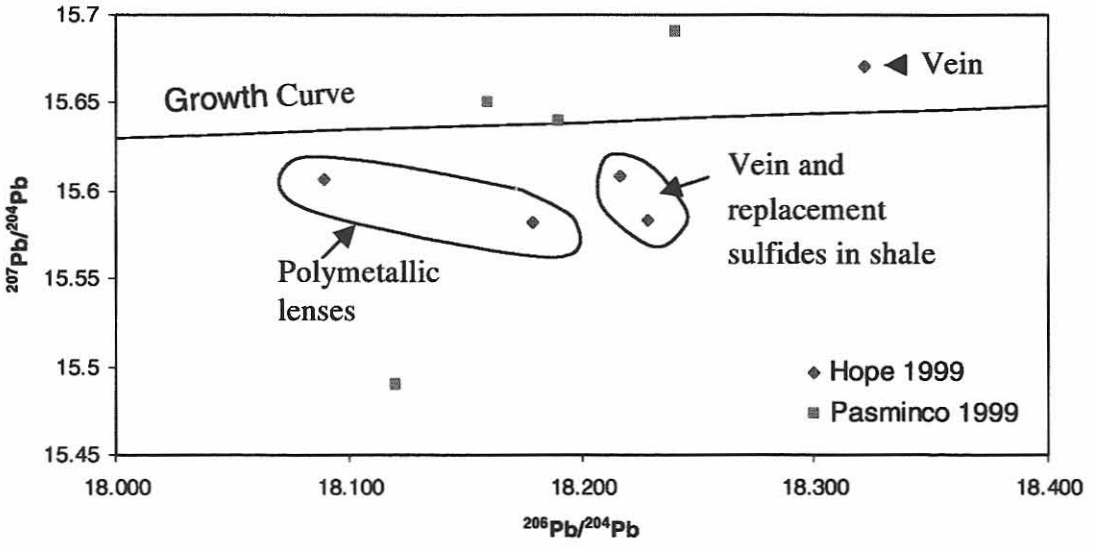

B)

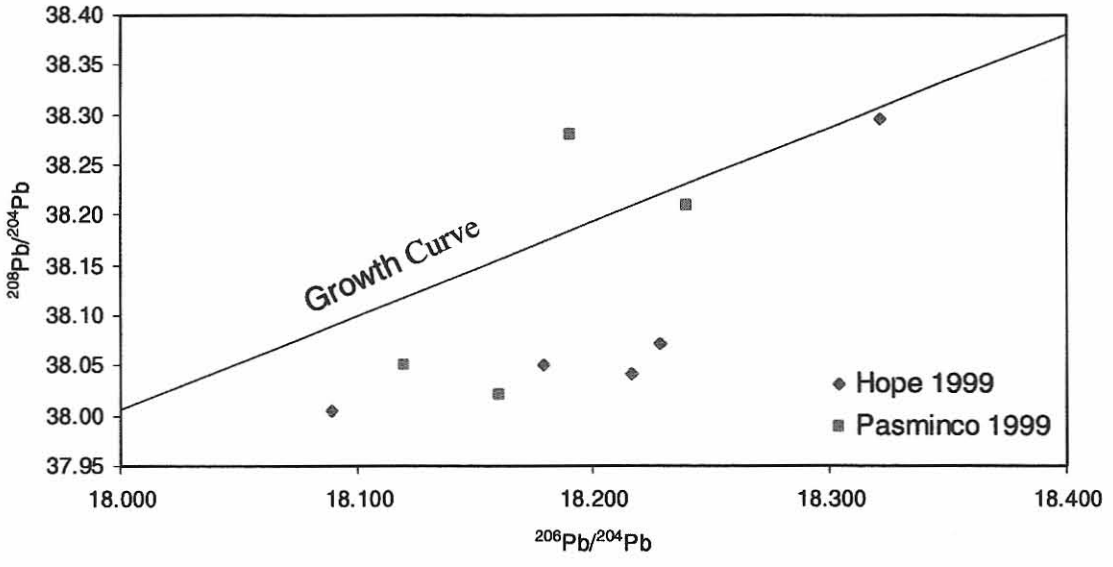

Figure 6.9 Lead isotopic compositions of samples obtained from the Beatrice Prospect. A) $^{207}Pb/^{204}Pb$ vs $^{206}Pb/^{204}Pb$, and B) $^{208}Pb/^{204}Pb$ vs $^{206}Pb/^{204}Pb$. The growth curves of Cumming and Richards (1975) are also shown.

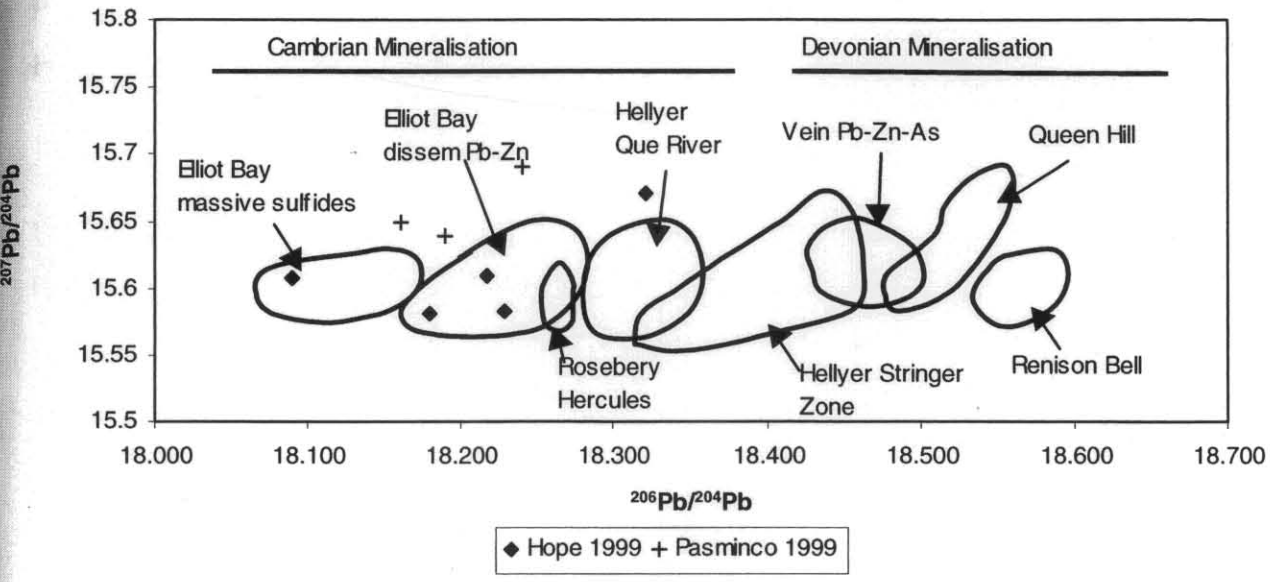

Figure 6.10 Plot of lead isotope compositions taken from the Beatrice Prospect. Samples place within the field defining Cambrian mineralisation (modified from Gulson et al. 1987).

from Elliot Bay to Hellyer indicates younger ages for mineralisation to the north. Due to the location of Beatrice, approximately half way between Mt Jukes and Rosebery, the lower $^{206}Pb/^{204}Pb$ ratio may be consistent with the progression to older mineralisation towards the south of the Belt.

Based on petrography, it is evident that lead obtained from samples 3-16 and 3-10 predate deformation, and represent the most prospective form of mineralisation. These samples have the lowest radiogenic signature, followed by lead obtained from replacement (predating deformation) and veinlet mineralisation from in the shale. The highest lead isotopic ratios were obtained from veins in the Quartz Feldspar Porphyry.

Gulson and Porritt (1987) indicate that Pb-Zn mineralisation, occurring as disseminated or veinlet sulfides in Cambrian quartz and granitic porphyries or in adjacent altered volcaniclastics have $^{206}Pb/^{204}Pb$ ratios averaging 18.24, similar to the $^{206}Pb/^{204}Pb$ ratios obtained from the Beatrice Prospect (18.19). Gulson and Porritt (1987) infer a genetic relationship between the intrusion of the porphyries and mineralisation. Two possible igneous bodies may be responsible for mineralisation within the prospect; the overlying Quartz Feldspar Porphyry, (which appears unlikely) or the interpreted ridge of sub surface

Cambrian Granite lying to the east of the prospect, outlined by Large et al. (1996). Petrographic observations show that mineralised veins in the Quartz Feldspar Porphyry at Beatrice are late features, with sharp vein edges and localised vein controlled alteration.

The lead sample taken from the inferred late, stage-2 vein within the Quartz Feldspar Porphyry has the highest values in all three ratios, which may indicate that this lead has been isotopically modified, possibly during deformation. Original Cambrian derived lead may have entrained more radiogenic material during remobilisation, broadening the data set to represent a composite between Cambrian and Devonian signatures.

Gulson and Porritt (1987) discuss the problem of relatively uniform isotopic signatures (such as the Beatrice dataset) and the absence of an orebody, with particular reference to the Lake Selina area. The homogenous lead isotope composition indicates that the mineralisation of Selina formed as part of a major hydrothermal system, similar to that which gives rise to VHMS deposits. However, the conditions necessary to concentrate metals into a viable deposit were precluded. Gulson and Porritt (1987) suggest that metal bearing fluids may have boiled prior to reaching the sea floor, possibly due to a limited depth of seawater and insufficient hydrostatic pressure.

6.5 Zinc Ratio

6.5.1 Introduction

The relationship of Zn to Pb transported in a saturated ore solution is controlled by temperature and salinity only, and is independent of pH, fO_2 and activity of dissolved sulfur (Huston and Large 1987). The zinc ratios [100Zn/(Zn + Pb)] observed in polymetallic massive sulfide deposits such as the Rosebery, Hercules and Hellyer deposits are similar to those calculated for conditions typical for the deposition of sphalerite and galena at 150 -250°C from a 0.5-1.5 *m* NaCl solution.

Huston and Large (1987) suggested that the analysis and comparison of distribution patterns, means and standard variations of the zinc ratio of anomalous samples can provide an excellent method of distinguishing the metallogenic style and determining the likelihood of favorable VHMS mineralisation.

Volcanogenic massive sulfide deposits are characterized by zinc ratios displaying a normal distribution and a restricted range of means between 64 and 77 with relatively low standard deviations (less than 15). The less economically significant Cambrian vein-style deposits associated with felsic porphyries and Ordovician and Devonian deposits are characterized by a wide distribution of Zn ratios with lower means, generally around 40 (but ranging from 39 to 75) and standard deviations greater than 23 (Figure 6.11).

6.5.2 Results

The zinc ratio data from the Beatrice Prospect is based on assay results from 179 samples taken from drill core, that contain greater than 1000ppm for both Zn and Pb (Appendix 8). Data were plotted both as a whole set and subdivided according to lithology and style of mineralisation. The two styles are, shale hosted veinlet and replacement mineralisation, and veinlet and disseminated mineralisation hosted within the volcaniclastic units. The zinc ratios for both these styles are shown in Figure 6.12, along with the complete dataset. Figure 6.13 shows zinc ratios and locations within the sequence intersected by MS7 and MS3.

The zinc ratios for the entire dataset show similar patterns to the Cambrian VHMS deposits. The histogram shows a normal distribution with a mean of 63.64 with a slightly

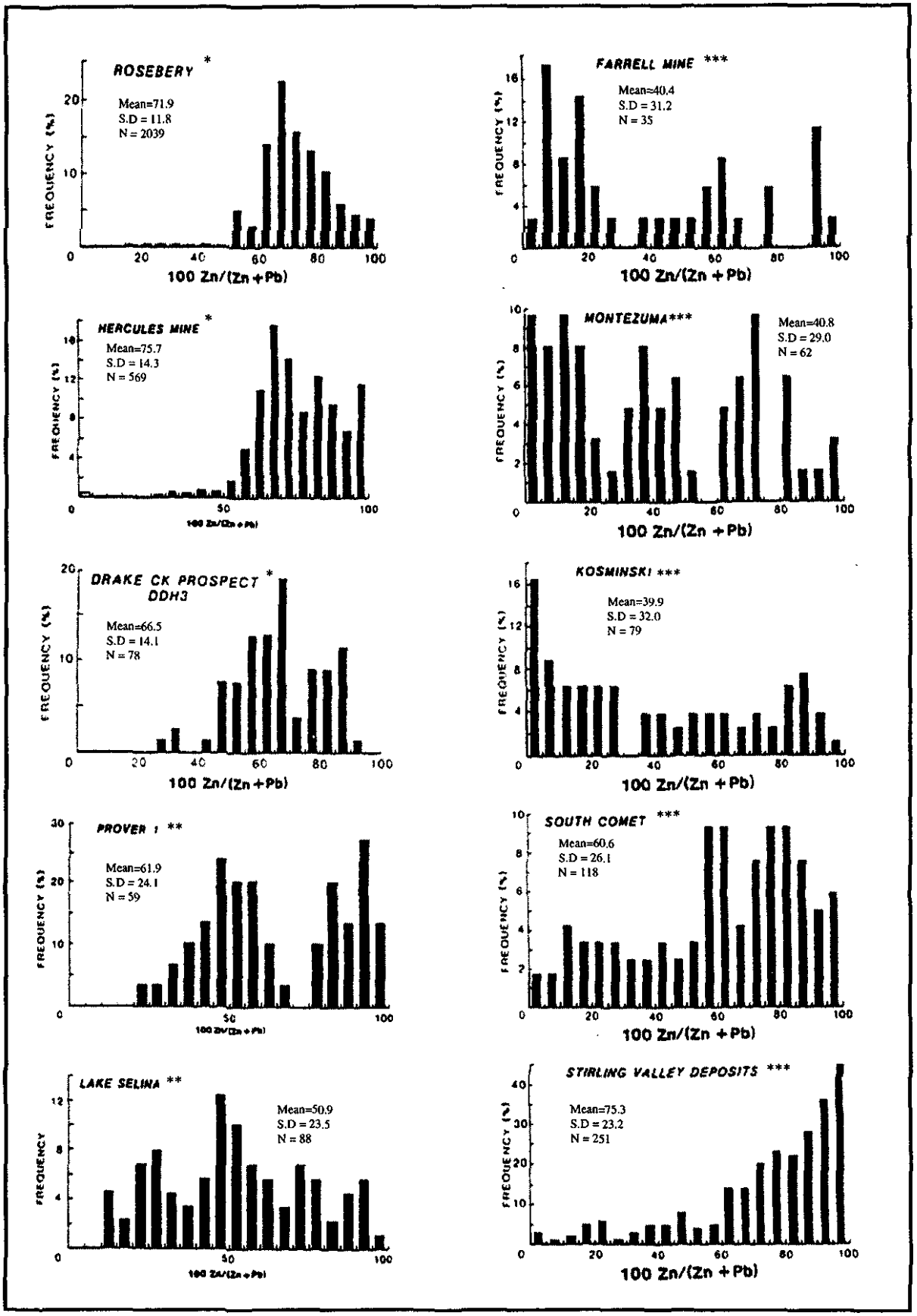

Figure 6.11 Zinc Ratio histograms for deposits in the Mt Read Volcanics. * VHMS deposits, ** Cambrian Pb-Zn vein-style mineralisation, *** Devonian vein-style mineralisation. (modified from Huston and Large 1987).

A)

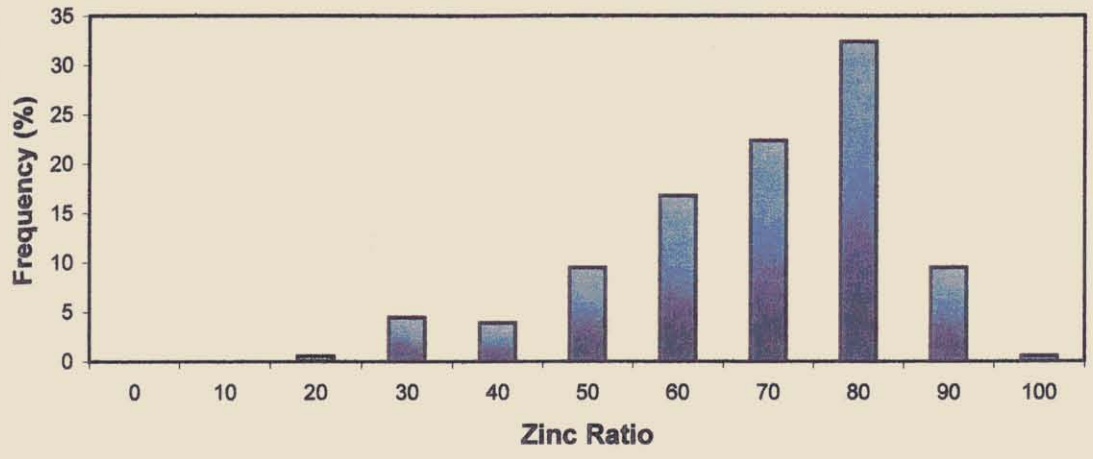

B)

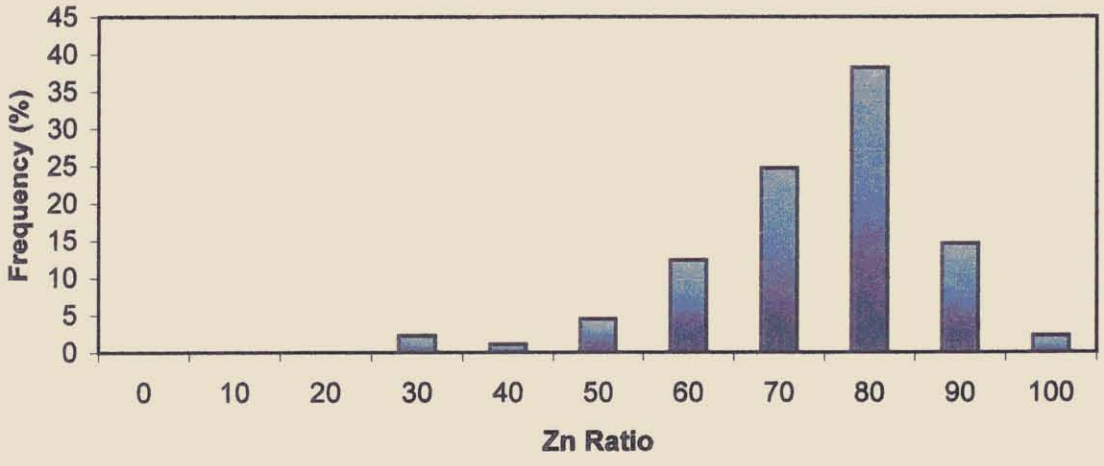

C)

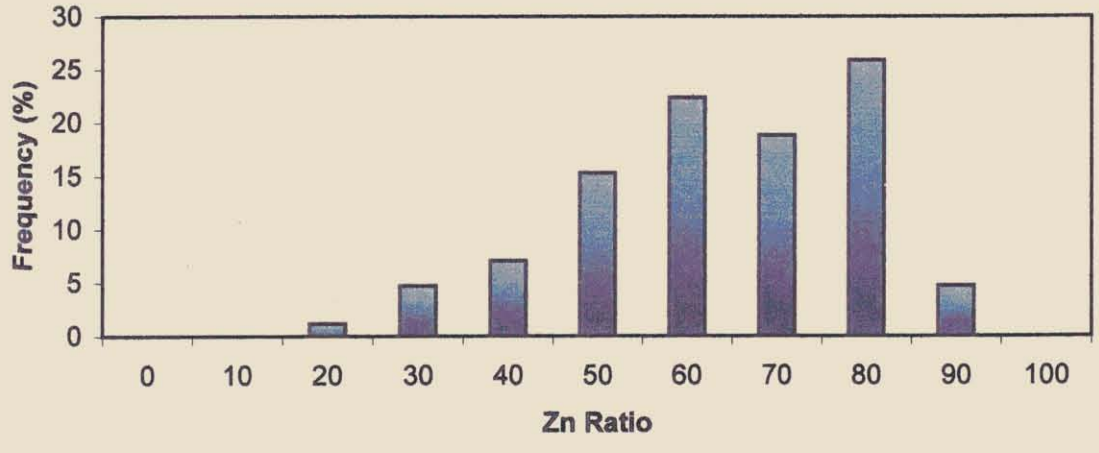

Figure 6.12. Zn ratio histograms for the Beatrice Prospect assay data
A) Whole data set. B) Shale hosted mineralisation
C) Volcaniclastic hosted mineralisation

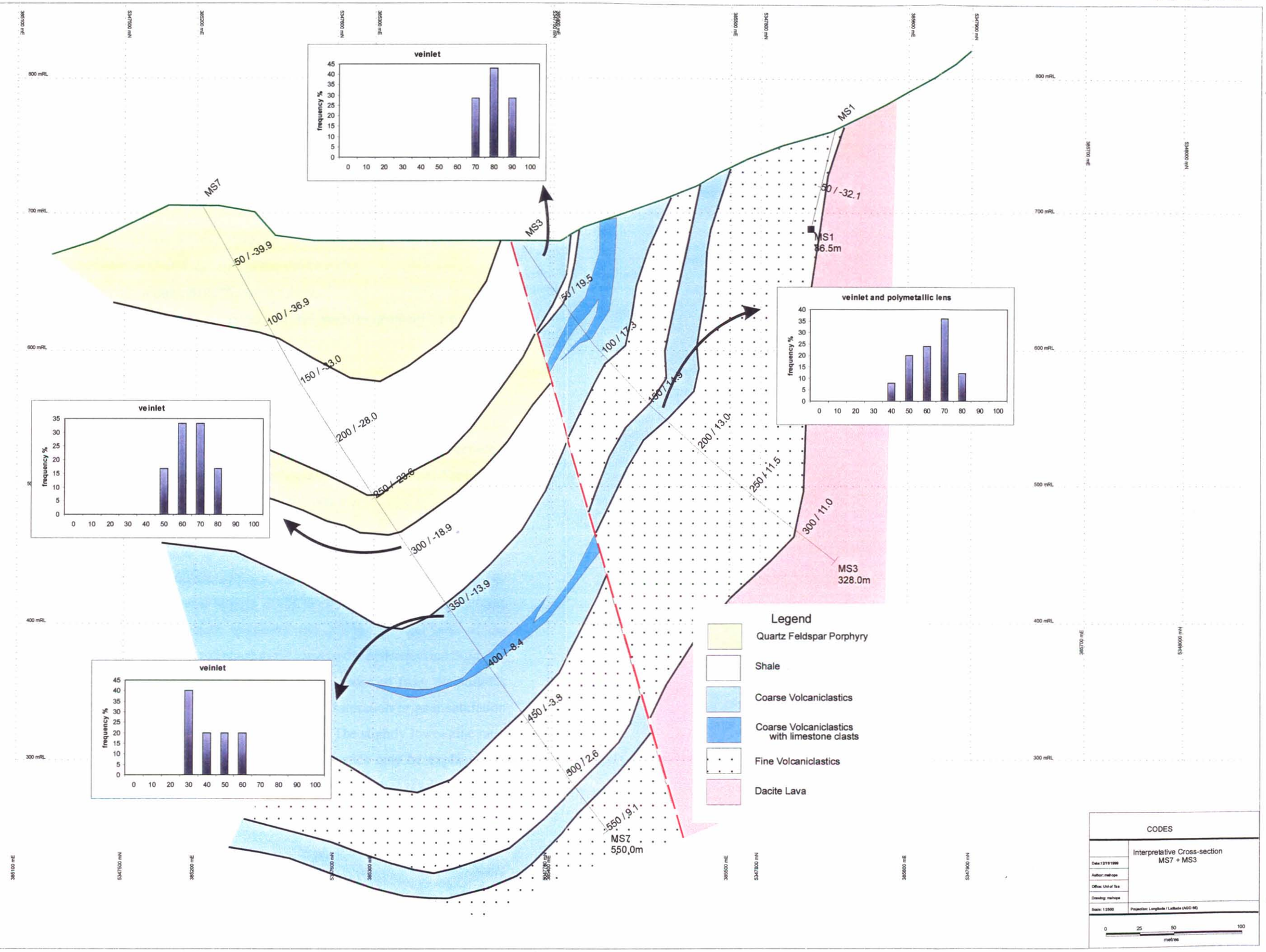

Figure 6.13 Zinc ratios for anomalous intersections (<1000ppm) based on lithology for MS7 and Ms3.

5 cm

larger standard deviation (15.7) than Cambrian VHMS deposits. The zinc ratio for mineralisation hosted within the black shale displays a good correlation with other VMS deposits of the Mount Read Volcanics, with a slightly higher mean (69.1) and a low standard deviation (13.3). Conversely the veinlet and disseminated mineralisation within the volcaniclastics has a lower mean (58.9) and a larger standard deviation (16.3).

6.5.3 Interpretation

Huston and Large (1987) stated that the zinc ratio may be controlled by four factors;

- The relative concentrations of lead and zinc in the source rocks
- The mechanisms of metal solution from the source rocks
- The saturation – non-saturation of base metal and the overall chemistry of the metal bearing solutions and
- The efficiency of metal deposition

The first two controls on zinc ratio may impart variations within the zinc ratio on a district scale, relating to the compositional variation in the source rocks but would not be expected to impart control on prospect scale inhomogeneity of the zinc ratio. The fourth factor, the efficiency of metal deposition, is complex and poorly constrained and is unlikely to significantly affect zinc ratios (Huston and Large 1987).

The most realistic cause for zinc ratio variability is the chemistry and saturation or non-saturation of base metals within the metal bearing fluids. If the ore bearing solutions were at or near saturation with respect to both sphalerite and galena the zinc ratio of the precipitating sulfides would be constant and equal to the ratio in the hydrothermal fluid.
As a result, the well-constrained spread of zinc ratio values observed from the sulfides within the Beatrice Prospect may be interpreted to reflect the saturation or near saturation of the ore bearing solutions with respect to both lead and zinc. The slightly lower zinc ratio and broader standard deviation observed within the volcaniclastics may be explained as either an effect of varying salinity and/or temperature or as the result of slight undersaturation of the ore bearing fluid with respect to lead and/or zinc.

Comparing the zinc ratio and lead isotope ratios of sulfides within the prospect on one diagram, as in Figure 6.14, may provide a powerful method of classifying the style and age of mineralisation and hence provide supporting evidence toward a genetic model.

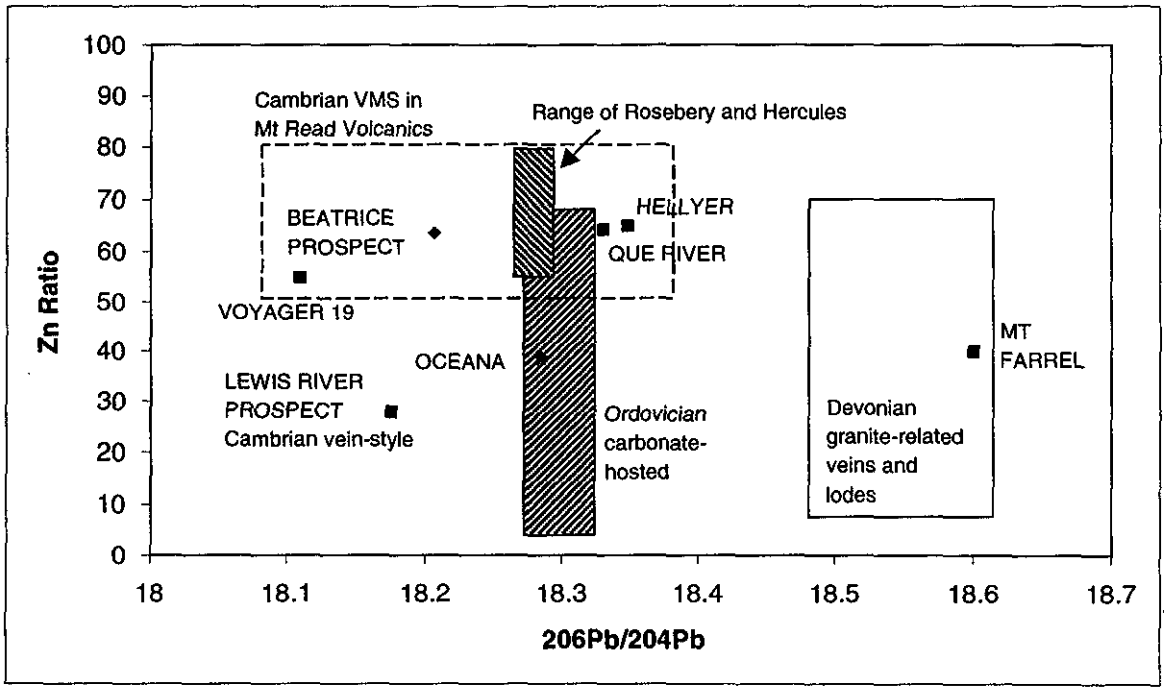

Figure 6.14 Plot of zinc ratio vs. 206Pb/204Pb ratio for the Beatrice Prospect; also shown are the fields of other western Tasmanian mineralisation styles. Mean values for each deposit are plotted as points and range values as a box. (Modified from Huston and Large 1987).

It is clearly evident from the combined use of zinc number and lead isotope ratios that Beatrice is similar to other known Cambrian VHMS deposits, suggesting lead-zinc saturation of a Cambrian hydrothermal fluid. This finding has favourable implications for the prospectivity of the area, suggesting that the general chemical conditions controlling lead and zinc deposition at Beatrice were similar to known high grade (and their associated low grade) deposits within the Mt Read Volcanic Belt.

6.6 Summary

A Microthermometric study of fluid inclusions has indicated that two populations exist in the quartz + carbonate ± chlorite ± feldspar ± base metal sulfides veins in the Quartz Feldspar Porphyry. A low temperature (~ 148°C), saline fluid (3.2 to 18.6 eq. wt% NaCl) containing substantial CaCl, and a second higher temperature (~268°C) high salinity (11-16 eq. wt% NaCl) fluid.

Carbon and oxygen isotope analyses have shown that calcite in bucky quartz + carbonate ± chlorite ± base metals veins in the Quartz Feldspar Porphyry and within the shale and volcaniclastic units have $\delta^{13}C$ and $\delta^{18}O$ values in the range of Cambrian carbonate defined by Khin Zaw (1991). The calculated isotopic composition of fluids responsible for stage 1-4 bucky quartz carbonate veinlets are $\delta^{13}C$ = -7.6 to –10‰ and $\delta^{18}O$ = -0.8 to –4.5‰ based on a temperature of 148°C from population 1 fluid inclusions. The $\delta^{18}O$ values are consistent with a meteoric water source. However, the isotopic composition of the fluid calculated from temperature estimates of population 2 inclusions (268°C yielding $\delta^{13}C$ values of -3.7 to –6.2‰ and $\delta^{18}O$ values of +2.4 to +6.1‰) are consistent with a metamorphic fluid. This metamorphic fluid can be modelled to explain the negative trend observed in the dataset. The interpretation that veins within the Quartz Feldspar Porphyry are of Devonian origin is supported by textural evidence. It is interpreted that vein carbonates have been precipitated during the Devonian deformation from metamorphic fluids interacting with felsic host rocks.

Analyses of sulfur isotopes for various sulfide morphologies show a broad range of $\delta^{34}S$ values and a complex source of sulfur. Polymetallic lenses within the volcaniclastic unit display tightly constrained $\delta^{34}S$ values of between 11.6 and 15.7‰ consistent with a mixed sulfur source, obtained from the abiotic reduction of seawater sulphate and sulfur leached from the underlying felsic volcanics, in a manner similar to VHMS style mineralisation. Higher $\delta^{34}S$ values measured from veinlet and replacement sulfides may reflect the increased involvement of reduced seawater sulfate. Unusually heavy $\delta^{34}S$ values obtained from sulfides within the shale unit strongly correlate with the presence of pyrite pseudomorphs of gypsum, and relate to the *in situ* reduction of sulfate minerals producing isotopically heavy sulfides.

Lead isotope values indicate a Cambrian age of mineralisation, based on the previous investigations of Gulson and Porritt (1987). Lead isotope ratios however show a broad range in values indicating either some isotopic modification associated with later deformation and the addition of more radiogenic material into the system, or the possiblity that mineralisation is associated with Cambrian igneous bodies. Two possible igneous bodies may be responsible; the Quartz Feldspar Porphyry, (which appears unlikely) or the interpreted ridge of sub surface Cambrian Granite lying to the east of the prospect, outlined by Large et al. (1996). As discussed in chapter 4.2.3, potassic alteration overprinted by chlorite + magnetite alteration located at depth indicates that granite related alteration occurs within the prospect, and may also be responsible for mineralisation.

Further evidence for the presence of VHMS mineralisation exists in the combined use of lead isotope values and zinc ratios. Zinc ratios display a relatively high mean (63.6) and low standard deviation (15.7) reflecting the saturation of the fluid with respect to both lead and zinc. The high mean, low standard deviation and normal distribution patterns of zinc ratios distinguish mineralisation within the prospect from both Cambrian and Devonian vein-style mineralisation. When plotted together, Beatrice samples plot in the centre of the lead isotope/zinc ratio field defining western Tasmanian Cambrian VHMS deposits. It is therefore inferred that Cambrian VHMS style mineralisation has occurred within the prospect. This interpretation is supported by the sulfur isotope ratios obtained from the small polymetallic lens and the petrographic evidence for pre - kinematic mineralisation.

Chapter 7
Synthesis and Discussion

7.1 Introduction

The major aims in this investigation were to:

- Document the various lithologies observed in the Itat Creek Area of the Beatrice Prospect and to define the styles and distributions of alteration assemblages observed in outcrop and in drillcore.
- Document the mineralogy, geochemistry and style of base metal occurrences and attempt the construction of a genetic model to assist the assessment of prospectivity of the area.

7.2 Summary

7.2.1 Geology of the Mount Sedgewick Anomalous Zone

The MSAZ consists of a westerly dipping sequence of felsic volcaniclastics, coherent quartz phyric lavas and shale, conformably overlying spherulitic quartz ± feldspar phyric lava of the Central Volcanic Complex. Overlying this sequence is the large quartz feldspar porphyry body, which obscures the host sequence west of the Itat Creek Valley. The Quartz Feldspar Porphyry appears to have formed several lenses, displaying peperitic margins at both top and bottom contacts indicating emplacement into wet sediments. Also present in the Quartz Feldspar Porphyry are monomict, graded breccias inferred to reflect fragmentation of coherent porphyry by fluidised flow and polymict breccias indicating the entrainment of clastic material by coherent porphyry.

A marine depositional environment for the host rocks is indirectly inferred on the basis of siliceous sponge spicules (first identified by this study) in the shale unit. The existence of mass flow breccias containing clean limestone clasts in the underlying coarse volcaniclastic unit may further constrain the depositional environment of the host rocks, implying the proximity or connection of the depositional basin with a near shore environment. This interpretation may be supported by the existence of evaporite laminae within the shale unit. The existence of gypsum crystals (now pseudomorphed by pyrite) may have formed *in situ* on a shallow hypersaline bottom, or sourced from shallow water

slumped and/or current reworked platform deposits to be deposited into a deeper water environment. Evaporitic palaeo-environments have not been previously recognised in either the CVC or Lynchford Member of the Tyndall Group.

7.2.2 Alteration

Three distinct alteration assemblages were delineated within the MSAZ. Ubiquitous sericite alteration occurs throughout the volcaniclastic units, typically forming lenses of fine grained aggregates reflecting the sericitisation of original glassy pumiceous fragments. On textural evidence, widespread sericite alteration is inferred to be unrelated to mineralisation, resulting instead from the conversion of diagenetic clays to sericite during regional metamorphism.

Chlorite alteration in the host sequence correlates with the major mineralising event. The intensity of chlorite alteration increases systematically towards zones of anomalous sulfide concentration. Typically fine to medium grained aggregates of chlorite within the fine grained volcaniclastic unit progressively coalesce to form pervasive zones approaching the upper contact between fine and coarse volcaniclastic units where sulfides are concentrated.

A third alteration assemblage, consisting of weak to moderate potassic alteration overprinted by chlorite + magnetite alteration, is defined at the bottom of holes MS7 and MS8 and to a lesser extent at the base of MS3 and MS2. This alteration assemblage is consistent with alteration associated with Cambrian high K, magnetite series granites, as mapped at Lake Selina by Hunns (1987), and at Jukes by Doyle (1990) and Wyman (1998). The source of this alteration may be the long semi continuous ridge of Cambrian Granite interpreted to lie at depth, east of the prospect along the eastern margin of the Mt Read Volcanic Belt. (Large et al. 1996).

The spatial correlation between chlorite alteration and base metal concentration is supported by the Ishikawa Alteration index (AI) which shows a systematic increase towards zones of pervasive chlorite alteration and base metal concentration. Its use in combination with the Chlorite Carbonate Pyrite Index (CCPI) enables the comparison of geochemistry with alteration assemblage, and the classification of alteration trends. Hydrothermally altered samples show a systematic increase to high AI and CCPI values reflecting the increase in chlorite and pyrite and the destruction of plagioclase and original

volcanic glass. Another vector towards zones of more intense chlorite alteration and possible mineralisation is the depletion in Strontium, associated with the destruction of albite. No spatial variation in chlorite compositions was detected in downhole sample sets. It appears that the composition of hydrothermal chlorites equilibrated with host rocks during regional metamorphism. However anomalous higher magnesium chlorites, and ankeritic carbonate, exist in association with massive sphalerite in the large outcropping vein (MH6). Further study on these chlorites (easily detected by their anomalous blue interference colours under cross polarised light) may prove to be useful vector towards high grade mineralisation.

7.2.3 Mineralisation

Known base metal sulfides exist within the prospect in numerous forms. In the volcaniclastic units, mineralisation is manifested as discordant veinlets and rare small (<3cm) lenses consisting of sphalerite, galena, pyrite and chalcopyrite. Sulfide species in the shale unit are diverse, containing arsenopyrite, pyrrhotite and marcasite in addition to sphalerite, galena, pyrite and chalcopyrite. Sulfides in the shale unit exist as bedding parallel and discordant veinlets in addition to selective replacements rimming carbonate and evaporite laminae, and replacing fine grained lithic clasts in minor mass flows. Base metal lenses in the volcaniclastic units indicate pre to syn kinematic precipitation, with brittle fracturing of pyrite and the diffuse alignment of sphalerite and chalcopyrite with the dominant cleavage. Mineralisation within the shale also exhibit pre to syn deformational features with pyrite (after gypsum) and arsenopyrite grains rotated into alignment with the cleavage. These early formed grains exhibit pressure shadows infilled by fibrous quartz, sparry calcite and remobilised sulfides.

Sulfides are typically concentrated in the volcaniclastic units at the upper contacts between fine and coarse grained units, existing as fine anastomosing veinlets parallel to the contact. This feature is peculiar insofar as greater porosity and permeability would be expected for the coarse volcaniclastic unit, suggesting hydrothermal fluids would pass through, rather than be ponded at this contact.

7.2.4 Fluid inclusions, zinc ratios and stable and radiogenic isotopes

Isotopic studies indicate that mineralisation at the Beatrice Prospect occurred during the Cambrian. Lead isotopes display a moderate spread centred within the field of Cambrian ores defined by Gulson et al. (1987). Lead isotopic values in stage II veins in the Quartz

mineralisation is replacive and vein related, and not bedded as suggested by Boyd (1994). Wilde and Kerr (1990) downgraded the prospect as not favourable for VHMS style deposits, based on the presence of K-feldspar alteration. However, the isotopic evidence presented within this study indicates that, geochemically, sulfide occurrences are most akin to Cambrian VHMS style mineralisation, displaying zinc ratio, lead and sulfur signatures similar to known stratiform sulfide deposits. Even so, the absence of stratiform or syngenetic mineralisation within the volcaniclastics and shale unit does pose a problem when formulating a genetic model.

The presence of potassically altered rocks cross cut by a chlorite + magnetite assemblage, in the lower part of the sequence intersected by MS7 and MS8, is similar to the alteration related to high K, magnetite series granites. However, sulfur isotopic data indicate that, base metals and sulfur are not directly related to the granite interpreted to lie at depth east of Itat Creek. Nevertheless, emplacement of the Cambrian Granite may have acted as a heat source to drive convection of seawater through felsic volcaniclastics and lavas of the Central Volcanic Complex. If sufficiently heated (>200°C; Green and Taheri, 1992) convecting fluids would be capable of inorganically reducing seawater sulfate and leaching metals from wall rocks and ultimately producing the chloritisation and sulfide mineralisation observed with the fine and coarse volcaniclastics.

Haas (1971) indicated seawater depth is the primary factor that determines whether or not rising hydrothermal fluids boil on its ascent to the seafloor. Under high hydrostatic pressure (greater than 1000 to 1500metres) fluids ascend to the seafloor without boiling, concentrating base metal precipitation at the seawater rock interface to form stratiform ore deposits. In shallow water environments sub-seafloor phase separation gives rise to footwall brecciation and stockwork mineralisation. The presence of limestone clasts and evaporite laminae may indicate that deposition of the host sequence occurred within shallower environments resulting in boiling, dispersion and precipitation of base metals within the host sequence before concentration on the sea floor. As a result mineralisation within the prospect may not be manifested in a stratiform deposit similar to other VHMS deposits within the Mt Read Volcanic belt, but as a stockwork of anastomosing veinlets deposited in the subseafloor volcanic pile.

Petrographic evidence indicates that base metals have been mobile during deformation, resulting in remobilisation of galena, sphalerite and chalcopyrite into pressure fringes adjacent to pyrite euhedra. This remobilisation during deformation has not substantially modified the isotopic composition nor zinc ratio of these sulfides.

Fluid inclusions obtained from mineralised quartz carbonate veins within the Quartz Feldspar Porphyry indicate two distinct populations: a low temperature (~149°C) and high temperature fluid (~268°C), both of variable, high salinity. The most likely explanation for the similar $\delta^{13}C$ and $\delta^{18}O$ values obtained from the veins within the Quartz Feldspar Porphyry is that they relate to deformation during the Devonian. This interpretation is supported by textural evidence indicating stage 1-4 veins represent late stage cross cutting features. The high eutectic temperatures obtained from fluid inclusions indicate a fluid containing significant quantities of Ca in addition to Na, K, Cl and H_2O. The high CaCl content of the metamorphic fluid may in part be attributed to the fluxing of fluids through the underlying sedimentary sequence containing both evaporites and carbonates.

References

Allen, R.L. and Cas, R.F. (1990) The Rosebery controversy: distinguishing prospective submarine ignimbrite-like units from true subaerial ignimbrites in the Rosebery-Hercules Zn-Cu-Pb Massive Sulfide District, Tasmania. Geological Society of Australia: Abstracts 25: 31-32.

Barrett, T. J. and MacLean, W.H. (1994) Mass changes in hydrothermal alteration zones associated with VMS deposits of the Noranda area. Explor. Mining Geol. Vol. 3 (2): 131-160.

Beales, F.W. and Jackson, S.A. (1967) An aspect of sedimentary basin evolution; the concentration of Mississippi Valley-type ores during late stages of diagenesis. Bulletin of Canadian Petroleum Geology. Vol. 15-4.

Boyd, D. (1994) in Halley, S., Vicary, M. and Boyd, D. (1995) Exploration Licenses EL 102/87, 55/89 and 12/92 Annual Report for the period April 1994 to March 1995. Unpublished report to RGC Exploration Pty. Ltd. (MRT CR 95-3721).

Callaghan, T. (1998) The geology of the Mt. Julia Deposit, Henty Goldmine. Unpublished M.Sc. Thesis. University of Tasmania

Cathelineau, M. and Nieva, D. (1985) A chlorite solid solution geothermometer; the Los Azufres (Mexico) geothermal system. Contrib. Mineral. Petrol. Vol 91:235-244.

Claypool, G.E., Holser, W.T., Kaplan, I.R., Sakai, H. and Zale, I. (1980) The age curves of sulfur and oxygen in marine sulfate and their initial interpretation. Chemical Geology. Vol 28: 199-206.

Corbett, K.D. (1992) Stratigraphic-Volcanic Setting of Massive Sulfide deposits in the Cambrian Mount Read Volcanics, Tasmania. Ecomonic Geology. Vol 87: 564-586.

Corbett, K.D. and Solomon, M. (1989) Cambrian Mt. Read Volcanics and Associated Mineral Deposits. Ch 4 in Burrett, C. F and Martin, E.L. (Eds) Geology and Mineral Resources of Tasmania. Geological Society of Australia. Special Publication 15.

Cox, S.F and Etheridge, M.A. (1983) Crack-seal fibre growth mechanisms and their significance in the development of oriented layer silicate microstructures. Tectonophysics. Vol 92 (1-3): 147-170.

Crawford, A.J., Corbett, K.D. and Everard, J.L. (1992) Geochemistry of the Cambrian Volcanic-Hosted Massive Sulfide-Rich Mount Read Volcanics, Tasmania, and Some Tectonic Implications. Economic Geology. Vol 87: 597-619

Cumming, G.L. and Richards, J.R. (1975) Ore lead isotope ratios in a continuously changing earth. Earth Planetary Science Letters. Vol 28: 155-177.

Davidson, G. (1997) Carbon/Oxygen Isotopes – Their principles and uses in the exploration and understanding of fossil hydrothermal systems. Exploration Geochemistry and Hydrothermal Geochemistry. Course Work Manual 12: 327-358.

Davidson, G. and Kitto, P. (1997) The sulfur isotope signature of Cambrian faults in the Mt Read Volcanic Belt, and their implications for sulfur enrichment in submarine volcanosedimentary rift basins. AMIRA. P.291A.

Deer, W.A., Howie, R.A. and Zussman, J. (1966) An introduction to the Rock-Forming Minerals. Longman Scientific & Technical.

Denwar, K. P. (1998) Beatrice Prospect Literature Review. Exploration Licence EL6/98. Unpublished Pasminco Exploration Report. EL6/98.

Doyle, M.G., (1990) The Geology, Mineralisation and alteration of the Jukes Proprietary prospect, Tasmania. Unpublished BSc.Hons Thesis, University of Tasmania.

Eastoe, C. J., Solomon, M. and Walshe, J. L. (1987) District – Scale Alteration Associated with Massive Sulfide Deposits in the Mount Read Volcanics, Western Tasmania. Economic Geology. Vol. 82

Finlow-Bates, T. and Stumpfl, E.F. (1981) The behaviour of so-called immobile elements in hydrothermally altered rocks associated with volcangenic submarine-exhalative ore deposits. Mineralium Deposita. Vol 16.

Gemmell, J.B. & Large, R.R. (1992) Stringer System and Alteration Zones Underlying the Hellyer Volcanic-Hosted Massive Sulfide Deposit, Tasmania, Australia. Economic Geology. Vol. 87

Gemmell, J.B., (1998) Alteration and Stringer Zones associated with VHMS Deposits: in Ore deposit studies and exploration models, Volcanic-hosted massive sulfide deposits. Codes Short Course Manual 7

Gemmell, J.B., Large, R.R., and Khin Zaw. (1998) Palaeozoic volcanic-hosted massive sulfide deposits. AGSO Journal of Australian Geology & Geophysics, Vol. 17 (4)

Ghazban, F., Schwarcz, H.P., Ford, D.C. (1990) Carbon and Sulfur Isotope Evidence for In Situ Reduction of Sulfate, Nanisivik Lead-Zinc Deposits, Northwest Territories, Baffin Island, Canada. Economic Geology, Vol 85

Govett, G.J.S (1983) Handbook of Exploration Geochemistry: Rock Geochemistry in Mineral Exploration. Elseveier Scientific Publishing Company.

Green, G.R. (1983) The geological setting and formation of the Rosebery volcanic-hosted massive sulfide ore body, Tasmania. Unpublished Ph.D. Thesis. University of Tasmania

Green, G.R., Solomon, M. and Walshe, J.L. (1981) The formation of the volcanic-hosted massive sulfide at Rosbery, Tasmania. Economic Geology. Vol 76: 304-338.

Green, G.R. & Taheri, J. (1992). Stable isotopes and geochemistry as exploration indicators. Bull. Geol. Surv. Tasm. 70: 84-91.

Green, G.R., Ohmoto, H., Date, J., and Takahashi, T. (1983). Whole-Rock Oxygen isotope Distribution in the Fukazawa-Kosaka Area, Hokuroku District, Japan, and Its

Potential Application to Mineral Exploration: in Skinner, B. J., The Kuroko and Related Volcanogenic Massive Sulfide Deposits. Economic Geology. Monograph 5

Guilbert, J. and Park, C. (1986) The Geology of Ore Deposits. Ch. 4f. Freeman.

Gulson, B.L., and Porritt, P.H. (1987) Base metal exploration of the Mount Read Volcanics, Western Tasmania: Pt.II. Lead isotope signatures and genetic implications. Economic Geology. Vol. 82

Gulson, B.L., Large, R.R., and Porritt, P.H. (1987) Base metal exploration of the Mount Read Volcanics, Western Tasmania: Pt.III. Application of Lead Isotopes at Elliott Bay. Economic Geology. Vol. 82

Herrmann, W. (1998) Use of immobile elements and chemostratigraphy to determine precursor volcanics. CODES AMIRA / ARC P439.

Hunns, S.R. (1987) Mineralisation at the Lake Selina Prospect. Unpublished Honours Thesis. University of Tasmania.

Huston, D.L. and Large, R.R. (1987) Genetic and Exploration Significance of the Zinc Ratio (100Zn/(Zn + Pb)) in Massive Sulfide Systems. Economic Geology. Vol 82: 1521-1539.

Huston et al (1992) Laser ablation sulfur isotope analysis at the University of Tasmania-preliminary results from a new technique with research and exploration applications. Bulletin of the Geological Survey of Tasmania 70: 93-95.

Ishikawa, Y., Sawaguchi, T., Iwaya, S., & Horiuchi, M. (1976) Delineation of prospecting targets for Kuroko deposists based on modes of vocanism of underlying dacite and alteration halos. Mining Geology, Vol. 26, (in Japanese with English abs.)

Jenkins, D.R. (1991) Red Hills Unpublished Honours Thesis. University of Tasmania.

Jiang, Wei-The, Peacor, D.R. and Busek. P.R. (1994) Chlorite Geothermometry? – Contaminations and Apparent Octahedral Vacancies. Clays and Clay Minerals. Vol 42 (5): 593-605.

Kharaka. Y.K., Maest, A.S., Carothers, W.W., Law, L.M., Lamothe, P.J. and Fries, T.L. (1987) Geochemistry of metal-rich brines from central Mississippi Salt Dome basin, U.S.A. Applied Geochemistry. Vol 2:543-561.

Khin Zaw (1991) Rosebery-Hercules. Unpublished Ph.D. Thesis. University of Tasmania

Khin Zaw and Cooke, D. (1997) Fluid Inclusions. In Exploration Geochemistry and Hydrothermal Geochemistry. Master of Economic Geology Course Work Manual 12. CODES. University of Tasmania.

Khin Zaw and Large, R. (1992): The precious metal-rich South Hercules mineralization, western Tasmania: a possible subsea-floor replacement volcanic-hosted massive sulfide deposit. Economic-Geology. Vol 87(3): 931-952

Kitto, P.A. (1994) Structural and Geochemical Controls on Mineralisation at Renison, Tasmania. Unpublished Ph.D. Thesis. University of Tasmania.

Kranidiotis, P and MacLean, W. H. (1987) Systematics of Chlorite Alteration at the Phelps Dodge Massive Sulfide Deposit, Matagami, Quebec. Economic Geology. Vol 82: 1898-1911.

Large, R.R., Doyle, M., Raymond, O., Cooke, D., Jones, A. and Heasman, L. (1996) Evaluation of the role of Cambrian granites in the genesis of world class VHMS deposits in Tasmania. Ore Geology Reviews. Vol 10: 215-231.

Large, R.R., Gemmell, B.G. and Herrmann, W. (1998) Summary of geochemical and mineralogical vectors to ore, based on the seven case studies in P439. CODES AMIRA / ARC P439.

Large, R.R. (1992) Australian Volcanic-Hosted Massive Sulfide Deposits: Features, Styles, and Genetic Models. Economic Geology. Vol. 87: 471-510.

McCrea, T. (1950) The isotopic chemistry of carbonates and a palaeotemperature scale. Journal of Chemistry and Physics. Vol 18: 849-857.

McNeill, A.W. and Corbett, K.D. (1992) Geology and mineralisation of the Mt Murchison area. Division of Mines and Mineral Resources. Mt Read Volcanics Project Geological Report. 3

McPhie, J. and Allen, R.L (1992) Facies Architecture of Mineralised Submarine Volcanic Sequences: Cambrian Mount Read Volcanics, Western Tasmania. Economic Geology. Vol87: 587-596

McPhie, J., Doyle, M. and Allen, R.L (1993) Volcanic Textures: A guide to the interpretation of textures in volcanic rocks. CODES Key Research Centre. University of Tasmania.

Nash, J.T. (1976) Fluid Inclusion petrology data for porphyry copper deposits and applications to exploration. US Geological Survey. Professional Papers. Vol 907-D: 1-16

Noonan, D. J. (1990) Lake Margaret EL 5/85 Tasmania, Technical Progress Report for the year ended October 1990. Aberfoyle Report TCR 90-3190.

Ohmoto, H. and Rye, R.O. (1979) Isotopes of sulfur and carbon. In Barnes, H. L. (Ed) Geochemistry of Hydrothermal Ore Deposits. John Wiley and Sons.

Pemberton, J. and Corbett, K.D. (1992) Stratigraphic-facies associations and their relationship to mineralisation in the Mount Read Volcanics. Bulletin of the Geological Survey of Tasmania 70:167-176.

Perkins, C. and Walshe, J.L. (1993) Geochronology of the Mount Read Volcanics, Tasmania, Australia. Economic Geology. Vol 88: 1176-1197.

Peter, J.M. (1986) Genesis of hydrothermal vent deposits in the southern trough of the Guymas Basin, Gulf of California: a mineralogical and chemical study. Unpubl. MsC. Thesis, University of Toronto.

Pontifex, I.R. (1998) Mineralogical Report No. 7666. Pontifex & Associates Pty. Ltd.

Roedder, E. (1984) Fluid Incluison as samples of ore fluids. In Barnes, H. L. (Ed) Geochemistry of Hydrothermal Ore Deposits. John Wiley and Sons.

Sangster, D.F. (1968) Relative sulfur isotopic abundance of ancient seas and stratabound sulfide deposits. Proc. Geol. Assoc. Canada. Vol. 19.

Solomon, M., Eastoe, C.J., Walshe, J.L. & Green, G.R. (1988) Mineral Deposits and Sulfur Isotope Abundances in the Mount Read Volcanics between Que River and mount Darwin, Tasmania. Ecomonic Geology, Vol. 83:1307-1328

Southgate, P.N., Lambert, I.B., Donnelly, T.H., Henry, R., Etminan, H. and Weste, G. (1989) Depositional environments and diagensis in Lake Parakeelya: a Cambrian alkalike playa from the Officer Basin, South Australia. Sedimentology. Vol 36: 1091-1112.

Taylor. H.P. (1979) Oxygen and Hydrogen Isotope Relationships in Hydrothermal Mineral Deposits. In Barnes, H. L. (Ed) Geochemistry of Hydrothermal Ore Deposits. Second Edition. John Wiley and Sons.

Tompkins, L.A., Rayner, M.J., Groves, D.I., and Roche, M.T., (1994) Evaporite: In Situ Sulphur Source for Rythmically Banded Ore in the Cadjebut MVT Zn-Pb Deposit, Western Austral. Economic Geology, Vol 89.

Walshe, J.L. (1986) A six-component chlorite solid solution model and the conditions of chlorite in hydrothermal and geothermal systems. Economic Geology, Vol 81: 681-703.

Warren, J.K. (1996) Evaporites, brines and base metals: what is an evaporite? Defining the rock matrix. Australian Journal of Earth Sciences. Vol 43: 115-132.

White, M.J and McPhie, J. (1996) Stratigraphy and Palaeovolcanology of the Cambrian Tyndall Group, Mt Read Volcanics, western Tasmania. Australian Journal of Earth Sciences. Vol 43: 147-159

Windchester, J.A. and Floyd, P.A. (1977) Geochemical discrimination of different magma series and their differentiation products using immobile elements. Chemical Geology. Vol 20.

Wilde, A.R. and Kerr, T.L. (1990) Exploration Licence 102/87, 1989-1990 Annual Report. Unpublished report to BHP exploration. (MRT Report CR 90-3102)

Wyman, B. (1998) Chlorite alteration associated with syn-volcanic granites and Cu-Au mineralisation: A pilot study along the Jukes Road. CODES AMIRA / ARC P439.

Zheng, Y.F. and Hoefs, J. (1993) Carbon and Oxygen isotopic covariations in hydrothermal calcites. Mineralium Deposita. Vol 28:79-89.

Appendix 1

Diamond Drill Logs

660136

PASMINCO EXPLORATION

DIAMOND DRILL HOLE LOGGING

Hole_ID MS1	Project Q'town
Hole_Type DDH	Tenement_No.
Year	Prospect BEATRICE
Geologist M. HOPE	Date 22/3/99

Depth	Lithology Code	Lithology Colour	Comments	Alteration Up to 3 codes w. intensities (1-3)	Mineralisation Up to 3 codes with %	Graphic Log	preferred std field	preferred std field
0			Scree					
			3.1m yellow/brown sericite altered fine volcaniclastic dark dendritic chl features 5.4m 8cm rhyolitic clast showing voids = dissolution of carb veins					
			pyrolusite veining zonation away from fractures 					
10								
			13.2m Coarse volcaniclastic containing <1cm clasts of aphyric pink rhyolite	Weak to mod sericite alt chl increases to mod.				
			19.5m fine ashy green volcaniclastic					
20								
				Weak pervasive sericite alt				
			strongly foliated sericitic g/m c 1cm aphyric clast	moderate chl spotting in sericitic ground mass				
30								
				chl spots increasing in size to 3mm				
				Ser3 Chl3	moderate mineralisation			
				alt increasing chl spots larger & coalescing				
40								

PASMINCO EXPLORATION

DIAMOND DRILL HOLE LOGGING

660137

Hole_ID	Project
Hole_Type	Tenement_No.
Year	Prospect
Geologist	Date

Depth	Lithology Code	Colour	Comments	Alteration Up to 3 codes w. intensities (1-3)	Mineralisation Up to 3 codes with %	Graphic Log	preferred std field	preferred std field
				chl alt pervasive mod-strong	veinlet & dissem gn, sph & py		50 40°	
				Ser 3				
			foliation defined by sericite. pseudobreccia - chl in sericite matrix	chl alt pervasive mod-strong	weak - mod dissem py veinlet qtz, py ± sph ± Qtz common		50 22°	
60			rare <2mm rounded pink/cream aphyric rhyolite clasts 1-2mm Quartz pebbles					
			Some gn & sph not associated with veins. fine disseminated mineralisation	Ser 3	mod - veinlet & dissem gn, py, sph			
				Ser 3 chl 3				
70			6.4m. Graded mass flow flamme more abundant right at top. Clasts of aphyric Pink/green rhyolite	Relatively fresh rock				
80					weak dissem py			

660138

PASMINCO EXPLORATION

DIAMOND DRILL HOLE LOGGING

Hole_ID	Project
Hole_Type	Tenement_No.
Year	Prospect
Geologist	Date

Depth	Lithology Code	Lithology Colour	Comments	Alteration Up to 3 codes w. intensities (1-3)	Mineralisation Up to 3 codes with %	Graphic Log	preferred std field	preferred std field
90								
			8cm rounded rhyolite clast Abundant <3cm limestone clasts (not seen in last unit)	Weak sericite alt				
100			lithic/fiamme unit	Ser 1-3 Sericite alt increasing	qtz carb qtz veinlets			
110			coarse lithic sandstone					
			Strongly foliated abundant veinlet & dissem py, sph 114m - Qtz/lithic sandstone top grading into coarse lithic breccia	Ser 3 Chl 3 Ser 3	5-10% total		moderately broken core	
120								

660139

PASMINCO EXPLORATION

DIAMOND DRILL HOLE LOGGING

Hole_ID	Project
Hole_Type	Tenement_No.
Year	Prospect
Geologist	Date

Depth	Lithology Code	Lithology Colour	Comments	Alteration Up to 3 codes w. intensities (1-3)	Mineralisation Up to 3 codes with %	Graphic Log	preferred std field	preferred std field
130			Clasts comprise ~60% typically rhyolite - limestone and shale limestone more common at base 7cm shale clast			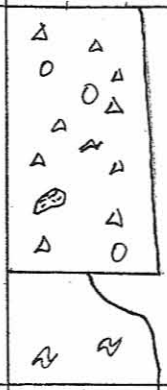		
140			Poorly graded mass flows			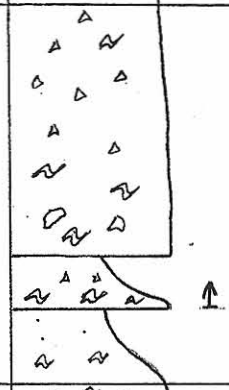		
150			Abundant sericite altered fiamme	Ser 3		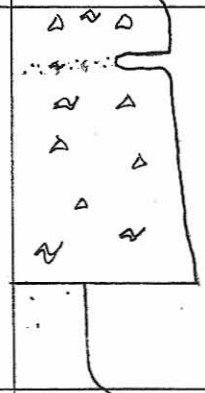		
160			Angular limestone clasts Qtz-Chl spotting of fine volcaniclastic			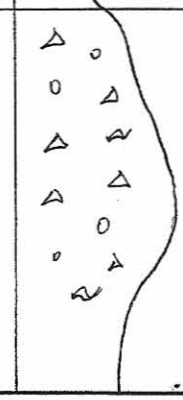		

660140

PASMINCO EXPLORATION

DIAMOND DRILL HOLE LOGGING

Hole_ID	Project
Hole_Type	Tenement_No.
Year	Prospect
Geologist	Date

Depth	Lithology Code	Lithology Colour	Comments	Alteration Up to 3 codes w. intensities (1-3)	Mineralisation Up to 3 codes with %	Graphic Log	preferred std field	preferred std field
			Well graded mass flow			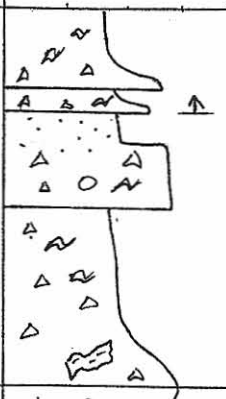		
			Subrounded to angular abundant limestone clasts					
170			Abundant limestone clasts <7cm Qtz xtals & sericite chert y augen texture					
			fspar phyric rhyolite clast with chl alt halo					
180			Subround rhyolite clasts					
			fine bedded clast showing microfault					
			limestone, shale & rhyolite clasts to 3cm but typically ~4mm					
190								
			sericitic volcaniclastic breccia. well sorted/bedded volcaniclastic sandstone containing small shale clasts	Ser 2				
200			Gradational contact into black shale				50 20°	

660141

PASMINCO EXPLORATION

DIAMOND DRILL HOLE LOGGING

Hole_ID	Project
Hole_Type	Tenement_No.
Year	Prospect
Geologist	Date

Depth	Lithology Code	Lithology Colour	Comments	Alteration Up to 3 codes w. intensities (1-3)	Mineralisation Up to 3 codes with %	Graphic Log	preferred std field	preferred std field
					strong veinlet Pyrite Arsenopyrite also present		50 30°	
210					2cm blebs of py in assoc E carb			
				Ser 3				
			216.5m Green grey shale rounded dark grey chloritic clasts				50 5°	
220								
			Abundant carbonate spots <1mm		strongly pyritic dissem bedded & veinlet - large framboidal py			
				Ser 2				
230					weak veinlet qtz & sph - 10cm zone of strong py & carb veins			
							50	
			Grey Green shale				50 20°	
							50 10°	
			237m Coarse volcanic sandstone abundant Qtz lithics in chl g'm - limestone & rhyolite clasts <4cm	Ser 2-3 Chl 3			strongly foliated	
240								

FASMINCO EXPLORATION

DIAMOND DRILL HOLE LOGGING

Hole_ID	Project
Hole_Type	Tenement_No.
Year	Prospect
Geologist	Date

Depth	Lithology Code	Lithology Colour	Comments	Alteration (Up to 3 codes w. intensities (1-3))	Mineralisation (Up to 3 codes with %)	Graphic Log	preferred std field	preferred std field
			Poorly sorted subrounded to sub angular cherty & shale clasts up to 10mm	Ser 3 Chl 2			8cm black shale clast flattening compaction ~40° CA	
			Badly broken pyritic black shale					
			Qtz fspar Porphyry	Chl 2				
				Chl 1-2				
250			uniform black shale moderately cleaved rare carbonate laminations		moderate Py bedding & veinlets		So 15°	
							So 10°	
260								
			bedding becoming more disrupted		moderate Py ± carb vein		So 25-30°	
			266.7m 30cm fault zone					
270								
			271m peperitic contact	Ser 2-3 Chl 2	Sph in Qtz chl carb veins			
280								

PASMINCO EXPLORATION

DIAMOND DRILL HOLE LOGGING

Hole_ID MSL	Project Qtown
Hole_Type DDH	Tenement_No.
Year	Prospect Beatrice
Geologist MAH	Date 18/3/99

Depth	Lithology Code	Lithology Colour	Comments	Alteration (Up to 3 codes w. intensities (1-3))	Mineralisation (Up to 3 codes with %)	Graphic Log	preferred std field	preferred std field
10			Glacial scree weathered black shale & minor dolerite, i.e. QFP					
20			Well sorted feldspathic sandstone Pyritic black shale				S0 60°	
30			20m green/grey, well sorted bedded sandstone, with minor shale bands. Sandstone containing f'spar grains & lithics - disseminated Py		pyritic shale		S0 5-20°	
40			Pyritic black shale		Py bedded & c Carb Qtz veins		S0 5° S0 32° S0 18° S0 27°	

PASMINCO EXPLORATION

DIAMOND DRILL HOLE LOGGING

Hole_ID	Project
Hole_Type	Tenement_No.
Year	Prospect
Geologist	Date

Depth	Lithology Code	Lithology Colour	Comments	Alteration (Up to 3 codes w. intensities (1-3))	Mineralisation (Up to 3 codes with %)	Graphic Log	preferred std field	preferred std field
							So 12°	
			Gradational contact Interbedded sand/siltstone flame structures - silt into sand.		weakly pyritic disseminated		So 23° So 20°	
50			lithics & flamme gradational contact back to black shale containing finely bedded white calcareous beds		veinlet. dissem & blebby py common			
60			coarse volcaniclastic containing aphyric volcanic clasts & limestone large aphyric clast ~9cm				Broken core	
			flamme & aphyric clasts in fspar, chl gm		weak pyrite & minor gn			
70			Clasts of fspar phyric lava (~3cm) shale & limestone (limestone surrounded) clasts commonly ~3-6mm - Possible weak up hole grading					
			10cm pink lava clast 10cm light pink Qtz phyric lava clast					
80								

PASMINCO EXPLORATION

DIAMOND DRILL HOLE LOGGING

Hole_ID	Project
Hole_Type	Tenement_No.
Year	Prospect
Geologist	Date

Depth	Lithology Code	Lithology Colour	Comments	Alteration Up to 3 codes w. intensities (1-3)	Mineralisation Up to 3 codes with %	Graphic Log	preferred std field	preferred std field
90						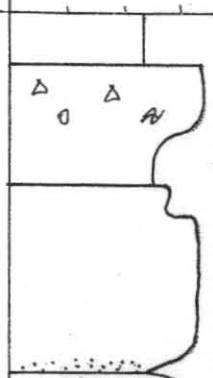		
100			Units conformable ± coarse base of mass flow			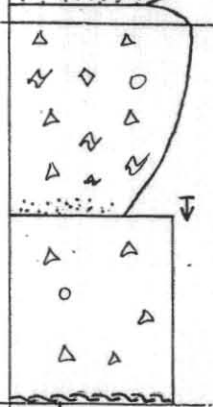	So 5°	
110			Shale grey green - lithic/fiamme sandstone ± abundant <4mm shale clasts gradational contact very similar 46m but less defined bedding black shale strong veined	Ser 2	py in assoc ± Qtz carb veins, also as beds/blebby	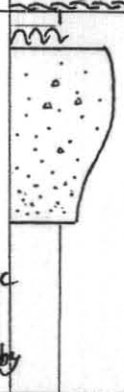		
120			Dark nodules - assoc ± blebby py Dark green/grey well bedded Sandstone		py ± qn, sph in vein	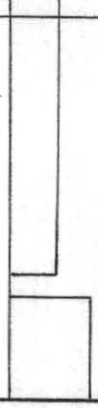	So 20° So //	

PASMINCO EXPLORATION

DIAMOND DRILL HOLE LOGGING

Hole_ID	Project
Hole_Type	Tenement_No.
Year	Prospect
Geologist	Date

Depth	Lithology Code	Colour	Comments	Alteration Up to 3 codes w. intensities (1-3)	Mineralisation Up to 3 codes with %	Graphic Log	preferred std field	preferred std field
			Volcanic sandstone clasts in dark grey shale		weak sphgn in Qtz carb veinlet			
130			Strongly foliated swirling colouration green, grey, black texture					
			Typical black shale				So 10°	
140							So // LCA	
				mod-strong Sericite-silica	moderately pyritic minor sph veinlets			
			limestone & shale clasts <25mm in shale matrix	mod ser				
150					Veinlet py & sph in Qtz carb			
				mod sericite				
			Aphyric - & zones of coarse Qtz pebbles	mod sericite & silica				
160			Qtz phyric clasts in Qtz pebble sericite matrix					

PASMINCO EXPLORATION

DIAMOND DRILL HOLE LOGGING

Hole_ID	Project
Hole_Type	Tenement_No.
Year	Prospect
Geologist	Date

Depth	Lithology Code	Lithology Colour	Comments	Alteration Up to 3 codes w. intensities (1-3)	Mineralisation Up to 3 codes with %	Graphic Log	preferred std field	preferred std field
			sharp contact relationship unknown (fault?)					
			Black shale				So 0-10°	
			dark elongate blebs					
					moderate bedded & veinlet pyrite			
170			finely laminated pyritic beds				So // CA	
							So 5°	
180								
				Mod ser chl at contact				
190			Qtz-fspar Porphyry					
			?finer grained near contact : quenched.		Abundant Qtz, Carb Chl veins			
200								

PASMINCO EXPLORATION

DIAMOND DRILL HOLE LOGGING

Hole_ID	Project
Hole_Type	Tenement_No.
Year	Prospect
Geologist	Date

Depth	Lithology Code	Lithology Colour	Comments	Alteration Up to 3 codes w. intensities (1-3)	Mineralisation Up to 3 codes with %	Graphic Log		preferred std field	preferred std field
210			rare chl grains altered amphibole	moderate Sericite					
220			minor breccia	weak sericite Pink grey					
230				Colour Pink colour fresh porphyry					
240				weak to mod sericite alt of gm					

PASMINCO EXPLORATION

DIAMOND DRILL HOLE LOGGING

Hole_ID	Project
Hole_Type	Tenement_No.
Year	Prospect
Geologist	Date

Depth	Lithology Code	Lithology Colour	Comments	Alteration Up to 3 codes w. intensities (1-3)	Mineralisation Up to 3 codes with %	Graphic Log		preferred std field	preferred std field
					minor CPY in 30mm Qtz Carb Chl vein				
250			Brecciated zone	strong chl silica alt	minor PY ±gn				
				mod chl ser alt					
260									
				weak to moderate Chl-Ser±fgm					
280			weak foliation associated with sericite alt ~60°LCA weakly brecciated	moderate sericite Chlorite alteration of ground mass	minor sph gn in qtz carb veins sph bbbs 20mm				

PASMINCO EXPLORATION

DIAMOND DRILL HOLE LOGGING

Hole_ID	Project
Hole_Type	Tenement_No.
Year	Prospect
Geologist	Date

Depth	Lithology Code	Lithology Colour	Comments	Alteration Up to 3 codes w. intensities (1-3)	Mineralisation Up to 3 codes with %	Graphic Log	preferred std field	preferred std field
290				moderate sericite chlorite alt. fspars becoming altered to sericite	Weak sph gn min in 1% rare Qtz Carb veins			
300			Peperitic contact Block shale c mod Qtz Carb veining				50 60 LCA	
310				mod ser. chl alt	pyritic contact			
320				weak to moderate sericite increase of chl to mod.				

PASMINCO EXPLORATION

DIAMOND DRILL HOLE LOGGING

Hole_ID	Project
Hole_Type	Tenement_No.
Year	Prospect
Geologist	Date

Depth	Lithology			Alteration	Mineralisation	Graphic Log		preferred std field	preferred std field
	Code	Colour	Comments	Up to 3 codes w. intensities (1-3)	Up to 3 codes with %				
330					2-3mm gn in Carb veins				
340				Weak to moderate sericite chlorite alteration	coarse sph gn in Qtz Carb vein				
350									
360									

PASMINCO EXPLORATION

DIAMOND DRILL HOLE LOGGING

Hole_ID MS7	Project Q'town
Hole_Type DDH	Tenement_No. EL 6/98
Year 1999	Prospect Beatrice
Geologist MAH	Date 26/3/99

Depth	Lithology Code	Lithology Colour	Comments	Alteration (Up to 3 codes w. intensities (1-3))	Mineralisation (Up to 3 codes with %)	Graphic Log (1/16, 1/2, 4, 8, 32)	preferred std field	preferred std field
			Glacial Scree QFP dominated					
			7-109.1m Qtz fspar porphyry					
20								
			24-28m clastic porphyry cemented by carb-chl ± FeOx	Mod chl				
			Pink coloured QFP Kspar alteration of ground mass	moderate				
40								
			abundant Qtz carb ± chl veins					
60					minor malachite in Qtz chl carb vein			
				minor sericite	chl veinlets ± cpy & gn			
80								

PASMINCO EXPLORATION

DIAMOND DRILL HOLE LOGGING

660153

Hole_ID	Project
Hole_Type	Tenement_No.
Year	Prospect
Geologist	Date

Depth	Lithology Code	Lithology Colour	Comments	Alteration Up to 3 codes w. intensities (1-3)	Mineralisation Up to 3 codes with %	Graphic Log 1/10 1/2 4 8 12	preferred std field	preferred std field
100			hornblende intact	relatively unaltered very weak sericite				
			sharp contact - possibly peperitic log 2m well laminated, weakly calcareous interbedded shale flame structures & graded beds	sericite increases toward contact but fspar still intact	weak sph py at contact; disseminated py		so 46°; so 55°	
120							so 60°	
					minor py sph in qtz carb ± chl vein		so 22°; so 45°	
140							so 52°	
					disseminated py in assoc ± carb rich beds		so 34°; so 58°	
160								

PASMINCO EXPLORATION

DIAMOND DRILL HOLE LOGGING

660154

Hole_ID	Project
Hole_Type	Tenement_No.
Year	Prospect
Geologist	Date

Depth	Lithology Code	Lithology Colour	Comments	Alteration Up to 3 codes w. intensities (1-3)	Mineralisation Up to 3 codes with %	Graphic Log 1/16 1/4 1 4 8 12	preferred add field	preferred add field
			strong Qtz Carb veining strongly broken core				So 50°	
			Black nodules appear and start to increase					
180							So 60°	
			pyrite in close association with dark nodules		dark sph ! py in carb vein		So 48°	
					Sph in Carb veinlet			
			strongly broken core - fault		Sph ! qz in Carb veinlets minor cpy			
200							So 42°	
							So 53°	
				Mn Carb veins				
							So 70°	
220			strongly cleaved and chl altered					
							So 80°	
			231.2m sharp pegmatic contact	Strong ser. of qm alt of some fspar				
			phenocrysts flow. aligned ~ 50° LCA					
240								

PASMINCO EXPLORATION

DIAMOND DRILL HOLE LOGGING

660155

Hole_ID	Project
Hole_Type	Tenement_No.
Year	Prospect
Geologist	Date

Depth	Lithology Code	Lithology Colour	Comments	Alteration Up to 3 codes w. intensities (1-3)	Mineralisation Up to 3 codes with %	Graphic Log 1/10 1/2 4 8	preferred old field	preferred old field
260			Well developed peperitic contact	Mod ser alt	minor sph as veinlets & dissem material			
			261.2m weakly peperitic contact Black shale - less carbonate localised microfaulting		weak veinlet py sph on in carb veins		So 65° So 56°	
300			-pyrite abundant in assoc & carbonate beds & veins -bedding disrupted by microfaults				So 50° So 35°	
320			series of lithic rich beds containing volcanic & shale material & Qtz grains & flamme Dark green fine/med volcaniclastic		abundant py in Carb veins sph, semi aligned & foliation			

PASMINCO EXPLORATION

DIAMOND DRILL HOLE LOGGING

660156

Hole_ID	Project
Hole_Type	Tenement_No.
Year	Prospect
Geologist	Date

Depth	Lithology Code	Lithology Colour	Comments	Alteration Up to 3 codes w. intensities (1-3)	Mineralisation Up to 3 codes with %	Graphic Log tp ½ 4 8 12	preferred add field	preferred add field
			Chlorite spotting in fine grained tops of mass flow units		cpy±gn veinlets in framme			
			limestone clasts ± framme more abundant					
340								
			limestone clasts at base	weak chl spotting			So 25°	
			351-1-356.4m well graded limestone framme rich unit with well bedded top	weak carb spotting			So 45°	
				chl alt. increases to mod.			So 45°	
			Coarse volcaniclastics rhyolitic, limestone clasts ± framme - more massive units	chl increases gn as to mod/strong	veinlets ± disseminated sph ± py			
				mod-strong sericite				
380				strong chl	gn±sph assoc c chl±py			
			medium grained volcanic sandstone ± rare rhyolite clasts ± framme ± limestone	Weak to mod ser of gm				
			Coarse limestone breccia	chl 3				
				mod to strong chl 3	gn±sph rim on carb clast			
					rare veinlet gn±fracture controlled disse		So 55°	

MINCO EXPLORATION

DIAMOND DRILL HOLE LOGGING

660157

Hole_ID	Project
Hole_Type	Tenement_No.
Year	Prospect
Geologist	Date

Depth	Lithology Code	Lithology Colour	Comments	Alteration Up to 3 codes w. intensities (1-3)	Mineralisation Up to 3 codes with %	Graphic Log 1/10 1/2 4 8 12	preferred std field	preferred std field
					gn py sph in chl			
			dacite & limestone clasts to 6cm	relatively unaltered				
120								
			graded mass flow units with coarse 8-10cm limestone & minor rhyolite clasts				So 52° LCA	
			green ashy volcaniclastic grading into coarse carb clast rich base	weak chl				
0				mod sericite				
			Pumiceous mass flow unit & strong pink kspar/chl/hem-hag alt. producing pseudobreccia	weak kspar alteration strong kspar alt & xtalline hematite				
460								
			series of Qtz-fspar veins xcut by Qtz chl selective kspar alt of pumice limestone clasts still present rimmed & hematite dusting					
				mod chl				
				chl spotting	minor sph cpy increasing			
580								

Appendix 2

Wholerock Geochemical Analyses

	1-1	1-2	1-3	1-4	1-6	1-9	1-14	3-2	3-9	3-12	3-20	3-23
SiO2 wt%	71.8	74.1	71.3	71.4	68.5	61.8	69.1	68.5	68.8	67.5	76.3	67.8
Al2O3wt%	11.9	11.5	9.2	12.3	13	13.2	11.2	13.1	11.5	6.85	10.9	12.2
TiO2_ppm	2000	2000	1900	2500	3100	3200	2700	3500	2900	1200	2400	3000
Fe2O3_ppm	66000	69500	104000	63000	29500	48000	66500	67000	22000	177000	60000	102000
MnO_ppm	4400	1900	7800	2100	2700	3400	17800	3200	4200	9700	900	1700
MgO_ppm	7900	7700	7300	3900	4500	7000	7900	14400	3400	10400	4800	7300
CaO_ppm	1000	700	1000	500	37500	66000	2700	8700	48000	800	1900	1100
Na2O_ppm	700	500	-500	-500	800	1600	600	600	800	-500	-500	500
K2O_ppm	32500	29500	17400	33500	52000	42500	53000	53000	57000	2500	32000	36000
P2O5_ppm	390	410	290	370	480	500	400	790	450	210	270	440
SO3_ppm	8260	5670	18400	17800	4210	1660	3450	11600	6300	5510	8410	41000
LOI_ppm	31500	25500	33500	29000	49000	79500	41500	31000	54000	46500	24500	49500
S_ppm	3230	1830	6850	7320	1250	440	1400	4070	2480	1870	2960	33000
Zr_ppm	280	293	262	321	292	267	255	250	258	172	275	298
Sr_ppm	-5	5	-5	6	48	62	23	32	73	6	6	9
Rb_ppm	179	166	117	189	235	209	193	212	223	25	168	226
Ba_ppm	375	435	270	385	1270	560	2430	1930	1970	78	470	470
Nb_ppm	10	11	8	10	10	8	10	10	9	7	12	10
Y_ppm	51	50	39	46	37	35	45	30	40	24	40	31
C_ppm												
OrgC_ppm												
CO3_ppm												
CCPI	69.000934	72.01493	86.81747	66.96697	39.17051	55.4995	58.125	60.2963	30.52885	98.94403	67.28972	74.96571
AI	95.961995	96.875	98.01587	100	59.59916	42.27156	94.85981	87.87484	55.31136	97.72727	96.33508	96.43653
P2O5/TiO2	0.195	0.205	0.152632	0.148	0.154839	0.15625	0.148148	0.225714	0.155172	0.175	0.1125	0.146667
Ti/Zr	4.2820317	4.092044	4.347406	4.668882	6.36439	7.184832	6.347482	8.392782	6.738391	4.18245	5.231864	6.035078
Rb/Sr	35.8	33.2	23.4	31.5	4.895833	3.370968	8.391304	6.625	3.054795	4.166667	28	25.11111
Ba/Sr	75	87	54	64.16667	26.45833	9.032258	105.6522	60.3125	26.9863	13	78.33333	52.22222
Mg number	10.690122	9.974093	6.55885	5.829596	13.23529	12.72727	10.61828	17.69042	13.38583	5.549626	7.407407	6.678866

	7-9	7-12	7-16	7-13	7-27	8-27	3-26	3-28	9-2	5-1	7-1	8-17
SiO2 wt%	73.7	69.2	71.7	72.9	65.6	73.3	68.1	72	66.6	65.3	52.2	48.2
Al2O3wt%	15	12.3	13.2	11.8	12.9	14.6	12.4	13.7	12.9	14.2	13.2	13.2
TiO2_ppm	3200	3600	2400	2100	3300	2600	3700	2700	3300	4200	4000	3100
Fe2O3_ppm	41000	49500	19700	24500	52500	43500	63000	54500	41500	49000	108000	109000
MnO_ppm	800	2000	500	500	1300	1000	1600	1300	4800	1500	21000	50500
MgO_ppm	8000	10200	5000	5400	6000	6700	8900	5900	7700	29500	27500	28500
CaO_ppm	3400	9000	12800	10900	17700	6700	9200	7800	39500	23000	24500	58500
Na2O_ppm	12300	24000	37500	33000	1000	1200	1400	1300	800	700	1400	700
K2O_ppm	54000	50500	49000	42000	72500	64500	78000	63500	53500	39500	37500	18600
P2O5_ppm	570	620	410	360	520	310	620	420	530	720	10600	6230
SO3_ppm	2300	2100	-100	-100	250	740	120	2110	1210	23500	46000	35500
LOI_ppm	16000	21500	18000	16200	34000	19700	22500	22000	50500	56000	77500	94500
S_ppm	630	690	50	130	110	240	90	640	400	14500	35000	21500
Zr_ppm	306	325	164	156	323	307	281	306	276	131	138	117
Sr_ppm	36	55	120	190	53	45	68	49	52	35	52	63
Rb_ppm	197	192	145	137	298	286	282	267	236	190	196	98
Ba_ppm	1860	1810	1390	1160	2460	2420	2680	2080	2150	575	980	590
Nb_ppm	12	12	13	11	11	13	11	14	12	9	10	7
Y_ppm	36	30	21	18	44	34	33	42	37	23	37	31
C_ppm										12200	10300	25000
OrgC_ppm										7390	2820	3160
CO3_ppm										24000	37500	110000
CCPI	42.497832	44.48584	22.21223	28.50334	44.31818	43.3132	47.52148	48.24281	47.53623	66.13311	77.69495	87.69133
AI	79.79408	64.78122	51.77373	51.91676	80.76132	90.01264	89.12821	88.40764	60.29557	74.43366	71.50715	44.30856
P2O5/TiO2	0.178125	0.172222	0.170833	0.171429	0.157576	0.119231	0.167568	0.155556	0.160606	0.171429	2.65	2.009677
Ti/Zr	6.1247637	8.396688	6.826869	7.052758	5.647317	8.473278	6.465028	4.795876	16.22134	13.52495	10.37569	8.719774
Rb/Sr	5.4722222	3.490909	1.208333	0.721053	5.622642	6.355556	4.147059	5.44898	4.538462	5.428571	3.769231	1.555556
Ba/Sr	51.666667	32.90909	11.58333	6.105263	46.41509	53.77778	39.41176	42.44898	41.34615	16.42857	18.84615	9.365079
Mg number	16.326531	17.08543	20.24291	18.0602	10.25641	13.34661	12.3783	9.768212	15.65041	37.57962	20.2952	20.72727

	8-19	8-8	8-10	8-13	9-1	Tasgran	Tasmonz
SiO2 wt%	70.1	71.3	63.6	62.9	71.6	73.2	58.4
Al2O3wt%	12.8	13.2	14.1	9.85	13.9	13.7	17.2
TiO2_ppm	2600	2400	4300	4600	2600	2900	6200
Fe2O3_ppm	23000	46000	121000	49500	24000	22000	54000
MnO_ppm	1900	1700	4800	500	600	400	1200
MgO_ppm	5400	7500	15900	29500	4500	6100	29500
CaO_ppm	22500	3700	1200	26500	29500	18500	56500
Na2O_ppm	12300	1800	-500	2100	27000	27500	53500
K2O_ppm	56000	78500	33500	39000	31500	46000	30000
P2O5_ppm	550	450	800	830	510	1030	1480
SO3_ppm	1560	1330	5210	19400	290	-100	-100
LOI_ppm	47000	16300	35500	66000	37000	7900	8000
S_ppm	570	490	2050	12400	200	700	90
Zr_ppm	165	164	283	155	170	169	167
Sr_ppm	99	93	9	55	179	157	359
Rb_ppm	219	221	192	192	113	254	112
Ba_ppm	1650	4670	1190	745	960	375	595
Nb_ppm	11	9	12	11	11	13	9
Y_ppm	19	18	43	28	25	33	20
C_ppm				17600			
OrgC_ppm				9020			
CO3_ppm				43000			
CCPI	29.369183	39.98505	80.57681	65.77852	32.75862	27.65748	50
AI	63.825364	93.98907	98.60279	70.54583	38.91892	53.10907	35.10324
P2O5/TiO2	0.2115385	0.1875	0.186047	0.180435	0.196154	0.355172	0.23871
Ti/Zr	15.35265	10.98292	9.122589	13.32188	11.98969		
Rb/Sr	2.2121212	2.376344	21.33333	3.490909	0.631285	1.617834	0.311978
Ba/Sr	16.666667	50.21505	132.2222	13.54545	5.363128	2.388535	1.657382
Mg number	19.014085	14.01869	11.61432	37.34177	15.78947	21.70819	35.32934

Appendix 3

Electron Microprobe Analysis

Label	7-15_3	7-15_3	7-15_3	7-15_3	7-15_4	7-15_4	7-15_5	7-15_6	1-7_1.	1-7_1.	1-7_4.	1-7_4.	1-7_5.	1-7_5.	1-7_6.	1-7_7.	1-7_8.	1-7_8.	1-7_8.	1-9_1.	1-9_1
SiO2	46.42	38.23	47.04	37.13	48.37	46.44	48.23	45.18	55.4	49	49.5	49.5	49.2	48.7	46.1	49.2	48.4	52.3	47.6	47.9	47.4
TiO2	0.17	0.08	0.21	0.19	0.16	0.15	0.14	0.4	0.22	0.23	0.13	0.14	0.05	0.04	0.07	0.12	0.2	0.26	0.12	0.32	0.38
Al2O3	27.89	24.67	28.14	24.27	28.32	27.41	28.68	27.53	25.5	29.5	31.2	31.3	31.6	31.3	29.8	31.1	29.3	28.6	28.9	31	30.4
Cr2O3	0.01	0.05	0	0	0.01	0	0.05	0.01	0	0	0	0.05	0.02	0.01	0	0	0	0.01	0.06	0	0.05
FeO	8.12	19	5.49	19.63	5.77	7.36	5.85	9.39	1.27	4.63	3.18	2.91	2.85	3	8.01	3.61	5.42	2.74	5.36	4.26	4.14
MgO	0.88	2.04	1.46	2.22	1.33	1.15	1.26	1.7	1.09	1.36	1.26	1.25	1.1	1.1	1.6	1.3	1.6	1.3	1.65	1.15	1.15
Na2O	0.07	0.05	0.07	0.04	0.06	0.08	0.05	0.04	0.65	0.05	0.07	0.09	0.11	0.11	0.08	0.09	0.09	0.36	0.07	0.07	0.06
K2O	10.41	6.31	11.23	6.04	11.33	10.72	10.83	9.82	7.74	10.4	10.2	10.3	10.2	10.5	9.35	10.1	10.6	9.56	10.5	11.1	10.6
F	0.22	0.18	0.37	0.13	0.35	0.25	0.21	0.17	0.32	0.4	0.4	0.37	0.26	0.31	0.33	0.29	0.42	0.33	0.39	0.16	0.14
Cl	0.04	0.03	0.03	0.03	0.01	0.02	0.03	0.02	0.01	0.01	0.01	0.01	0.03	0.01	0	0.02	0.01	0	0.01	0	0.01
H2O(c)	4.17	3.81	4.13	3.78	4.23	4.14	4.29	4.18	4.33	4.25	4.32	4.33	4.36	4.31	4.21	4.36	4.23	4.37	4.18	4.38	4.32
O=F	0.09	0.08	0.16	0.05	0.15	0.1	0.09	0.07	0.14	0.17	0.17	0.16	0.11	0.13	0.14	0.12	0.18	0.14	0.16	0.07	0.06
O=Cl	0.01	0.01	0.01	0.01	0	0	0.01	0	0	0	0	0	0.01	0	0	0	0	0	0	0	0
Sum Ox%	98.3	94.36	98	93.38	99.78	97.59	99.51	98.36	96.4	99.6	100	100	99.6	99.2	99.5	100	100	99.6	98.8	100	98.5
mg numbe	9.778	9.696	21.01	10.16	18.73	13.51	17.72	15.33	46.2	22.7	28.4	30	27.8	26.8	16.6	26.5	22.8	32.2	23.5	21.3	21.7
Si	6.495	5.871	6.544	5.791	6.603	6.535	6.584	6.358	7.41	6.61	6.59	6.58	6.56	6.54	6.33	6.56	6.55	6.93	6.54	6.44	6.47
Ti	0.018	0.01	0.022	0.022	0.016	0.016	0.014	0.042	0.02	0.02	0.01	0.01	0.01	0	0.01	0.01	0.02	0.03	0.01	0.03	0.04
Al/Al IV	1.505	2.129	1.456	2.209	1.397	1.465	1.416	1.642	0.59	1.39	1.41	1.42	1.44	1.46	1.67	1.44	1.45	1.08	1.47	1.56	1.53
Al VI	3.095	2.337	3.158	2.252	3.16	3.08	3.198	2.924	3.43	3.3	3.47	3.48	3.53	3.5	3.16	3.44	3.22	3.38	3.21	3.36	3.36
Cr	0.002	0.006	0	0	0.002	0	0.005	0.002	0	0	0	0.01	0	0	0	0	0	0	0.01	0	0.01
Fe2+	0.95	2.44	0.639	2.561	0.659	0.866	0.668	1.105	0.14	0.52	0.35	0.32	0.32	0.34	0.92	0.4	0.61	0.3	0.62	0.48	0.47
Mg	0.183	0.466	0.302	0.516	0.27	0.241	0.257	0.357	0.22	0.27	0.25	0.25	0.22	0.22	0.33	0.26	0.32	0.26	0.34	0.23	0.24
Na	0.02	0.014	0.02	0.011	0.016	0.022	0.013	0.011	0.17	0.01	0.02	0.02	0.03	0.03	0.02	0.02	0.02	0.09	0.02	0.02	0.02
K	1.857	1.237	1.993	1.201	1.973	1.924	1.886	1.762	1.32	1.79	1.73	1.74	1.73	1.8	1.64	1.72	1.83	1.61	1.84	1.9	1.85
F	0.096	0.089	0.164	0.063	0.149	0.11	0.091	0.076	0.14	0.17	0.17	0.16	0.11	0.13	0.14	0.12	0.18	0.14	0.17	0.07	0.06
Cl	0.008	0.007	0.006	0.007	0.002	0.004	0.007	0.004	0	0	0	0	0.01	0	0	0	0	0	0	0	0
OH	3.895	3.904	3.829	3.93	3.849	3.886	3.902	3.92	3.86	3.83	3.83	3.84	3.88	3.86	3.86	3.88	3.82	3.86	3.83	3.93	3.94
Sum Cat#	18.13	18.51	18.13	18.56	18.1	18.15	18.04	18.2	17.3	17.9	17.8	17.8	17.8	17.9	18.1	17.9	18	17.7	18	18	18
XMg	0.161	0.16	0.321	0.168	0.291	0.217	0.278	0.244	0.61	0.34	0.41	0.43	0.41	0.4	0.26	0.39	0.34	0.46	0.35	0.33	0.33
Oct	4.247	5.259	4.121	5.35	4.107	4.203	4.143	4.43	3.81	4.12	4.09	4.07	4.07	4.06	4.42	4.12	4.17	3.97	4.18	4.11	4.11
Int	1.877	1.25	2.013	1.212	1.99	1.946	1.899	1.773	1.49	1.81	1.75	1.76	1.76	1.83	1.66	1.74	1.85	1.71	1.86	1.92	1.86

Microprobe analysis of white mica

Label	1-9_2	1-9_2	1-9_3	1-9_3	1-9_4	1-9_4	1-9_6	7-7_1	7-7_1	7-7_2	7-7_2	7-7_5	7-7_5_
SiO2	48.7	47.1	48.2	46.5	47.8	47.4	57	47.6	47.8	47.9	47.7	48.1	39.8
TiO2	0.3	0.27	0.35	0.18	0.38	0.28	0.17	0.25	0.23	0.24	0.34	0.2	0.18
Al2O3	30.4	31.9	31.4	33.1	31.1	31.4	28.4	31.8	31.8	31.1	31.7	29.4	29.4
Cr2O3	0	0.04	0	0	0	0	0.05	0	0	0	0	0	0.03
FeO	4.36	4.02	4.02	4.62	4.16	3.99	1.21	4.07	4.27	4.28	4.26	6.14	10.8
MgO	1.18	1.07	1.08	1.18	1.1	1.14	1.1	1.1	1.15	1.18	1.12	1.06	1.37
Na2O	0.06	0.07	0.09	0.09	0.08	0.09	0.59	0.09	0.09	0.1	0.1	0.1	0.1
K2O	10.6	11	10.8	10.3	10.8	10.7	8.19	10.9	10.7	11	11	10	8.84
F	0.19	0.16	0.18	0.17	0.12	0.2	0.12	0.17	0.18	0.17	0.14	0.26	0.19
Cl	0.02	0	0.03	0.01	0	0.01	0.01	0.01	0.01	0.01	0.01	0.01	0.03
H2O(c)	4.37	4.37	4.39	4.39	4.39	4.34	4.65	4.38	4.39	4.38	4.41	4.28	3.95
O=F	0.08	0.07	0.08	0.07	0.05	0.08	0.05	0.07	0.08	0.07	0.06	0.11	0.08
O=Cl	0	0	0.01	0	0	0	0	0	0	0	0	0	0.01
Sum Ox%	100	99.9	100	100	99.9	99.5	101	100	100	100	101	99.4	94.6
mg number	21.3	21	21.2	20.3	20.9	22.2	47.6	21.3	21.2	21.6	20.8	14.7	11.2
Si	6.54	6.36	6.45	6.24	6.45	6.42	7.25	6.39	6.4	6.44	6.39	6.54	5.89
Ti	0.03	0.03	0.04	0.02	0.04	0.03	0.02	0.03	0.02	0.02	0.03	0.02	0.02
Al/Al IV	1.46	1.64	1.55	1.76	1.56	1.59	0.75	1.61	1.6	1.56	1.62	1.46	2.11
Al VI	3.35	3.43	3.4	3.47	3.38	3.41	3.51	3.42	3.41	3.37	3.39	3.26	3.02
Cr	0	0	0	0	0	0	0.01	0	0	0	0	0	0
Fe2+	0.49	0.45	0.45	0.52	0.47	0.45	0.13	0.46	0.48	0.48	0.48	0.7	1.34
Mg	0.24	0.21	0.22	0.24	0.22	0.23	0.21	0.22	0.23	0.24	0.22	0.21	0.3
Na	0.02	0.02	0.02	0.02	0.02	0.02	0.15	0.02	0.03	0.03	0.03	0.03	0.03
K	1.82	1.89	1.85	1.77	1.86	1.85	1.33	1.86	1.83	1.88	1.87	1.74	1.67
F	0.08	0.07	0.08	0.07	0.05	0.09	0.05	0.07	0.08	0.07	0.06	0.11	0.09
Cl	0	0	0.01	0	0	0	0	0	0	0	0	0	0.01
OH	3.91	3.93	3.92	3.92	3.95	3.91	3.95	3.93	3.92	3.93	3.94	3.89	3.9
Sum Cat#	17.9	18	18	18	18	18	17.3	18	18	18	18	18	18.4
XMg	0.33	0.32	0.32	0.31	0.32	0.34	0.62	0.32	0.33	0.33	0.32	0.24	0.19
Oct	4.11	4.13	4.1	4.24	4.11	4.12	3.87	4.13	4.14	4.11	4.13	4.2	4.68
Int	1.83	1.91	1.87	1.79	1.88	1.87	1.47	1.88	1.86	1.91	1.9	1.76	1.7

Microprobe analysis of white mica

Label	SiO2	FeCO3	MnCO3	MgCO3	CaCO3	BaCO3	SrCO3	ZnCO3	Sum Ox%	Witherite	Smithsor	Stonianit	Rhodoch	Magnesit	Sidérite	Calcite
7-15_3	3.16	49.72	28.65	3.92	2.84	0.01	0	0	88.29	0.003	0	0	29.038	5.416	49.992	3.3
7-15_4	0.14	2.26	1.62	0.31	94.44	0.01	0.08	0.18	99.05	0.007	0.142	0.054	1.429	0.375	1.978	95.678
7-15_4	0.12	2.16	2.92	0.29	94.06	0.06	0.07	0	99.68	0.03	0	0.05	2.561	0.349	1.879	94.743
7-15_5	0.06	1.86	3.06	0.22	95.4	0	0.12	0	100.72	0	0	0.079	2.66	0.263	1.604	95.205
7-15_5	0.28	0.43	6.83	0.13	92.67	0	0	0.04	100.37	0	0.029	0	5.945	0.153	0.369	92.597
7-15_6	0	2.72	1.61	0.38	96.72	0	0.03	0.18	101.64	0	0.139	0.019	1.388	0.445	2.33	95.811
1_3_3_	0.03	61.69	33.66	4.84	2.42	0.02	0.03	0.06	102.75	0.011	0.049	0.021	32.241	6.325	58.627	2.665
1_3_3_	0.04	53.08	45.18	2.43	2.37	0	0	0.22	103.31	0	0.196	0	43.433	3.186	50.629	2.622
1-7_2_	1.39	2.35	3.79	0.26	93.62	0.05	0.04	0	101.49	0.022	0	0.026	3.176	0.291	1.956	90.067
1-7_2_	0.36	1.66	4.19	0.22	94.37	0.02	0.07	0.03	100.93	0.01	0.023	0.047	3.617	0.26	1.421	93.45
1-7_2_	1.34	1.89	5.43	0.22	88.93	0.04	0.01	0	97.87	0.02	0	0.009	4.727	0.265	1.631	88.881
1-7_3_	0.62	0.69	3.61	0.1	96.46	0.01	0.06	0	101.54	0.003	0	0.037	3.066	0.113	0.585	94.189
1-7_3_	0.01	0.59	3.67	0.04	96.76	0.03	0.02	0	101.12	0.016	0	0.012	3.181	0.051	0.506	96.203
1-7_6_	0.02	1.58	3.44	0.13	95.77	0.02	0.22	0	101.18	0.009	0	0.151	2.981	0.157	1.357	95.284
1-7_6_	0.02	1.5	3.44	0.11	96.81	0.01	0.16	0.2	102.24	0.004	0.155	0.106	2.95	0.134	1.279	95.474
mh6_1_	0.02	26.39	13.18	11.34	49.56	0.03	0	1.91	102.44	0.018	1.565	0	11.784	13.827	23.405	50.891
mh6_1_	0.02	26.12	12.36	12.07	48.73	0	0	2.21	101.5	0	1.832	0	11.158	14.857	23.399	50.533
mh6_2_	0.02	26.86	12.94	12.37	48.66	0.07	0	0.63	101.55	0.036	0.51	0	11.509	15	23.692	49.693
mh6_2_	0.01	26.29	13.21	12	48.69	0	0	0.7	100.91	0	0.579	0	11.839	14.664	23.372	50.099
1-9_1_	0.09	5.51	3.41	0.41	90.18	0	0.08	0.08	99.75	0	0.065	0.054	3.011	0.488	4.818	91.327
1-9_1_	0.01	5.53	3.81	0.47	89.11	0	0.08	0.04	99.06	0	0.03	0.059	3.391	0.572	4.886	91.06
1-9_2_	0.05	1.46	2.43	0.11	96.75	0	0.15	0.01	100.96	0	0.006	0.103	2.107	0.131	1.254	96.253
1-9_2_	2.41	2.07	3.99	0.19	90.67	0	0.09	0	99.41	0	0	0.057	3.332	0.214	1.715	86.992
1-9_4_	0.07	1.89	6.39	0.21	90.52	0.02	0.07	0	99.17	0.012	0	0.049	5.662	0.249	1.658	92.117
1-9_4_	0.17	2.88	3.57	0.44	91.33	0	0	0.1	98.49	0	0.083	0	3.169	0.53	2.536	93.188
1-9_5_	0.03	0.97	2.81	0.06	95.3	0	0	0	99.17	0	0	0	2.476	0.072	0.845	96.498
1-9_5_	0.03	3.03	2.78	0.24	93.43	0	0.06	0	99.56	0	0	0.038	2.452	0.283	2.644	94.485
1-9_6_	3.79	3.05	1.67	1.24	86.86	0	0.1	0	96.71	0	0	0.064	1.381	1.402	2.507	82.632
1-9_6_	0.96	3.43	2.14	0.62	90.03	0.06	0.04	0.15	97.43	0.03	0.124	0.027	1.886	0.744	2.995	91.084
7-9_1_	1.39	8.27	11.16	0.45	78.91	0	0.13	0.14	100.46	0	0.115	0.086	9.616	0.533	7.07	78.099
7-9_1_	5.42	3.39	6.76	0.28	81.1	0	0.18	0.14	97.27	0	0.102	0.113	5.425	0.309	2.699	74.799
7-9_3_	0.77	5.28	9.66	0.48	83.3	0.08	0.23	0.03	99.83	0.041	0.023	0.155	8.44	0.575	4.579	83.632
7-9_6_	0.86	4.02	11.43	0.37	80.94	0	0.09	0.15	97.87	0	0.125	0.063	10.183	0.454	3.557	82.828
7-9_6_	0.86	4.1	8.2	0.34	84.73	0.04	0.15	0	98.42	0.022	0	0.103	7.231	0.407	3.589	85.76

Microprobe Analyses of Carbonate

Label	SiO2	FeCO3	MnCO3	MgCO3	CaCO3	BaCO3	SrCO3	ZnCO3	Sum Ox%	Witherite	Smithsor	Stonianit	Rhodoch	Magnesit	Sidérite	Calcite
7-7_3_	0.33	47.92	50.66	1.3	2.54	0	0	1.05	103.8	0	0.921	0	48.637	1.703	45.644	2.805
7-7_3_	0.93	49.01	50.5	0.57	1.13	0.02	0	0.44	102.6	0.014	0.382	0	48.207	0.745	46.414	1.239
7-7_5_	0.02	58.24	36.83	4.8	2.76	0	0	0.26	102.91	0	0.232	0	35.282	6.267	55.357	3.032
7-7_5_	0.02	24.31	23.95	1.45	51.8	0	0.06	0.36	101.95	0	0.304	0.041	21.838	1.802	21.998	54.259
7-7_5_	0.03	9.5	14.37	0.68	75.69	0	0.01	0	100.27	0	0	0.004	12.86	0.826	8.432	77.781
7-7_6_	1.49	49.48	47.69	1.36	1.54	0	0	1.06	102.6	0	0.913	0	44.952	1.743	46.272	1.664
7-7_6_	0.12	50.73	50.23	0.67	1.09	0	0.05	0.56	103.44	0	0.498	0.035	48.667	0.881	48.762	1.21
7-7_8_	0.03	54.32	46.7	0.67	0.91	0	0	1.33	103.97	0.002	1.186	0	45.483	0.884	52.494	1.023
7-7_8_	0.02	54.07	47.94	0.42	0.74	0.03	0	0.98	104.2	0.018	0.867	0	46.497	0.553	52.031	0.827

Microprobe Analyses of Carbonate

Sample	SiO2	TiO2	Al2O3	Cr2O3	FeO	MnO	MgO	CaO	Na2O	K2O	H2O(c)	Sum Ox%	mg number
MH7-15	23.35	0.06	19.95	0.01	40.5	0.86	5.1	0	0	0.15	10.66	100.73	11.18421
MH7-15	23.46	0.07	20.04	0.02	40.27	0.88	5.12	0.01	0.02	0.03	10.68	100.8	11.28002
MH7-15	23.5	0.05	19.84	0.03	39.67	0.72	5.21	0.15	0.02	0.1	10.62	99.9	11.60873
MH7-15	23.46	0.02	19.78	0.04	39.39	0.78	5.41	0.06	0.01	0.06	10.61	99.8	12.07589
MH7-15	25.94	0.04	20.48	0	35.19	0.6	4.64	0.03	0.01	1.36	10.79	99.17	11.64951
MH1-3	22.35	0.03	21.67	0.04	42.79	0.89	2.75	0.01	0	0	10.61	101.29	6.038647
MH1-3	22.11	0	21.86	0	42.96	1.04	2.53	0	0	0	10.59	101.26	5.561662
MH1-3	22.89	0.05	20.13	0	42.93	0.95	2.84	0.01	0.01	0.01	10.5	100.5	6.204938
MH1-3	22.37	0.04	21.03	0	43.26	0.95	2.74	0	0.02	0.02	10.55	101.07	5.956522
MH1-3	22.48	0.05	20.97	0.02	42.58	1	2.79	0.06	0.05	0.02	10.53	100.67	6.149438
MH1-3	22.65	0.01	20.62	0	43.32	0.93	2.86	0.01	0.01	0.04	10.55	101.04	6.193157
MH1-3	22.68	0.03	20.7	0.04	43.75	0.93	2.9	0.01	0	0.01	10.61	101.76	6.216506
MH1-3	23.26	0.06	19.86	0	42.3	0.92	3.24	0	0	0.02	10.52	100.31	7.114625
MH1-3	22.67	0	20.15	0	43.27	0.94	3.09	0.03	0.01	0	10.51	100.73	6.665229
MH1-7	23.15	0.02	19.88	0	42.95	0.39	3.64	0	0.02	0	10.56	100.72	7.812835
MH1-7	22.99	0.01	19.69	0.01	42.45	0.37	3.52	0.01	0.01	0.02	10.45	99.61	7.657168
MH1-7	26.38	0.07	21.16	0	37.17	0.26	3.1	0	0.01	1.67	10.92	101.03	7.698038
MH1-7	23.02	0.04	19.5	0	41.87	0.61	4.02	0	0.06	0.02	10.47	99.61	8.760078
MH1-7	22.58	0.06	20.8	0	39.22	2.75	4.44	0.01	0.03	0	10.61	100.54	10.16949
MH1-7	22.36	0	20.7	0.02	40.71	1.46	4.1	0.03	0.02	0.02	10.53	100.11	9.149743
MH1-7	31.2	0.06	22.93	0	31.35	0.26	2.68	0.03	0.03	3.17	11.61	103.34	7.875404
MH1-7	23.69	0.01	20.01	0.04	41.71	0.4	3.41	0.03	0	0.32	10.58	100.4	7.557624
MH1-7	23	0.05	19.88	0.05	43.23	0.41	3.76	0	0.02	0	10.58	101.06	8.001702
MH1-7	22.67	0.07	19.79	0	42.24	0.72	3.61	0.01	0.01	0.02	10.43	99.62	7.873501
MH6	26.63	0	19.44	0.01	27.95	0.75	14.73	0.02	0	0.01	11.47	101.36	34.51265
MH6	26.11	0.05	19.27	0.03	30.15	0.59	13.45	0	0	0.01	11.35	101.39	30.84862
MH6	25.76	0	19.47	0	31.86	0.54	12.23	0	0	0.01	11.26	101.35	27.73872
MH6	25.53	0	19.18	0	32.43	0.47	11.62	0.03	0	0.05	11.13	100.57	26.37911
MH1-9	25.18	0.22	21.22	0	38.95	0.17	3.99	0.03	0.01	0.74	10.92	101.47	9.292035
MH1-9	23.17	0.05	20.83	0	40.73	0.21	3.96	0.06	0	0.06	10.58	99.75	8.861043
MH1-9	25.41	0.08	21.53	0	38.61	0.16	3.96	0.05	0.03	0.92	10.98	101.97	9.302326
MH1-9	23.43	0.01	21.09	0	41.34	0.2	4.2	0.06	0.01	0.03	10.75	101.39	9.222661
MH1-9	36.2	0.15	24.26	0	25.37	0.14	2.59	0.09	0.04	4.25	12.31	105.59	9.263233
MH1-9	23.28	0	20.73	0	40.93	0.2	4.39	0.05	0.01	0.02	10.65	100.33	9.686673

Microprobe Analyses of Chlorite

Sample	SiO2	TiO2	Al2O3	Cr2O3	FeO	MnO	MgO	CaO	Na2O	K2O	H2O(c)	Sum Ox%	mg number
MH1-9	22.76	0.03	21.05	0	41.46	0.23	3.92	0	0	0	10.58	100.08	8.638167
MH7-9	22.75	0.03	26.46	0.01	37.22	0.28	2.99	0.43	0.17	0.26	11.06	101.93	7.435961
MH7-9	22.48	0.02	19.55	0.02	43.2	0.36	3.96	0.02	0.03	0.02	10.46	100.22	8.396947
MH7-9	22.4	0.05	20.14	0	42.45	0.44	3.36	0.05	0.08	0.05	10.42	99.56	7.334643
MH7-9	25.07	0.03	20.52	0.01	39.22	0.45	3.18	0.04	0.04	1.15	10.73	100.45	7.5
MH7-9	22.64	0.01	20.42	0	42.93	0.48	3.59	0	0	0	10.56	100.87	7.717111
MH7-9	23	0.05	20.12	0.03	41.49	0.41	3.63	0.03	0.06	0.23	10.49	99.64	8.045213
MH7-9	23.32	0.04	20.26	0.03	42.47	0.35	3.34	0.02	0.01	0.28	10.6	100.97	7.290985
MH7-9	22.55	0.08	19.95	0	43.05	0.39	3.55	0.01	0	0.03	10.47	100.14	7.618026
MH7-7	22.62	0.04	20.37	0	39.98	0.79	4.41	0.05	0.03	0.04	10.47	99.02	9.93467
MH7-7	23.19	0.05	19.59	0.02	40.04	0.72	4.7	0.02	0	0.1	10.51	99.4	10.50514
MH7-7	23.07	0.02	20.34	0	41.59	0.67	4.41	0.02	0.03	0.03	10.64	100.99	9.586957
MH7-7	22.53	0.06	20.99	0.01	40.12	0.72	4.85	0.03	0.02	0.02	10.6	99.95	10.78497
MH7-7	23.5	0.06	19.64	0.04	41.5	0.8	4.14	0	0	0.1	10.59	100.52	9.07099
MH7-7	23.3	0.04	20.81	0	40.54	0.73	4.34	0.01	0.02	0.15	10.69	100.91	9.670232
MH7-7	23.38	0.03	20	0.01	41.92	0.71	4.34	0.01	0.01	0	10.66	101.24	9.381755
MH7-7	22.95	0	20.62	0.01	40.86	0.68	4.32	0.04	0	0.01	10.6	100.31	9.561753

Microprobe Analyses of Chlorite

Appendix 4

Fluid Inclusions

Beatrice Prospect

Fluid Inclusion data from quartz stage 2 veins

Sample	Type	Te	T(min)	wt% NaCl	Th
MH4-11	1a	-44.5	-8	11.70	145
MH4-11		-51.2	-12.6	16.53	166
MH4-11		-44.2	-12.7	16.62	168
MH4-11		-46	-9	12.85	160
MH4-11			-8.1	11.81	
MH4-11		-46.9	-10	13.94	155.7
MH4-11			-10.6	14.57	149.6
MH4-11			-10.2	14.15	145.3
MH4-11		-53.6	-13.9	17.70	150
MH4-11			-10.2	14.15	154.2
MH4-11		-50.6	-14.9	18.55	158
MH4-11			-7	10.49	151
MH1-11		-41.7	-7.3	10.86	
MH1-11		-38.9	-2.4	4.03	125
MH1-11		-42.1	-1.9	3.23	
MH1-11		-44	-6.2	9.47	126
MH1-11		-47	-4.8	7.59	
MH1-11		-49.1	-7.9	11.58	114
MH1-11		-43.8	-6.6	9.98	152.9
MH1-11					160
MH1-11			-7.6	11.22	262.6
MH1-11			-8.4	12.16	265.6
MH1-11			-10.6	14.57	276
MH1-11			-12.1	16.05	

Appendix 5

Carbon-Oxygen Isotopes

Sample Name	Description	host rock	Delta 45	Delta 46	Delta 13C wrt PDB	Precision Delta 13C	Delta 18O wrt PDB	Precision Delta 18O	Delta 18O wrt SMOW
MH30	spherical siderite alteration in volcaniclastic	vc	2.641	-1.584	-3.434	0.002	-14.510	0.005	15.902
MS2 MH2/	calcite, vein - tension gash	vc	1.935	-6.956	-4.003	0.003	-19.811	0.008	10.438
MS1 MH11	vein, qtz + chl+ sph + gn	qfp	2.622	-6.508	-3.289	0.001	-19.371	0.005	10.891
MS3 MH4	calcite replacement? Vein	vc	1.616	-7.059	-4.338	0.003	-19.913	0.012	10.333
MS5 MH3	bedded	shale	0.284	-5.313	-5.811	0.004	-18.186	0.006	12.112
MS6 MH1	calcite. Vein + fspar in QFP	qfp	2.637	-8.370	-3.210	0.007	-21.209	0.005	8.996
MS7 MH7	siderite alteration in volcaniclastic	vc	3.327	-4.297	-2.615	0.006	-17.190	0.008	13.139
MS7 MH17	fine grained 3cm carbonate clast in vc	vc	4.922	-7.020	-0.831	0.003	-19.881	0.010	10.365
MS8 MH2	Calcite veined contact b/w shale & QFP	qfp	1.551	-8.374	-4.362	0.005	-21.211	0.012	8.995
MS8 MH3	Calcite, coarse with qtz chl, and arsenopyrit	qfp	0.343	-6.429	-5.710	0.002	-19.288	0.002	10.977
MS8 MH4a	vein carb + qtz + fspar	qfp	1.577	-6.968	-4.382	0.003	-19.822	0.003	10.426
MS8 MH4b	vein carb + qtz + chl	qfp	2.484	-7.480	-3.403	0.003	-20.330	0.003	9.903
MS8 MH12a	bedded not calcite	shale	1.283	-5.969	-4.728	0.003	-18.836	0.008	11.443
MS8 MH12b	vein carb	shale	0.527	-4.687	-5.573	0.004	-17.569	0.004	12.749
MS8 MH14	clastic? Carbonate beds	shale	2.170	-6.764	-3.760	0.002	-19.623	0.002	10.631

Transducer (mBar)	Reference Ion Gauge	Sample Ion Gauge
0	8.23E-08	8.19E-08
0	8.11E-08	8.30E-08
0	1.04E-07	1.06E-07
25.8	1.06E-07	1.04E-07
34.2	1.03E-07	1.05E-07
32.8	1.04E-07	1.03E-07
20.4	1.03E-07	1.03E-07
24.1	1.02E-07	1.03E-07
30.7	1.03E-07	1.02E-07
20.5	1.03E-07	1.04E-07
12.0	1.03E-07	1.04E-07
23.7	1.03E-07	1.03E-07
17.1	1.04E-07	1.03E-07
33.0	1.03E-07	1.04E-07
9.4	1.03E-07	1.03E-07

Appendix 6

Sulfur Isotopes

Sample No.	Mineral	Sample Description	^{34}S CDT
3-10	py	Euhedral crystals of pyrite associated with anhedral galena and sphalerite in chlorite altered volcaniclastic	13.665
3-10	gn	anhedral galena in assoc' with sphalerite and pyrite	14.037
3-10	sph	anhedral sphalerite	15.669
3-16	py	Euhedral crystals of pyrite associated with anhedral galena,sphalerite and minor chalcopyrite in chlorite altered volcaniclastic	12.412
3-16	gn	anhedral galena in polymetallic lens	11.639
3-16	sph	anhedral sphalerite in polymetallic lens	13.77
4-1	py	Euhedral pyrite sub aligned with veinlets hosted within black shale	6.279
4-1	sph	Anhedral sphalerite in pyrite, carbonate, quartz veinlet	9.68
MH39	gn	Anhedral galena and sphalerite in quartz, chlorite, carbonate veinlet hosted within volcaniclastic	17.154
MH39	sph	veinlet hosted within volcaniclastic	19.955
MH6	sph	Outcropping Anhedral sphalerite vein hosted within chloritic volcaniclastic	15.249
T36721	?	RGC samples	15.8
T36722	?	RGC samples	14.9
T36720	py	RGC samples	15.8
MH38	sph	Anhedral veinlet sphalerite hosted within chloritic volcaniclastic	21.48325
7-7	py	Coarse andedral pyrite within chlorite carbonate altered volcaniclastic	20.43254
7-7	gn	fine veinlet sphalerite in chlorite carbonate altered volcaniclastic	19.38694
8-15	sph	Sub euhedral sphalerite within clasts? Replacement? Within clastic bed within shale	19.57011
8-15	py	veinlet pyrite within clastic bed within shale	12.13114
8-10	sph	Anhedral veinlet sphalerite within shale hosted carbonate bed containing arsenopyrite and pyrrhotite	25.73283
8-10	py	coarse euhedral veinlet pyrite	33.00572
8-10	gn	anhedral veinlet galena	30.62137
4-11	sph	Bucky quartz carbonate vein within Quartz Feldspar Porphyry containing anhedral massive sphalerite and galena	22.94199
4-11	gn	Bucky quartz carbonate vein within Quartz Feldspar Porphyry containing anhedral massive sphalerite and galena	14.59742
8-11	py	pyrite pseudomorphs of gypsum with euhedral arsenopyrite	31.0237
8-11	po	Veinlet anhedral pyrrhotite, with chalcopyrite, arsenopyrite and minor sphalerite	30.33694

S isotopes

Appendix 7

Lead Isotopes

lead isotopes

MS3-16						
	1	2	3	ave	std	RSD(%)
206/204	18.087	18.115	18.065	18.089	0.025	0.139
207/204	15.517	15.632	15.672	15.607	0.081	0.516
208/204	37.959	37.955	38.1	38.005	0.083	0.218
208/206	2.0988	2.0951	2.1098	2.101	0.008	0.364
207/206	0.8579	0.8629	0.8675	0.863	0.005	0.555

MS8-15						
	1	2	3	ave	std	RSD(%)
206/204	18.116	18.276	18.294	18.229	0.098	0.537
207/204	15.522	15.652	15.576	15.583	0.065	0.419
208/204	38.101	38.191	37.923	38.072	0.136	0.358
208/206	2.1032	2.0902	2.0738	2.089	0.015	0.705
207/206	0.8569	0.8564	0.8515	0.855	0.003	0.348

MS7MH4						
	1	2	3	ave	std	RSD(%)
206/204	18.207	18.261	18.181	18.216	0.041	0.224
207/204	15.622	15.607	15.597	15.609	0.012	0.080
208/204	38.023	38.081	38.02	38.042	0.034	0.090
208/206	2.0872	2.085	2.0921	2.088	0.004	0.173
207/206	0.8578	0.8544	0.8581	0.857	0.002	0.237

MS1MH11						
	1	2	3	ave	std	RSD(%)
206/204	18.28	18.35	18.334	18.321	0.037	0.202
207/204	15.662	15.713	15.637	15.671	0.039	0.246
208/204	38.124	38.381	38.384	38.296	0.149	0.390
208/206	2.0856	2.0907	2.0926	2.090	0.004	0.172
207/206	0.8563	0.856	0.8525	0.855	0.002	0.244

MS3-10				average	std	RSD%
206/204	18.182	18.136	18.219	18.179	0.041	0.228
207/204	15.577	15.557	15.612	15.582	0.028	0.178
208/204	38.045	37.977	38.127	38.04967	0.075	0.198
208/206	2.092	2.0926	2.0923	2.0923	0	0.015
207/206	0.8563	0.8576	0.8568	0.8569	0.001	0.077

Pasminco				
Sample ID:	deposit	206/204	207/204	208/204
241738	PasBeatric	18.16	15.65	38.02
241738	PasBeatric	18.19	15.64	38.28
241738	PasBeatric	18.12	15.49	38.05
241738	PasBeatric	18.24	15.69	38.21

Appendix 8

Assay results

hole ID	Sample No	Depth from	depth to	Ag ppm	As ppm	Cu	Pb	Zn	
MS1	MS1-4	4	7.2	0	0	100	100	800	
MS1	MS1-7.2	7.2	13.7	0	0	100	300	600	
MS1	MS1-13.7	13.7	19.4	0	0	100	300	1100	
MS1	MS1-19.4	19.4	25	0	0	100	800	2500	
MS1	MS1-25	25	30	0	0	100	1200	3700	
MS1	MS1-30	30	32	0	0	100	1700	2900	
MS1	MS1-32	32	34	0	0	100	1500	5000	
MS1	MS1-34	34	36	0	0	100	1200	3200	
MS1	MS1-36	36	38	0	0	100	1000	4000	
MS1	MS1-38	38	40	0	0	100	700	15000	
MS1	MS1-40	40	42	0	0	100	400	3000	
MS1	MS1-42	42	44	0	0	100	1800	3200	
MS1	MS1-44	44	46	0	0	100	1300	1000	
MS1	MS1-46	46	48	0	0	100	300	400	
MS1	MS1-48	48	50	0	0	100	1100	600	
MS1	MS1-50	50	52	0	0	100	2200	1700	
MS1	MS1-52	52	54	0	0	100	4700	1900	
MS1	MS1-54	54	56	0	0	200	15000	2400	
MS1	MS1-56	56	58	0	0	100	1000	800	
MS1	MS1-58	58	60	0	0	100	2000	2200	
MS1	MS1-60	60	61	0	0	100	2800	8500	
MS1	MS1-61	61	62	0	0	100	3000	8800	
MS1	MS1-62	62	63	0	0	100	12800	17000	
MS1	MS1-63	63	64	0	0	100	6200	15800	
MS1	MS1-64	64	65	0	0	200	12500	16500	
MS1	MS1-65	65	66	0	0	100	20000	13700	
MS1	MS1-66	66	67	0	0	200	10200	24700	
MS1	MS1-67	67	68	0	0	200	7400	24200	
MS1	MS1-68	68	69	0	0	100	5500	3500	
MS1	MS1-69	69	70	0	0	100	800	1100	
MS1	MS1-70	70	72	0	0	100	1500	2300	
MS1	MS1-72	72	74	0	0	100	700	1100	
MS1	MS1-74	74	76	0	0	100	500	800	
MS1	MS1-76	76	78	0	0	100	400	1000	
MS1	MS1-78	78	80	0	0	100	300	500	
MS1	MS1-80	80	85	0	0	100	200	300	
MS1	MS1-85	85	90	0	0	100	200	300	
MS1	MS1-90	90	96	0	0	100	200	300	
MS1	MS1-96	96	97.1	0	0	100	100	100	
MS1	MS1-97.1	97.1	98.5	0	0	100	700	1600	
MS1	MS1-98.5	98.5	104	0	0	100	400	900	
MS1	MS1-104	104	110	0	0	100	200	400	
MS1	MS1-110	110	111	0	0	100	1300	1700	
MS1	MS1-111	111	112	0	0	1400	30000	79000	
MS1	MS1-112	112	113	0	0	1400	23000	22000	
MS1	MS1-113	113	114	0	0	100	700	1900	
MS1	MS1-114	114	115	0	0	100	900	500	
MS1	MS1-115	115	116	0	0	100	800	1700	
MS1	MS1-116	116	117	0	0	100	200	500	
MS1	MS1-117	117	118	0	0	100	600	700	
MS1	MS1-118	118	119	0	0	100	300	400	
MS1	MS1-119	119	120	0	0	100	500	700	
MS1	MS1-120	120	130	0	0	100	400	400	
MS1	274901	120	122	4	0	104	1165	1557	
MS1	274902	122	124	-2	0	5	922	506	
MS1	274903	124	126	-2	0	4	454	402	
MS1	274904	126	128	-2	0	8	182	290	
MS1	274905	128	130	-2	0	11	76	226	
MS1	MS1-130	130	140	0	0	100	100	200	
MS1	274906	130	132	-2	0	5	58	185	
MS1	274907	132	134	-2	0	-4	44	214	
MS1	274908	134	136	-2	0	-4	49	168	
MS1	274909	136	138	-2	0	6	50	173	
MS1	274910	138	140	-2	0	-4	21	92	

MS1	MS1-140	140	160	0	0	100	100	100
MS1	274911	140	142	-2	0	-4	25	91
MS1	274912	142	144	-2	0	-4	55	131
MS1	274913	144	146	-2	0	13	74	173
MS1	274914	146	148	-2	0	5	47	250
MS1	274915	148	150	-2	0	4	83	322
MS1	274916	150	152	-2	0	-4	49	145
MS1	274917	152	154	-2	0	-4	52	110
MS1	274918	154	156	-2	0	6	46	118
MS1	274919	156	158	-2	0	6	32	103
MS1	274921	158	160	-2	0	15	66	127
MS1	MS1-160	160	170	0	0	100	200	400
MS1	274922	160	162	-2	0	6	50	174
MS1	274923	162	164	-2	0	10	60	307
MS1	274924	164	166	-2	0	8	101	536
MS1	274925	166	168	-2	0	8	115	293
MS1	274926	168	170	-2	0	10	254	827
MS1	MS1-170	170	180	0	0	100	300	700
MS1	274927	170	172	-2	0	-4	161	433
MS1	274928	172	174	-2	0	11	292	789
MS1	274929	174	176	-2	0	29	121	376
MS1	274930	176	178	-2	0	18	236	741
MS1	274931	178	180	-2	0	33	505	985
MS1	MS1-180	180	190	0	0	100	200	700
MS1	274932	180	182	-2	0	31	331	906
MS1	274933	182	184	-2	0	10	305	793
MS1	274934	184	186	-2	0	7	190	1301
MS1	274935	186	188	-2	0	-4	135	448
MS1	274936	188	190	-2	0	13	114	613
MS1	MS1-190	190	196.7	0	0	100	500	1100
MS1	274937	190	192	-2	0	23	506	1158
MS1	274938	192	194	-2	0	47	292	1019
MS1	274939	194	196.7	-2	0	35	373	1461
MS1	MS1-196.7	196.7	200	0	0	100	100	200
MS1	MS1-200	200	205	0	0	100	1200	2300
MS1	274941	200	202	-2	0	48	269	1218
MS1	274942	202	204	2	0	86	1822	2101
MS1	274943	204	206	-2	0	45	325	1891
MS1	MS1-205	205	210	0	0	100	1200	1100
MS1	274944	206	208	2	0	49	137	619
MS1	274945	208	210	4	0	58	1536	1547
MS1	MS1-210	210	215	0	0	100	1400	2600
MS1	274946	210	212	7	0	69	5900	1626
MS1	274947	212	214	6	0	71	2414	5930
MS1	274948	214	216	3	0	44	1358	1554
MS1	MS1-215	215	220	0	0	100	600	700
MS1	274949	216	218	3	0	13	120	87
MS1	274950	218	220	2	0	12	78	203
MS1	MS1-220	220	225	0	0	100	300	600
MS1	274951	220	222	2	0	41	179	310
MS1	274952	222	224	2	0	34	150	168
MS1	274953	224	226	-2	0	5	234	398
MS1	MS1-225	225	230	0	0	100	400	700
MS1	274954	226	228	-2	0	-4	85	92
MS1	274955	228	230	-2	0	4	467	1476
MS1	MS1-230	230	235	0	0	100	600	1400
MS1	274956	230	232	2	0	4	402	1189
MS1	274957	232	234	-2	0	-4	117	111
MS1	274958	234	236	2	0	65	291	1199
MS1	MS1-235	235	240	0	0	100	500	2300
MS1	274959	236	238	2	0	24	745	3034
MS1	274961	238	240	-2	0	12	78	171
MS1	MS1-240	240	243.1	0	0	100	100	100
MS1	MS1-243.1	243.1	245	0	0	100	1100	1300
MS1	MS1-245	245	245.5	0	0	100	1900	2200

MS1	MS1-245.5	245.5	248.9	0	0	100	400	800
MS1	MS1-248.9	248.9	250	0	0	100	300	700
MS1	MS1-250	250	255	0	0	100	200	400
MS1	274962	250	252	2	0	48	111	311
MS1	274963	252	254	3	0	55	100	323
MS1	274964	254	256	2	0	52	113	337
MS1	MS1-255	255	260	0	0	100	200	400
MS1	274965	256	258	-2	0	56	125	320
MS1	274966	258	260	2	0	68	119	358
MS1	MS1-260	260	265	0	0	100	400	500
MS1	274967	260	262	2	0	71	198	434
MS1	274968	262	264	2	0	65	310	654
MS1	274969	264	266	2	0	56	259	417
MS1	MS1-265	265	270	0	0	100	400	700
MS1	274970	266	268	2	0	63	263	503
MS1	274971	268	270	3	0	64	308	790
MS1	MS1-270	270	271.4	0	0	100	300	3100
MS1	274972	270	272	2	0	39	247	1401
MS1	MS1-271.4	271.4	280	0	0	100	200	200
MS1	274973	272	274	-2	0	15	106	353
MS1	274974	274	276	-2	0	5	87	69
MS1	274975	276	278	-2	0	7	74	155
MS1	274976	278	280	-2	0	8	80	73
MS1	MS1-280	280	290	0	0	100	100	100
MS1	MS1-290	290	300	0	0	100	100	100
MS1	MS1-300	300	310	0	0	100	100	100
MS1	MS1-310	310	320	0	0	100	100	100
MS1	MS1-320	320	329.1	0	0	100	300	200

hole ID	Sample No	Depth from	depth to	Ag ppm	Au ppı	Cu	Pb	Zn
MS3	MS3-10.4	10.4	12	0	0	30	1000	2800
MS3	MS3-12	12	13.4	0	0	20	500	1500
MS3	MS3-13.4	13.4	14.8	0	0	30	2800	5000
MS3	MS3-14.8	14.8	16.8	0	0	50	300	1000
MS3	MS3-16.8	16.8	18.8	0	0	30	200	800
MS3	MS3-18.8	18.8	20.8	0	0	20	200	500
MS3	MS3-20.8	20.8	22.8	0	0	20	200	600
MS3	MS3-22.8	22.8	24.8	0	0	30	200	600
MS3	MS3-24.8	24.8	26.8	0	0	20	200	900
MS3	MS3-26.8	26.8	28.8	0	0	20	200	1500
MS3	MS3-28.8	28.8	30.8	0	0	60	1200	2500
MS3	MS3-30.8	30.8	32.7	0	0	30	800	2400
MS3	MS3-32.7	32.7	36.5	0	0	20	400	1000
MS3	MS3-36.5	36.5	38.5	0	0	20	500	700
MS3	MS3-38.5	38.5	40.5	0	0	20	300	1400
MS3	MS3-40.5	40.5	42.3	0	0	20	700	1600
MS3	MS3-42.3	42.3	44.3	0	0	50	700	1200
MS3	MS3-44.3	44.3	46.3	0	0	50	1200	8400
MS3	MS3-46.3	46.3	48.3	0	0	60	1900	5600
MS3	MS3-48.3	48.3	50.3	0	0	60	1500	4800
MS3	MS3-50.3	50.3	51.3	0	0	90	1200	6800
MS3	MS3-51.3	51.3	53.3	0	0	50	900	1900
MS3	MS3-53.3	53.3	55.3	0	0	40	700	1100
MS3	MS3-55.3	55.3	57.3	0	0	30	1200	1200
MS3	MS3-57.3	57.3	59.3	0	0	60	1000	2300
MS3	MS3-59.3	59.3	61.3	0	0	30	600	4000
MS3	MS3-61.3	61.3	66.4	0	0	30	400	1000
MS3	MS3-66.4	66.4	71.4	0	0	30	300	700
MS3	MS3-71.4	71.4	76.4	0	0	20	300	600
MS3	MS3-76.4	76.4	81.4	0	0	20	200	400
MS3	MS3-81.4	81.4	86.4	0	0	20	400	600
MS3	MS3-86.4	86.4	91.4	0	0	20	700	700
MS3	MS3-91.4	91.4	96.4	0	0	20	300	700
MS3	MS3-96.4	96.4	101.4	0	0	60	1500	1300
MS3	MS3-101.4	101.4	106.4	0	0	40	700	1100
MS3	MS3-106.4	106.4	111.6	0	0	120	2500	2800
MS3	MS3-111.6	111.6	112.6	0	0	570	6800	15800
MS3	MS3-112.6	112.6	113.6	0	0	160	5800	6900
MS3	MS3-113.6	113.6	114.6	0	0	130	2600	6400
MS3	MS3-114.6	114.6	115.6	0	0	90	3600	2400
MS3	MS3-115.6	115.6	116.6	0	0	60	3500	2200
MS3	MS3-116.6	116.6	118.6	0	0	150	5500	4800
MS3	MS3-118.6	118.6	120.6	0	0	60	500	500
MS3	MS3-120.6	120.6	122.6	0	0	30	600	1000
MS3	MS3-122.6	122.6	124.6	0	0	90	1000	3100
MS3	MS3-124.6	124.6	126.6	0	0	140	2400	5600
MS3	MS3-126.6	126.6	128.6	0	0	210	3500	7000
MS3	MS3-128.6	128.6	130	0	0	160	1400	1900
MS3	MS3-130	130	132	0	0	920	1800	2500
MS3	MS3-132	132	134	0	0	70	400	200
MS3	MS3-134	134	136	0	0	110	4600	8500
MS3	MS3-136	136	138	0	0	210	7200	6300
MS3	MS3-138	138	140	0	0	120	4500	9500
MS3	MS3-140	140	142	0	0	60	1400	900
MS3	MS3-142	142	144	0	0	80	3200	6900

MS3	MS3-144	144	146	0	0	70	7200	8100
MS3	MS3-146	146	148	0	0	70	3200	6500
MS3	MS3-148	148	150	0	0	70	900	6300
MS3	MS3-150	150	152	0	0	30	500	400
MS3	MS3-152	152	154	0	0	20	300	500
MS3	MS3-154	154	156	0	0	50	400	600
MS3	MS3-156	156	160	0	0	20	300	200
MS3	MS3-160	160	165	0	0	30	400	600
MS3	MS3-165	165	170	0	0	50	600	400
MS3	MS3-170	170	175	0	0	50	3700	3200
MS3	MS3-175	175	180	0	0	60	4700	6900
MS3	MS3-180	180	185	0	0	60	3600	7500
MS3	MS3-185	185	190	0	0	50	800	4500
MS3	MS3-190	190	196.8	0	0	70	1300	4800
MS3	MS3-196.8	196.8	197.3	0	0	70	100	500
MS3	MS3-197.3	197.3	200	0	0	140	800	7400
MS3	MS3-200	200	205	0	0	80	700	5100
MS3	MS3-205	205	210	0	0	70	900	600
MS3	MS3-210	210	215	0	0	50	100	1700
MS3	MS3-215	215	220	0	0	70	300	1700
MS3	MS3-220	220	225	0	0	60	800	300
MS3	MS3-225	225	230	0	0	120	100	500
MS3	MS3-230	230	235	0	0	210	200	500
MS3	MS3-235	235	240	0	0	220	200	600
MS3	MS3-240	240	245	0	0	170	100	200
MS3	MS3-245	245	250	0	0	130	200	200
MS3	MS3-250	250	255	0	0	20	100	100
MS3	MS3-255	255	260	0	0	30	200	100
MS3	MS3-260	260	265	0	0	20	200	200
MS3	MS3-265	265	268	0	0	50	100	200
MS3	MS3-268	268	270	0	0	1100	200	300
MS3	MS3-270	270	272	0	0	40	100	200
MS3	MS3-272	272	274	0	0	60	100	200
MS3	MS3-274	274	276	0	0	20	100	200
MS3	MS3-276	276	278	0	0	80	200	1500
MS3	MS3-278	278	280	0	0	50	200	400
MS3	MS3-280	280	282	0	0	30	200	600
MS3	MS3-282	282	284	0	0	150	200	500
MS3	MS3-284	284	286	0	0	150	200	200
MS3	MS3-286	286	290.6	0	0	70	300	500
MS3	MS3-290.6	290.6	291.4	0	0	40	400	500
MS3	MS3-291.4	291.4	295.6	0	0	90	500	200
MS3	MS3-295.6	295.6	300	0	0	40	300	200
MS3	MS3-300	300	305	0	0	50	3200	100
MS3	MS3-305	305	310	0	0	30	500	100
MS3	MS3-310	310	315	0	0	30	1100	600
MS3	MS3-315	315	320	0	0	20	300	400
MS3	MS3-320	320	325	0	0	30	500	600
MS3	MS3-325	325	328	0	0	20	200	300

hole ID	Sample N	From	To	Ag ppm	Au ppm	Pb	Zn	Cu
MS7	274301	24	25	-0.1	-0.01	-50	170	7
MS7	274302	25	26	-0.1	-0.01	54	164	-5
MS7	274303	26	27	-0.1	-0.01	56	194	-5
MS7	274304	27	28	-0.1	-0.01	-50	184	-5
MS7	274305	109.3	111	1.5	-0.01	480	3546	47
MS7	274306	111	113	1.1	-0.01	371	1430	43
MS7	274307	113	115	1.1	-0.01	229	860	48
MS7	274308	115	117	0.8	-0.01	74	253	51
MS7	274309	117	119	1.2	-0.01	83	166	92
MS7	274310	119	120	0.9	-0.01	78	181	83
MS7	274311	120	122	0.7	-0.01	82	285	41
MS7	274312	122	124	0.7	-0.01	82	224	44
MS7	274313	124	126	0.9	-0.01	90	264	33
MS7	274314	126	128	0.9	-0.01	91	259	43
MS7	274315	128	130	1.2	-0.01	68	148	81
MS7	274316	130	132	0.8	-0.01	230	708	57
MS7	274317	132	134	0.9	-0.01	354	1892	41
MS7	274318	134	136	0.8	-0.01	103	300	51
MS7	274319	136	138	0.6	-0.01	-50	199	62
MS7	274321	138	140	0.3	-0.01	-50	103	94
MS7	274322	140	142	0.2	-0.01	-50	176	76
MS7	274323	142	144	0.1	-0.01	-50	116	59
MS7	274324	144	146	0.1	-0.01	-50	106	58
MS7	274325	146	148	0.1	-0.01	-50	94	86
MS7	274326	148	150	-0.1	-0.01	-50	85	47
MS7	274327	150	152	-0.1	-0.01	-50	88	49
MS7	274328	152	154	-0.1	-0.01	-50	96	45
MS7	274329	154	156	0.2	-0.01	-50	116	61
MS7	274330	156	158	0.5	-0.01	137	294	67
MS7	274331	158	160	0.8	-0.01	216	210	62
MS7	274332	160	162	0.6	-0.01	113	217	51
MS7	274333	162	164	0.8	-0.01	130	162	80
MS7	274334	164	166	1	-0.01	422	410	110
MS7	274335	166	168	0.9	-0.01	134	231	57
MS7	274336	168	170	0.6	-0.01	131	221	151
MS7	274337	170	172	0.3	-0.01	114	211	64
MS7	274338	172	174	0.6	-0.01	131	174	45
MS7	274339	174	176	0.6	-0.01	159	274	34
MS7	274341	176	178	0.9	-0.01	305	431	77
MS7	274342	178	180	1.6	-0.01	534	593	60
MS7	274343	180	182	1.7	-0.01	614	1179	86
MS7	274344	182	183	1.9	-0.01	466	1590	85
MS7	274345	183	184	1.5	-0.01	343	1695	95
MS7	274346	184	185	1.4	-0.01	367	728	76
MS7	274347	185	186	2.5	-0.01	1020	4261	98
MS7	274348	186	187	1.7	-0.01	364	1163	105
MS7	274349	187	188	1.6	-0.01	318	957	59
MS7	274350	188	189	1.5	-0.01	275	1527	68
MS7	274351	189	190	1.7	-0.01	296	1440	78
MS7	274352	190	191	1.8	-0.01	484	1277	104
MS7	274353	191	192	2.9	-0.01	1327	2195	60
MS7	274354	192	193	1.9	-0.01	1456	3016	53
MS7	274355	193	194	2.6	-0.01	837	3600	56
MS7	274356	194	195	1.7	-0.01	176	957	53
MS7	274357	195	196	1.4	-0.01	167	2113	76

MS7	274358	196	197	0.9	-0.01	425	1842	59
MS7	274359	197	198	1.3	0.02	800	1106	53
MS7	274361	198	199	0.5	-0.01	218	349	45
MS7	274362	199	200	0.5	-0.01	167	140	60
MS7	274363	200	202	0.4	-0.01	150	156	58
MS7	274364	202	204	0.3	-0.01	123	157	47
MS7	274365	204	206	0.6	-0.01	256	370	48
MS7	274366	206	208	0.5	-0.01	376	513	45
MS7	274367	208	210	0.4	-0.01	103	203	40
MS7	274368	210	212	1.3	-0.01	351	579	49
MS7	274369	212	214	0.6	-0.01	264	590	58
MS7	274370	214	216	0.8	-0.01	331	853	82
MS7	274371	216	218	0.6	-0.01	367	492	61
MS7	274372	218	220	0.3	-0.01	133	362	57
MS7	274373	220	222	0.2	-0.01	143	339	40
MS7	274374	222	224	0.4	-0.01	138	413	52
MS7	274375	224	226	0.5	-0.01	129	442	50
MS7	274376	226	228	0.5	-0.01	143	443	48
MS7	274377	228	230	0.6	-0.01	166	494	54
MS7	274378	230	231.8	0.7	-0.01	254	672	65
MS7	274379	231.8	234	0.2	-0.01	167	435	10
MS7	274381	252	254	-0.1	-0.01	60	169	12
MS7	274382	254	255.8	0.4	-0.01	285	2152	44
MS7	274383	255.8	258.4	0.4	-0.01	250	986	22
MS7	274384	258.4	261.2	0.2	-0.01	191	370	10
MS7	274385	261.2	263	1.2	-0.01	618	1520	66
MS7	274386	263	265	1.2	-0.01	670	1216	53
MS7	274387	265	267	0.6	-0.01	159	359	38
MS7	274388	267	269	0.7	-0.01	230	405	46
MS7	274389	269	271	0.8	-0.01	270	444	43
MS7	274390	271	273	0.7	-0.01	257	552	50
MS7	274391	273	275	0.7	-0.01	430	770	51
MS7	274392	275	277	0.8	-0.01	322	666	40
MS7	274393	277	279	0.5	-0.01	226	503	40
MS7	274394	279	281	0.5	-0.01	213	480	49
MS7	274395	281	283	0.5	-0.01	229	384	47
MS7	274396	283	285	0.7	-0.01	247	550	47
MS7	274397	285	287	1.7	-0.01	844	3069	66
MS7	274398	287	289	1.4	-0.01	610	2108	90
MS7	274399	289	291	1.3	-0.01	485	1314	90
MS7	274401	291	293	1.1	-0.01	381	1121	66
MS7	274402	293	295	1.1	-0.01	451	1727	66
MS7	274403	295	297	1.6	-0.01	697	2110	54
MS7	274404	297	299	1.1	-0.01	371	1470	46
MS7	274405	299	301	1.8	-0.01	825	2106	75
MS7	274406	301	303	2.3	-0.01	1192	3298	76
MS7	274407	303	305	1.7	-0.01	980	1839	52
MS7	274408	305	307	1.8	-0.01	1121	1495	63
MS7	274409	307	309	1.3	-0.01	915	327	44
MS7	274410	309	311	0.7	-0.01	581	363	37
MS7	274411	311	313	1.3	-0.01	958	900	32
MS7	274412	313	315.1	1.4	0.02	1084	462	59
MS7	274413	315.1	316.1	2	-0.01	976	2654	43
MS7	274414	316.1	317.2	2	-0.01	1267	2871	57
MS7	274415	317.2	319	3.6	-0.01	831	1340	23
MS7	274416	319	321	1.3	-0.01	1035	1281	29

MS7	274417	321	323	3	-0.01	1288	1288	68
MS7	274418	323	325	13	-0.01	1084	1350	117
MS7	274419	325	327	0.2	-0.01	80	259	-5
MS7	274421	327	329	0.2	-0.01	95	439	11
MS7	274422	329	331	1.2	-0.01	227	675	40
MS7	274423	331	333	0.2	-0.01	55	168	7
MS7	274424	333	335	2.6	-0.01	373	457	80
MS7	274425	335	337	0.3	-0.01	105	244	27
MS7	274426	337	339	0.2	-0.01	78	208	7
MS7	274427	339	341	0.2	-0.01	-50	270	37
MS7	274428	341	343	0.2	-0.01	62	486	-5
MS7	274429	343	345	0.5	-0.01	170	491	28
MS7	274430	345	347	0.3	-0.01	96	219	6
MS7	274431	347	349	0.3	-0.01	115	285	7
MS7	274432	349	351	0.4	-0.01	120	297	11
MS7	274433	351	353	0.3	-0.01	90	192	9
MS7	274434	353	355	2	-0.01	167	213	6
MS7	274435	355	357	0.3	-0.01	85	180	-5
MS7	274436	357	359	0.6	-0.01	200	336	-5
MS7	274437	359	361	0.3	-0.01	180	272	44
MS7	274438	361	364	0.2	-0.01	671	897	94
MS7	274439	364	365	1.2	-0.01	2637	1775	95
MS7	274441	365	366	0.4	-0.01	927	1019	11
MS7	274442	366	368	0.5	-0.01	887	804	29
MS7	274443	368	370	0.3	-0.01	438	320	17
MS7	274444	370	372	0.6	-0.01	314	249	14
MS7	274445	372	374	0.5	-0.01	566	269	87
MS7	274446	374	375	1.7	-0.01	4800	1620	297
MS7	274447	375	376	2.2	0.14	6591	2562	419
MS7	274448	376	377	0.5	-0.01	1297	972	33
MS7	274449	377	378	0.7	-0.01	1356	1481	7
MS7	274450	378	380	0.6	-0.01	722	862	6
MS7	274451	380	382	0.3	-0.01	161	283	13
MS7	274452	382	384	0.3	-0.01	74	168	20
MS7	274453	384	386	0.2	-0.01	-50	227	27
MS7	274454	386	388	0.3	-0.01	70	139	31
MS7	274455	388	390	0.4	0.6	181	229	36
MS7	274456	390	392	0.6	-0.01	523	594	31
MS7	274457	392	394	0.8	-0.01	925	883	87
MS7	274458	394	396	1.1	-0.01	2010	852	70
MS7	274459	396	398	1.9	-0.01	843	254	34
MS7	274461	398	400	0.7	-0.01	1133	435	12
MS7	274462	400	401	1	-0.01	2699	884	52
MS7	274463	401	402	1.2	-0.01	1770	1130	85
MS7	274464	402	403	0.8	-0.01	1055	799	29
MS7	274465	403	404	0.8	-0.01	1316	961	32

Appendix 9

Literature Review

Alteration Geochemistry and its use in the exploration for volcanic hosted massive sulfide deposits

Marcus Hope
Bachelor of Science

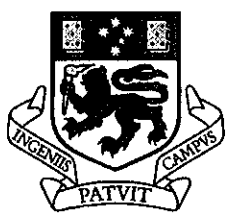

UNIVERSITY OF TASMANIA

A literature review submitted in partial fulfilment of the requirements of the Degree of Bachelor of Science with Honours

CODES SRC

School of Earth Sciences, University of Tasmania

June 1999

Abstract

Alteration zones associated with VHMS deposits are typically much larger than the deposits themselves. The recognition of the mineralogical, chemical and isotopic zonations in alteration systems is critical in the development of vectors for exploration. A review of the literature indicates that numerous geochemical techniques can be used to understand alteration systems associated with VHMS deposits and provide indications of where the sulfide body, if any, would be.

A change in alteration assemblage, in its self, is a direct indicator towards the centre of the alteration system. Reflecting the spatial change in physical and chemical conditions within the alteration system. and also the controlling factor on the chemistry of the rocks in the alteration zone.

Sodium depletion is an almost ubiquitous feature in VHMS associated footwall alteration, reflecting the destruction of feldspar and the formation of phyllosilicates. Exploration companies frequently use it in defining alteration zones. It does not, however, provide a direct vector towards ore. The best direct geochemical vector is the alteration index (AI) [$100(MgO + K_2O)/(Na_2O + CaO + MgO + K_2O)$] developed by Ishikawa. The combined use of this alteration index with the chlorite-carbonate-pyrite index (CCPI) [$100(MgO + FeO)/(MgO + FeO + Na_2O + K_2O)$] not only provides a method of measuring the degree of alteration but also the likely style of alteration. Trace element ratios may also be used as a vector towards ore, Ba/Sr and Rb/Sr ratios are related to the sericitisation of feldspar and commonly show an increasing towards massive sulfide deposits.

Whole-rock $\delta^{18}O$ isotope studies are valuable in broad reconnaissance exploration due to the extent of $\delta^{18}O$ anomalies far exceeding that of elemental anomalies, they may also be useful in metamorphosed terrain as $\delta^{18}O$ zoning is more resistant than mineral assemblages to metamorphic re-equilibration.

Lead isotopes, zinc ratios and sulfur isotope studies provide methods of discriminating between favorable and uneconomic mineralisation styles and between fertile and barren alteration systems.

Mineral chemistry may provide another vector towards sulfide ore, with phyllosilicates containing higher Fe/Mg ratios and increasing Al towards the more intensely altered core of some alteration systems. Ore related carbonates, particularly dolomite display an increase in Fe/Mg ratio towards the ore body. However caution should be used when using mineral chemistry, as contradictory patterns are common.

Table of Contents

List of Figures

1. Introduction

Volcanic hosted massive sulfide (VHMS) deposits are a class of polymetallic deposits which have significantly contributed to the total production of zinc, copper, silver and gold in Australia and overseas. The majority of VHMS deposits are small; about 80% of all known deposits rangING in size from 0.1 to 10mt (Evans 1993). There are however, some large tonnage and/or very rich "world class" VHMS deposits which make them very attractive targets for base metal explorers.

The VHMS deposits hosted by the Mount Read Volcanics in western Tasmania have been classified as Cambrian analogues of the Tertiary Kuroko – style deposits of Japan (Lydon 1988). The VMS deposits of the New Brunswick camp and the Archean Cu – Zn deposits of the Canadian Shield also display many geochemical similarities with Kuroko deposits and have been included in this review to enhance understanding of the processes of VHMS mineralisation and provide possible exploration vectors.

The recognition of mineralogical, chemical and isotopic zonation within hydrothermally altered wallrocks is fundamental in a VHMS exploration program because alteration zones associated with VHMS ore deposits frequently present much larger targets than the ore deposits themselves.

2. Mineral zonation and morphology of alteration systems

The textural, mineralogical and chemical characteristics of hydrothermal alteration zones are highly variable due to a number of factors. These include: 1) The physical and chemical properties of the hydrothermal fluid, 2) the permeability, rigidness and chemical reactivity of the sediments or rocks below the seafloor, and 3) hydrostatic pressures (ie. water depth) (Luff et al.1992).

2.1. Mineral zonation

Several alteration assemblages are associated with VHMS deposits and each form a halo of variable extent around the orebodies. The types of alteration halos recognised in the footwall rocks below the Kuroko, Mt Read, and some of the Canadian deposits have many similarities. Footwall alteration is dominated by the formation of phyllosilicates and typically displays a mineralogical zonation. This zoning is particularly evident where well

developed alteration pipes exist and typically consists of a central zone of massive chlorite surrounded by a zone of less chlorite and minor sericite, followed by a sericite – chlorite zone, all enveloped by a zone of dominantly sericitic alteration (Gemmell 1998). The chlorite to sericite (or illite) zonation has been interpreted to represent an outwardly decreasing thermal gradient. This interpretation is consistent with the pattern of sulfide zonation within the stringer alteration pipe which characteristically consists of a chalcopyrite–pyrite rich core with sphalerite rich margins (Lydon 1988).

The Kuroko VHMS deposits of Japan are an example of alteration zones that are unmetamorphosed and undeformed. Footwall alteration surrounding Kuroko deposits are divided into three mineralogical zones; 1) a siliceous core surrounded by highly silicified and sericitised rocks with minor chlorite. 2) An intermediate zone that envelopes the upper part of the siliceous zone and surrounds the ore body, consisting of sericite, Mg-chlorite and montmorillonite and 3) a widespread outer zone that consist of zeolite and clay alteration.

Patchy carbonate (typically ferroan carbonate) alteration may occur within the sulfide deposit and may extend from the outer edge of the chlorite zone through the sericite zone (Gemmell 1998). In some cases silica alteration overprints the chlorite alteration immediately below the thickest development of massive sulfide. This is seen at Hellyer (Gemmell et al. 1998) and at Brunswick No.12, where SiO_2 increases by up to 300% (Lentz and Goodfellow 1996). A composite of the various alteration features reported for VHMS alteration pipes is shown in Figure 1.

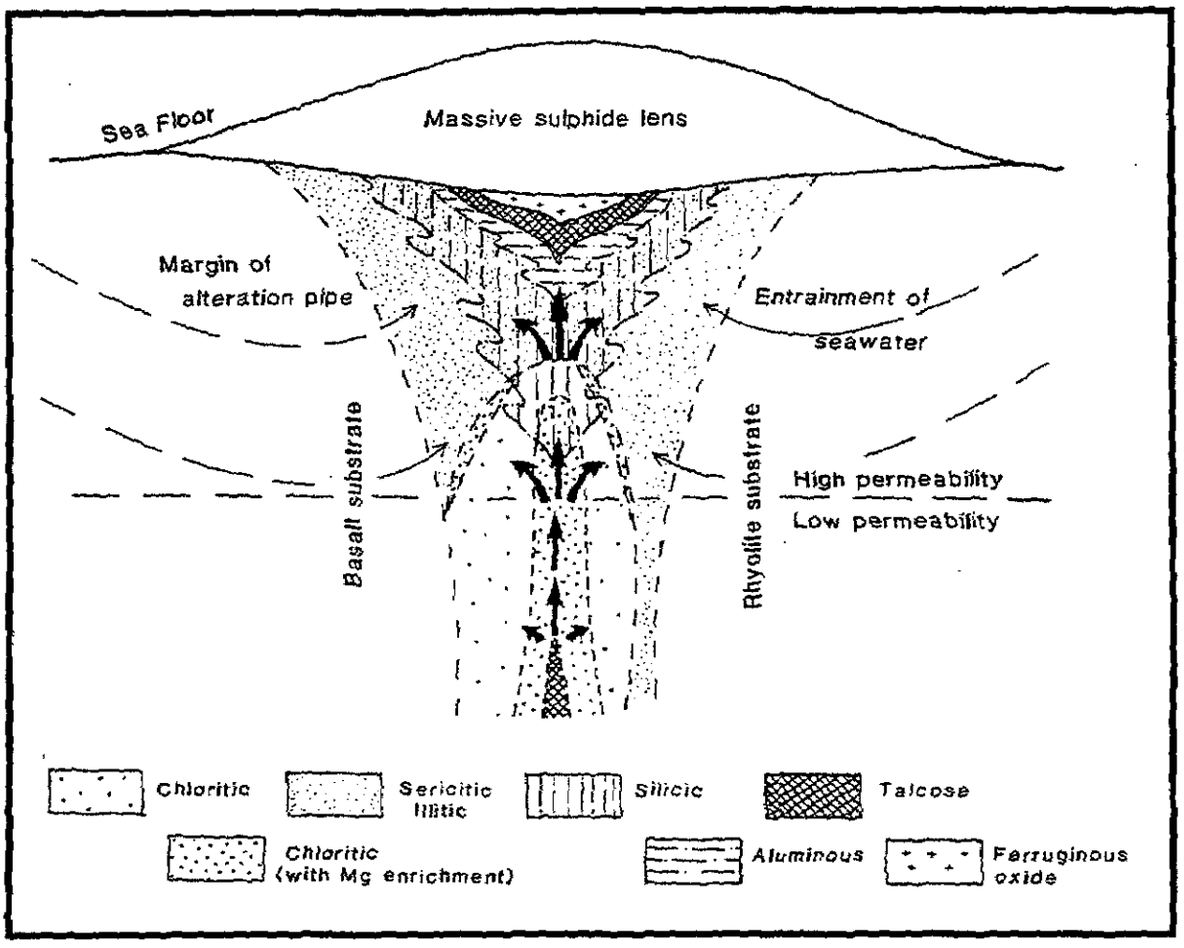

Figure 1. Composite representation of the various alteration assemblages reported for alteration pipes of VHMS deposits (from Lydon, 1988)

Stratabound or semi-conformable footwall alteration zones are more common than alteration pipes and are dominated by quartz-sericite ± pyrite alteration with patchy development of chlorite and carbonate.

Hangingwall alteration is of very low intensity compared to footwall alteration, is commonly lacking in sulfides and is best developed above the thickest portions of the massive sulfide body (Gemmell et al. 1998). Weakly developed sericite-chlorite-quartz alteration is the most common form, however, carbonate and feldspar alteration have also been documented at Hellyer and Heath Steele (Drown 1990, Lentz et al.1997). At Heath Steele, New Brunswick and at Hellyer the hanging-wall alteration is thought to reflect continued hydrothermal reaction after the hanging wall rocks were deposited.

Albitisation is a common alteration feature surrounding many deposits, replacing plagioclase within the outer (montmorillanite) zone around Kuroko deposits (Green et al. 1983). Within the Brunswick camp deposits, albite replaces plagioclase and alkali feldspar within the distal footwall and hangingwall (Lentz et al. 1997, Luff et al. 1992).

Albite pseudomorphs are in turn replaced by quartz, chlorite and sericite within the Brunswick deposits as rocks become more altered and the pH of the altering fluid decreases to stabilize white mica and chlorite (Lentz et al 1997). The hydrolysis of albite to mica marks the almost complete removal of sodium from within the zone of alteration.
It is frequently difficult to determine whether albitisation is related to alteration associated with mineralisation, or if it reflects regional metamorphic de-calcification of plagioclase and/or advanced diagenetic alteration (Herrmann pers comm. 1999).

2.2 Morphology

The morphology of footwall alteration zones vary according to the nature of the host rocks and the influence of brittle structures which may have focussed the hydrothermal fluids (Gemmell 1998). The morphology and spatial relationships of alteration zones and VHMS deposits have been summarized and discussed by Gemmell (1998).

Mound type sulfide deposits formed above competent non-porous lavas and sediments typically have alteration zones that are pipe like, carrot shaped or tabular and cross cut footwall stratigraphy. These reflect zones of structurally induced permeability that focussed mineralising fluids during their ascent to the seafloor.

Alteration pipes may be associated with stringer mineralisation and are developed below most major mound-style VHMS deposits. Alteration pipes are characteristic of the Precambrian VHMS deposits of the Canadian Shield and also exist beneath the deposits at Brunswick No. 12 (Lentz and Goodfellow 1996), and the Tasmanian deposits; Hellyer (Gemmell and Large 1992), Hercules and Red Hills (Eastoe et al. 1987). The alteration pipes beneath Hellyer and Brunswick No.12 and the identification of syn-volcanic coeval fault structures illustrates the importance of focused fluid flow in controlling the discharge of hydrothermal fluids onto the seafloor.

VHMS deposits that are hosted in porous and permeable volcaniclastic rocks generally have sheet-like footwall alteration zones. They are interpreted to have formed by lateral dispersion of hydrothermal fluids, which may have been originally structurally focused, but has dispersed when they encountered porous and permeable strata (Gemmell 1998). Stratabound alteration is often extensive with alteration extending 200m below the ore horizon and for several square kilometres around the deposit. Stratabound alteration zones exists beneath several of the Mount Read deposits including Rosebery and Mt Lyell

(Eastoe et al. 1987). An extreme example of this blanket style alteration is observed at Mt Lyell, where a very large hydrothermal system has pervasively altered approximately 10km^3, forming an assemblage dominated by sericite ± chlorite ± pyrite (Eastoe et al. 1987). The importance of stratigraphic permeability on hydrothermal fluid mobility has been documented at Thalanga, North Queensland by Herrmann and Hill (in prep. 1999), where semi-stratiform stringer alteration reflects the focussing of ascending fluids along permeable volcaniclastic layers between coherent rhyolite units.

3. Whole Rock Geochemistry

Geochemical changes within the footwall alteration system generally correspond to the different alteration assemblages. Typically magnesium, iron, manganese and sulfur increase within the chlorite zone. Within the sericite, quartz ± chlorite alteration zone there are sporadic enrichments of potassium and sulfur. Within both alteration zones sodium and calcium are depleted (Gemmell et al. 1998).

Sodium depletion is the most common feature of footwall alteration, and is the most sensitive indicator among the major oxides (FeO, MgO, CaO, K_2O, SiO_2 and Na_2O) of the intensity of alteration. Studies by Urabe and Scott (1983) on the South Bay deposit in northwestern Ontario, indicate that sodium depletion is the only major element to show a consistent systematic lateral change within the alteration halo, while other major components and oxygen isotope ratios show no change. Studies by Hashiguchi et al. (1983) of the Kosaka and Fukazawa Kuroko deposits show that the areal extent of strong Na_2O depletion (<0.32-0.36% Na_2O) haloes are two to three times larger than the known extent of ore.

5 cm

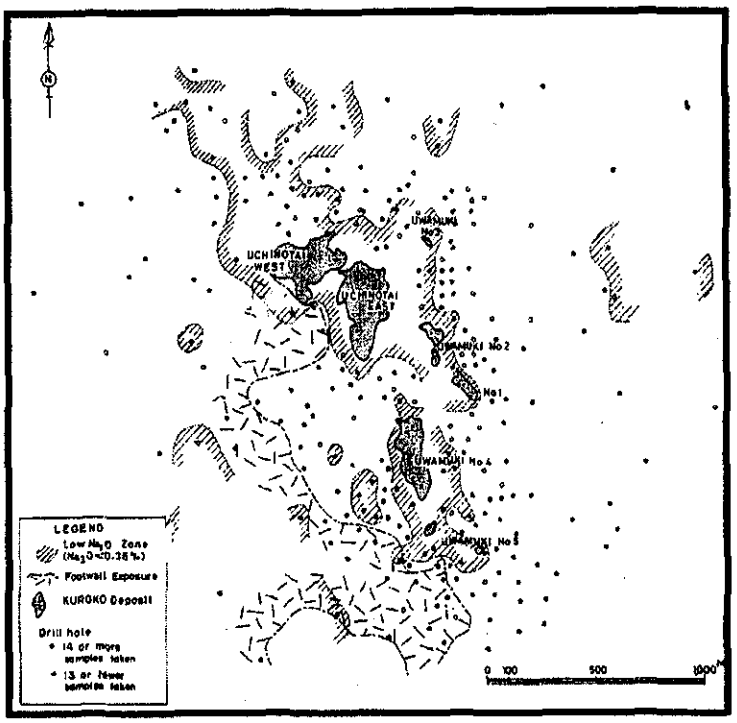

Figure 2. Distribution map of low Na_2O anomalies in the Kosaka area. Note the close correlation between Na_2O anomalies and distal, small orebodies. (Taken from Hashiguchi et al 1983).

Na_20 contents typically decrease from values of 2 to 4% in unaltered volcanics to less than 0.5% in the outer sericite–quartz alteration zone and commonly less than 0.2% in the chlorite rich alteration zone (Large 1992). Recognition of the variation of Na_2O contents in footwall rocks, therefore, are an important and easily used tool in the exploration of VHMS deposits particularly in detailed prospect scale exploration programs.

Barrett and MacLean's (1994) study of mass changes associated with VHMS deposits of the Noranda area, Quebec, indicate that sodium depletion, although certainly advantageous in exploration is complicated by the fact that Na_2O depletion zones can be caused by a variety of fluids not necessarily related to ore forming hydrothermal systems. Meteoric water may alter wallrocks surrounding later tectonic fault zones and deplete sodium, it will not however provide significant Fe and Mg additions. Lentz et al's (1997) study of the alteration of the Heath Steele B Zone massive sulfide deposit accounted for this by using a ratio of (Fe + Mg) / (K + Na). This ratio increased progressively toward the ore horizon, from <1 to almost 100, indicating the increase in chlorite at the expense of mica and feldspar.

The problem identified by Barrett and MacLean (1994), is overcome by using the alteration index (AI) developed by Ishikawa et al. (1976) for quantifying the intensity of alteration through the calculation of major element mass changes associated with feldspar destruction and chloritisation. The alteration index has the form:

$$AI = \frac{100\ (MgO + K_2O)}{(Na_2O + CaO + MgO + K_2O)}$$

Studies of the Hellyer alteration system by Gemmell and Large (1992) using the alteration index clearly showed an increase in AI values associated with increasing alteration intensity, from AI = 36 within the unaltered footwall andesite to AI = 91 within the proximal siliceous core.

Large (pers. comm. 1998) developed an alteration index called the chlorite-carbonate-pyrite index (CCPI) that accounts for the degree of chlorite, carbonate and/or pyrite alteration in volcanic rocks.

$$CCPI = \frac{100\ (MgO + FeO)}{(MgO + FeO + Na_2O + K_2O)}$$

These two indexes, when plotted together on a AI vs CCPI boxplot provide a method of visually discriminating the effects and intensities of chloritisation, sericitisation, carbonatisation and albitisation associated with VHMS deposits.

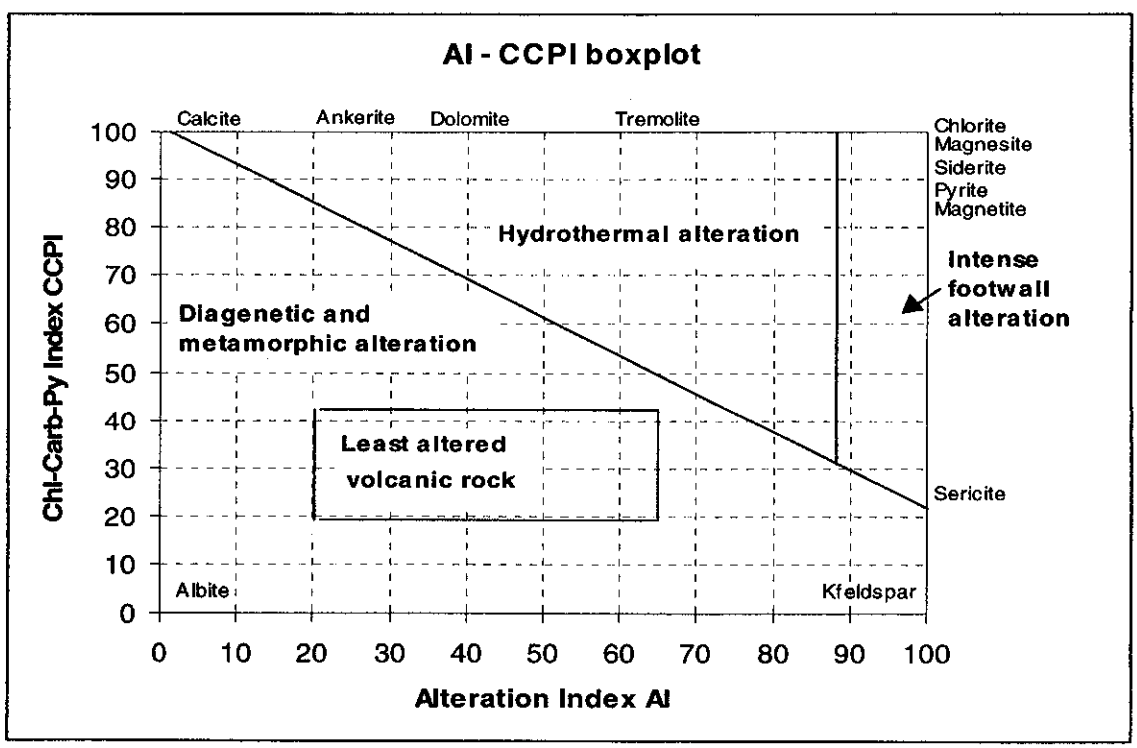

Figure 3. Alteration index AI versus carbonate–chlorite-pyrite index CCPI.

The AI – CCPI boxplot provides an estimate of the major alteration mineral assemblages and the likely alteration facies; footwall, hangingwall and diagenetic/metamorphic alteration. Therefore, its application in identifying alteration trends and locating the likely position within a hydrothermal alteration system makes it a very useful tool in the exploration of VHMS deposits.

Barrett and MacLean (1994) also suggested the study of changes in trace element abundance to further delineate VHMS alteration zones and determine vectors towards mineralisation. Changes in trace element abundances associated with alteration systems has long been known. Green et al's (1983) studied the alteration zones within the Fukazawa-Kosaka area and showed that strontium content decreases from 100ppm in the distal montmorillonite zone to less than 10ppm in the proximal sericite-chlorite zone.

Lentz et al. (1997) observed an increase in barium content 2 to 5 times greater than background in the hanging wall alteration zone of Heath Steele. Moreover, they found a considerable decrease in Sr and Rb towards the ore horizon. Whole rock arsenic and antimony also increase proximally in association with S, Cu and Co reflecting saturation in sulfides. Maclean and Hoy (1991) also observed an increase of 430ppm Ba and 46ppm Rb and a decrease of 41ppm for Sr for the Horne Mine. However, barium was not added as barite as in Kuroko and Tasmanian deposits but as a trace component in sericite. Gemmell and Large (1992) observed significant increases in Ba (increase from 700 to 2300ppm) and decreases in Sr (decrease from 300 to 20ppm) with proximity to the centre of the alteration system at Hellyer.

The above changes in the major and trace elements are related to mineral assemblages. The destruction of primary plagioclase results in the loss of Na, Ca and Sr. Mg, Fe and Mn increase within the chlorite zone, in addition to S, Ba, Tl and Sc, and in the sericite, quartz± chlorite zones there are sporadic increases in K, S, Ba, Rb and Sc.

4. Mineral Chemistry Vectors

4.1 Chlorite Chemistry

Urabe et al (1983) observed a significant compositional variation in the chemistry of chlorite both laterally and vertically away from the Seneca, South Bay and Corbet deposits. Urabe et al (1983) suggested that the Fe/ (Fe + Mg) ratio of chlorite can be used as a vector

within hydrothermal alteration zones associated with VHMS deposits. Chlorite compositions become more iron rich away from these deposits with Fe/(Fe + Mg) ratios increasing systematically from 0.3 at the center to 0.5 at the margin of the alteration halo for Seneca and 0.65 - 0.9 and 0.3 - 0.6 for South Bay and Corbet respectively.
Proximal iron depletion was also observed at Thalanga (Herrmann & Hill in prep.) and at the Hellyer deposit, where Jack (1989) determined that chlorites within the Hellyer alteration zone are magnesium rich, Fe/(Fe+Mg) = 0.14 – 0.28, whereas chlorites within the footwall andesites outside the stringer zone are more iron rich {Fe/(Fe+Mg) = 0.44 – 0.46}.

The opposite relationship is observed at the Heath Steele B Zone Massive Sulfide Deposit, New Brunswick (Lentz et al. 1997), Brunswick No 12 (Luff et al. 1992) Horne Mine, Noranda, Quebec (Maclean & Hoy 1991) and at Hercules (Eastoe et al, 1987). Lentz et al. (1997) observed that chlorite within both the hangingwall and footwall increases in abundance relative to white mica and also becomes more iron rich towards the ore horizon. Eastoe et al. (1987) observed a more complex distribution, where footwall chlorite containing anomalously high magnesium in an aureole extending 0.8km on either side of a narrow iron chlorite enriched, pyritic zone beneath the center of the deposit.

In some hydrothermal systems the composition of chlorite parallels variations in the whole rock Fe/Mg ratios related to the introduction of Mg from seawater, (Urabe et al. 1983). However, bulk chemistry and the composition of chlorites can be biased by the presence of iron bearing minerals such as pyrite, pyrrhotite, siderite and magnetite in VHMS alteration assemblages. As a result, within the zone of more intense pyritic alteration, chlorite will become increasingly more magnesium rich as iron may be incorporated in pyrite.

Bischoff and Dickson (1975) (cited in Urabe. 1983) demonstrated through experimental studies on seawater / rock reactions that magnesium is the first element to be removed from the seawater during the initial stages of water / rock interaction. Therefore, the alteration zone enriched in bulk magnesium and/or containing low Fe/(Fe + Mg) chlorites is most likely to reflect the zone of initial interaction between the seawater and the host rock. This is supported by Lentz & Goodfellow's (1993) study of the Brunswick No. 12 massive sulfide deposit. They inferred that similar compositional zonation reflected a modification of the hydrothermal fluid from a lower $\alpha Fe/\alpha Mg$ fluid in the peripheral alteration zone to high $\alpha Fe/\alpha Mg$ fluid with moderate to high $f(H_2S)$, coincident with the

stringer – sulfide zone. This supports an interpretation of a higher proportion of seawater being involved in the peripheral alteration compared to the more chemically modified fluid responsible for the stringer – sulfide zone alteration and mineralisation.

Urabe et al. (1983) further inferred that a fluid flow direction (from magnesium rich to less magnesian zones) can be deduced from gradients in the whole rock Fe/(Fe + Mg) ratio. This zonation may account for the complex distribution of chlorite compositions observed by Eastoe et al. (1987) for the Hercules footwall, where magnesium content of chlorite increases towards the central feeder which contains strongly magnesium depleted chlorites.

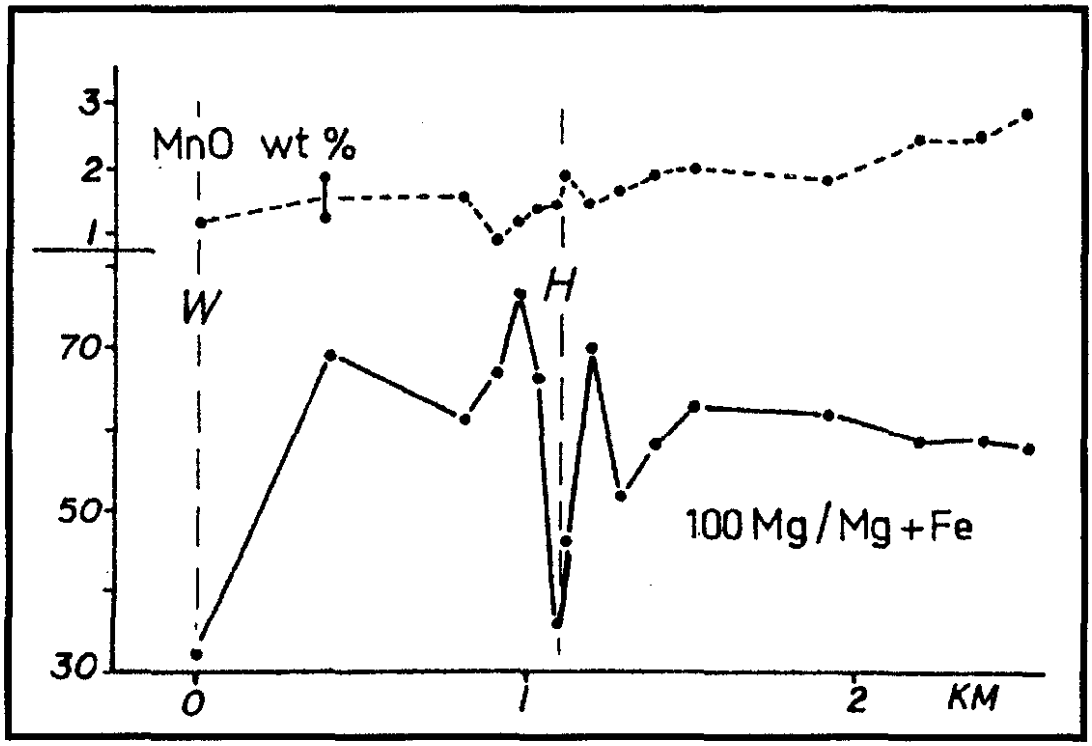

Figure 4. Variations in Mg/Mg + Fe and Mn content in chlorites from the Hercules footwall. Analyses are plotted as a function of position. W = Williamsford deposit; H = Hercules deposit, central feeder.(Taken from Eastoe et al. 1987)

The use of chlorite chemistry as a geothermometer has been studied by numerous authors and has been summarized by Green and Taheri (1992). Empirical thermometers typically rely on the measurement of the abundance of tetrahedrally coordinated aluminium within the chlorite structure.

$$[Mg, Fe^{2+}, Mn, Al]_{12}[(Si, Al, Fe^{3+})_8O_{20}]\ [OH]_{16}$$

Where the first group of cations are octohedrally coordinated in the structure and the second group are tetrahedrally coordinated by oxygen.

Tetrahedrally coordinated aluminum increases with increasing temperature. This empirical thermometer is best used between 200° and 300°C. The use of chlorite composition to define temperature of formation results in its use to map paleotemperature gradients within the hydrothermal system, and hence, may define higher temperature zones associated with ascending mineralised fluids.

The chemical composition of chlorite provides a useful parameter in quantifying hydrothermal alteration systems associated with VHMS systems. However, due to the complexity governing the composition of chlorite, and the noted reversal in compositional zonation, chlorite chemistry should only be used as one of several indicators within a multi facetted exploration program.

4.2 White Mica Chemistry

Studies by Lentz & Goodfellow (1993) and Lentz et al. (1997) indicated that white mica compositional zonation, which parallels the composition of chlorites, exists in the footwall alteration systems of the Brunswick No.12 and the Heath Steele B zone massive sulfide deposits. Proximal white micas have higher Fe/(Fe + Mg) ratios and lower manganese than the mica in the peripheral alteration haloes. In addition, aluminium content increases (with respect to Mg + Fe ions in the octahedral site) with increasing alteration intensity, resulting in mica compositions trending towards end – member muscovite compositions adjacent to sulfide zones (Lentz et al. 1997). This is also observed in the South Bay massive sulfide deposit (Urabe and Scott 1983).

Lentz and Goodfellow (1993) also indicate that proximal footwall phengitic muscovite is locally enriched in barium. Barium contents of phengite at Heath Steele however, are irregular, with Ba content decreasing towards the ore horizon in the footwall, but enriched in the hangingwall.

4.3 Carbonate Chemistry

Carbonate alteration is a common, but poorly documented feature of footwall alteration zones associated with VHMS deposits. It may exist beneath the deposit, within the deposit or in some cases enveloping the deposit (Gemmell 1998).

Ore related carbonates are typically Fe, Mg and Mn varieties. Ferroan carbonate occurs within the proximal alteration zone of the Brunswick No.12 massive sulfide deposit associated with Fe – rich chlorite, muscovite and quartz (Lentz et al. 1997). At Hellyer, rhombs and rounded nodules of dolomite ranging in size from 0.1 to 5mm occur within a

fine grained chloritic matrix at the basal contact of the massive sulfide and adjacent to the siliceous core zone (Gemmell and Large 1992).

At South Bay, siderite and ferroan dolomite coexists within the immediate footwall and siderite is also found within the massive sulfide ore (Urabe & Scott 1983). Iron and magnesium contents in ferroan dolomite show lateral variation relative to the distance from the ore, where the iron content of dolomite decreases systematically towards the orebody over distances of tens to hundreds of metres.
There is no spatial trend in Mn content of carbonates at Thalanga, however, there is a subtle increase in Fe content (<0.005 up to 0.020 cations) of dolomite towards the central sulfide lens (Herrmann & Hill in prep.).

5. Rare Earth Elements

Graf (1977) suggests that the Rare Earth Elements (REE), due to their coherent and somewhat predictable geochemical properties can indicate the types of alteration reactions which take place within hydrothermal systems responsible for the formation of massive sulfide deposits.

Just as inferences regarding magmatic processes can be made based on REE patterns and their known fractionation patterns, a similar approach can be used in the study of hydrothermal systems. REE concentrations in a hydrothermal solution interacting with host rocks will be controlled by the concentrations of the REE in the rock, the partitioning behaviour of the REE between the rock phases and the solution, and the types of alteration reactions which take place. If the hydrothermal solution is released into seawater and precipitates a massive sulfide body or other exhalite, the REE pattern of both the resulting chemical sediment and the altered footwall rocks can provide information regarding the hydrothermal system responsible for their formation (Graf 1977).

Typically the most obvious/visual feature when observing the REE pattern of altered footwall rocks is the negative europium anomaly which reflects the loss of soluble Eu^{2+} to the reduced hydrothermal fluid during the alteration of plagioclase (Graf 1977). This negative europium anomaly, observed within the altered footwall has since been recognized in many volcanic hosted massive sulfide alteration systems. (Whitford et al 1988, Barrett & Sherlock 1996, Peter & Goodfellow 1996).

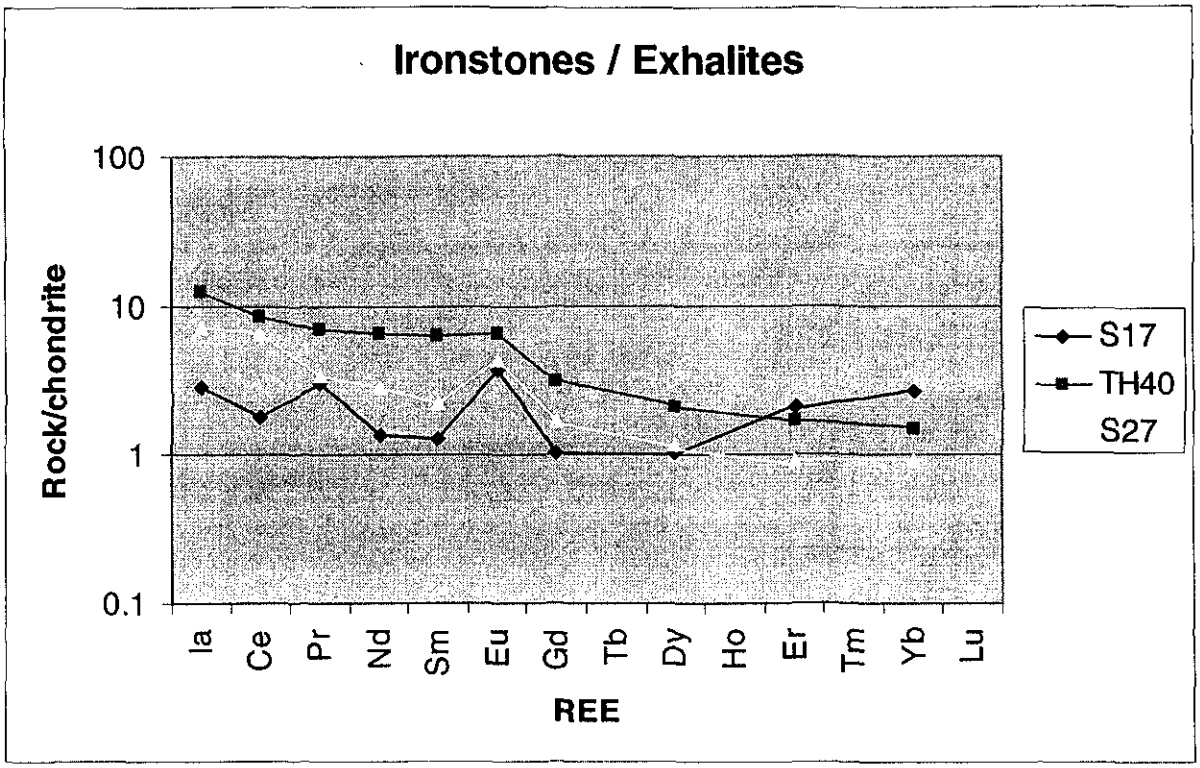

Figure 6. Rare earth element plots of exhalites and ironstone normalised to the chondritic values of Evensen et al (1978). Characterised by low REE concentrations, slight LREE enrichment and positive Eu anomalies. Samples from the Mount Windsor ironstones. S17: from the Thalanga ore horizon; TH40 and S27: ironstones from the Trooper Creek Formation. (Data from Duhig et al. 1992)

Positive Eu anomalies are absent from exhalites associated with the Kuroko deposits of Japan and from many modern deep-sea sediments. This reflects that this anomaly is not preserved in modern and ancient oxidised oceans because of the rapid oxidation of hydrothermal Eu^{2+} to Eu^{3+} (Peter & Goodfellow 1996). Nevertheless, the recognition of these chemical sediments based on mineralogy and other REE patterns may help to recognize favorable horizons for exhalitive and massive sulfide deposits (Urabe et al 1983, Whitford et al 1988, Duhig et al 1992).

6. Stable Isotopes

6.1 Lead.

Lead isotopes have been used for distinguishing between VHMS and other styles of uneconomic mineralisation on the West Coast of Tasmania. Gulson & Porritt (1987) indicated that the Cambrian volcanogenic deposits (Mount Lyell, Rosebery, Hercules, Que River and Hellyer) have lead isotope signatures that differ substantially from those associated with post – Cambrian mineralisation. Cambrian stratiform massive sulfide samples exhibit the least radiogenic values ($^{206}PB/^{204}Pb$ = 18.06 to 18.14), Devonian vein-style Pb-Zn-As mineralised samples form the most radiogenic group ($^{206}PB/^{204}Pb$ = 18.44

to 18.53)A third group of values with intermediate radiogenic values come from disseminated and vein-style Pb-Zn mineralised samples associated with quartz porphyry bodies which are considered to post-date the episode of massive sulfide formation. (Gulson et al. 1987).

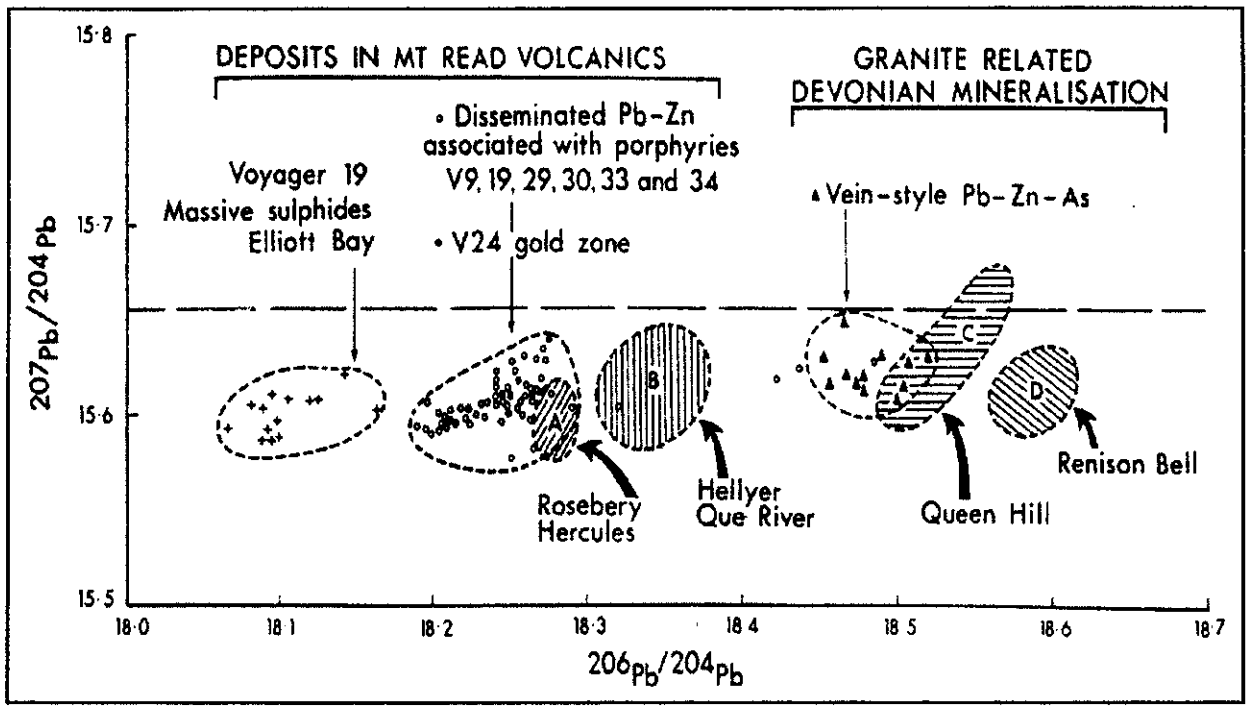

Figure 7. Lead isotope data for western Tasmanian ore deposits (Taken from Gulson et al. 1987).

The use of lead isotopes can therefore be used within an exploration program to differentiate between geochemical anomalies produced by massive sulfide mineralisation or from less prospective Devonian and Cambrian vein systems. Prioritisation of prospects for their relevance to possible VHMS style base metal deposits, may be based on Pb isotope data from a variety of geochemical samples including anomalous soil samples and drill hole intersections.

6.2 Sulfur.

Sulfur isotope geochemistry has a long history with respect to massive sulfide deposit research, and has been used to determine temperature of sulfide deposition and the mechanisms of sulfide deposition (i.e. role of pH and fO_2) and the origin of sulfur. Studies by Solomon et al (1988) and Gemmell and Large (1992) on the Mount Read Volcanics have shown that VHMS deposits have a sulfur isotope signature that reflects the supply of sulfur from a combination of reduced seawater sulfate and from volcanic rock sources.

Large (1989) indicated that sulfur isotope studies on pyrite and base metal sulfides have generally proved less successful as an exploration tool within the Paleozoic VHMS deposits of western Tasmania. $\delta^{34}S$ values typically range between +0 and +17‰ for Paleozoic volcanic hosted massive sulfide deposits (Gemmell et al 1998). Tasmanian deposits have a $\delta^{34}S$ range between +5‰ and +20‰. Green and Taheri (1992) however suggested that barren pyritic alteration systems can be distinguished and excluded based on their lower (< +5‰) $\delta^{34}S$ values. Low $\delta^{34}S$ values reflect leaching of sulfur from the surrounding volcanic rocks due to alteration by fluids of lower temperature (<200°C) than those required to inorganically reduce seawater sulfate or to transport sufficient base metals together with H_2S to form an orebody.

Studies of the Hellyer deposit and associated alteration zones by Gemmell and Large (1992) resulted in the formation of a temporal and spatial model for the evolution of sulfur isotope values, and a possible vector towards focused mineralisation. In most cases the massive sulfide ores and main-stage stringer veins show restricted $\delta^{34}S$ values with variation of only ~5‰. Sulfides within the barite-rich stratiform ore and the lateral (early and late stage) veins show more positive $\delta^{34}S$ values with variations of 5 to 15‰ heavier than the massive sulfide ores (Large 1992). The heavier $\delta^{34}S$ ratios for sulfides within the lateral stringers and the barite cap has been interpreted to reflect an increasing involvement of reduced seawater sulfate due to mixing of the hydrothermal fluid with heated seawater at the top of the deposit and/or within the lateral stringer zone (Large 1992; Gemmell and Large 1992).

Miocene Kuroko deposits generally have lower $\delta^{34}S$ values reflecting the lower $\delta^{34}S$ value of seawater during the Miocene. $\delta^{34}S$ values for sulfide minerals within Kuroko deposits form a tight cluster between +2 and +8‰, contrasting the wide range measured within the host rocks (-50 to +10‰). The recognition of characteristic sulfur isotopic signatures, reflecting the mixing of reduced seawater and primary volcanic rock sulfur and the recorded variation in $\delta^{34}S$ values away from the centre of hydrothermal systems (Gemmell and Large 1992) may provide a basis for developing sulfur isotope vectors towards mineralisation.

6.3 Oxygen.

Regional studies (Cathles 1993) and district scale studies (Green et al 1983, Green & Taheri 1992, Maclean and Hoy 1991) have shown that the distribution of whole rock $\delta^{18}O$

values can define areas of high temperature fluid flow in areas of VHMS mineralisation. The dominant control on $\delta^{18}O$ (and alteration assemblage) within hydrothermal systems is the temperature at which the hydrothermal fluid alters the rock (Brauhart et al 1998). The $\delta^{18}O_r$ value is also affected by the water/rock ratio. Where the water/rock ratio is large (>1) the $\delta^{18}O$ of the water dominates, resulting in the initial $\delta^{18}O$ value of the rock being modified to a value that is consistent with alteration by a fluid with a $\delta^{18}O$ close to the seawater value of 0‰ (Green & Taheri 1992). Consequently, zones of low $\delta^{18}O_r$ values can be considered characteristic of areas that have undergone high – temperature fluid fluxing in association with silica leaching proximal to zones of hydrothermal discharge.

Comparisons made by Green et al (1983) in the Fukazawa area indicated that the areal extent of the $\delta^{18}O$ anomaly of the footwall rocks is far larger than the geochemical anomalies associated with Na, K, Mg, Ca, Sr, Cu, Pb, Zn and S. In addition, as the variablity of $\delta^{18}O$ values within a site is much less than that of the elemental compositions, the analysis of whole-rock $\delta^{18}O$ values is a useful method of exploration during the reconnaissance stage, whereas other geochemical methods are more suitable for detailed exploration during the developmental stage within a prospect.

Conversely, the area of fluid recharge in a convection system is much greater than the area of discharge. If the area of recharge that fed discharge and produced the massive sulfide mineralisation could be mapped, the dimensions of the massive sulfide exploration target would be increased by an order of magnitude or more. Cathles (1993) indicates that as seawater contains far more ^{18}O than is in equilibrium with rock at low temperatures, the $\delta^{18}O$ of rocks within the zone of recharge for the hydrothermal system would be increased. This concentric zonation from a broad (~30km diameter) zone of ^{18}O enrichment to a small inner $^{18}O_r$ depleted zone reflects the transition from cold water recharge to high temperature discharge within the hydrothermal system and hence a vector to focused, mineralised hydrothermal fluids and possible massive sulfide deposition. MacLean and Hoy (1991) however point out that $\delta^{18}O$ enrichment can occur within the proximal alteration zone when intense silicification has occurred.

The amount of isotopic alteration is proportional to the amount of fluid circulation. As a result, the intensity and volume of the isotopic alteration may provide a method of quantitatively assessing the size and longevity of a discovered paleohydrothermal system and hence its potential to generate massive sulfide mineralisation (Cathles 1993).

In addition to isotopic alteration being proportional to the amount of fluid circulation, whole rock oxygen isotope zonations would be preserved during metamorphism, providing metamorphism took place under low water – rock ratio conditions. As a result, oxygen isotopes may be of greater exploration significance in greenschist facies metavolcanic terranes, such as the Mount Read Volcanics, where original clay – zeolite mineralogical zonation associated with mineralisation would be destroyed / masked by later metamorphism (Green & Taheri 1992).

6.4 Strontium

Studies by Farrell and Holland (1983) and Whitford et al (1992) have further reinforced the proposed genetic model for VHMS / seawater circulation based on strontium isotope studies within the Miocene Kuroko and Paleozoic Mt Read VHMS districts. Their studies have also defined $^{87}Sr/^{86}Sr$ values of barite associated with VHMS systems, and which may be used to assess the likely metallogenic association of minor mineral occurrences and therefore be used as an exploration tool.

Whitford et al (1992) put forward an interesting scenario regarding exploration for Tasmanian deposits based on $^{87}Sr/^{86}Sr$ ratios. As the measured $^{87}Sr/^{86}Sr$ of stratiform barites are higher than both the initial $^{87}Sr/^{86}Sr$ ratios calculated for the host volcanic rocks and the ratio inferred for Cambrian Seawater, Whitford et al (1992) suggest the possible interaction of hydrothermal fluids with old continental crust material. If this hydrothermal fluid has contacted old continental crust beneath the volcanic pile and obtained ore metals from it, Whitford suggests that exploration for VHMS deposits formed from these systems may be warranted beyond the confines of the volcanics.

7. Zinc Ratio

Volcanogenic massive sulfide deposits are the most significant base metal resource within the Mount Read Volcanics of western Tasmania. The exploration for these deposits is however complicated by the presence of other uneconomic styles of Pb – Zn mineralisation.

The analysis and comparison of distrbution pattern, mean and standard variatio of the "zinc ratio" [100Zn/(Zn + Pb)] of anomalous samples can provide an excellent method in

distinguishing between the metallogenic style and hence provide a prospect screening mechanism for the favourable VHMS mineralisation (Huston and Large, 1987).

Volcanogenic massive sulfide deposits are characterized by zinc ratios displaying a normal distribution and a restricted range of means between 64 and 77 with relatively low standard deviations (less than 15). Alternatively, Cambrian vein-style mineralisation associated with felsic porphyries and Ordovician and Devonian mineralisation are characterized by having a wide distribution pattern with lower means, generally around 40 (but ranging from 39 to 75) and standard deviations greater than 23.

Huston and Large (1987) indicate that the Zinc Ratio should not be used in isolation to determine the style of mineralisation. However they indicate that its use in conjunction with lead isotopes can be a powerful method of discriminating between different ages and styles of mineralisation. This makes it a useful prospect screening mechanism for targeted VHMS mineralisation.

8. Conclusion

There are broad geochemical similarities between the alteration systems of the Archean Canadian Shield, the Kuroko, the New Brunswick and the Mount Read deposits. These similarities reflect their broadly similar genesis. Differences observed between these deposits are attributable to differences in host rocks (degree of fractionation, relative proportions of volcanic and sedimentary rock), differences in ore composition, alteration mineralogy, fluid chemistry, structural and permeability controls, depositional environment and whether deposits are proximal or distal to the primary source of mineralising fluids.

There are however, consistent geochemical patterns associated with the alteration process of VHMS mineralisation. The recognition of these patterns may provide useful vectors for exploration at the reconnaissance stage right through to detailed mining development.

The recognition of alteration mineralogy and zonation is critical in the exploration of VHMS deposits. Within footwall sequences, dominated by intermediate to mafic volcanics, alteration will typically exhibit a chlorite rich core surrounded by sericite±quartz. If the footwall sequence is dominated by felsic volcanics the core of the alteration system is generally sericite dominated with a halo of chlorite.

Oxygen isotope ratios show a consistent relationship with alteration assemblages. The fact that $\delta^{18}O$ values show a systematic increase from low isotopic values within the most intensely altered zone to higher values within the less altered periphery and out into the unaltered host rocks. Therefore its use as an exploration tool may be extremely useful for VHMS prospectors. Comparisons made by Green et al (1983) regarding the areal extent of $\delta^{18}O$ and the geochemical anomalies produced by Na, K, Mg, Ca, Sr, Cu, Pb, Zn and S indicate that the extent of anomalous $\delta^{18}O$ values is far greater. They therefore suggest that the analysis of whole rock oxygen may be a useful broad scale exploration tool in the reconnaissance stage of exploration.

Mass change calculations in the footwall alteration zone reflect the alteration mineralogy and generally show that altered rocks have experienced losses of Na_2O and CaO, increases in FeO and MgO and variable SiO_2 and K_2O gains/losses. Sodium depletion is the most common feature of footwall altered rocks, and in some cases, such as South Bay may be the only major element to show systematic mass changes within the alteration zone. The high spatial correlation between Na_2O depletion and ore protrusions documented by

Hashigushi et al (1983) suggest that the mapping of sodium depletion haloes may be advantageous during detailed prospect exploration or mine development programs. The use of the alteration index (AI) vs. chlorite-carbonate-pyrite index (CCPI) boxplot may further identify geochemical trends within altered host rocks and provide a vectors towards more intensely altered rocks and possible mineralisation.

Trace element abundance can be used as a vector towards sulfide deposition, with Ba/Sr and Rb/Sr ratios generally increasing towards zones that have undergone more intense alteration. Strontium typically decreases as a result of feldspar being destroyed and barium increases as either the major constituent in barite or as a trace element in sericite.

The use of mineral chemistry as a vector towards volcanic hosted massive sulfide deposits has generally proved inconclusive, with chlorite, white mica and carbonate compositions showing spatial variations within several systems. The Fe/(Fe + Mg) content of chlorite has been observed to display a spatial variation within the altered rocks of known VHMS systems. Urabe et al (1983) suggested that typically chlorite content becomes more iron rich away from mineralisation. This observation holds true for the Canadian deposits of Seneca, South Bay and Corbet and also at Hellyer. However, this zonation contradicts laboratory studies and empirical evidence from the Brunswick camp, Horne mine and at Hercules.

The composition of white mica typically parallels that of chlorite, with Fe/(Fe + Mg) content of phengitic muscovite also displaying spatial variations within the alteration system. The aluminium content of white mica also correlates with alteration intensity, with mica compositions trending towards end-member muscovite proximal to mineralisation.
Carbonate mineralogy associated with volcanic hosted massive sulfide deposits have been documented to typically consist of Fe, Mg and Mn varies. Studies by Urabe and Scott (1983) and Herrmann and Hill (in prep.) indicate that the Fe/Mg ratio of dolomites increase towards sulfide deposits.

The spatial variations observed in the composition of carbonates and micas may provide a method of determining the location within a hydrothermal system. However, due to their known discrepancies and observed reversals in zonation the application of mineral chemistry for exploration should be used with caution.

Several techniques appear applicable in distinguishing the metallogenic source of anomalous samples and small base metal showings, and the likelihood of VHMS style mineralisation. The distinctive mean value (64-77), low standard deviation (less than 15) and normal distribution of zinc ratios [100Zn/(Zn +Pb)] associated with VHMS mineralised samples differs greatly to the wide distribution patterns, lower means and high standard deviations of uneconomic Cambrian and Devonian vein style mineralisation. As a result prospects can be screened quickly for the likely metallogenic source of sulfides.

The use of zinc ratio patterns in conjunction with lead isotopes has proven to be a powerful method in discriminating between different ages and styles of mineralisation, within the Mount Read Volcanics. Green and Taheri (1992) also indicate that the use of sulfur isotopes may also delineate between fertile and barren hydrothermal systems, providing an even greater ability to distinguish prospective targets.

The importance of alteration geochemistry as a vital tool in the exploration of VHMS deposits can not be underestimated. It may provide a vector towards host rocks effected by hydrothermal alteration and a method of quantifying and interpreting the intensity and style of alteration. Alteration geochemistry may also provide a method of discriminating between styles of mineralisation that is cost-effective. The application of alteration geochemistry in exploration however, must be integrated into a multi-disciplinary exploration program which combines detailed geological mapping with volcanic facies interpretation, alteration mapping and geophysical methods.

References

Barrett, T. J. and MacLean, W. H. (1994) Mass changes in hydrothermal alteration zones associated with VMS deposits of the Noranda area. Explor. Mining Geol., Vol. 3 (2)

Barrett, T. J. and Sherlock, R.L (1996). Volcanic Stratigraphy, Lithogeochemistry, and Seafloor Setting of the H-W Massive Sulfide Deposit, Myra Falls, Vancouver Island, British Columbia. Explor. Mining Geol., Vol. 5 (4)

Brauhart, C. W., Huston, D. L., & Andrew, A. S. (1998) Part II. Alteration mapping by oxygen isotopes. AGSO Research Newsletter 29. November.

Cathles, L. M. (1993) Oxygen isotope alteration in the Noranda Mining District, Abitibi Greenstone Belt, Quebec. Economic Geology. Vol. 88

Duhig, N. C., Stolz, J., Davidson, G. J., and Large, R. R. (1992). Cambrian Microbial and Silica Gel Textures in Silica Iron Exhalites from the Mount Windsor Volcanic Belt, Australia: Their Petrography, Chemistry, and Origin. Economic Geology. Vol.87

Eastoe, C. J., Solomon, M. and Walshe, J. L. (1987) District – Scale Alteration Associated with Massive Sulfide Deposits in the Mount Read Volcanics, Western Tasmania. Economic Geology. Vol. 82

Evans, A. M. (1993) Ore Geology and Industrial Minerals: An Introduction. Blackwell Science, Geoscience Texts.

Evensen, N. M., Hamilton, P. J. & O'Nions, R. K. (1978) Rare earth abundances in chondritic meteorites. Geochim. Cosmochim. Acta, 42: in Rollinson, H. R. (1996) Using Geochemical Data: evaluation, presentation, interpretation. Addison Wesley Longman Limited.

Farrell, C. W. & Holland, H. D. (1983) Strontium Isotope Geochemistry of the Kuroko Deposits: in Skinner, B. J., The Kuroko and Related Volcanogenic Massive Sulfide Deposits. Economic Geology. Monograph 5

Gemmell, J. B. & Large, R. R. (1992) Stringer System and Alteration Zones Underlying the Hellyer Volcanic-Hosted Massive Sulfide Deposit, Tasmania, Australia. Economic Geology. Vol. 87

Gemmell, J. B., (1998) Alteration and Stringer Zones associated with VHMS Deposits: in Ore deposit studies and exploration models, Volcanic-hosted massive sulfide deposits. Codes Short Course Manual 7

Gemmell, J. B., Large, R. R., and Khin Zaw. (1998) Palaeozoic volcanic-hosted massive sulfide deposits. AGSO Journal of Australian Geology & Geophysics, Vol. 17 (4)

Govett, G. J. S (1983) Handbook of Exploration Geochemistry: Rock Geochemistry in Mineral Exploration. Elseveier Scientific Publishing Company.

Graf, J. L. (1977). Rare Earth Elements as Hydrothermal Tracers During the Formation of Massive Sulfide Deposits in Volcanic Rocks. Economic Geology. Vol. 72.

Green, G. R. & Taheri, J. (1992). Stable isotopes and geochemistry as exploration indicators. Bull. Geol. Surv. Tasm. 70: pg84-91.

Green, G. R., Ohmoto, H., Date, J., and Takahashi, T. (1983). Whole-Rock Oxygen isotope Distribution in the Fukazawa-Kosaka Area, Hokuroku District, Japan, and Its Potential Application to Mineral Exploration: in Skinner, B. J., The Kuroko and Related Volcanogenic Massive Sulfide Deposits. Economic Geology. Monograph 5

Gulson, B. L., Large, R. R., and Porritt, P. H. (1987) Base metal exploration of the Mount Read Volcanics, Western Tasmania: Pt.III. Application of Lead Isotopes at Elliott Bay. Economic Geology. Vol. 82

Gulson, B. L., and Porritt, P. H. (1987) Base metal exploration of the Mount Read Volcanics, Western Tasmania: Pt.II. Lead isotope signatures and genetic implications. Economic Geology. Vol. 82

Hashiguchi, H., Yamada, R., & Inove, T. (1983) Practical Applications of low Na20 Anomalies in Footwall Acid lava for Delimiting Promising Areas around the Kusaka and Fukazawa Kuroko Deposits, Akita Prefecture, Japan.: in Skinner, B. J., The Kuroko and Related Volcanogenic Massive Sulfide Deposits. Economic Geology. Monograph 5

Herrmann, W. & Hill, A. P. (in prep.) Carbonate alteration associated with the Thalanga VHMS deposit, North Queensland. Centre for Ore Deposit Research, University of Tasmania.

Ishikawa, Y., Sawaguchi, T., Iwaya, S., & Horiuchi, M. (1976) Delineation of prospecting targets for Kuroko deposists based on modes of vocanism of underlying dacite and alteration halos. Mining Geology, V.26, (in Japanese with English abs.)

Jack, D. J. (1989). Hellyer host rock alteration. Unpub. Masters thesis, University of Tasmania

Large, R. R. (1992) Australian Volcanic-Hosted Massive Sulfide Deposits: Features, Styles, and Genetic Models. Economic Geology. Vol. 87

Large, R. R. (1998) Written Communication. Practical Notes, KEA336 Ore Deposit Geology. University of Tasmania.

Lentz, D. R. & Goodfellow, W. D. (1996) Intense silicification of footwall sedimentary rocks in the stockwork alteration zone beneath the Brunswick No.12 massive sulphide deposit, Bathurst, New Brunswick. Canadian Journal of Earth Sciences. Vol. 33

Lentz, D. R. & Goodfellow, W. D. (1993) Character, Distribution, and Origin of Hydrothermal Alteration features of the Brunswick No.12 massive sulfide deposit, Brunswick, New Brunswick. Exploration & Mining Geology. Vol. 2

Lentz, D. R., Hall, D. C. & Hoy, L. D. (1997) Chemostratigraphic, alteration, and oxygen isotopic trends in a profile through the stratigraphic sequence hosting the Heath Steele B Zone massive sulfide deposit, New Brunswick. The Canadian Mineralogist. Vol. 35

Lentz, D. R., Hall, D. C. and Hoy, L. D. (1997) Chemostratigraphic, alteration, and oxygen isotopic trends in a profile through the stratigraphic sequence hosting the Heath Steele B zone massive sulfide deposit, New Brunswick. Canadian Mineralogist. Vol. 35 (4).

Luff, W.M., Goodfellow, W. D. & Juras, S. J. (1992) Evidence for a feeder pipe and associated alteration at Brunswick No. 12 massive sulfide deposit. Exploration and Mining Geology. Vol. 1

Lydon, J. W. (1988) Volcanogenic Massive Sulfide Deposits Part 1: A descriptive model. in Ore Deposit Models. Geoscience Canada Reprint Series 3.

MacLean, W. H., & Hoy, L. D., (1991) Geochemistry of Hydrothermal Altered Rocks at the Horne Mine, Noranda, Quebec. Economic Geology Vol. 86

Peter, J. M., & Goodfellow, W. D. (1992) Mineralogy, bulk and rare earth element geochemistry of massive sulphide-associated hydrothermal sediments of the Brunswick Horizon, Bathurst Mining Camp, New Brunswick. Canadian Journal of Earth Science. Vol. 33

Solomon, M., Eastoe, C. J., Walshe, J. L. & Green, G. R. (1998) Mineral Deposits and Sulfur Isotope Abundances in the Mount Read Volcanics between Que River and mount Darwin, Tasmania. Ecomonic Geology, Vol. 83

Urabe, T. & Scott, S. D. (1983) Geology and footwall alteration of the South Bay massive sulfide deposit, northwestern Ontario, Canada. Canadian Journal of Earth Sciences. Vol. 20

Urabe, T., Scott, S. D., and Hattori, K. (1983) A Comparison of Footwall-Rock Alteration and Geothermal Systems beneath Some Japanese and Canadian Volcanogenic Massive Sulfide Deposits: in Skinner, B. J., The Kuroko and Related Volcanogenic Massive Sulfide Deposits. Economic Geology. Monograph 5

Whitford, D. J., Korsch, M. J. & Solomon, M. (1992) Strontium Isotope Studies of Barites: Implications for the origin of base metal mineralisation in Tasmania. Economic Geology Vol. 87

Whitford, D. J., Korsch, M. J., Porritt, P. M., and Craven, S. J., (1988) Rare-Earth element Mobility around the Volcanogenic Polymetallic Massive Sulfide Deposit at Que River, Tasmania, Australia. Chemical Geology, Vol. 68. Pg105-119.

Appendix 10

Rock Catalogue

Catalog#	Field#	Rock Name	Description	AMG Northing	AMG Easting	DDH	Depth	Group	Preps
112938	MHMS1-1	v'clastic	f/ ashy v'clastic, ser gm, 2-3mm chl spotting,gn with carb	5347742	385491.5	MS1	36.3	Tyndall Group	PS,WR,R
112939	MHMS1-2	v'clastic	ashy v'clastic, chl-sph,gn,ser. More chl in gm also chl spotting	5347742	385491.5	MS1	40.6	Tyndall Group	PS,WR,R
112940	MHMS1-3	v'clastic	chl vclastic, small rhyo clast, strong vein minn	5347742	385491.5	MS1	54.7	Tyndall Group	PS,WR,R
112941	MHMS1-4	v'clastic	str chl-ser v'clastic 1cm fiamme veinlet and dissem gn,sph,py	5347742	385491.5	MS1	62.8	Tyndall Group	WR,R
112942	MHMS1-5	v'clastic	chl-ser v'clastic, veinlet gn & sph in close assoc.	5347742	385491.5	MS1	67	Tyndall Group	PS,R
112943	MHMS1-6	v'clastic	med/coarse v'clastic qz xtal, fiamme, aphyric rhyolite clasts	5347742	385491.5	MS1	76	Tyndall Group	WR,R
112944	MHMS1-7	v'clastic		5347742	385491.5	MS1	110.8	Tyndall Group	PS,R
112945	MHMS1-9	v'clastic	coarse v'clastic, ser fiamme,angular limestone clasts	5347742	385491.5	MS1	164.5	Tyndall Group	PS,WR,R
112946	MHMS1-11	Qtz-fspar porp	qz/fspar porphyry, 3cm qz carb,chl,sph w' gn vein	5347742	385491.5	MS1	273.4	Tyndall Group	PS,R,Cl,Pbl,Fl
112947	MHMS1-14	v'clastic	coarse v'clastic, rhy'c clasts and chl veining and replacement of pum	5347742	385491.5	MS1	18.1	Tyndall Group	WR,R
112948	MHMS2-2	v'clastic	coarse chl ser alt v'clastic w. cal vein	5347487	385254	MS2	107	Tyndall Group	Cl,R
112949	MHMS2-9	qtz fspar phyri	fine grained top to mass flow unit -Kfspar alt	5347487	385254	MS2	154.6	Tyndall Group	PS,R
112950	MHMS2-15	Qtz rhyolite?	recrystallized qz in microcrystalline qtz gm	5347487	385254	MS2	296.8	CVC?	PS,R
112951	MHMS3-2	v'clastic	dark chl alt v'clastic w' fiamme, shale and veinlet sph	5347487	385318.6	MS3	32	Tyndall Group	WR,R
112952	MHMS3-4	v'clastic	contact b/w coarse v'clastic and fine v'clastic w. sph min & cal veining	5347588	385318.6	MS3	61.2	Tyndall Group	Cl,R
112953	MHMS3-9	v'clastic	v'clastic relatively unaltered, fiamme qz xtals	5347588	385318.6	MS3	109.4	Tyndall Group	WR,R
112954	MHMS3-10	ore	3cm massive sulphide clast? In chl spotted/altered volcanic	5347588	385318.6	MS3	111.7	Tyndall Group	PS,R,Pbl, Slgn,s
112955	MHMS3-12	v'clastic	near massive chl,w' gn sph in carb veins	5347588	385318.6	MS3	115.3	Tyndall Group	WR,R
112956	MHMS3-16	ore	mod chl seri alt volcanic sst w' wispy py gn sph min	5347588	385318.6	MS3	137.1	Tyndall Group	PS,R, Pbl,Slpy,g
112957	MHMS3-20	v'clastic	green coloured coarse volcanic sst	5347588	385318.6	MS3	200.25	Tyndall Group	WR
112958	MHMS3-23	v'clastic	chl spotted ser alt volcanic sst w' py	5347588	385318.6	MS3	273.2	Tyndall Group	WR,R
112959	MHMS3-24	v'clastic	massive chl vein w' chalco vein	5347588	385318.6	MS3	285.1	Tyndall Group	PS,R
112960	MHMS3-26	v'clastic	domainal fspar chl alt of v'clastic	5347588	385318.6	MS3	308.2	CVC?	WR,R
112961	MHMS3-28	v'clastic	domainal fspar chl alt of pumic v'clastic	5347588	385318.6	MS3	326.6	CVC?	WR,R
112962	MHMS4-1	shale	shale w' coarse euhedral py sub aligned w' veins & bedding? Sph	5347888	385518.3	MS4	109.7	Tyndall Group	PS,R,Slpy,sph
112963	MHMS4-2	shale	intermixing of black and green shale	5347888	385518.3	MS4	131.8	Tyndall Group	TS,R
112964	MHMS4-11	qz fspar porph	qz fspar porph w. qz carb gn sph vein	5347888	385518.3	MS4	335.4	Tyndall Group	Slsph,gn,Fl
112965	MHMS5-1	qz fspar porph	mod grained qz fspar porphyry w'weak ser of fspar	5348341	384882.7	MS5	13	Tyndall Group	WR,R
112966	MHMS5-3	shale	shale	5348341	384882.7	MS5	49.7		Cl
112967	MHMS5-4	shale	calcareous shale dominated clastic bx - py clasts .	5348341	384882.7	MS5	52.9	Tyndall Group	PS,R
112968	MHMS6-1	qz fspar porph	qz cal, vein controlled fspar alt of qz fspar porph	5347110	384976.9	MS6	69	Tyndall Group	Cl,R

Catalog#	Field#	Rock Name	Description	AMG Northing	AMG Easting	DDH	Depth	Group	Preps
112969	MHMS7-1	qz fspar porph	qz,fspar,porph, fspar alt w' mag blebs	5347510	385087.7	MS7	77	Tyndall Group	WR,R
112970	MHMS7-4	shale	black shale w' vein gn & py, gn dissem/bled from vein	5347510	385087.7	MS7	263.6	Tyndall Group	PS,R,Pbl
112971	MHMS7-6	v'clastic	coarse limestone rich volcaniclastic w' sph& gn min in ser clast	5347510	385087.7	MS7	376.05	Tyndall Group	PS,R
112972	MHMS7-7	v'clastic	str chl v'clastic w' fe rich carb? W' min sph,gn & chalco also large Py	5347510	385087.7	MS7	393.8	Tyndall Group	PS,R,Cl,Slpy,gn
112973	MHMS7-9	v'clastic	pumic v'clastict w' pink alt fspar w' chl alt blebby py in assoc w'chl veins	5347510	385087.7	MS7	451.2	Tyndall Group	PS,WR,R
112974	MHMS7-11	v'clastic	fspar alt v'clastic w.chl alt and minor py	5347510	385087.7	MS7	467.75	Tyndall Group	R
112975	MHMS7-12	v'clastic	fine grain v'clastic with fspar,hem chl alt +-ser w' chalco vein	5347510	385087.7	MS7	478	Tyndall Group	WR,R
112976	MHMS7-13	v'clastic	fine v'clastic w' coarse sections. W' chl - jasper?-chl rim typical alt assem	5347510	385087.7	MS7	481.7	Tyndall Group	PS,WR,R
112977	MHMS7-15	v'clastic	fine v'clastic cut by qtz veins w' ser alt Chl blebs w' fspar/hem	5347510	385087.7	MS7	489.45	Tyndall Group	PS,R
112978	MHMS7-16	v'clastic	fine v'clastic w' fine red carb/sph spots	5347510	385087.7	MS7	542.6	Tyndall Group	WR,R
112979	MHMS7-17	v'clastic	coarse limestone rich v'clastic	5347510	385087.7	MS7	432.3	Tyndall Group	Cl,R
	MHMS7-27	v'clastic	unaltered v'clastic, with carb clasts	5347510	385087.7	MS7	353.3	Tyndall Group	WR
112980	MHMS8-2	shale	veined contact cal,qz,chl and sph gn min	534826	385110	MS8	373.2	Tyndall Group	R
112981	MHMS8-3	qz,fspar porph	str qz, chl, cal veined qz fspar porph	534826	385110	MS8	373.4	Tyndall Group	R
112982	MHMS8-8	shale	weakly py black shale	534826	385110	MS8	465.8	Tyndall Group	WR,R
112983	MHMS8-10	shale	shale w' carb beds replaced/ veinlet sph w' veinlet py gn & apy	534826	385110	MS8	561.9	Tyndall Group	PS,R,Slsph,py,g
112984	MHMS8-11	shale	py beds with pyrite rossettes	534826	385110	MS8	564.8	Tyndall Group	PS,R,Slpy,po
112985	MHMS8-12	shale	calcareous black shale showing calc replaced concretions	534826	385110	MS8	565.4	Tyndall Group	R
112986	MHMS8-13	shale	calcareous black shale showing calc replaced concretions	534826	385110	MS8	568.8	Tyndall Group	WR,R
112987	MHMS8-14	v'clastic	shale w' coarse carb rich beds? W' sph, py min & siliceous fossils	534826	385110	MS8	571.05	Tyndall Group	PS,R,Cl
112988	MHMS8-15	v'clastic	med/coarse bx- shale,carb rich clasts min replacement? Of carb clasts?	534826	385110	MS8	582	Tyndall Group	PS,R,Pbl,Slsph,l
112989	MHMS8-17	qz,fspar porph	qz,fspar,porph mod/str ser alt of fspar and chl of amphibole	534826	385110	MS8	604.7	Tyndall Group	WR,R
112990	MHMS8-19	qz,fspar porph	qz,fspar,porph mod/str silica +- mod chl alt w' minor py	534826	385110	MS8	649.3	Tyndall Group	WR,R
112991	MHMS8-27	v'clastic	green mod/coarse v'clastic with chl ser alt of pum	534826	385110	MS8	670	Tyndall Group	WR,R
112992	MHMS9-1	shale	black shale, w. cal py veins	534826	385110	MS9	178.9	Tyndall Group	WR,R
112993	MHMS9-2	qz fspar porph	mod unalt qz fspar porph	534826	385110	MS9	272.2	Tyndall Group	WR,R
112994	MHMS9-3	qz fspar porph	monomict qz fspar porph bx in black shale matrix	534826	385110	MS9	48.8	Tyndall Group	R
112995	MHMS9-4	shale	large spherical concretion in py, carb bed	534826	385110	MS9	153.5	Tyndall Group	R

	Field#	Rock Name	Description	AMG Northing	AMG Easting	DDH	Depth	Group	Preps
112996	MH5	re xtline qtz	med coarse fpar rich v'clastic - str ser alt. Gn sph py min	5347684	385387			Tyndall Group	PS,R
112997	MH6	ore	massive sph vein?. Host - min fine chl alt v'clastic	5347680	385386.5			Tyndall Group	PS,R,Slsph
112998	MH11	Qtz rhyolite	fine grained qtz phyric lava	5347708	385416			Tyndall Group	TS, R
112999	MH30	v'clastic	rnd carb alt of fine v'clastic	5347973	385487			Tyndall Group	Cl,R
113000	MH38	v'clastic	strong veinlet sph min in chl alt v'clastic	5347651	385315.5			Tyndall Group	PS,R,Slsph
113001	MH39	vein	shale clast in v'clastic? With large gn vein	5347649	385316.5			Tyndall Group	PS,R,Slsph,gn
113002	MH40	Qtz rhyolite?	recrystallized qz in microcrystalline qtz gm	5347740	385439			CVC?	PS,R
113003	MH15	qz rhyolite	fine grained qtz phyric lava	534768.4	385425.6			CVC?	TS, R